Baseband Compensation Principles for Defects in Quadrature Signal Conversion and Processing

GERT-JAN VAN ROOYEN

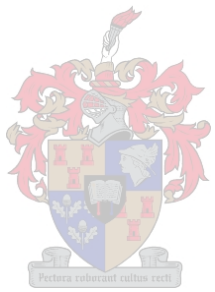

Dissertation presented for the Degree of Doctor of Philosophy at the University of Stellenbosch

PROMOTER: Prof. J.G. Lourens

April 2004

Declaration

I, the undersigned, hereby declare that the work contained in this dissertation is my own original work and that I have not previously in its entirety or in part submitted it at any university for a degree.

Opsomming

Sleutelwoorde: sagteware-gedefinieerde radio, SDR, haaksfasige menging, haaksfasige modulasie, haaksfasige demodulasie, digitale kompensasie, sagteware-radio, direk-digitale sintese, DDS.

'n Gewilde stelling is dat digitale seinomsetting in sagteware-gedefinieerde kommunikasiestelsels so na as moontlik aan die antenna moet geskied deur gebruik te maak van hoëspoed omsetters. Hierdie verhandeling stel alternatiewe ontwerpsbeginsels voor, en toon aan dat hierdie beginsels die eersgenoemde stelsel se akkuraatheid verbeter, terwyl stelselbuigsaamheid gehandhaaf word.

Dit word eerstens voorgestel dat digitale kompensasie gebruik word om die effekte van hardeware-onakkuraathede in die RF-koppelvlak van sagteware-gedefinieerde radio's om te keer. Nuwe kompensasietegnieke, wat seinartefakte weens koppelvlak-onakkuraathede kan onderdruk, word aangebied. Die mate waartoe hierdie artefakte onderdruk kan word, word slegs beperk deur die akkuraatheid waarmee dit gemeet en digitaal voorgestel kan word. 'n Algemene kompensasiebeginsel word neergelê waarin die voorwaardes vir optimale kompensasie vasgelê word.

Tweedens word voorgestel dat 'n duidelike onderskeid getref word tussen seinverwerkingskompleksiteit en seinverskuiwing in RF-koppelvlakke. Daar word getoon dat konvensionele SDR-stelsels dikwels nie hierdie beginsel handhaaf nie. 'n Alternatief, naamlik haaksfasige menging, word voorgehou as 'n tegniek wat duidelik onderskei tussen seinverskuiwing en seinverwerking. Akkurate kompensasietegnieke is egter nodig om effektief van sulke mengers gebruik te maak.

Haaksfasige mengers word voorgestel as veeldoelige koppelvlakke vir sagteware-gedefinieerde radio's, en haaksfasige modulasie- en demodulasietegnieke word voorgestel as plaasvervangers vir bestaande tegnieke. Die inherente hardeware-onakkuraathede word geanaliseer en gesimuleer, en geskikte kompensasietegnieke word afgelei en getoets. Laastens word die teoretiese resultate met 'n praktiese prototipe bevestig.

Abstract

Keywords: software-defined radio, SDR, quadrature mixing, quadrature modulation, quadrature demodulation, digital compensation, software radio, direct-digital synthesis, DDS.

An often-stated goal of software-defined transceiver systems is to perform digital signal conversion as close to the antenna as possible by using high-rate converters. In this dissertation, alternative design principles are proposed, and it is shown that the signal processing techniques based on these principles improve on the prior system's accuracy, while maintaining system flexibility.

Firstly, it is proposed that digital compensation can be used to reverse the effects of hardware inaccuracies in the RF front-end of a software-defined radio. Novel compensation techniques are introduced that suppress the signal artefacts introduced by typical front-end hardware. The extent to which such artefacts may be suppressed, is only limited by the accuracy by which they may be measured and digitally represented. A general compensation principle is laid down, which formalises the conditions under which optimal compensation may be achieved.

Secondly, it is proposed that, in the design of such RF front-ends, a clear distinction should be drawn between signal processing complexity and frequency translation. It is demonstrated that conventional SDR systems often neglect this principle. As an alternative, quadrature mixing is shown to provide a clear separation between the frequency translation and signal processing problems. However, effective use of quadrature mixing as design approach necessitates the use of accurate compensation techniques to circumvent the hardware inaccuracies typically found in such mixers.

Quadrature mixers are proposed as general-purpose front-ends for software-defined radios, and quadrature modulation and demodulation techniques are presented as alternatives to existing schemes. The inherent hardware inaccuracies are analysed and simulated, and appropriate compensation techniques are derived and tested. Finally, the theory is verified with a prototype system.

Bedankings

Ek wil graag baie dankie sê aan die volgende persone wat die voltooiing van hierdie proefskrif moontlik gemaak het:

- Eerstens, aan my promotor, prof. Johan Lourens: vir jou vertroue, entoesiasme en leiding sedert hierdie stuk navorsing meer as ses jaar gelede klein-klein as 'n skripsie begin het. Telkens wanneer ek op die details gefokus het, het jy die groter moontlikhede raakgesien—baie dankie! Ek waardeer alles wat jy gedoen het om my voortgesette studies moontlik te maak.

- Aan Adriana: baie dankie vir jou geduld, liefde en begrip tydens die lang proses om hierdie werk te voltooi. Jou ondersteuning het vir my geweldig baie beteken.

- Aan my ma: dankie vir hope liefde en bemoediging, en veral vir 'n ouerhuis waar ek keer op keer kon opdaag om te ontspan en heerlik te eet op tye wanneer dinge te besig geraak het.

- Aan my skoonouers: dankie vir al die lekkernye wat gereeld van die plaas af by my aangekom het!

- Aan Carine: dankie vir jou voortreflike (en vleiende) proefleeswerk.

- Aan my studente, veral die M-studente wat soms gesukkel het om afsprake tussen my skrywery deur te reël: dankie vir julle geduld, en vir alles wat ek deur julle navorsing kon leer.

- Aan my vriende, wat my kort-kort herinner het dat daar soveel goeie redes is hoekom 'n mens groot stukke werk wil kláármaak.

List of Publications

The following publications have resulted from the work documented in this dissertation:

International journal publications

[49] VAN ROOYEN, G.-J. and LOURENS, J. G., "A Quadrature Baseband Approach to Direct Digital Synthesis." *IEEE Transactions on Broadcasting,* September 2000, Vol. 46, No. 3, pp. 227–230.

International conference publications

[52] VAN ROOYEN, G.-J. and LOURENS, J. G., "Baseband Digital Synthesis and Analysis for High-Frequency Software Radio Applications." *Proceedings of IEEE Africon,* October 2002, Vol. 1, pp. 371–376.

[55] WITKOWSKY, J. and VAN ROOYEN, G.-J., "A Hardware Emulator Testbed for Software Defined Radio." *Proceedings of IEEE Africon,* October 2002, Vol. 1, pp. 383–388.

Patents

[51] VAN ROOYEN, G.-J. and LOURENS, J. G., "Baseband Digital Signal Processing System with Digital Spur Compensation." October 2002. South African Patent Application 2002/7909.

Local journal publications

[50] VAN ROOYEN, G.-J. and LOURENS, J. G., "Advances in Direct Digital Frequency Synthesis." *Elektron,* July 2001, pp. 39–42.

Numbers in square brackets refer to the corresponding entry in the Bibliography.

Contents

List of Figures

List of Tables

Nomenclature

Acronyms

ADC	analogue-to-digital converter
AM	amplitude modulation
ASK	amplitude-shift keying
BPSK	binary phase-shift keying
CD	compact disc
CDMA	code division multiple access
CMOS	complementary metal-oxide semiconductor
CODEC	coder-decoder
COTS	commercial off-the-shelf
DAC	digital-to-analogue converter
DC	direct current
DDFS	direct-digital frequency synthesis
DDS	direct-digital synthesis
DFT	discrete Fourier transform
DNL	differential non-linearity
DSB	double sideband
DSP	digital signal processor
FIR	finite impulse response
FM	frequency modulation
FPGA	field-programmable gate array
FFT	fast Fourier transform
FSK	frequency-shift keying
IF	intermediate frequency
HF	high-frequency range (3–30 MHz)
IC	integrated circuit
INL	integral non-linearity
LPF	low-pass filter
LSB	least significant bit
LSB	lower sideband in SSB modulation
MSB	most significant bit
NCO	numerically controlled oscillator

NRZ	non-return to zero
PC	personal computer
PLL	phase-locked loop
PM	phase modulation
PSK	phase-shift keying
QAM	quadrature amplitude modulation
QBB	quadrature baseband
QBB-DDS	quadrature-baseband direct-digital synthesis
QPSK	quadrature phase-shift keying
RDL	relative distortion level
RDS	radio data system
RC	resistor-capacitor
RF	radio frequency
RX	receiver
ROM	read-only memory
SABS	South African Bureau of Standards
SBR	software-based radio
SDR	software-defined radio
SFDR	spurious-free dynamic range
SR	software radio
SNR	signal-to-noise ratio
SQNR	signal-to-quantisation-noise ratio
SSB	single sideband
SSB-DDS	single-sideband direct-digital synthesis
S+H	sample and hold
THD	total harmonic distortion
TX	transmitter
UHF	ultra-high frequency range (0.3–3 GHz)
USB	upper sideband in SSB modulation
VCO	voltage-controlled oscillator
VHF	very high frequency range (30–300 MHz)

Variables

symbol	unit	description
$a(t)$	v(t)	amplitude component of a modulating signal
a_0	V	maximum amplitude of a quadrature-deviation error signal
a_1	V	maximum offset of a quadrature-deviation error signal
a_i	V	instantaneous amplitude

symbol	unit	description
B	Hz	bandwidth of a modulated signal
B_0	Hz	bandwidth of a modulating baseband signal
C		signal-to-quantisation noise offset
C	bits/s	channel capacity
d		number of sine samples per quantisation error cycle
D		number of DAC bits
D_ϵ	dB	distortion associated with offset error
D_κ	dB	distortion associated with phase error
D_ρ	dB	distortion associated with amplitude deviation
f	Hz	continuous frequency
Δf	Hz	DDS frequency resolution
$f(t)$	V	general time-domain signal
f_d	Hz	FM deviation frequency
f_o	Hz	frequency of an output sinusoid
f_s	Hz	sampling frequency
F_c	Hz	discrete-time carrier frequency
$F(\omega)$		general frequency-domain signal
h_{-2}	$\mathrm{W} \cdot \mathrm{Hz}$	random walk frequency noise constant
h_{-1}	W	flicker frequency noise constant
h_0	W/Hz	white frequency noise constant
h_1	$\mathrm{W/Hz}^2$	shot phase noise constant
h_2	$\mathrm{W/Hz}^3$	white phase noise constant
H	dBc	harmonic spur size
I		in-phase channel of a quadrature modulator or demodulator
I_{in}	A	input current
I_{out}	A	output current
$I(t)$	$v(t)$	in-phase component of a quadrature baseband signal
j		defined as $\sqrt{-1}$
$J_n(\beta)$		Bessel function of the first kind, of order n
k_a		modulation index for AM
k_f		frequency deviation constant for FM
k_z		filter impedance scaling factor
k_ϕ		phase deviation constant for PM
$m(t)$	$v(t)$	modulating input signal for FM or PM
$m_p(t)$	$v(t)$	analytic non-baseband signal
$m_\epsilon(t)$	$v(t)$	demodulated error signal
M		number of ADC bits
$M(t)$	$v(t)$	local oscillator signal
$M_I(t)$	$v(t)$	in-phase local oscillator signal

symbol	unit	description
$M_Q(t)$	$v(t)$	quadrature-phase local oscillator signal
n		number of sampled sine cycles per quantisation error cycle
N		input complexity of an algorithm
N_0	W/Hz	white frequency noise constant
ΔN_ϕ	dB	change in clock jitter noise floor
P_o	W	normalised power in a demodulated error signal
Q		quadrature-phase channel of a quadrature (de–) modulator
Q		bandpass quality factor
$Q(t)$	$v(t)$	quadrature-phase signal of a quadrature (de–) modulator
r	$v(t)$	magnitude of a phasor
R		number of bits in a phase accumulator
R	Ω	arbitrary resistance
$s(t)$	$v(t)$	complex-valued downmixed signal after quadrature demodulation
$s_d(t)$	$v(t)$	desired complex-valued downmixed signal
$s_\epsilon(t)$	$v(t)$	erroneous complex-valued downmixed signal
$s_\rho(t)$	$v(t)$	quadrature-downmixed signal with amplitude deviation
S		number of bits in each sine lookup table entry
$S(f)$	W	power density spectrum
S_κ	dBc	spur size due to phase error
S_ρ	dBc	spur size due to amplitude error
$S_{\rho\kappa}$	dBc	spur size due to combined phase and amplitude deviation
SFDR_ϵ	dB	SFDR associated with offset error
SFDR_κ	dB	SFDR associated with phase error
SFDR_ρ	dB	SFDR associated with amplitude deviation
$\mathrm{SFDR}_{\mathrm{sb}}$	dB	total sideband SFDR
SNR_q	dB	signal-to-quantisation noise ratio
SNR_φ	dB	signal-to-phase noise ratio
t	s	continuous time
T	s	discrete time period
$v_g(t)$	$v(t)$	filter input voltage
$v_o(t)$	$v(t)$	filter output voltage
V_{err}	V	maximum INL deviation from the ideal straight line
V_{max}	V	maximum DAC output voltage
V_{ref}	V	reference voltage
W		number of bits used to index a DDS lookup table
$y(t)$	$v(t)$	RF signal
$y_d(t)$	$v(t)$	desired RF signal
$y_\epsilon(t)$	$v(t)$	erroneous RF signal
$Y(\omega)$		Fourier transform of an RF signal

symbol	unit	description
α	V	amplitude of a local oscillator leakthrough signal
α_g	%	relative amplitude of SMIQ carrier leakthrough
β		FM modulation index
γ	rad	phase of a local oscillator leakthrough signal
γ_g	rad	phase of SMIQ carrier leakthrough
$\delta(\omega)$		dirac delta function
ε_i	V	I-channel offset
ε_q	V	Q-channel offset
$\theta(t)$	rad	phase and frequency component of a modulating signal
$\mathbf{\Theta}(t)$	rad	random process: uniformly distributed angle
κ	rad	quadrature phase error at the I-Q channels
κ_f	rad	phase mismatch contributed by filter
κ_g	rad	quadrature phase impairment in SMIQ modulator
λ	rad	phase error in a quadrature mixer's local oscillator signals
ρ_0	V	absolute amplitude deviation in an I-Q channel
ρ		relative amplitude deviation in an I-Q channel
ρ_f		amplitude deviation contributed by filter
ρ_g		relative amplitude impairment in SMIQ modulator
τ	s	continuous time in an integrand
ϕ_0	rad	phase angle at time $t = 0$
$\phi_{\max}$		maximum phase accumulator value
$\phi(nT)$		value of a phase accumulator at discrete time nT
$\phi(t)$		value of a phase accumulator at continuous time t
$\Delta\phi$		discrete phase increment
ϕ_i	rad	instantaneous phase
$\phi_\epsilon(t)$	rad	erroneous phase angle due to quadrature deviation
ω	rad/s	continuous frequency
ω_c	rad/s	carrier frequency of an FM signal
ω_d	rad/s	FM deviation frequency
ω_i	rad/s	instantaneous signal frequency
ω_m	rad/s	frequency of a modulating input sinusoid
ω_n	rad/s	negative baseband frequency
ω_p	rad/s	positive baseband frequency
$\Delta\omega$	rad/s	DDS frequency resolution
$\Delta\omega$	rad/s	local oscillator frequency mismatch

Operations

$\mathcal{F}\{\cdot\}$	Fourier transform
$\mathcal{I}m\{x\}$	imaginary part of a complex value
$\mathcal{R}e\{x\}$	real part of a complex value
$O(\cdot)$	order of complexity of an algorithm
$\dot{x}$	time derivative of x
$[x]_{\max}$	maximum value of the argument
$[x]_{\min}$	minimum value of the argument
$*$	convolution operator
$\lceil x \rceil$	ceiling function (smallest integer $\geq x$)
$\langle x \rangle_M$	modulo-M arithmetic
$[\cdot]_{\text{LPF}}$	low-pass filtering
$\hat{\omega}$	approximation of variable ω
$\hat{a}(t)$	Hilbert transform of function $a(t)$
$\tilde{a}(t)$	analytic representation of $a(t)$: $\tilde{a}(t) = a(t) + j\hat{a}(t)$

Chapter 1

Introduction

It is perhaps unusual for a discourse on signal theory to start by noting the importance of the software revolution of the late twentieth century. The growth of the digital industry in the latter half of the last century has, however, had a remarkable influence on nearly every aspect of engineering, and on many other aspects of society. We have seen computers develop from expensive assets to consumer items. In contrast, we have seen software products develop into constantly maintained and updated assets that can easily outlive the hardware on which they run. Half a century ago, software was a tool used to harness the computing power of the hardware. Today, hardware has become a platform needed to support the capabilities of constantly developing software.

This software revolution brought several new paradigms to engineering in general: object-oriented design, rapid application development, object re-use, development libraries, live updates and patches, reusable design patterns—to name just a few. These advances made possible the explosive growth of the software industry, and have spurred the need for similar developments in other fields of engineering. In particular, the telecommunications industry (especially mobile communications) has been strongly affected, with a growing requirement for continuous rapid advance in technology.

Consequently, many traditional design methodologies in telecommunications are fast becoming obsolete. "Soldered" analogue radios are making place for software-based systems that serve engineers' need for quick development, and users' need for upgradability and customisability. The research detailed in this dissertation was performed in this context of software-defined telecommunications sytems, and will advocate new design philosophies in this relatively young field of digital synthesis and processing of analogue signals.

The greatest hurdle to harnessing the full power of these so-called "software radio" systems, is that the signal quality in such systems is often still inferior to that of their analogue counterparts. The purpose of the principles presented in this document is to improve the quality of signals generated and processed by software-based communications systems, and thus to promote the viability of software radio in general.

1.1 Software radio

The goal of software radio is to replace traditional analogue radio functionality by software signal processing. Such an approach offers great flexibility in radio systems, powerful signal processing techniques and a reduced rate of hardware obsolescence in an environment of evolving communication standards.

The software radio is often defined in its "ideal" form, consisting of a general-purpose, reprogrammable digital processor that interfaces directly to the antenna (on the radio signal side) and the user (on the application side) [26, 27, 4]. Such an ideal software radio is not limited to specific frequency bands or communication modes.

There are serious practical issues in the implementation of such a radio, such as the realisation of multiband antenna structures, and the direct digitisation, synthesis and processing of signals at radio frequencies [26]. For this reason, most practical software-based radio implementations employ some form of analogue signal processing, usually in the form of superheterodyne mixing and filtering [3]. Such a system, where signal translation and filtering is performed in the analogue front-end, but all remaining signal processing is performed by software, is called a *software-defined radio* [4].

1.2 The signal frequency problem

The necessity to opt for a software-defined radio with an analogue front-end for signal translation places the SDR designer in a quandary: At what intermediate frequency (IF) should radio signals be sampled? Selecting a low IF allows low-speed data conversion and processing, but several stages of mixing and filtering may be required to obtain a reasonable alias-free translation of the signal at the low IF. On the other hand, selecting a high IF allows wide-bandwidth signals to be sampled, and minimises mixing and filtering. A high sampling rate and signal processing rate is, however, required. This in turn exacerbates conversion noise in the signal, lowering the signal quality (see Chapter 4).

1.3 The baseband solution

Chapter 2 will focus on an alternative technique for the frequency translation problem, using quadrature mixing techniques to perform direct signal translation between baseband and radio frequencies. These techniques, sometimes also called zero-IF transceivers [3] or direct-conversion transceivers [34], sidestep the use of an intermediate frequency altogether by representing the baseband signal using complex numbers. They allow low-speed, low-cost data converters and digital processors to be used to perform software-defined radio functions.

Although these quadrature modulation and demodulation techniques are not novel [12, 3, 34, 10], they are less widely known than the heterodyne mixing techniques. When cited in literature, quadrature signal conversion is usually criticised for its stringent requirement of

high-precision hardware. An authorative text on SDR front-ends states as recently as 2002: [3]

> A significant problem with direct conversion architecture is the introduction, by the process, of a DC offset. ... One of the predominant reasons designers of SDR receivers or transmitters are likely to reject direct conversion architecture has to do with the difficulty of generating a wideband quadrature local oscillator. ... The local oscillator ... will have to maintain precise phase quadrature, and precise amplitude balance over [a] range of frequencies.

One of the main objectives of this dissertation is to present simple techniques to reverse the effects of such non-idealities. As a result, it will be shown that quadrature conversion does not merely present a viable alternative to the traditional heterodyne front-end, but that it represents a generally preferable signal processing paradigm.

1.4 Digitisation versus digital compensation

As touched upon in Section 1.2 above, the use of heterodyne mixing places difficult design constraints on the RF front-end of an SDR. The generally cited solution to this problem is to eventually avoid the use of an IF by sampling at radio frequencies. Brannon *et al.* writes: [5]

> ...the challenge of moving the analog-digital boundary closer to the antenna is the critical step in establishing the foundation for increasing the content and capability of digital signal processing (DSP) in the radio.

This assertion firstly relies on the belief that future technology will be capable of converting and processing signals at a "high enough" rate to avoid heterodyne mixing. It further assumes that there in fact exists a rate "high enough" to process radio signals in general. Clearly, no reasonably foreseeable technology will allow the direct sampling and processing of arbitrarily high parts of the frequency spectrum. Consequently, it will always be possible to construct hardware radios that can make use of parts of the signal spectrum inaccessible to these RF-sampling software radios. This dissertation challenges such a definition of software radio that forces it to be perpetually inferior to hardware-based techniques.

The motivation for the direct-sampling ideal is clear: Hardware-based signal processing (including the use of an extensive analogue front-end on an SDR) is fraught with inaccuracies; software-based signal processing, on the other hand, can be done with mathematical precision. The conventional conclusion drawn from this observation is that as much of the signal processing as possible should be performed in software—hence the ideal of digitising directly at the antenna.

The research presented here attempts to show that the same premises can lead to an alternative conclusion that is also more practically realisable: The use of an RF front-end for signal translation is justified, as long as it does not compromise the flexibility and

accuracy of the software radio. It will be shown that it is possible to compensate for hardware deficiencies, in particular those caused by quadrature mixing, up to the point where

(a) the effects of these deficiencies can longer be measured reliably; or

(b) the parameters used to compensate for these inaccuracies are directly limited by the numeric resolution of the digital system.

Such a system would still meet the software-radio objective of complete software reconfigurability. It will be argued that such a system is likely to have higher signal fidelity than that of a system attempting to sample at radio frequencies.

1.5 Scope of the dissertation

1.5.1 Central proposition

The central proposition of the dissertation may be stated as follows:

> **Proposition A:**
> A digital processing system can always compensate for deterministic distortion effects in its analogue front-end (limited only by the accuracy of its numeric representation, and by the accuracy with which the distortion effects can be measured) under the condition that all these analogue inaccuracies are cascades of invertible transforms, and that their net effect is fully known.

This dissertation attempts to give a thorough analysis of this central proposition, its context, its implications and its applications.

1.5.2 Preliminary observations

A new design philosophy

As was highlighted in Section 1.4 (Digitisation versus digital compensation), the conventional approach to digital transceiver systems such as software radio has been to avoid analogue components as much as possible, due to their inherent non-idealities. The alternative design philosophy proposed by this dissertation relaxes this requirement by emphasising *digital control* over the entire signal path, instead of placing the emphasis on *digitisation*. This can make analogue front-end design much simpler, because, instead of requiring signal converters that function as close as possible to the theoretical ideal (and often at radio frequencies), more signal processing can be done in the analogue domain, using lower-quality components.

Separating translation and processing

Traditionally, digital signal processing has been placed in contraposition to analogue processing. This is made manifest in the often-stated goal of the "ultimate" software radio:

to completely replace analogue signal processing components with functionally equivalent software. Joseph Mitola writes: [26]

> The placement of the A/D/A converters as close to the antenna as possible and the definition of radio functions in software are the hallmarks of the software radio.

He qualifies this assertion by noting the flexibility of this idealised architecture:

> The key difference [between software radios and software-controlled hardware radios] is the total programmability of software radios, including programmable RF bands, channel access modes, and channel modulation.

This dissertation's central proposition suggests that a software radio's digital capabilities can be better employed to *complement* analogue hardware. In particular, this can be done without forfeiting the advantages associated with software radios, as defined by Mitola [26].

This approach makes the quadrature-baseband proposition of Section 1.3 not merely an interesting alternative "hybrid" configuration, but a fundamental technique of frequency translation. Moreover, it underlines an important distinction between signal translation and signal processing that forms a basic principle of the research presented here:

> **Proposition B:**
> The Shannon-Hartley law implies that signal (information) processing and frequency translation are distinct components of any transceiver system: Signal processing concerns the embedding and extraction of *information* into and from a signal. *Signal processing complexity is a function of information rate.* Frequency translation involves the placement of a signal at a prescribed or convenient position in the frequency spectrum. It does not affect the information content in any way, and is thus only a function of the translation distance. This implication of the Shannon-Hartley law should be considered in the design of SDR systems.

Developing the implications of this separation between translation and processing is perhaps the most important contribution of the research described in this document. It will be illustrated that it is more practical to address frequency translation in the analogue domain, and that quadrature mixing is, in general, the best tool for this purpose.

This approach stands in stark contrast to the current software radio paradigm, where signal processing is done at as high a sampling rate as possible in order to minimise analogue frequency translation (consequently placing large demands on processing and conversion requirements). The architectures proposed in this dissertation all have a digital complexity of $O(N)$, where N is the information rate of the received or transmitted signal. This means that signal processing demands scale with the *bandwidth* and *dynamic resolution* of the modulated signal, rather than with the signal's absolute frequency. After all, a signal's centre frequency is something fairly arbitrary, dictated by spectrum allocation and convenience—it should not affect the complexity of signal processing.

The Shannon-Hartley law states that information capacity can be expressed as a function of bandwidth and dynamic resolution, in the familiar relationship

$$C = B \log_2(\mathrm{SNR} + 1)\,, \tag{1.1}$$

where C represents a signal's information capacity, B its occupied bandwidth, and SNR the signal-to-noise ratio—its dynamic resolution [40]. Proposition B above implies that a software transceiver's signal processing complexity is a linear function of C. On the other hand, B dictates the temporal complexity of the system (that is, how fast samples must be processed) and the SNR (the signal-to-quantisation noise ratio in particular) dictates the resolution complexity of the system—typically the word length of the digital logic and the data converters.

1.5.3 Document outline

The rest of the dissertation is structured as follows:

- Chapter 2 briefly reviews the conventional techniques of direct-digital synthesis, and then presents an alternative, namely quadrature modulation. The mathematical theory of quadrature modulation is developed, and its advantages are illustrated. It is shown how general modulation schemes can be achieved by using quadrature modulation.

  The chapter then also presents the use of quadrature mixing for digital signal reception and demodulation. Quadrature demodulation is the receiver-side counterpart of quadrature modulation, and is developed here from first principles.

- Chapter 3 focuses on software-defined radio. The chapter covers the basic principles, the use of quadrature modulation and demodulation, and the basic types of signal impairment that can be expected. A brief introduction to digital compensation is given to lay the foundation for the following chapters.

Up to this point, a broad background has been given on digital modulation and demodulation techniques, with special reference to the quadrature approach. These chapters serve to establish the context for the main development of the dissertation, which follows in the next two chapters. In these following chapters, the non-idealities in the hardware front-end are carefully scrutinised, and methods are developed to compensate for their effects.

- Chapter 4 presents a study of digital-to-analogue and analogue-to-digital converters. Converters are always present in software radios and related architectures, and typically represent the point in the signal path where the most severe signal distortion takes place. For this reason, a dissertation on SDR-related signal quality should make a careful study of these devices, in order to understand the ways in which they affect the signal, and to determine whether means can be found to minimise or even eliminate this distortion. This chapter is mostly an overview of established signal converter theory.

- Chapter 5 represents a main contribution of the document, and studies the distortion effects found in typical quadrature mixers. The chapter shows that it is possible to fully predict the effects of the non-idealities. These effects may be measured in the frequency domain, and the causes of the distortion are simple to deduce from the measured effects.

- Chapter 6 demonstrates that is is possible to compensate for the non-idealities described in the previous chapter. This is used to strengthen the assertion that quadrature modulation and demodulation are the techniques of choice for SDR-related platforms. As a result, processing and conversion requirements can be relaxed.

  The theory presented in this chapter represents the most significant and novel contribution made by the research documented in this text.

The last two chapters (7 and 8) form a denouement to the research: The proposed compensation techniques are evaluated against practical measurement in a quadrature-based SDR system (Chapter 7), thereby illustrating that compensated signal conversion and processing can be achieved in practice. Chapter 8 takes all the results together in conclusion, and discusses the implications of the research, as well as possible future avenues.

Chapter 2

Quadrature mixing

The conventional technique for digitally synthesising radio signals is called direct-digital synthesis (DDS). This chapter will briefly look at DDS and its difficulties, and present quadrature modulation as an attractive alternative. It will then be shown that quadrature demodulation provides the same advantages at the receiver side.

The study of quadrature mixing presented here provides background to the understanding of Proposition B. This chapter does not concentrate on novel techniques; rather, it gives an original development of the theory of quadrature mixing as background for the central thesis of the dissertation. It will be demonstrated that, when performing quadrature mixing, the signal processing complexity is proportional to the signal's bandwidth, rather than its intermediate or broadcast centre frequency.

2.1 Direct-digital synthesis

It is assumed that the reader is familiar with DDS as signal synthesis technique (a summary of direct-digital synthesis is included as Appendix A). The conventional approach to using DDS in the transmission stage of software-defined radios is to produce a modulated signal at a conveniently chosen intermediate frequency. On the one hand, it is desirable to have this intermediate frequency as high as possible: This reduces the need for expensive mixing and filtering. Figure 2.1 illustrates the resulting problem. Consider a DDS output signal generated at an intermediate frequency of 10 MHz. If this signal must be broadcast at 110 MHz, mixing must be performed by multiplying the signal in the time domain with a carrier of 100 MHz. This produces output components at both 90 MHz and 110 MHz, and sharp filtering is required to remove the alias component at 90 MHz. In practical DDS systems, several stages of mixing and filtering might be required to adequately suppress the alias signal [14]. If the DDS signal is generated at a high intermediate frequency, the demands on the mixing and filtering circuitry are relaxed.

High frequency output, however, requires a high-speed DAC, which is more expensive and likely to contribute significantly more noise [46]. Furthermore, there is a trade-off between converter speed and resolution for a given unit cost. As a result, it is also advantageous to

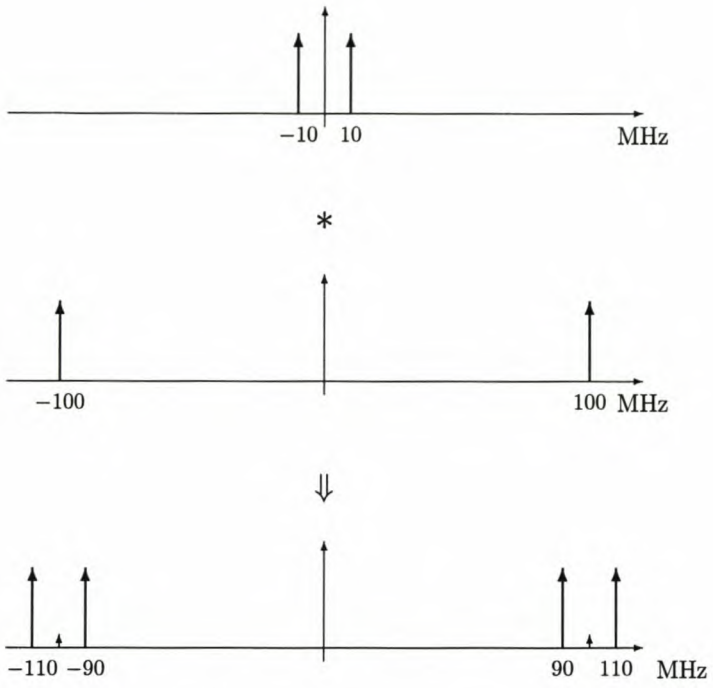

Figure 2.1: *When real-valued signals are mixed, alias components are produced.*

keep the intermediate frequency as low as possible. Conventional SDR receivers suffer from the same trade-off in their downmixing and digitisation stage.

The quadrature-baseband (or "zero-IF") approach to direct digital synthesis, introduced next, provides a solution to the output frequency dilemma: By using this technique, it is possible to produce, for example, a modulated FM radio broadcast signal directly in the baseband, with the sampling frequency as low as 200 kHz. Furthermore, single-stage upmixing with minimal filtering is quite sufficient, because quadrature modulation sidesteps the problem of alias signals.

2.2 Quadrature modulation

All real signals can be seen as having an equal negative frequency component for each positive frequency component in the Fourier frequency domain [43]. On the other hand, complex-valued signals of the form

$$f(t) = Ae^{j\omega_o t} = A\cos\omega_o t + Aj\sin\omega_o t \tag{2.1}$$

do not share this characteristic of being reflected around $\omega = 0$. Consequently, it is possible to multiply complex-valued signals without having to deal with alias signals. What if it were possible to digitally generate a complex signal? Such a signal could, for example, perform frequency modulation around any centre frequency, even around zero herz. Without the problem of aliasing, such a complex-valued signal could easily be upmixed to any desired output frequency.

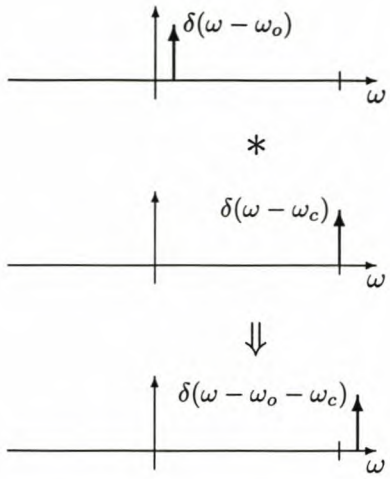

Figure 2.2: *Translation of a complex signal.*

2.2.1 A complex-signal solution

It turns out that it is indeed possible to generate and upmix a complex signal, and to transmit the real part. This approach has been successfully applied before [48, 12, 10], and is repeated here for completeness. It is similar to the author's exposition of the subject in [49, 50]. The technique shares similarities with single-sideband modulation [43]. The single-frequency (sinusoidal) case will be developed first, since this presents the simplest derivation of the technique. In Section 2.2.2 it will be shown that it is trivial to extend the single-frequency case to general Fourier-transformable signals.

If it were possible to generate a single frequency component at ω_o, without a reflection on the opposite Fourier transform frequency axis, the signal would be represented by a single impulse in the frequency domain,

$$F(\omega) = 2\pi\delta(\omega - \omega_o)\,. \tag{2.2}$$

By taking the inverse Fourier transform of this equation, the equivalent time-domain signal is found to be

$$f(t) = 1 \cdot e^{j\omega_o t} = \cos\omega_o t + j\sin\omega_o t\,, \tag{2.3}$$

which is similar to Equation 2.1. From these equations it can also be seen that, unless a signal has identical components at both ω_o and $-\omega_o$ on the Fourier transform frequency axis, the signal has both a real and an imaginary part.

Next, consider the concept of frequency translation. A complex signal with frequency ω_o (either positive or negative) can be translated to $\omega_c + \omega_o$ by convolving it in the frequency domain with a frequency of ω_c. This is illustrated in Figure 2.2. Mathematically, this frequency translation can be described as follows:

$$\delta(\omega - \omega_o) * \delta(\omega - \omega_c) = \delta(\omega - \omega_o - \omega_c)\,, \tag{2.4}$$

where the 2π factors were omitted for simplicity. In the time domain, this translates to

$$e^{j\omega_o t} \cdot e^{j\omega_c t} = e^{j(\omega_o+\omega_c)t} . \tag{2.5}$$

The goal of quadrature modulation is to easily translate the baseband signal to the centre frequency of choice, ω_c. After upmixing, the (complex) output signal would be

$$\begin{aligned} s_c(t) &= e^{j\theta(t)} \cdot e^{j\omega_c t} \\ &= e^{j[\theta(t)+\omega_c t]} \\ &= \cos[\omega_c t + \theta(t)] + j \sin[\omega_c t + \theta(t)] . \end{aligned} \tag{2.6}$$

Of course, a complex-valued output signal cannot be generated and transmitted. In a practical application, only the real part of this signal will be taken:

$$\begin{aligned} s(t) &= \mathcal{R}e\{s_c(t)\} \\ &= \cos[\omega_c t + \theta(t)] . \end{aligned} \tag{2.7}$$

As a result, the output signal will once again be symmetrical around $\omega = 0$. The positive frequency axis will not, however, contain any alias signals. Consequently, no bandpass filter is required to remove alias signals created by upmixing. By combining Equations 2.6 and 2.7, the complete operation can be seen:

$$\begin{aligned} s(t) &= \mathcal{R}e\{[\cos\theta(t) + j\sin\theta(t)] \\ &\qquad \cdot[\cos\omega_c t + j\sin\omega_c t]\} \\ &= \mathcal{R}e\{[\cos\theta(t)\cos\omega_c t - \sin\theta(t)\sin\omega_c t] \\ &\qquad + j[\sin\theta(t)\cos\omega_c t + \cos\theta(t)\sin\omega_c t]\} \\ &= \cos\theta(t)\cos\omega_c t - \sin\theta(t)\sin\omega_c t . \end{aligned} \tag{2.8}$$

The result is surprisingly simple. Suppose that a complex signal, $e^{j\theta(t)}$, has to be translated in frequency by ω_c, and the real part of the result is all that is of interest. Equation 2.8 describes how to achieve such a frequency translation. The sine and cosine of the modulated phase, $\theta(t)$, must be calculated, and multiplied with the sine and cosine, respectively, of ω_c. When the two products are subtracted, the result will be the real part of the frequency translation. This can be used to generate a modulated signal directly from the baseband.

For an accessible introduction to complex signals and negative frequencies, the reader is referred to the tutorial by Smith [41]. The term *quadrature modulation* stems from the use of two identical baseband signals with a quadrature phase relationship to each other. Equation 2.8 is often written in the form

$$s(t) = I(t)\cos\omega_c t - Q(t)\sin\omega_c t . \tag{2.9}$$

$I(t)$ and $Q(t)$ are called the *in-phase* and *quadrature* components, respectively, of the complex baseband signal.

2.2.2 Generalisation

The analysis so far focused on the synthesis of a single sinusoidal component of a given frequency. This is easily extended to a signal modulating in amplitude, phase, frequency or a combination of these. Also, it can be shown that quadrature upmixing can be performed on baseband signals that represent more than one modulating sinusoid.

Multitone signals

The frequency translation performed to upmix the complex baseband signal to a broadcast frequency is linear. This can be seen by requiring an output signal consisting of the sum of sinusoids of independent amplitude and phase:

$$s(t) = \sum_{i=1}^{N} a_i \cos(\omega_i + \phi_i)\,. \tag{2.10}$$

It will later be shown that any of a_i, ω_i or ϕ_i may be time-varying, so that it is possible to synthesise modulating signals. The current proof will consist of showing that the digital synthesis of a sum of complex exponentials,

$$f(t) = \sum_{i=1}^{N} a_i e^{j[(\omega_i - \omega_c)t + \phi_i]}\,, \tag{2.11}$$

will result in the desired signal after quadrature mixing with the carrier frequency, ω_c. On page 11 it was shown that the process of quadrature mixing can be expressed as the real part of the multiplication of a complex baseband signal with a complex exponential at the carrier frequency. Applying this to Equation 2.11 yields

$$\begin{aligned} s'(t) &= \mathcal{R}e\left\{ e^{j\omega_c t} \cdot \sum_{i=1}^{N} a_i e^{j[(\omega_i - \omega_c)t + \phi_i]} \right\} \\ &= \sum_{i=1}^{N} a_i \, \mathcal{R}e\left\{ e^{j[(\omega_i - \omega_c + \omega_c)t + \phi_i]} \right\} \\ &= \sum_{i=1}^{N} a_i \cos(\omega_i + \phi_i)\,, \end{aligned} \tag{2.12}$$

which was to be proven. Consequently, quadrature-baseband DDS can be used to synthesise multitonal signals of independent amplitude, phase and frequency. This can be achieved by separating the complex exponentials that must be synthesised (Equation 2.11) into their real and imaginary parts, so that

$$I(t) = \sum_{i=1}^{N} a_i \cos\left[(\omega_i - \omega_c)t + \phi_i\right] \tag{2.13}$$

and

$$Q(t) = \sum_{i=1}^{N} a_i \sin\left[(\omega_i - \omega_c)t + \phi_i\right]\,, \tag{2.14}$$

which can consequently be synthesised and mixed according to Equation 2.9.

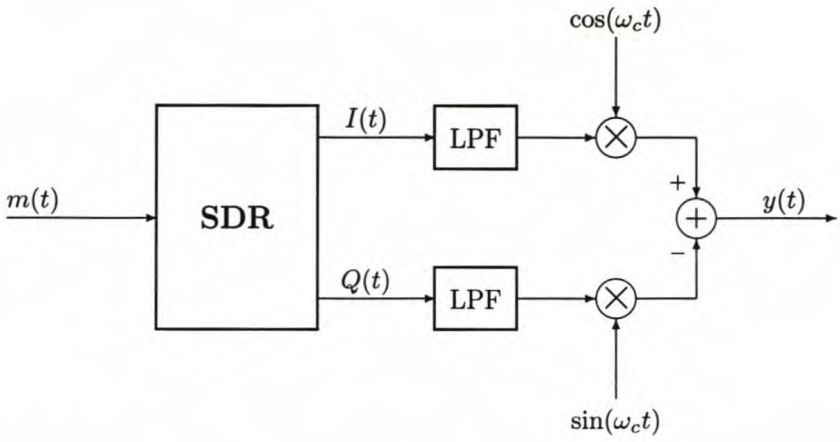

Figure 2.3: *Block diagram of a DDS-based quadrature modulator.*

Dynamic signals

The use of the term "quadrature modulation" implies an interest in synthesising a signal that is time-variant in some or other way. For this reason, it is important to show that the techniques presented in this chapter can be applied to such dynamic signals.

This is demonstrated by noting that Equations 2.11 through 2.12 hold equally well when a_i, ω_i and ϕ_i are variant in time. While it is true that an ambiguity develops between frequency and phase when one or both are time-variant,[1] this does not affect the accuracy of the frequency translation that takes place during quadrature mixing, whether the modulation is seen to take place in phase, frequency or both. Once again, the linearity of the operation ensures that quadrature mixing can be expressed in terms of familiar modulating expressions.

2.2.3 Quadrature modulator overview

A practical implementation of Equation 2.9 is shown in Figure 2.3. It shows the generation of two quadrature signals in the baseband using direct-digital synthesis. As this technique is well suited to software radio modulation techniques, it is referred to in this document as *quadrature modulation.* Alternative terms are *quadrature-baseband direct digital synthesis* [49] and *single-sideband direct digital synthesis* [10]. The main advantage of the quadrature baseband technique is that signal synthesis is performed at much lower frequencies than required by the conventional DDS technique. This has the following advantages:

- Only minimal low-pass filtering is required to remove the alias sampling components, reducing the system complexity.
- Since the demands on filtering are relaxed, only a single quadrature upmixing stage is

[1]The ambiguous relationship between frequency and phase, and the related concept of "instantaneous" frequency, are touched upon again in Chapter 5.

required.

- As will be seen in Chapter 4, digital-to-analogue converters perform better at lower frequencies and produce less signal distortion.
- The lower sampling frequency causes a smaller computational load on the signal processor and better modulation schemes can be implemented on less powerful digital technology.
- Overall, the system complexity is no longer a function of the *absolute* output frequency (the RF signal), but of the *signal bandwidth* – as suggested by Proposition B.

These advantages provide strong encouragement to seriously consider quadrature modulation as a viable alternative to the single-signal DDS technique. The greatest disadvantage of quadrature modulation is that two matched signals, instead of a single output, need to be produced. This requirement has the following repercussions:

- Two digital-to-analogue converters (DACs) are required. DACs are expensive components in a DDS system, and this requirement could substantially affect system costs.
- The amplitudes of $I(t)$ and $Q(t)$ have to be matched. The quadrature local oscillator signals must also be matched in amplitude. The effects of poorly matched amplitudes will be investigated in Section 5.5.
- There must be no DC offset on either the I or Q channels (this is often also a requirement with standard DDS). The effects of DC offset will be analysed in Section 5.6.
- Quadrature mixers usually suffer from local oscillator leakthrough. This means that an unwanted component appears at the carrier frequency in the upmixed signal. This phenomenon will also be investigated in Section 5.6.
- In practice it is not always simple to generate signals with exactly ninety degrees phase difference. Output filters could affect this phase accuracy, and quadrature mixers are never completely accurate. Section 5.7 will take a closer look at this problem.

An important objective of this dissertation is to carefully consider and analyse both the advantages and disadvantages of quadrature modulation and its counterpart, quadrature demodulation, in order to determine whether they form viable alternatives to the single-signal synthesis and analysis techniques. In particular, it will be shown that computationally simple methods can be used to compensate for the most significant disadvantages of quadrature systems.

2.2.4 An experimental prototype

Quadrature modulation using direct-digital synthesis was first proposed and tested in undergraduate research conducted by the author in 1998 [48]. A successful quadrature modulator

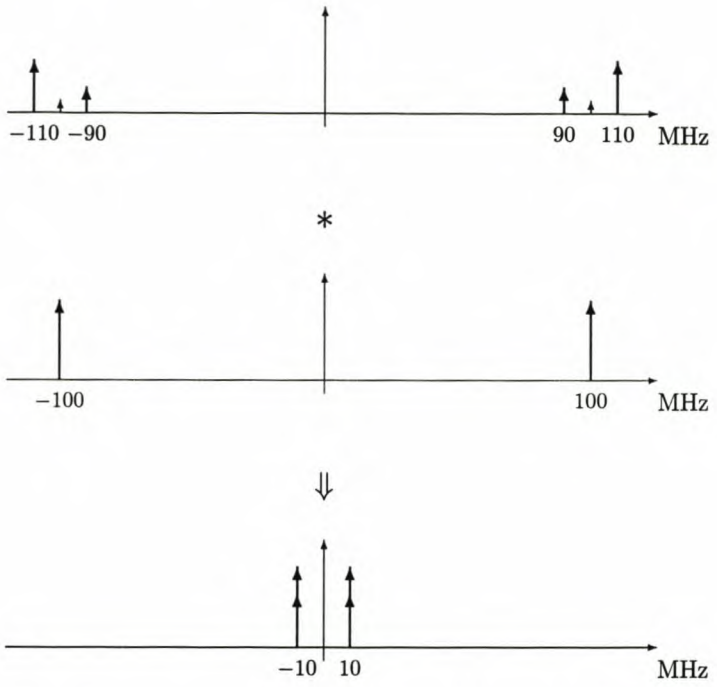

Figure 2.4: *There is an ambiguity inherent in single-signal downmixing (heterodyning): Both the desired signal at* 110 Mhz *and its poorly filtered reflection around the mixing frequency are superimposed in the baseband.*

implementing FM radio modulation[2] was built with a 66-MHz Motorola DSP56002, with an output sampling rate of only 380 kHz. Both amplitude and phase employed 16-bit resolution. Although not suited for more sophisticated testing, this prototype confirmed that it is possible to generate broadcast-quality FM radio using quadrature modulation, by transmitting audio in the commercial radio band.

This concludes the study of ideal quadrature modulation techniques in an SDR transmitter. The focus now shifts to replicating these techniques in an ideal receiver.

2.3 Quadrature demodulation

At the turn of the twenty-first century, many software-defined radio receivers simply make use of single-signal quantisation—sometimes at the transmission frequency, but mostly at an intermediate frequency (IF) [45, 26, 6, 16]. This poses much the same aliasing problems encountered in single-signal modulation—not only the desired signal is mixed down, but also its reflection around the mixing frequency, as shown in Figure 2.4. Careful filtering is required prior to mixing in order to combat its effects. As is the case for single-signal

[2]Commercial FM radio broadcasting requires a centre frequency in the range 88–108 MHz and frequency deviation of 75 kHz.

synthesis, several stages of mixing and filtering could be required in order to downmix a signal to a frequency where it can be converted and processed conveniently. This increases the overall system complexity and cost.

Once again, quadrature mixing provides an attractive alternative. Although the reception side is slightly different from the quadrature upmixing presented in Chapter 2, many of the principles are the same. In particular, it allows alias-free frequency translation of signals. Also, because the resulting downmixed signal is complex-valued, full knowledge of the original signal's magnitude and phase is retained. This information can be exploited to develop robust digital demodulation algorithms that outperform their analogue counterparts.

2.3.1 Complex downconversion

The alias-free upmixing technique of Section 2.2 encourages one to find a way to achieve similar results in complex downmixing for signal reception. The goal here is to find a way to translate a received RF signal to the baseband whilst avoiding the mixing ambiguities and aliasing associated with heterodyne mixing.

Firstly, note that it is only the positive-frequency components of the received signal that are of interest. Since a real signal is received, the negative-frequency components are complex conjugates of their positive-frequency counterparts, and therefore contribute no additional information to the demodulation process.

Suppose that the signal of interest is a single sinusoid at $\omega_c + \omega_o$ rad/s. (Of course, a true information-bearing signal will have to be time-variant in some or other way, and may consist of several such sinusoids. For simplicity, the following analysis will again initially postpone these concerns for the sake of clarity. The generalisation of the theory is presented in Section 2.3.2.) Consequently, the Fourier frequency-domain description of the signal is

$$F(\omega) = 2\pi\delta(\omega - \omega_c - \omega_o)\,. \tag{2.15}$$

It is now desired to translate this signal to baseband, so that it again lies at ω_o (the original modulating frequency). If the signal can be convolved in the frequency domain with an impulse at $-\omega_c$, the desired signal is found:

$$\delta(\omega - \omega_c - \omega_o) * \delta(\omega + \omega_c) = \delta(\omega - \omega_o)\,, \tag{2.16}$$

where the factor 2π is omitted for simplicity. Note that it is assumed in this signal translation that the exact carrier frequency and phase is known. Although this is true in some receivers (e.g. pilot-tone systems), it is most often not the case. Section 2.3.2 will show that this need not pose a problem, and that signal translation need not be impaired if only a rough estimate of the carrier frequency is used.

Since the received RF signal is real-valued, it also contains a negative-frequency component that will also be mixed down. This component lies at

$$F(\omega) = 2\pi\delta(\omega + \omega_c + \omega_o)\,. \tag{2.17}$$

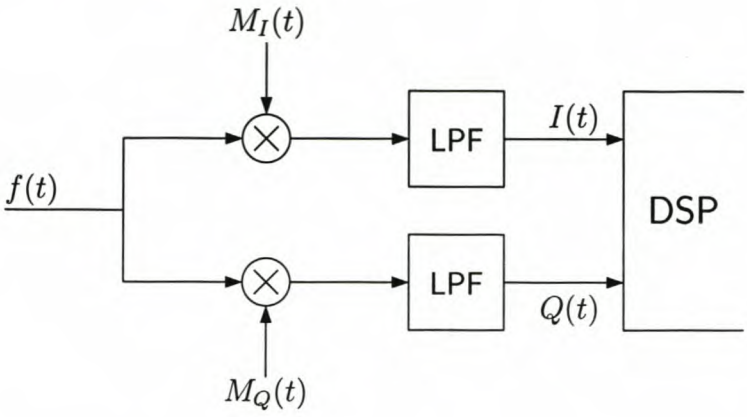

Figure 2.5: *Block diagram of a quadrature demodulator.*

After the downmixing of Equation 2.16, this component lies at $-2\omega_c - \omega_o$, which is much further from the baseband than the original RF signal was. It can easily be removed by low-pass filtering after mixing.

This means that it is possible to perform alias-free frequency translation on a real-valued signal—if this signal can be convolved with a frequency-domain impulse at the carrier frequency. As was shown on page 10, an impulse in the Fourier frequency domain corresponds to a complex exponential in the time domain, so that

$$M(t) = 1 \cdot e^{-j\omega_c t} = \cos\omega_c t - j \sin\omega_c t\,. \tag{2.18}$$

From this it follows that, if $f(t)$ is the received RF signal, and $s(t)$ the downmixed signal, then

$$\mathcal{R}e\{s(t)\} = 2\,[f(t) \cdot \cos\omega_c t]_{\text{LPF}} \tag{2.19}$$

and

$$\mathit{Im}\{s(t)\} = -2\,[f(t) \cdot \sin\omega_c t]_{\text{LPF}}\,, \tag{2.20}$$

where $[\cdot]_{\text{LPF}}$ denotes low-pass filtering. The arbitrary gain factor 2 is included simply for mathematical convenience. The real and imaginary components of $s(t)$ can now be converted to digital form, and further demodulation and processing can be done on the complex-valued signal. Equations 2.19 and 2.20 are implemented in the block diagram of Figure 2.5, and may be written in the compact form

$$s(t) = 2\left[f(t) \cdot e^{-j\omega_c t}\right]_{\text{LPF}}\,. \tag{2.21}$$

Note that complex-valued signals can distinguish between positive and negative frequencies. For example, if the received signal is a frequency-modulating signal, the downmixed $s(t)$ will be seen to vary its instantaneous frequency between negative and positive values, as the original RF signal varies around the carrier frequency.

2.3.2 Generalisation

In the development thus far it has been assumed that the input signal is a single sinusoid, and that the original carrier or centre frequency is known exactly. It will now be shown that the frequency-translating properties of quadrature mixing hold—even when these assumptions are not met.

Multitone signals

Equation 2.19 is linear, and may be applied individually to terms in the received signal $s(t)$. Let the input signal be expressed as the sum of sinusoids of independent amplitude and phase, i.e.

$$f(t) = \sum_{i=1}^{N} a_i \cos(\omega_i + \phi_i)\,. \tag{2.22}$$

In the next section it will be shown that any a_i, ω_i and ϕ_i may be time-varying (in other words, the compound signal may be dynamically changing). Applying the complex mixing steps of Section 2.3.1 to the compound signal now yields

$$\begin{aligned} f(t) \cdot M(t) &= e^{j\omega_c t} \sum_{i=1}^{N} a_i \cos(\omega_i + \phi_i) \\ &= \sum_{i=1}^{N} a_i e^{j\omega_c t} \cos(\omega_i + \phi_i)\,. \end{aligned} \tag{2.23}$$

Equation 2.23 shows that the complex mixing of a sum of sinusoids can be expressed as the sum of single-sinusoid mixing stages. As this was shown in Section 2.3.1 to result in frequency translation, the final complex-valued received signal (after low-pass filtering) can be derived as

$$s(t) = \sum_{i=1}^{N} a_i e^{j[(\omega_i - \omega_c)t + \phi_i]}\,, \tag{2.24}$$

which means that all frequency components have shifted to the baseband, with their respective amplitudes, phase offsets and relative frequencies unaffected. Clearly, any signal that can be expressed as the sum of various sinusoids (that is, any signal that has a Fourier transform) can be translated by quadrature mixing, because each frequency component is translated correctly. By the Dirichlet conditions, all energy signals (i.e. all physically realisable waveforms) have Fourier transforms, which makes the result developed here generally applicable to physical signals.

Dynamic signals

Almost all practical signals of interest are time-variant in some or other way—modulation may be defined as varying one or more signal parameters in time, usually based on an information source. It is therefore important that the quadrature frequency-translation process is valid for such dynamic signals.

If, in the exposition of Section 2.3.1, the RF input signal is taken to be

$$f(t) = a(t) \cdot \cos \phi(t) \,, \tag{2.25}$$

it can be regarded as a carrier component of which any or all of the signal parameters (amplitude, phase and frequency) may be time-variant. Following exactly the same derivation as was used for the static signal, the complex-valued downmixed signal is found as

$$s(t) = a(t) \cdot e^{j[\phi(t) - \omega_c t]} \,, \tag{2.26}$$

which is, once again, identical to the positive frequency component of the original signal, with a shift of ω_c in the instantaneous frequency at any moment in time. All the signal parameters, namely the amplitude, phase and instantaneous frequency (relative to the carrier frequency) have been retained. Consequently, quadrature downmixing may be used for time-variant signals.

Poor carrier frequency estimate

Thus far it was assumed that a received signal was modulated onto a specific carrier or centre frequency, and that this signal's frequency and phase are exactly known on the receiver side. This is not generally the case, and the effect of a poorly matched receiver carrier frequency must be investigated.

Consider a received signal component with the following instantaneous amplitude, frequency and phase:

$$f(t) = Ae^{j[(\omega_c + \omega_o)t + \phi]} \,, \tag{2.27}$$

where ω_o represents a (possibly negative) frequency deviation from the centre frequency, ω_c. Of course, these parameters may be time-variant, and several such frequency components may exist in the received signal. As has already been established, this does not affect the quadrature frequency translation.

Ideally, the received signal would have been translated to a complex representation exactly at the baseband, i.e.

$$s(t) = Ae^{j(\omega_o t + \phi)} \,, \tag{2.28}$$

giving a signal from which, in particular, the exact frequency deviation, ω_o, can be estimated. Suppose, however, that the carrier frequency, ω_c, is not exactly known on the receiver side, and is roughly estimated as $\hat{\omega}_c$. Now the the received signal is

$$s'(t) = Ae^{j[(\omega_o + \omega_c - \hat{\omega}_c)t + \phi]} \,. \tag{2.29}$$

This means that the instantaneous frequency of the received signal is overestimated by $\omega_c - \hat{\omega}_c$. The signal amplitude and phase are not affected. The following conclusions are drawn:

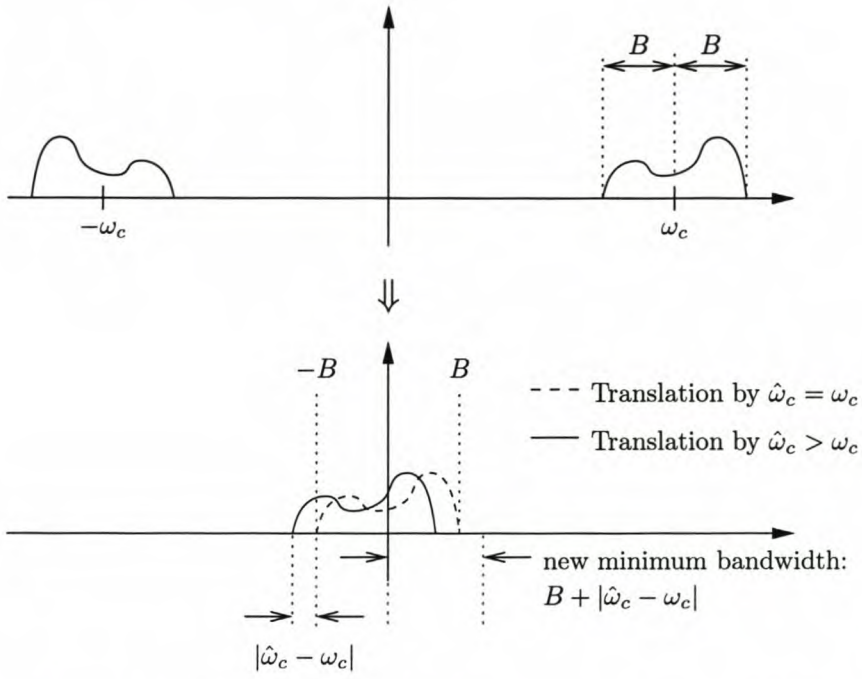

Figure 2.6: *An incorrect estimate of the carrier frequency during quadrature downmixing causes the required minimum baseband bandwidth to increase by* $|\omega_c - \hat{\omega}_c|$.

- Modulation systems that do not embed information in the signal frequency (such as amplitude or phase modulated systems) are not affected by poor frequency estimate. The baseband bandwidth is increased somewhat (as will be demonstrated shortly), but this is a relatively benign side effect.

- Many frequency-based modulation systems are not affected either. An example is audio frequency modulation (as is used in commercial radio broadcasting), where a slight frequency offset merely adds DC offset to the demodulated signal. This is easily remedied by a DC block filter, or can even be ignored in some applications.

- Even in systems where the exact instantaneous signal frequency is important (such as in FSK transmission), it should be emphasised that *no information is lost in the frequency translation process.* If uncertainty regarding the correct downmixed frequency exists, it is because the carrier frequency was uncertain in the first place. It is usually much better to address this problem in the baseband digital domain than in the RF analogue domain. Digital signal processing can be used to estimate the carrier frequency error, and correction can be done in software. One straightforward way to achieve this is by adding an additional software-based quadrature mixing stage, where the digitised baseband signal is translated with a correction frequency.

An incorrect estimate of the carrier frequency causes an increase in the bandwidth requirements of the baseband system. This is illustrated in Figure 2.6. Because the frequency translation error has a magnitude of $|\omega_c - \hat{\omega}_c|$, the maximum absolute frequency in the

baseband signal increases by the same amount. This could mean that digital-to-analogue converters might have to function at somewhat higher sampling frequencies due to the frequency error, although these sampling frequencies are still much lower than would have been the case had direct sampling at the RF frequency (or even an IF frequency) been attempted.

2.4 Narrowband applications

Quadrature mixing greatly facilitates the use of extreme narrowband signals (where the ratio between the centre frequency and bandwidth is very high). Alternative signal translation techniques usually require sharp bandpass filtering of the RF signal, so that all out-of-band components are sufficiently removed. Theoretically, quadrature mixing requires no such filtering: The entire frequency spectrum is shifted up or down depending on the local oscillator frequency—out-of-band components are removed in the baseband by using simple low-pass filters. Practically, some form of bandpass filtering is usually required in receivers to limit the input power to the quadrature mixer.

This frequency translation effectively means that, when using quadrature mixing, a signal's bandwidth can be considered completely independent of its centre frequency. This greatly reduces filter complexity, since a bandpass filter's required order depends on both its centre frequency and its bandwidth; a low-pass filter has no such restriction [44]. Even at high centre frequencies, signals with comparatively narrow bandwidths can be addressed in close proximity, in ways not viable with other technologies. Quadrature mixing therefore improves the efficient use of the spectrum without increasing system complexity. This conclusion is directly related to Proposition B, that states that bandwidth and frequency translated should be considered separately. The generation of such a narrowband signal will be demonstrated using the prototype of Chapter 7.

2.5 Concluding remarks

In this chapter, it was shown that quadrature mixing in a software radio's RF front-end allows a clear separation between signal processing and signal translation (Proposition B). When quadrature modulation or demodulation is used, a complex-valued baseband signal is used in the baseband, and the signal processing rate depends on the bandwidth of this signal. The complex-valued baseband representation is a general representation compatible with traditional analogue modulation schemes.

The quadrature mixing stage in the RF front-end is conceptually simple, and represents signal translation without any additional signal processing. It is possible to perform single-stage mixing from the baseband to the broadcast frequency, and *vice versa*.

The treatment of the subject in this chapter has assumed ideal quadrature mixing, but under this assumption, the technique presented holds significant merit, by Proposition B. Furthermore, it will be shown in Chapter 6 that non-idealities in physical systems may

be removed (as per Proposition A), thus retaining the advantages of the idealised system introduced in this chapter.

Chapter 3

Software-defined radio

Perhaps the most direct and relevant applications of the signal translation and compensation techniques presented in this research, lie in the field of software-defined radio (SDR). This is certainly not to say that this is the only (or even the most important) application of the research, or that this is a dissertation "on the topic of" SDR. Rather, SDR presents a relevant context in which the applicability of the research may be evaluated.

For this reason, physical-layer software radio theory is briefly covered in this chapter, and much of the research documented in later chapters will consider the SDR-related implications of their results. In particular, the types of noise and distortion associated with SDR are investigated. The purpose is to identify analogue inaccuracies that may be modelled as invertible transforms, in order to show the use of software compensation in SDR-related systems. This also lays the basis for the prototype SDR developed in Chapter 7.

3.1 Introduction to SDR

Software-defined radio (SDR), software radio (SR) and their collective technology (sometimes called "software-based radio", or SBR) are very broad fields that cover all aspects of communications system design. These include, among others, the physical layer, software design, network implementation, service provider functionality and user application design. Only the physical-layer aspects of software-defined radio are directly relevant to the quadrature-baseband compensation principles that will be developed in the later chapters of this document. Therefore, this chapter will focus on the signal synthesis and digitisation aspects of SDR only.

Software-defined radio (SDR) may be defined as follows: [4]

> An *SDR* is defined as a radio in which the receive digitization is performed at some stage downstream from the antenna, typically after wideband filtering, low noise amplification, and down conversion to a lower frequency in subsequent stages—with a reverse process ocurring for the transmit digitization. Digital signal processing in flexible and reconfigurable functional blocks defines the characteristics of the radio.

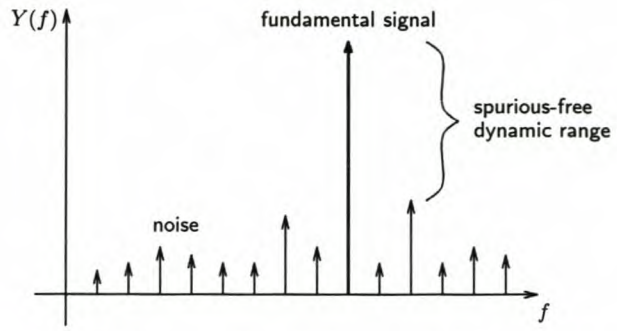

Figure 3.1: *The spurious-free dynamic range (SFDR) of a signal is the ratio between the fundamental signal power and that of the highest unwanted (spurious) component.*

SDR is usually considered a compromise to the stricter definition of "true" software radio, where the greatest possible part of the signal path lies in the digital domain: [4]

> As technology progresses, an SDR can move to an almost total *SR*, where the digitization is at (or very near to) the antenna and all of the processing required for the radio is performed by software residing in high-speed digital signal processing elements.

This text will generally use the term "software-defined radio"—firstly, because this is the most general practical implementation of the technology in use today, and therefore also the most familiar term in use. More significantly, however, the use of the term supports the principle proposed by the dissertation that digitisation directly at the antenna does not necessarily represent an optimal design solution, and that arbitrary-accuracy signal conversion techniques can be used to rather perform signal processing in the baseband. In fact, Proposition B (p. 5) emphasises that the complex baseband signal is a more parsimonious representation of the modulated signal information, and should therefore often be the configuration of choice.

3.2 Spurious-free dynamic range

When analysing synthesised signals, ways are needed to describe the quality of a generated waveform. In traditional communications theory, the signal-to-noise ratio (SNR) is an important measure of transmission clarity. SNR, however, is more suited to describe systems dominated by white-noise characteristics. In digital signal synthesis and analysis, it is possible for a processed signal to have a fairly low average SNR, but with some harmonically related "spurs" several decibels above the average noise level. Kester [19] writes:

> The assumption that the quantisation noise appears as white noise and is spread uniformly over the Nyquist bandwidth is simply not true in a DDS system.

Because these spurs have a serious effect on signal quality, a better measure of software-defined radio performance is given by the size of the highest spur compared to the desired signal (see Figure 3.1). This is called the spurious-free dynamic range (SFDR), and is a popular measure of DDS, quadrature mixing and SDR performance [1, 10, 15]. It is possible to refine the SFDR model by taking into account the receiver's third-order intercept point [3, p. 40].

3.3 Deterministic distortion effects

The use of compensation techniques to counter the effects of invertible inaccuracies (Proposition A) lies central to this dissertation. Deterministic distortion effects are unwanted signal components that are caused by inaccuracies in signal conversion, filtering and mixing. These effects will always cause the same distortion signal in a given output signal, and generally maintain any periodicity in the transmitted and received signals. Hence, distortion tends to give rise to undesired harmonic components, a topic that will be explored further later in this chapter. Such deterministic distortion effects stand in contrast to undesired stochastic signals, such as thermal noise or quantisation effects,[1] which cannot be predicted.

The deterministic distortion effects considered in this research are converter non-linearities and quadrature inaccuracies. This focus stems from the identification of the quadrature mixer and the ADC/DAC stages as the main components of the proposed RF front-end. In general, other deterministic inaccuracies may also be identified: amplifier non-linearities, or undesired filter roll-off and phase shift. The principles developed for converter non-linearities and quadrature inaccuracies are intended to be general enough for extrapolation to other forms of distortion.

Since deterministic distortion effects are predictable, one is led to believe that ways can be found to compensate for the distortion. This possibility will be fully explored in Chapter 6.

3.3.1 Signal conversion

Probably the most significant noise sources in a software-defined radio are the signal conversion stages, where digital-to-analogue and analogue-to-digital conversion takes place. Apart from the inevitable (and irreversible) quantisation effects, converters suffer from non-linear transfer functions, gain and offset errors, and transition glitches, to name just a few. Chapter 4 will provide a detailed study of these effects, and show that these effects are reversible by digital compensation, because they are deterministic and measurable, and can therefore be modelled and inverted in software.

---

[1] Quantisation error is considered to be random if the signal to which it is applied is not known (i.e. if it can also be modelled as a random process).

3.3.2 Quadrature mixing non-idealities

It was already mentioned in Section 2.2.3 that the following effects cause distortion in a quadrature modulated or demodulated signal:

- Amplitude mismatch between the I and Q signals or between the quadrature local oscillator signals.
- Non-zero offset on the I and Q signals.
- A phase difference other than 90° between the I and Q signals, or between the mixer's sine and cosine signals.
- Local oscillator leakthrough in the quadrature mixer.

If these errors are time-invariant, they should always cause the same distortion effects in the mixer's output signal. Chapter 5 will examine each of these non-idealties in detail, and investigate its effects on the transmitted and demodulated signals. In Chapter 6, techniques will be developed to compensate for these distortion effects.

3.4 Digital compensation

One of the main contributions of this research is the development of compensation principles that increase the accuracy of analogue-digital signal processing to within measurement and numeric representation accuracy. The principle is to develop models for hardware inaccuracies, in order to develop digital compensation techniques to compensate for these non-idealities. Proposition A (p. 4) qualifies this compensation as follows:

> ...under the condition that all these analogue inaccuracies are cascades of invertible transforms, and that their net effect is fully known.

In this section, the above qualification will be developed further. This general development provides motivation for deriving precise distortion models, for which specific compensation techniques may later be found.

Consider the diagram in Figure 3.2, representing a cascade of distortion transforms. For example, $\mathcal{A}\{x\}$ might represent quadrature mixing distortion, and $\mathcal{B}\{x\}$ the amplitude distortion ("integral nonlinearity") of an ADC. If one assumes invertibility,

$$\mathcal{A}\{\mathcal{A}^{-1}\{x\}\} = x \qquad \text{and} \qquad \mathcal{B}\{\mathcal{B}^{-1}\{x\}\} = x\,. \tag{3.1}$$

The distorted signal is given by

$$f'(t) = \mathcal{B}\{\mathcal{A}\{f(t)\}\}\,. \tag{3.2}$$

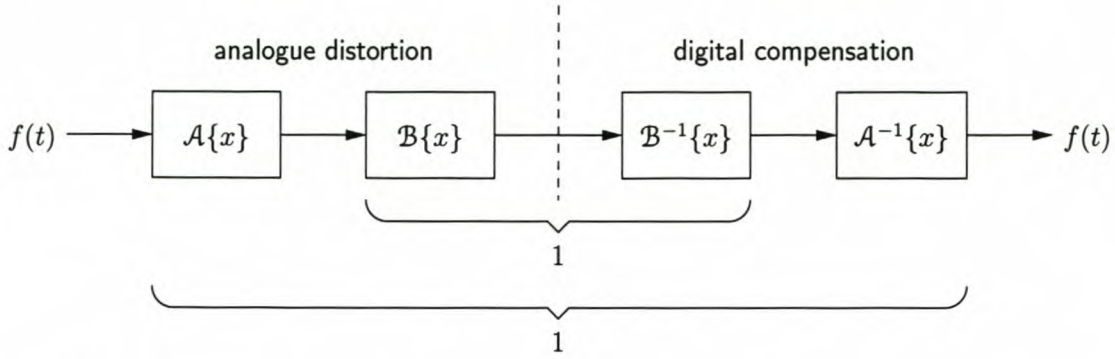

Figure 3.2: *To compensate for distortion modelled as invertible transforms, compensation transforms must be applied in reverse order on the signal flow.*

To reconstruct the original signal, the inverse transforms must be applied in reverse order:

$$\begin{aligned}\mathcal{A}^{-1}\{\mathcal{B}^{-1}\{f'(t)\}\} &= \mathcal{A}^{-1}\left\{\mathcal{B}^{-1}\left\{\mathcal{B}\left\{\mathcal{A}\left\{f(t)\right\}\right\}\right\}\right\} \\ &= \mathcal{A}^{-1}\{\mathcal{A}\{f(t)\}\} \\ &= f(t)\,. \end{aligned} \tag{3.3}$$

For example, $\mathcal{B}^{-1}\{x\}$ could be an inverse ADC amplitude distortion mapping, and $\mathcal{A}^{-1}\{x\}$ may represent quadrature compensation. In general, this compensation must be performed in reverse order, because it cannot be assumed that the inverse transforms are commutative:

$$\mathcal{A}^{-1}\{\mathcal{B}^{-1}\{x\}\} \neq \mathcal{B}^{-1}\{\mathcal{A}^{-1}\{x\}\} \tag{3.4}$$

A notable exception is when $\mathcal{A}$ and $\mathcal{B}$ (and their inverses) are linear transforms, such as s-domain transfer functions. Cascades of such types of distortion can be shown to be commutative, because

$$\mathcal{A}\{\mathcal{B}\{F(s)\}\} = A(s) \cdot B(s) \cdot F(s) = B(s) \cdot F(s) \cdot A(s) \tag{3.5}$$

In summary, any distortion that can be modelled as an invertible mathematical transform may be reversed by digital compensation using its inverse. When several such distortion transforms occur in cascade, the inverse transforms must be cascaded in reverse order. In general, this order is a necessary condition for compensation. However, when several linear transforms (such as s-domain transfer functions) occur in cascade, their mutual order is interchangable.[2]

In the next chapter, inaccuracies in the signal converter stages (DAC and ADC) will be investigated, and it will be established to what extent these effects are invertible. It will

[2]The inversion of s-domain transfer functions finds application in the field of channel and filter equalisation [56, 43, 33]. Inversion generally involves finding the reciprocal of that part of the distortion transfer function with poles and zeros inside the frequency band of interest. The compensation transfer function need not address poles and zeros outside the frequency band of interest, and may introduce its own poles outside this band in order to meet convergence and stability constraints.

then be shown how distortion can be inverted in the digital domain, in order to compensate for these inaccuracies.

Chapters 5 and 6 will follow a similar approach for the quadrature mixing stages, by investigating quadrature inaccuracies and their invertibility. Following that, specific compensation techniques will be developed, and it will be shown that it is possible to suppress spurious frequency-domain effects to within the constraints of Proposition A.

When multiple hardware inaccuracies are combined, the principle introduced in this section will apply: Calibration and compensation must be performed in an "inside-out" fashion. This principle illustrates the central proposition of this dissertation, namely that it possible to digitally compensate for cascades of invertible transforms. Chapter 6 will give a practical application of this idea in the development of an automatic SDR calibration system.

Chapter 4

Inaccuracies in signal conversion

One of the main premises of this dissertation (and, indeed, of software radio), is that it is advantageous to process analogue waveforms digitally—that greater control over the shape, contents and interpretation of a waveform is possible when it is represented in the digital domain. The assumption here is that a digital signal can, in fact, be accurately synthesised into its analogue counterpart; also, that the digital representation of a signal is, in fact, an accurate description of the analogue signal being analysed.

The failure of this assumption is possibly the most serious limitation of software-defined radio. Inevitably, the signal is distorted when it crosses the boundary between the analogue and digital domains. Often, it turns out that this distortion is difficult to predict. A serious study of software-based signal synthesis and analysis must consider the signal conversion stage very carefully, because it is necessary to thoroughly understand the limitations imposed by signal converters.

For this reason, this chapter will present a short study of digital-to-analogue converter (DAC) and analogue-to-digital converter (ADC) inaccuracies. In particular, the effects of such distortion on typical SDR signals are investigated. Also, one of the purposes of this chapter is to establish the extent to which a one-to-one mapping between the analogue and digital domains can still be achieved. Because of the generally deterministic nature of converter distortion, the possibility of digital compensation must be considered—a topic that will be touched upon in Section 6.3 of this chapter, in support of Proposition A.

The chapter will therefore focus on the fundamental converter inaccuracies (usually directly attributable to architectural tolerances) with digital compensation in mind. Aggregate parameters, such as the total unadjusted error and the signal-to-noise and distortion ratio, are generally intended as synoptical measures of performance, rather than parametric descriptions of a circuit's behaviour. Hence, such parameters are less valuable in constructing invertible component models, and are of secondary importance in this discussion.

The limited functionality of converters, particularly at higher sampling rates, indirectly emphasises the need for Proposition B (separation between signal translation and signal processing). Converters process signal information by transforming it from one representation to another. Converter complexity should therefore also be a function of signal information

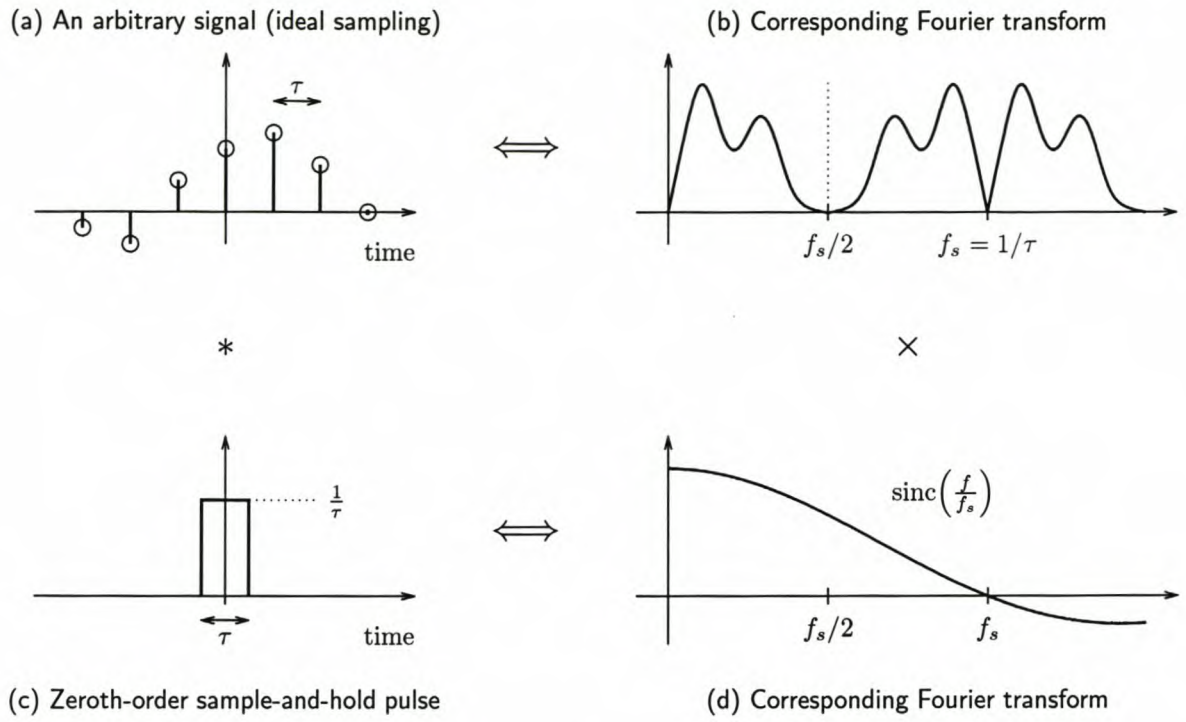

Figure 4.1: *A sample-and-hold response is effectively a rectangular pulse convolved with an ideal sampler. This causes the gain response shown in (d), which is multiplied by the ideal sampler's output spectrum in (b).*

rate (bandwidth), rather than be influenced by the absolute broadcast frequency.

4.1 Sample-and-hold distortion

The gain response of a zeroth-order hold function ("sample-and-hold") is present even in an ideal digital-to-analogue converter. Figure 4.1 illustrates this effect. If an ideal sampler were used to output an arbitrary signal, the sampled signal would be a train of scaled impulses, as is shown in Figure 4.1(a). The corresponding output spectrum is simply that of the sampled signal, reflected around the Nyquist frequency—see Figure 4.1(b).

In a zeroth-order sample-and-hold circuit, like that used in virtually all DACs, this ideal pulse train is convolved with a normalised rectangular pulse, similar to the one illustrated in Figure 4.1(c). The pulse has its own Fourier transform, namely the sinc function[1] shown in Figure 4.1(d). Since convolution in the time domain corresponds to multiplication in the Fourier (frequency) domain, the Fourier transform of the rectangular pulse acts like a filter on the signal spectrum—a low-pass filter with notches at the sampling frequency and its multiples.

Sample-and-hold distortion is typically not a serious problem in SDR transmitter design,

[1] $\text{sinc}(x) \equiv \frac{\sin \pi x}{\pi x}$

but it is an effect that must be kept in mind, especially when output filters are designed. At the half Nyquist frequency, the output signal is attenuated by about 3.92 dB. This is usually corrected with careful analogue low-pass filter design [19]. Alternatively, it is also possible to implement a predistortion filter in the digital domain. Sufficient oversampling minimises this distortion effect, and could simplify filter design. To prevent undesired amplitude-modulation effects in the synthesiser output, the amplitude response of the output channel must be flat for all possible output frequencies. When oversampling is employed, the filter need only compensate for sample-and-hold distortion within the designated signal band.

Sample-and-hold distortion is mostly associated only with signal synthesis, and generally does not affect signal reception. A possible exception is when upsampling is performed by the repetition of low-rate received samples, and a similar sample-and-hold effect is observed.

4.2 Linearity errors

An ideal digital converter should have a perfect linear response between exact minimum and maximum values. In an ADC, well-defined mimimum and maximum input voltages (or currents) should produce mimimum and maximum output codes. Similarly, the minimum and maximum input codes to a DAC should produce exact corresponding voltage (or current) levels on the DAC output.

Two different types of error compromise this ideal response. In this section, *linearity errors* are considered that involve the deviation of the minima and maxima, without influencing the converter's linearity between these points. These errors are generally simple to detect and correct. Errors that cause a DAC or ADC to deviate from the ideal straight-line response are called *non-linearity errors*, and are considered in the next section.

4.2.1 Offset error

Offset error measures how much the DAC output is shifted from the correct value when all input bits are '0'. For an ADC, it indicates the magnitude of the input required to set all output bits to '0'. Offset error can usually be minimised by adding an external trimming resistor, or by adjusting the digital offset of an SDR system.

4.2.2 Gain error

A DAC's gain error (or "gain drift") is the measure of the output signal's accuracy when all input bits are '1'. For an ADC, the gain error is measured by finding the input voltage (or current) required to set all output bits to '1', and determining how much it deviates from the desired reference input level. This gives an indication of how much the converter's gain deviates from the ideal, and is usually expressed as a percentage of the reference voltage (or current). It is usually simple to compensate for gain error by using an external trimming resistor, or by adjusting the digital gain of an SDR system.

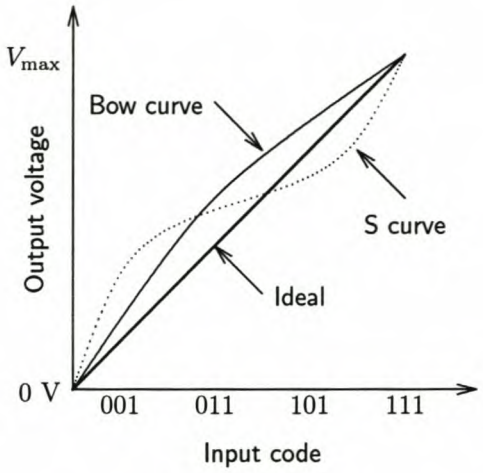

Figure 4.2: *Typical DAC integral non-linearity (INL) curves.*

There is an interplay between the definitions of the two linearity errors, and a converter's data sheet should indicate whether the specified gain error was measured before or after offset error calibration had been performed.

4.3 Non-linearity errors

The previous section looked at inaccuracies that affected the straight-line parameters of a converter's response. In this section, inaccuracies that cause a deviation from the straight-line response will be investigated.

4.3.1 Differential non-linearity

Ideally, a DAC's output should change exactly 1 LSB for a corresponding increase in the input code. Similarly, a 1-LSB increase to an ADC's input should produce a single increment in the output code. In practical converters, this does not always happen—imbalances in internal resistances produce inaccuracies. For a DAC, its differential non-linearity (DNL) reflects the maximum amount that a single-step change in output will deviate from the ideal.

4.3.2 Integral non-linearity

When a DAC's input code systematically sweeps from the lowest to the highest value at a fixed sampling rate, an ideal output would closely follow a straight line. Similarly, an ADC should produce a digitally sampled straight line when driven by a ramp function. In practical converters, small errors in successive quantisation steps tend to accumulate until the actual transfer function can stray significantly from the straight line (especially at midrange values). This summation of non-linearity errors is called *integral nonlinearity* or INL.

The shape of a DAC's integral non-linearity curve can have a significant influence on the quality of a synthesised signal. Crook and Cushing [9] show that INL curve shapes can be directly related to harmonic spurs in the output signal. Common curve shapes are shown in Figure 4.2. It can be shown that bow-shaped error patterns produce even-order harmonics, and S-shaped curves produce odd-order harmonics [9].

It should be noted that the harmonics produced by DAC inaccuracies are always harmonics of the output signal frequency, independent of the sampling rate. This is because these DAC errors are directly code-dependent, and therefore only dependent on the input signal. Consequently, the distortion signal shares the fundamental signal's periodicity, and harmonics of the fundamental output signal are generated [19].

An approximation to the size of the harmonic spur is [9]

$$H \approx 20 \log \left(\frac{V_{\text{err}}}{V_{\text{max}}} \right) \text{ dB}, \tag{4.1}$$

where V_{err} is the maximum INL deviation from the ideal straight-line transfer function. It will be shown in Section 6.3 that the generation of these harmonics can be exploited to compensate for converter non-linearities.

Although the work by Crook and Cushing [9] on the harmonics produced by integral non-linearity relates specifically to digital-to-analogue conversion, it applies just as well to ADCs. This is seen by observing that, in both cases, INL can be modelled as an undesired non-linear, continuous-valued transfer function in the conversion signal path. Whether this non-linear transfer function occurs during digital-to-analogue or analogue-to-digital conversion is immaterial—its effect on the signal is to produce spurious harmonics, as described above. It can be concluded that Crook and Cushing's results can be extended to signal reception.

4.3.3 Monotonicity

When a converter has a differential non-linearity error of greater than 1 LSB, it is possible that a rise in the converter input produces a *decrease* in its output (or vice versa). This phenomenon is called non-monotonicity, and produces high-frequency error components in the converted signal. Furthermore, the converter's transfer function becomes a quantised non-invertible function (a one-to-many mapping), which makes it difficult, and often impossible, to digitally compensate for monotonicity—a topic that will be pursued further in Section 6.3.

4.4 Other parameters

Converter data sheets often specify a large number of other parameters to help designers evaluate the typical performance of a device. Examples are the *total unadjusted error*, *absolute accuracy*, *signal-to-noise and distortion ratio*, *effective number of bits* and *total harmonic distortion*. These parameters are mostly cumulative descriptions of the non-idealities described in the previous sections, and present a higher-level representation of the converter

inaccuracies. Since the purpose of this chapter is to identify the atomic distortion effects in converters, the cumulative distortion parameters are of secondary concern. The interested reader is referred to the numerous available texts on the subject [5, 9, 15, 19, 36, 39].

It is, however, possible to identify additional primary, independent distortion effects to refine converter models. Such effects may include *aperture jitter*, *slew rate* and *aperture error* [5]. Although the compensation techniques of Section 6.3 will focus on the non-idealities introduced in the previous sections, the compensation principles may also be extended to these additional parameters and distortion models.

4.5 Measuring converter distortion

It was stated on page 33 that the presence of nonlinear DAC and ADC effects, such as INL, give rise to harmonics when a sinusoidal signal is converted. If the phase and magnitude of such harmonics can be measured, it may be possible to estimate the INL itself. This topic will be explored in more depth in Section 6.3, when the compensation of harmonics in quadrature signals is discussed.

Chapter 5

Inaccuracies in quadrature mixing

5.1 Overview

Chapter 2 introduced quadrature modulation and demodulation systems that cleanly separate signal translation and processing. This arrangement is strongly advocated by the research presented here, since it reduces signal conversion and processing complexity and allows single-stage frequency translation.

However, the idealised quadrature systems presented in the previous chapters imply several strong assumptions about the mixing stage. During quadrature modulation, the I and Q outputs from the DDS system were assumed to be perfectly matched in amplitude and without DC offset; all quadrature signals were assumed to be exactly 90° out of phase, and no leakthrough of the local oscillator into the output signal was taken into account. Likewise, the study of quadrature demodulation thus far assumed that the parallel signal paths have perfectly matched amplitudes, were mixed with perfect sines and cosines, and that no parasitic coupling occurs in any part of the mixing process. Of course, these assumptions usually fail to be met in real-life systems. This chapter will provide an original investigation on the effect of such inaccuracies on the spectral purity of the output signal, and lay

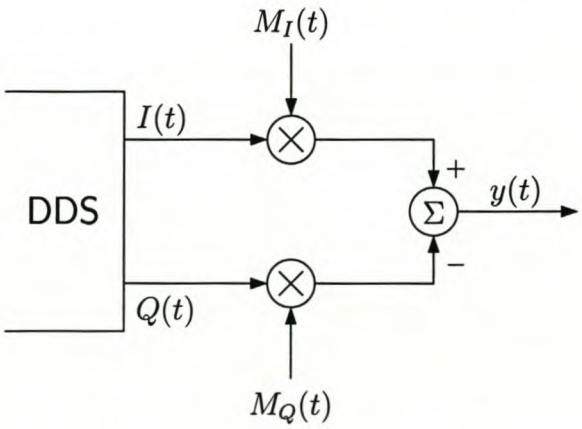

Figure 5.1: *Block diagram of a DDS-based quadrature modulator ("upmixing").*

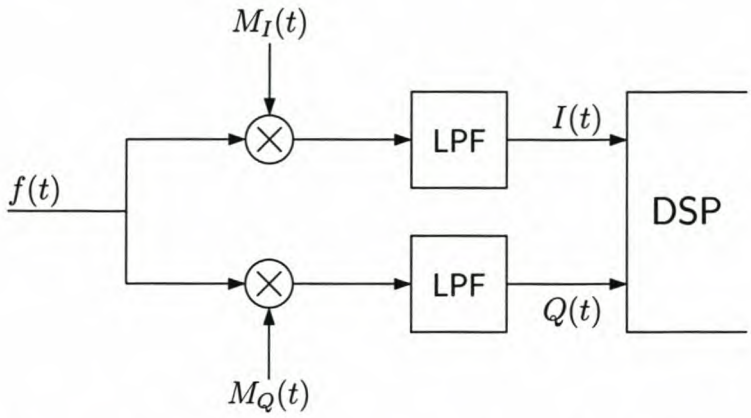

Figure 5.2: *Block diagram of a quadrature demodulator ("downmixing").*

the groundwork for the next chapter, which introduces novel techniques to compensate for such inaccuracies. The viability of such compensation is, in fact, the central thesis of this dissertation.

The transmitter side of the system under investigation is shown in Figure 5.1. The digital system performs digital-to-analogue conversion to produce two quadrature signals in the baseband, $I(t)$ and $Q(t)$. Ideally, these signals are perfect sinusoids that are identical in amplitude and instantaneous frequency,[1] and the Q-channel lags the I-channel with a phase difference of exactly 90°, or $\pi/2$ radians.

These signals are passed to a quadrature mixer, to be translated to the carrier frequency. The quadrature mixer multiplies $I(t)$ and $Q(t)$ with $M_I(t)$ and $M_Q(t)$ respectively. Both $M_I(t)$ and $M_Q(t)$ are sinusoidal signals at the carrier frequency, but the latter has an ideal phase lag of exactly $\pi/2$ radians. The Q-product is then subtracted from the I-product to produce the final modulated output, $s(t)$ (referred to here as the RF signal). In an ideal mixer, no spurious carrier-frequency component appears on the output—this phenomenon in physical mixers is called local oscillator leakthrough (or leakage), and is usually the result of parasitic coupling between the input and output ports.

The receiver side is very similar, as can be seen in Figure 5.2. A modulated input signal (also called the RF signal) is received and split into two identical input paths. The paths are mixed with the sine and cosine, respectively, of the carrier frequency.[2] Once again, the ideal demodulator assumes that these signals are in perfect quadrature relationship

[1]For an in-depth analysis of the concept of instantaneous frequency and its limitations, the reader is referred to Cohen (1995) [8].

[2]Or at least an estimate thereof. None of the quadrature demodulation techniques discussed in Chapter B require a local oscillator that is coherent in either phase or frequency. Instead, the estimate of the carrier frequency serves only to translate the signal to a complex baseband representation, in order to minimise the sampling rate. In most applications, the sampling frequency will be chosen well above the Nyquist limit, and a slight error in the carrier frequency estimation can easily be tolerated.

(equal amplitude and $\pi/2$ rad phase difference). After low-pass filtering, only the baseband components $I(t)$ and $Q(t)$ remain. These signals can be regarded as the real and imaginary components of a complex baseband signal, and can be sampled and demodulated by digital signal processing techniques.

In both the modulation and demodulation systems, low-pass filtering is performed as part of the conversion to and from the digital domain. In the idealised systems of Figures 5.1 and 5.2, these filters are assumed to have no effect on the I and Q signals' amplitude or phase; in other words, they are assumed to have unity amplitude response and equal, uniform group delay in the low-pass band in which the desired signal resides.

In order to clearly distinguish between the various components of a software-defined radio, the following terminology is defined:

- Baseband *modulation* refers to the (digital) generation of I and Q signals which contain modulated information.
- *Quadrature upmixing* refers only to the (analogue) signal multiplication stage during modulation, where $I(t)$ is mixed with $M_I(t)$ and $Q(t)$ is mixed with $M_Q(t)$, and then subtracted from each other to produce the RF signal.
- Collectively, the combined stages of baseband modulation and quadrature upmixing will be referred to as *quadrature modulation*, representing the entire conversion from modulating to modulated signal.
- Baseband *demodulation* refers to the digital signal processing method by which a modulated signal is recovered from I and Q signals.
- *Quadrature downmixing* refers only to the (analogue) signal multiplication stage during demodulation, where a received RF signal is split into two paths, and the resulting signals are multiplied with $M_I(t)$ and $M_Q(t)$, respectively. This produces baseband signals $I(t)$ and $Q(t)$.
- Collectively, the combined stages of quadrature downmixing and baseband demodulation will be referred to as *quadrature demodulation*, representing the entire conversion from modulated to demodulated signal.

5.2 Phasor notation

Prior to the main development of the chapter, a useful tool in the evaluation of quadrature errors will be introduced, namely the phasor locus.

$I(t)$ and $Q(t)$ contain the modulated signal's amplitude, phase and frequency information, relative to the in-phase carrier signal $M_I(t)$. As can be seen from Sections 2.2 and 2.3, the baseband signals always share the same amplitude and instantaneous frequency, and are

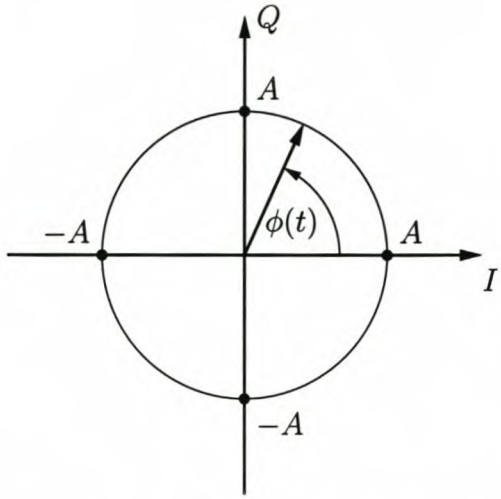

Figure 5.3: *Phasor representation of an ideal quadrature signal.*

always $\pi/2$ radians out of phase. Consequently, the I and Q signals can be written in the general form

$$\begin{aligned} I(t) &= \mathcal{R}e\left\{a(t)\, e^{j\phi(t)}\right\} \\ Q(t) &= Im\left\{a(t)\, e^{j\phi(t)}\right\}, \end{aligned}$$

where $a(t)$ represents the modulated signal's amplitude modulation component, and need not necessarily be real-valued; single-sideband modulation, in particular, has an analytic signal $a(t) = \tilde{m}(t)$. $\phi(t)$ contains the modulated phase (and, therefore, its modulated frequency). It can be shown that, for all possible $a(t)$ and $\phi(t)$, the quadrature signals will have the relationship

$$I^2(t) + Q^2(t) = |a(t)|^2 . \tag{5.1}$$

If $I(t)$ and $Q(t)$ are interpreted as the co-ordinates of a phasor at time t, the phasor will plot a rotating locus with radius $|a(t)|$. This is illustrated in Figure 5.3 for constant $a(t) = A$. The angle between the I-axis and the phasor is

$$\phi'(t) = \arctan \frac{\sin \phi(t)}{\cos \phi(t)} = \phi(t) . \tag{5.2}$$

The instantaneous frequency of the sinusoids $I(t)$ and $Q(t)$ is equal to the time derivative of their mutual phase argument, $\phi(t)$ [8]. This can be interpreted visually as the rate of change of the phasor angle in Figure 5.3. In other words, the speed of rotation of the phasor corresponds to the frequency of the quadrature signals. If the time derivative $\dot{\phi}(t)$ is positive, the phasor will rotate anti-clockwise. If $\dot{\phi}(t)$ is negative, the phasor will rotate clockwise. If $\dot{\phi}(t) = 0$, it means that $\phi(t)$ is a constant and that the phasor will remain stationary at that phase value.

For example, baseband frequency modulation is easily visualised in the phasor domain. Positive values of the modulating input signal produces a positive output frequency; this is

seen as an anti-clockwise rotation of the phasor. At the modulating signal's maxima, the speed of rotation is at its highest. As the modulating signal approaches DC, the phasor slows down until it stops momentarily at the modulating signal's zero crossing. When the input signal becomes negative, the phasor starts to rotate in a clockwise direction. The highest speed of clockwise rotation corresponds to the minima of the modulating input signal. In an FM scheme where, for example, a maximum frequency deviation of 75 kHz is used, the phasor will rotate at 75 000 cycles per second during maximum deviation.

In signals with modulating amplitude, the phasor locus will not be constrained to a closed curve like the circle shown in Figure 5.3, but will rotate freely across the plane. However, the closed-curve phasor representation will prove to be such a useful concept that this chapter will draw phasor diagrams as if they were generated by a constant (although possibly unknown) signal amplitude. This need not restrict the generality of the analysis: it just means that the phasor diagram must not be interpreted as the set of points in signal space to which a signal is limited. Rather, it should be seen as a signal's "trajectory" in signal space for the current instantaneous amplitude. From this point of view, an amplitude-modulating signal will be seen as a pulsating circle in the phasor domain.

5.3 Carrier-coherence as basis for study

A premise that must be established before the main development of the chapter, is the use of phase-coherent local oscillators in the transmitter and receiver mixers.

In Chapter 2 (p. 19) the notion of imperfect estimation of the transmitter mixing frequency at the receiver was investigated, and it was shown that such poor carrier frequency estimation does not seriously handicap the demodulation of received signals. In particular, it was shown that the mixing frequencies simply serve to translate a complex-valued signal in the frequency domain, without affecting the information content in the modulated signal. However, it should be noted that this analysis of Section 2.3.2 assumed ideal quadrature upmixing and downmixing, albeit with slightly different carrier frequencies.

When investigating the effects of quadrature inaccuracies on the modulation and demodulation process, it can no longer be assumed that the effects of non-coherent carriers are as benign as predicted by Section 2.3.2. This consideration will become particularly important when studying the effect of combined quadrature inaccuracies at the transmitter and receiver. In SDR applications, it is convenient not to maintain carrier coherence between transmitters and receivers, and therefore the non-coherent case can be considered to be particularly important.

In this chapter, the simpler (coherent) case, where the receiving mixer's local oscillator has exactly the same frequency as that of the transmitter, will be investigated first. Section 6.6 will then extend the results to the more general case where the receiver uses a carrier estimate that only approximates the transmission mixer's local oscillator frequency. The strong focus on the coherent-carrier case may be motivated as follows:

- By initially assumming that the transmitter and receiver employ the same local oscillator, the analysis can focus on the effect that quadrature inaccuracies have on the information content of the RF signal and the demodulated signal. A difference in carrier frequencies does not alter the information content of any of the signals, although it may lead to a misrepresentation of the information.

- Poor carrier frequency estimation can be viewed as an additional, separate stage of distortion. Furthermore, carrier synchronisation is a well-developed field, both in analogue and digital signal processing [56, 43, 32], and is straightforward to implement in a software-defined radio receiver.

- It will be shown in Section 6.6 that the quadrature compensation techniques developed for the coherent-reception case, can be extended to the noncoherent case.

This concludes the preliminary theory and remarks, and provides a foundation for the development of the main contributions of this chapter. The effects of quadrature amplitude mismatch, DC offset, LO leakthrough and phase mismatch on quadrature modulation and demodulation will now be investigated.

5.4 General distortion model

In this section, the cumulative effect of all forms of quadrature distortion is modelled. It will be shown that these effects are independent, and can be analysed separately.

5.4.1 Quadrature upmixing

For a transmission system suffering from quadrature distortion effects, the ideal upmixed signal described in Equation 2.9 (p. 11) can be modified to

$$\begin{aligned} y(t) &= \left[\varepsilon_i + (1+\rho)\cdot \mathcal{R}e\left\{a_i(t)\,e^{j\phi(t)}\right\}\right]\cdot\cos\omega_c t \\ &\quad - \left[\varepsilon_q + Im\left\{a_q(t)\,e^{j[\phi(t)-\kappa]}\right\}\right]\cdot\sin(\omega_c t-\lambda) \\ &\quad + \alpha\cos(\omega_c t+\gamma)\,. \end{aligned} \tag{5.3}$$

This generalised distortion model can be used to analyse the effects of quadrature inaccuracies on any form of quadrature modulation. Lines one and two of the equation represent the mixed I and Q signals, so that

$$\begin{aligned} I(t) &= \mathcal{R}e\left\{a_i(t)\,e^{j\phi(t)}\right\} \\ Q(t) &= Im\left\{a_q(t)\,e^{j[\phi(t)-\kappa]}\right\} \\ M_I(t) &= \cos\omega_c t \\ M_Q(t) &= \sin(\omega_c t-\lambda)\,. \end{aligned} \tag{5.4}$$

The expressions for $I(t)$ and $Q(t)$ are designed to make general analysis of modulation schemes possible. By placing specific constraints on $a_i(t)$, $a_q(t)$ and $\phi(t)$, a variety of modulation schemes can be obtained for a modulating input signal $m(t)$:[3]

- **FM**: $a_i(t) = a_q(t) = A, \quad \phi(t) = k_f \int_0^t m(\tau)\, d\tau$
- **AM**: $a_i(t) = a_q(t) = m(t), \quad \phi(t) = \omega_0 t$
- **SSB**: $a_i(t) = a_q(t) = \tilde{m}(t), \quad \phi(t) = \omega_0 t$ [4]

Note that these typical modulation schemes have $a_i(t) = a_q(t) = a(t)$, and that this simplification will be made throughout the text. The third line in Equation 5.3 contains a sinusoidal term that models local oscillator leakthrough into the output signal. The variables and constants in Equation 5.3 are as follows:

ρ: A constant describing the difference in amplitude between $I(t)M_I(t)$ and $Q(t)M_Q(t)$. When $\rho = 0$, the signals are of equal magnitude. When $\rho > 0$, the I-product is larger than the Q-product.

α: The magnitude of the carrier leakthrough component.

γ: The phase of the local oscillator leakthrough component, relative to that of $M_I(t)$.

ε_i: The spurious DC offset on $I(t)$.

ε_q: The spurious DC offset on $Q(t)$.

κ: The phase error (in radians) between $I(t)$ and $Q(t)$. When $\kappa = 0$, the signals should be exactly $\pi/2$ rad out of phase. When $\kappa > 0$, the signals are closer in phase.

λ: The phase error (in radians) between $M_I(t)$ and $M_Q(t)$. When $\lambda = 0$, the signals should be exactly $\pi/2$ rad out of phase. When $\lambda > 0$, the signals are closer in phase.

These cover the most significant types of non-ideality found in the quadrature mixing process, and may be considered a general model of the upmixing stage. Reorganisation of the terms in Equation 5.3 highlights the interplay between the various types of distortion:

$$\begin{aligned} y(t) \;=\; & \mathcal{R}e\left\{a_i(t)\, e^{j\phi(t)}\right\} \cdot \cos\omega_c t \;-\; Im\left\{a_q(t)\, e^{j[\phi(t)-\kappa]}\right\} \cdot \sin(\omega_c t - \lambda) \\ & + \rho \cdot \mathcal{R}e\left\{a_i(t)\, e^{j\phi(t)}\right\} \cdot \cos\omega_c t \\ & + \alpha\cos(\omega_c t + \gamma) + \varepsilon_i \cos\omega_c t - \varepsilon_q \sin(\omega_c t - \lambda)\,. \end{aligned} \tag{5.5}$$

[3] See Section B.1.4 (p. 171) for a more detailed discussion on how these quadrature modulation schemes are derived and used.

[4] $\tilde{m}(t)$ is the analytic representation of $m(t)$, so that $\tilde{m}(t) = m(t) + j\hat{m}(t)$. Note that $\hat{m}(t)$ is the Hilbert transform of $m(t)$.

The first line of the equation represents the desired upmixed signal, but with phase errors between the two terms. No other forms of distortion remain in these terms. Line 2 contains a modulated cosine produced by amplitude mismatch, and is also isolated from the other distortion parameters. The last line can be collected into a single sinusoid at the local oscillator frequency. Its amplitude and phase depends on the level of local oscillator leakthrough, the DC offset on $I(t)$ and $Q(t)$, and its phase can be affected by the phase accuracy between the quadrature local oscillator signals.

When analysing the effects of the various forms of quadrature distortion on the transmitted and received signal spectra, the terms in Equation 5.5 may be investigated separately; combined quadrature impairments will produce a superposition of these terms.

5.4.2 Quadrature downmixing

Although it would be possible to construct a similar distortion model for quadrature downmixing, it will be shown in the Sections 5.5 to 5.7 that it is always possible to model the distortion effects in a received signal as being generated by equivalent non-idealities in the transmitter. Therefore, a separate theory for quadrature downmixing is not required, and the text will focus on the effects of transmitter distortion on the RF and ideally downmixed signals.

The various parameters of Equation 5.3 will now be analysed individually.

5.5 Amplitude deviation

In a physical quadrature modulation system, it is possible that the I and Q output channels of the direct-digital synthesiser do not produce signals with perfectly matched amplitude. For example,

$$\begin{aligned} I(t) &= (1+\rho)\,\mathcal{R}e\{a(t)e^{j\phi(t)}\} \\ Q(t) &= Im\{a(t)e^{j\phi(t)}\}\,. \end{aligned} \tag{5.6}$$

This effect can typically be caused by unmatched DACs or by low-pass filters with poorly matched amplitude responses in the passband. Imperfections in the mixing circuit could also produce a slight discrepancy in the amplitudes of the two local oscillator signals:

$$\begin{aligned} M_I(t) &= (1+\rho)\cos\omega_c t \\ M_Q(t) &= \sin\omega_c t\,. \end{aligned} \tag{5.7}$$

Regardless of whether the amplitude deviation is found in the I-Q output channels or in the local oscillator signals, the resultant RF output signal can always be written in the form

$$y(t) = (1+\rho)\,\mathcal{R}e\{a(t)e^{j\phi(t)}\}\cdot\cos\omega_c t \;-\; Im\{a(t)e^{j\phi(t)}\}\cdot\sin\omega_c t\,. \tag{5.8}$$

Without loss of generality, the rest of this section will therefore only consider the effects of amplitude deviation at the I-Q outputs (Equation 5.6).

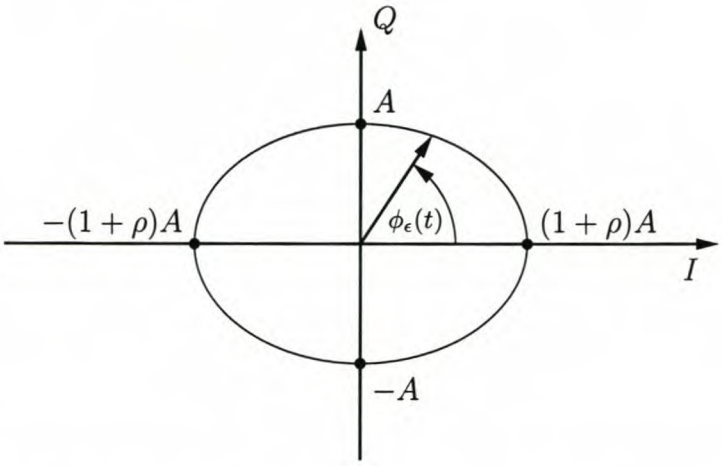

Figure 5.4: *The effect of amplitude deviation on the I-Q phasor locus, sketched for* $a(t) = A$.

When amplitude deviation occurs, a plot of the I-Q phasor locus produces an ellipse instead of a circle, as is illustrated in Figure 5.4 (drawn for the trajectory of $a(t) = A$). The ellipse's axes coincide with the I and Q axes, and the major axis of the ellipse corresponds to the channel with the largest amplitude. Consequently, the total power transmitted after unity-amplitude mixing is equal to a quarter of the squares of the minor and major radii.[5]

An example of the effect of amplitude deviation on the I-Q phasor locus can be seen in Figure 5.5, where the I-channel is 10% larger than the Q-channel. Because the FM signal is of constant amplitude, the baseband signal phasor stays on the elliptical locus.

5.5.1 Frequency spectrum of the upmixed signal

Preliminary considerations.

Important insights into the effects of amplitude deviation on the modulated signal can be gleaned by investigating the RF signal in the frequency domain. To do this, it is important to realise that the spectrum of a modulated signal may be time-variant in the frequency domain: For example, in FM the instantaneous frequency of the output signal varies according to the modulating input signal. Therefore, the frequency-domain plots considered in this chapter are idealised representations of the instantaneous frequency of a time-variant signal. They are idealised, because the implicit assumption is made that the instantaneous frequency of the signal varies very slowly in the time window from which the Fourier transform is taken. Consequently, the instantaneous frequencies are approximated as impulses in the frequency domain. In fact, a signal can only produce an impulse in the frequency domain when its frequency is invariant over all time—clearly not the case for information-bearing signals. When a finite time window is considered, or when the instantaneous frequency varies in

[5]See Appendix D.2.

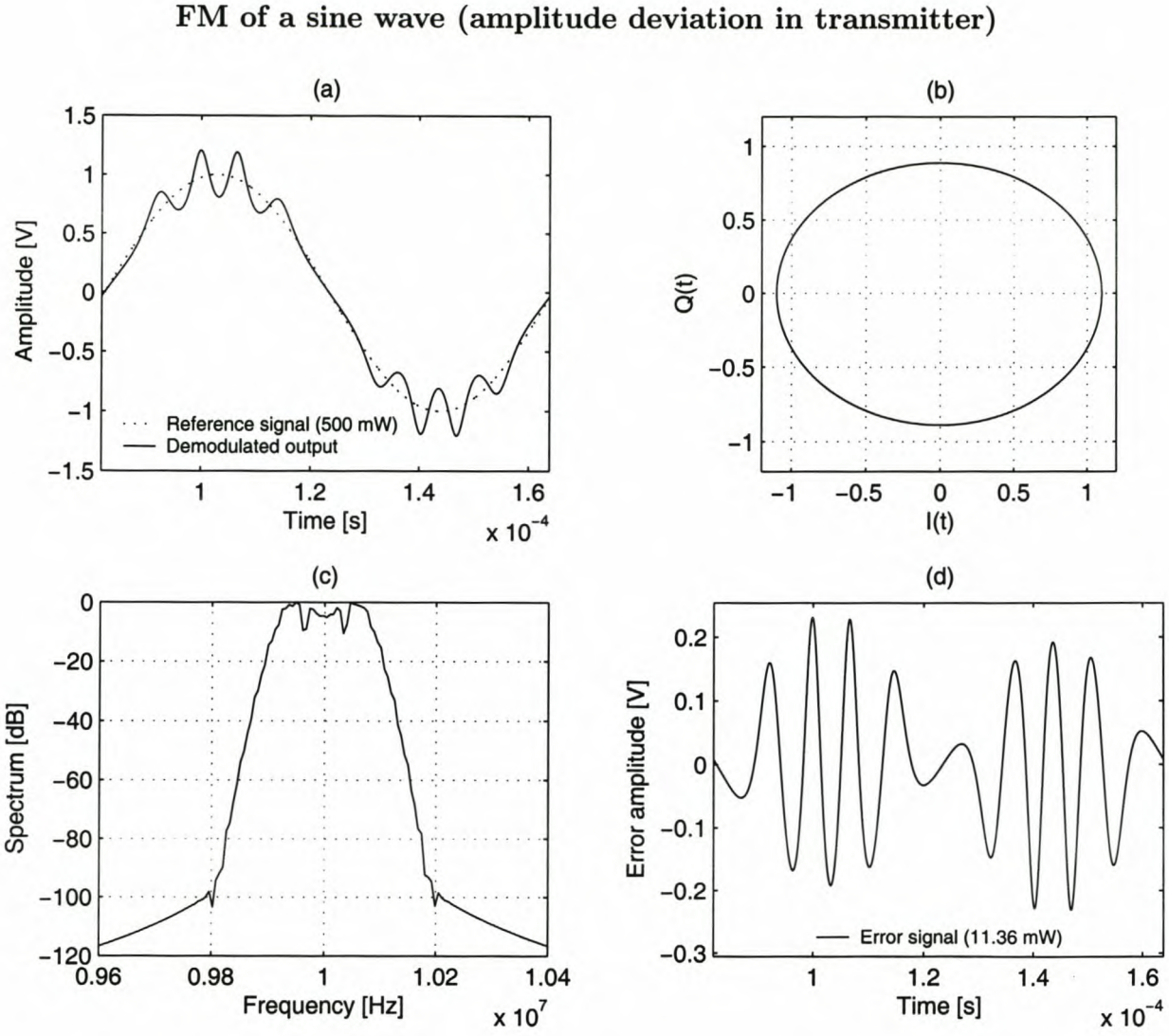

Figure 5.5: *Simulation of frequency modulation of an input sine wave, with the transmitter's I-channel amplitude amplified by 10.8%. 75 kHz frequency deviation was employed. (a) The demodulated signal shows an undesired distortion, which is at its worst at the maximum excursions of the desired signal. (b) The received signal's phasor has become elliptical, stretched in the direction of the I-axis. (c) Because of the symmetry of the FM signal's spectrum, any sideband present is obscured. (d) The error signal oscillates most rapidly and with highest amplitude near the desired signal's points of maximum excursion; at other points it is smaller, and oscillates slower (proportional to the speed of phasor rotation at that moment).*

Simulation reference: `ampdevfm`

that time window, the signal energy spills over the entire range of the Fourier frequency domain. The greater part of the energy is contained in a lobe centered around the average frequency. This interplay between windowing in the time and frequency domains is a result of the uncertainty principle in time-frequency analysis [8, p. 44].

This reasoning can be extended for the case of a time-varying amplitude of a (possibly frequency-modulating) carrier. An amplitude-modulating signal occupies a frequency band around the carrier frequency that is proportional to the bandwidth of $a(t)$, the modulating signal. Once more, an impulse at the carrier frequency occurs only when the signal amplitude stays constant over all time—something that is impossible if amplitude modulation is to take place. However, it will often be convenient to visualise an amplitude-modulating signal as a Dirac delta with a time-variant weight in the frequency domain. This is a good approximation if the modulating amplitude varies slowly in the time window from which the Fourier transform is taken.

The use of idealised impulses in the time-frequency domain can be justified under two conditions:

1. The idealisation must provide valid and useful information about the behaviour of the true signal.

2. The relationship between the idealisation and the true signal must always be clear.

The second condition can be met if the idealised frequency-domain impulse is interpreted as an indication of the *power* and *average location* of a time-variant frequency component occurring in a signal. In other words, the idealised frequency impulses show the size and position of signal lobes in the frequency domain. The analysis of the idealised impulses is useful, because the general behaviour of the impulses corresponds with the behaviour of the actual components in the time-frequency domain.

Application to amplitude deviation.

Firstly, note that Equation 5.8 can be written in the form

$$y(t) = \overbrace{\mathcal{R}e\{a(t)e^{j\phi(t)}\}\cos\omega_c t - \mathcal{I}m\{a(t)e^{j\phi(t)}\}\sin\omega_c t}^{\text{desired upmixed signal}} + \underbrace{\rho \cdot \mathcal{R}e\{a(t)e^{j\phi(t)}\}\cos\omega_c t}_{\text{error signal}} . \quad (5.9)$$

The frequency spectrum of the desired signal was already analysed in Figure 2.2 (p. 10), and furthermore depends on the specific modulation scheme and information content. Assume that, at time $t = \tau$, $a(\tau) = A$ so that the desired signal produces impulses of magnitude πA at frequencies $\omega_c + \dot{\phi}(\tau)$ and $-\omega_c - \dot{\phi}(\tau)$. Note that the constant A may be complex, as is the case for single-sideband amplitude modulation. Similarly, the factor $\rho A \cos\phi(t)$ in the error signal produces impulses of magnitude $\pi\rho A$ at the instantaneous frequencies $\dot{\phi}(\tau)$ and $-\dot{\phi}(\tau)$. The factor $\cos\omega_c t$ produces two components at $\pm\omega_c$ with amplitude π. Subsequently, the frequency transform of the complete error signal can be calculated by the

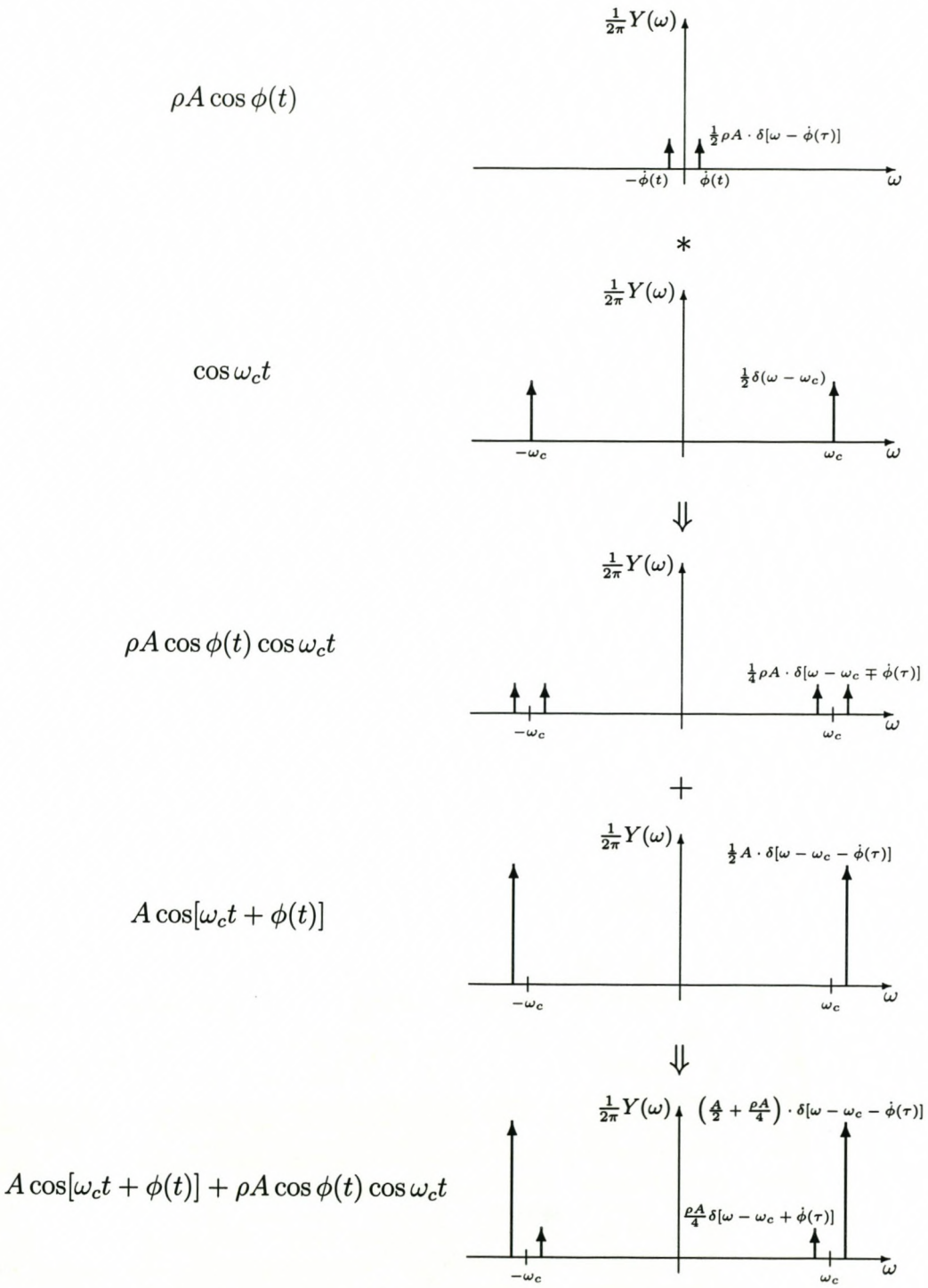

Figure 5.6: *Frequency diagram of I-Q mixing with amplitude deviation.*

convolution illustrated in Figure 5.6. By adding the spectra of the desired and the error signal, the frequency transform of the complete RF signal with amplitude deviation can be seen. Note that this visualisation applies equally well to a signal that is modulating in frequency, amplitude or both: If all parameters vary slowly in the Fourier time window, the "snapshot" of the signal can be approximated with a constant instantaneous frequency and amplitude.

Figure 5.6 shows that amplitude deviation causes a spurious frequency component to appear. This component has an amplitude of $\pi\rho a(t)/2$; the desired and the spurious frequency components appear at positions that are symmetric around the carrier frequency. A component of amplitude $\pi\rho a(t)/2$ is also added to the desired component. This means that the desired component is somewhat amplified for positive ρ (but attenuated for negative ρ). The ratio between the desired component and the largest spurious component, or spurious free dynamic range, is:

$$\mathrm{SFDR}_\rho = 20\log\left(\frac{2a(t)+\rho a(t)}{|\rho a(t)|}\right) = 20\log\left(\frac{2+\rho}{|\rho|}\right)\ \mathrm{dB}\,. \tag{5.10}$$

This equation gives a direct relationship between the size of amplitude mismatch, and a sideband component at a predictable frequency. Note that there is a one-to-one relationship between the quadrature error in the spur size—this means that, if it is necessary to estimate the level of amplitude distortion in a system, it would be possible to obtain it by measuring the signal spectrum. This concept will be further explored in the quadrature compensation theory of Chapter 6.

For example, consider Figure 5.7(c) on page 48. In this simulation, frequency modulation was performed on a input DC signal, which ideally should have generated a single frequency component above the centre frequency. However, due to amplitude mismatch of 10.8% ($\rho = 0.108$), a spurious sideband appears, exactly symmetrical to the desired component. Equation 5.10 predicts that the spur will lie 25.8 dB below the desired component, and this is exactly what is seen in the simulation. The spur's position and magnitude can be predicted precisely by the theory presented thus far.

The result of this section is generalised, and applies equally to multitone as to single-tone signals. Figure 5.8(c) shows the spectrum of an upmixed DSB-AM signal, which consists of three tones (one of them below the oscillator frequency). Each of the three large (desired) spurs produces an attenuated sideband spur, reflected around the oscillator frequency. Equation 5.10 predicts that, for $\rho = 1.08$, each of the sideband tones should be 25.8 dB lower than its desired counterpart. This corresponds to the simulation result, further confirming the validity of the theory.

The discussion thus far has focused on the effect of amplitude mismatch on the transmitted RF signal. The analysis now turns to the characteristics of the received signal.

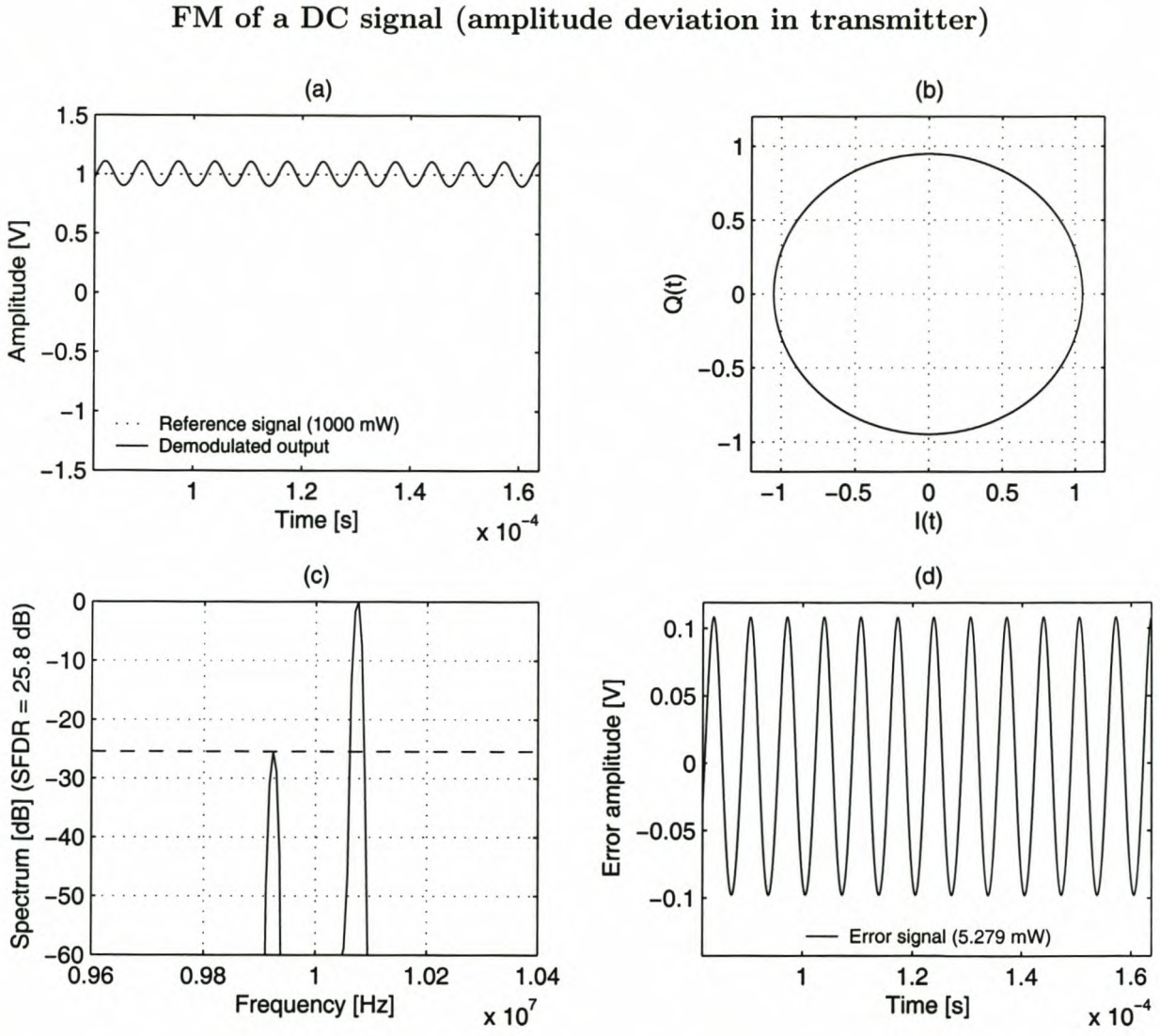

Figure 5.7: *Simulation of frequency modulation of an input DC signal, with the transmitter's I-channel amplitude amplified by 10.8%. 75 kHz frequency deviation was employed. (a) The demodulated signal shows an undesired 150-kHz oscillation. (b) The received signal's phasor has become elliptical, stretched in the direction of the I-axis. (c) A spurious sideband has appeared, symmetric around the centre frequency from the desired signal, and 25.8 dB below it. (d) The 150-kHz error signal can be seen as phasor rotation "leaking through" due to the amplitude error.*

Simulation reference: `ampdevdc`

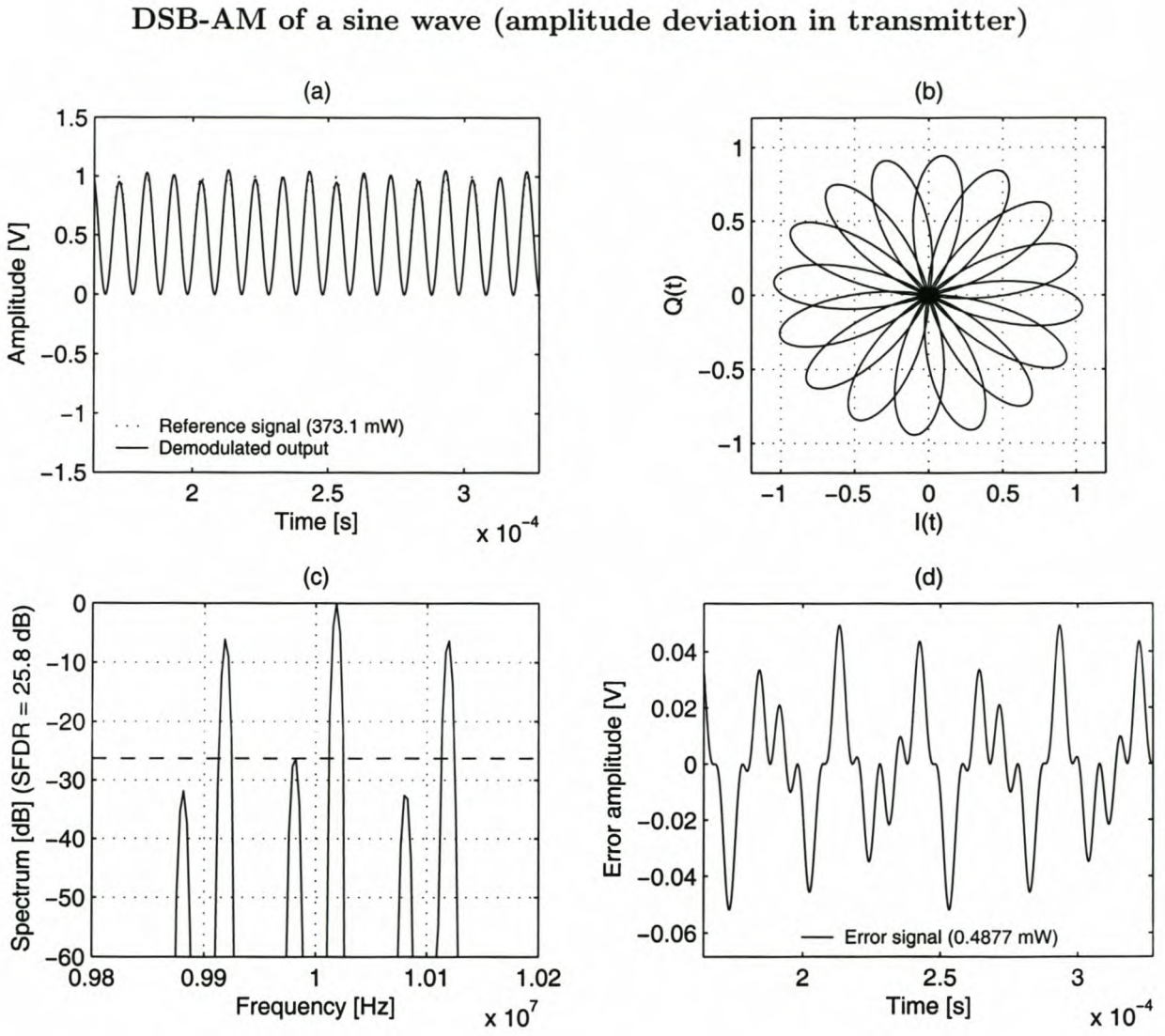

Figure 5.8: *Simulation of a DSB amplitude-modulated sine wave, with the transmitter's I-channel amplitude increased by 10.8%. In this simulation, the carrier frequency was chosen to be 18.75 kHz above the mixing frequency of 10 MHz. The modulating sinusoid has a frequency of 100 kHz. (a) The demodulated signal is no longer a single tone of constant amplitude. (b) The flower-like phasor of Figure B.3 has been stretched horizontally, proportional to the amount of amplitude deviation. (c) An attenuated version of the ideal signal spectrum (see Figure B.3) is reflected around the mixing frequency of 10 Mhz. The SFDR is 25.8 dB, which is the same as for the single-tone case (Figure 5.7). (d) The points of maximum excursion of the error signal is exactly proportional to the level of amplitude deviation.*

Simulation reference: `ampdevam`

5.5.2 Combined transmitter-receiver distortion

On the receiver side, unmatched amplitudes in both the transmitter and the receiver must be taken into account. For this analysis, coherent demodulation is first assumed—an interpretation for the non-coherent case will be presented at the end of the section.

Assume a complex-baseband modulated signal

$$s(t) = a(t) \cdot e^{j\phi(t)} . \tag{5.11}$$

After quadrature upmixing with amplitude deviation, Equation 5.9 (p. 45) yields

$$\begin{aligned} y(t) &= \mathcal{R}e\{a(t) \cdot e^{j[\phi(t)+\omega_c t]}\} + \rho_{\text{tx}} \cdot \mathcal{R}e\{a(t) \cdot e^{j\phi(t)}\} \cos\omega_c t & (5.12)\\ &= y_d(t) + y_\epsilon(t) . & (5.13) \end{aligned}$$

Next, the signal is transmitted and downmixed at the receiver. Because the downmixing is distributive, the desired and error terms may be considered separately. In the presence of amplitude deviation at the receiving mixer, the first part of the received signal may be written as

$$\begin{aligned} s_d(t) &= 2\left[(1+\rho_{\text{rx}}) \cdot y_d(t) \cos\omega_c t \; - \; j \cdot y_d(t) \sin\omega_c t\right]_{\text{LPF}} \\ &= s(t) + 2\rho_{\text{rx}} \cdot \mathcal{R}e\left\{a(t) \cdot e^{j\phi(t)}\right\}_{\text{LPF}} . \end{aligned} \tag{5.14}$$

Similarly, the downmixed version of $y_\epsilon(t)$ is

$$\begin{aligned} s_\epsilon(t) &= 2\Big[(1+\rho_{\text{rx}}) \cdot \rho_{\text{tx}} \cdot \mathcal{R}e\{a(t)\, e^{j\phi(t)}\} \cos^2\omega_c t \\ &\qquad - j\rho_{\text{tx}} \cdot \mathcal{R}e\{a(t)\, e^{j\phi(t)}\} \cos\omega_c t \sin\omega_c t\Big]_{\text{LPF}} . \end{aligned} \tag{5.15}$$

After trigonometric simplification and removal of double-frequency components (assuming that $\phi(t)$ has a bandwidth smaller than ω_c, as is usual in a communications system),

$$s_\epsilon(t) = \rho_{\text{tx}}(1+\rho_{\text{rx}}) \cdot \mathcal{R}e\left\{a(t)\, e^{j\phi(t)}\right\} . \tag{5.16}$$

The superposition $s(t) = s_d(t) + s_\epsilon(t)$ yields the complete received signal

$$s'(t) = s(t) \; + \; (\rho_{\text{tx}} + \rho_{\text{tx}}\rho_{\text{rx}} + \rho_{\text{rx}}) \cdot \mathcal{R}e\left\{a(t)\, e^{j\phi(t)}\right\} . \tag{5.17}$$

The first term in this equation is the desired downmixed signal. The second term represents a real-valued error component that will have a frequency spectrum that is symmetric around zero herz. Consequently, it will introduce a reflected sideband component in the baseband. Its magnitude depends on both the transmitter and receiver amplitude deviation constants. If follows that combined amplitude deviation in a transmitter-receiver system (with coherent carriers) can be modelled as an amplitude-mismatched transmitter in cascade with an ideal receiver. The transmitter has an equivalent normalised amplitude deviation

$$\rho' = \rho_{\text{tx}} + \rho_{\text{tx}}\rho_{\text{rx}} + \rho_{\text{rx}} , \tag{5.18}$$

which combines the deviation constants of the transmitter and the receiver.

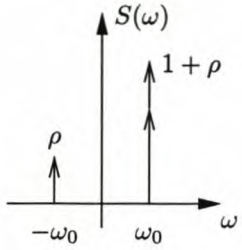

Figure 5.9: *Downmixed spectrum of a quadrature signal with amplitude mismatch. In this example, the desired signal is* $s(t) = e^{j\omega_0 t}$. *Receiver or coherent transmitter mismatch causes a spurious sideband to appear, proportional to the mismatch coefficient* ρ *and reflected around zero herz.*

This result implies that it is not necessary to consider receiver distortion as a separate case: Its effects on the received signal are similar to the transmitter case.

It will be seen in Section 6.6 that the coherent-carrier assumption ($\hat{\omega}_c = \omega_c$) is strictly necessary for this simplification to hold. Under this assumption it is always possible to "collect" total quadrature distortion effects at either the transmitter or receiver. In the more general case where the mixer frequencies differ, transmitter and receiver distortion effects must be modelled and compensated for separately. Even then, the result presented here provides a way to model receiver distortion as if it were generated by a fictional phase-coherent transmitter.

5.5.3 Frequency spectrum of the downmixed signal

It was shown in the previous section that amplitude mismatch in the transmitter or receiver causes the received complex baseband signal to take the form

$$s(t) = a(t)e^{j\phi(t)} + \rho \cdot \mathcal{R}e\left\{a(t)e^{j\phi(t)}\right\}, \tag{5.19}$$

where ρ is the cumulative effect of the transmitter and receiver amplitude distortion. While $a(t)e^{j\phi(t)}$ may uniquely address positive and negative frequencies, the real-valued error term has symmetric positive and negative sidebands. Its practical effect is demonstrated in Figure 5.9: A spurious sideband appears in the baseband spectrum, reflected around zero herz. This degrades the SFDR in the complex-valued baseband signal, and its effect on practical modulation schemes will be illustrated in the next section.

The simulation results presented in Figure 5.10 confirm the theory developed so far. In this single-tone experiment, the transmitter and receiver both had amplitude mismatch with $\rho_{\text{tx}} = \rho_{\text{rx}} = 4.125\%$. For the transmitter distortion, Equation 5.10 predicts an SFDR of 33.9 dB, which is exactly what is produced in Figure 5.10(a). After downmixing with $\rho_{\text{rx}} = 4.125\%$, Equation 5.18 states that the cumulative amplitude distortion factor is

$$\rho' = 2 \cdot 0.04125 + 0.04125^2 = 0.0842 \tag{5.20}$$

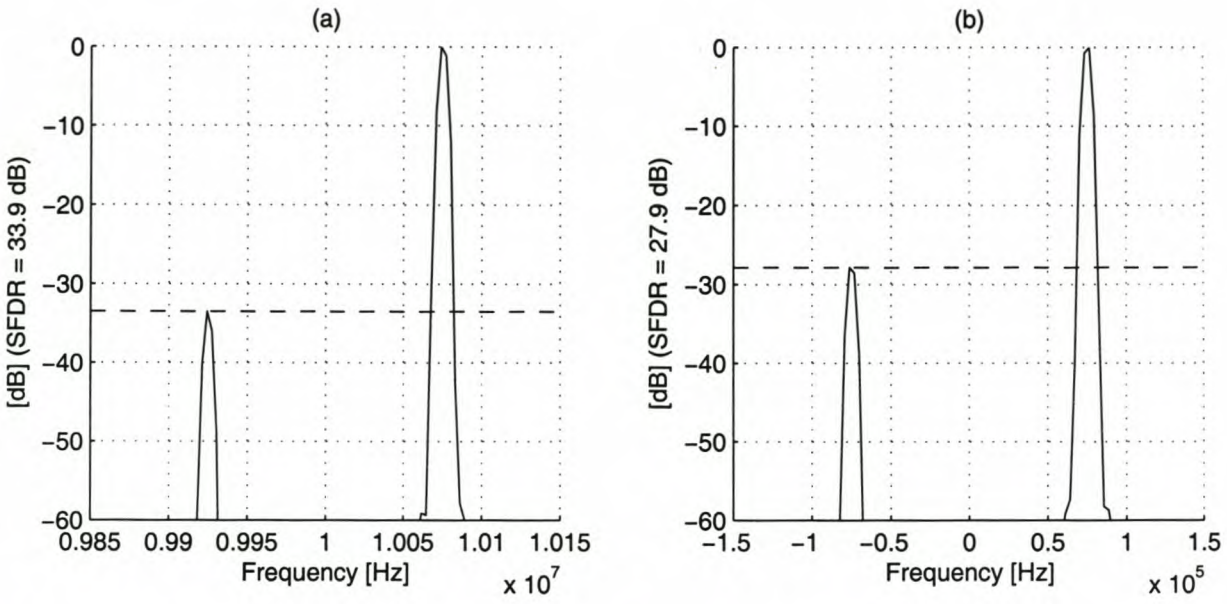

Figure 5.10: *Simulation of combined amplitude error in a quadrature transmitter and receiver. In this experiment,* $\rho_{\text{tx}} = \rho_{\text{rx}} = 4.125\%$. *(a) Frequency spectrum of the upmixed signal. (b) Frequency spectrum of the downmixed signal, showing the effect of both transmitter and receiver amplitude mismatch.*

which, according to Equation 5.10, should produce a spur 27.9 dB below the desired signal. This prediction is confirmed by the downmixed signal spectrum in Figure 5.10. The frequency spectrum of the downmixed signal contains its error component at a negative frequency, and is a reflection of the desired signal component. This agrees with the prediction of Equation 5.19.

5.5.4 Case studies

The general analysis presented above for amplitude deviation in quadrature mixers will now be applied to three practical analogue modulation schemes.

Frequency modulation

Let the phase angle of the phasor in Figure 5.4 be $\phi_\epsilon(t)$. From Equation 5.6 it follows that this (presumably erroneous) phase angle can be written in terms of the desired phase angle, $\phi(t)$, as follows:

$$\phi_\epsilon(t) = \arctan \frac{A \sin \phi(t)}{(1+\rho) A \cos \phi(t)} . \tag{5.21}$$

In this case, it makes sense to assume that $a(t) = A$, because the amplitude of an ideal frequency-modulated signal is usually constant. Because the frequency information relevant to FM is contained in the rate of change of the phase angle, the time derivative of

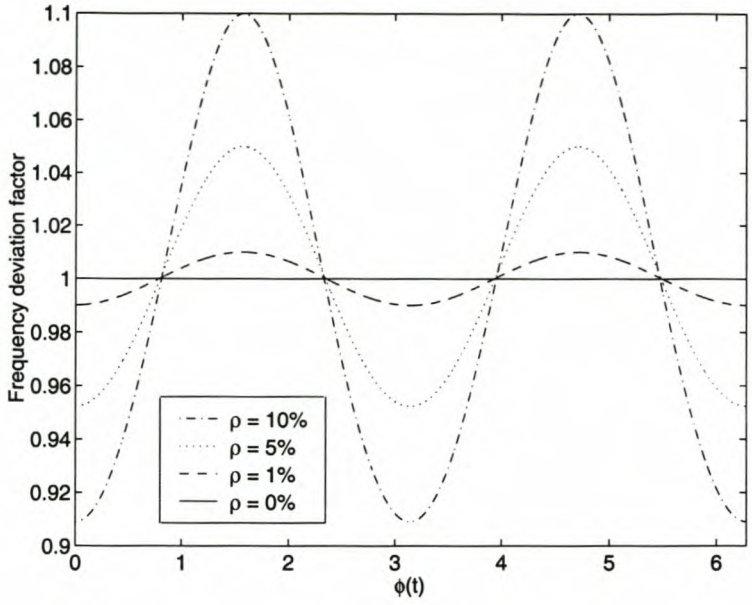

Figure 5.11: *The distortion wave $\dot{\phi}_\epsilon(t)/\dot{\phi}(t)$ for various values of the deviation factor ρ during quadrature frequency modulation. Note that the "distortion wave" represents the factor by which the demodulated signal varies from its ideal value.*

Equation 5.21 must be taken to find the instantaneous frequency. This is given by

$$\begin{aligned}\frac{d\phi_\epsilon(t)}{dt} &= \left(\frac{A^2(1+\rho)}{2A^2\rho\cos^2\phi(t) + A^2\rho^2\cos^2\phi(t) + A^2}\right)\frac{d\phi(t)}{dt} \\ &= \left(\frac{1+\rho}{\rho\cos^2\phi(t) + 2\rho\cos^2\phi(t) + 1}\right)\frac{d\phi(t)}{dt}. \end{aligned} \tag{5.22}$$

The distorted frequency is at its lowest when $\phi(t) = 0$ rad; at that point

$$\left[\frac{d\phi_\epsilon(t)}{dt}\right]_{\min} = \frac{1}{\rho+1}\cdot\frac{d\phi(t)}{dt}. \tag{5.23}$$

This corresponds to the speed of the phasor when it crosses the I-axis in Figure 5.4. Similarly, the distorted frequency reaches its zenith when $\phi(t) = \pi/2$ radians:

$$\left[\frac{d\phi_\epsilon(t)}{dt}\right]_{\max} = (\rho+1)\cdot\frac{d\phi(t)}{dt}. \tag{5.24}$$

This expression also gives the speed of the phasor when it crosses the Q-axis in Figure 5.4. Note that the minimum frequency always corresponds to the major axis of the phasor ellipse, and the maximum frequency to the minor axis. A plot of the distortion factor is given in Figure 5.11. Equation 5.22 gives an expression for the *actual* phasor frequency when amplitude deviation occurs, in terms of the *desired* phasor frequency. This expression may be manipulated into a desired signal component and an error signal, in order to find the

relative magnitude of the error:

$$\frac{d\phi_\epsilon(t)}{dt} = \overbrace{\frac{d\phi(t)}{dt}}^{\text{desired demodulated signal}} + \underbrace{\left(\frac{1+\rho}{2\rho\cos^2\phi(t) + \rho^2\cos^2\phi(t) + 1} - 1\right)\frac{d\phi(t)}{dt}}_{\text{error signal}} . \tag{5.25}$$

Equation 5.25 can be evaluated (e.g. numerically) to predict the distortion that amplitude deviation causes in a known signal. This is effectively what is done in the simulations presented in Figure 5.5 on page 44, where the power of both the desired signal and the error signal is calculated. From this, the signal-to-noise-and-distortion ratio (SINAD) can be calculated to determine the fidelity of the demodulated signal.

The DC-input FM signal simulation on page 48 produces a phasor rotating at a constant rate of 75 kHz (the maximum frequency deviation). The simulation shows that the subsequent distortion signal does oscillate at double the phasor frequency (i.e. 150 kHz), as predicted by Equation 5.22. For the sinusoidal input signal (p. 44), the phase rate of change depends on the instantaneous amplitude of the modulating input signal. This leads to a distortion signal with a frequency that varies correspondingly.

The error signal in the sinusoidal-input simulation (p. 44) is largest when the demodulated signal is largest, and goes to zero during the signal's zero crossings. This stems from the fact that the distortion factor of Equation 5.22 is multiplied with the desired output signal, thus effectively amplitude-modulating the error signal.

In summary, the simulations confirm and illustrate the theory presented thus far. Now that the effect of amplitude mismatch on an FM signal's spectrum has been investigated, a similar analysis will be done for amplitude modulation.

Double-sideband AM

The effect of imperfect quadrature mixing on an upmixed AM signal can, just as for FM, be derived from Equation 5.9. For an AM signal, $\phi(t) = \omega_0 t + \phi_0$ to produce a centre frequency at $\omega_c + \omega_0$:

$$y(t) = m(t)[1+\rho]\cos(\omega_0 t + \phi)\cos\omega_c t - m(t)\sin(\omega_0 t + \phi)\sin\omega_c t\,, \tag{5.26}$$

where $a(t) = m(t)$ is the modulating signal. Equation 5.26 can be written in the form

$$y(t) = \overbrace{m(t)\cos\left[(\omega_c + \omega_0)t + \phi_0\right]}^{\text{desired upmixed signal}} + \underbrace{m(t)\rho\cos(\omega_0 t + \phi_0)\cos\omega_c t}_{\text{error signal}} . \tag{5.27}$$

The result is identical to that of Equation 5.9, and the spectral diagram of Figure 5.6 applies—except that the frequency impulses representing the FM signal's instantaneous frequency are now replaced by the double-sided spectrum of the modulating signal. If $|\omega_0|$ is smaller than the bandwidth of the modulating signal, spectral overlap (aliasing) may occur.

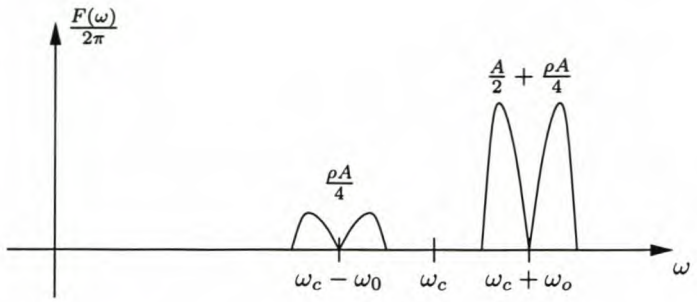

Figure 5.12: *Amplitude deviation in quadrature mixing also produces a sideband image of the desired signal. The magnitude of the desired and spurious spectra are indicated, relative to a maximum amplitude A.*

A special case is where $\omega_0 = 0$ (no frequency offset or channel selection). Here,

$$\begin{aligned} y(t) &= m(t)\cos(\omega_c t + \phi_0) + m(t)\rho\cos\phi_0\cos\omega_c t \\ &= m(t)\underline{/\phi_0} + m(t)\rho\cos\phi_0\underline{/0^\circ}\,. \end{aligned} \tag{5.28}$$

It is the magnitude of the phasor addition in Equation 5.28 that is of interest in amplitude modulation, and it can be calculated to be

$$|y(t)| = m(t)\sqrt{(\rho^2 + 2\rho)\cos^2\phi_0 + 1}\,. \tag{5.29}$$

The modulated amplitude is multiplied by a constant gain that depends on the amplitude deviation constant, ρ, and the relative angle ϕ_0. When $\phi_0 = 0$, $I(t) = m(t)$ and $Q(t) = 0$. This produces an undistorted modulated signal with the gain increased by ρ, the I-channel amplitude deviation factor. When $\phi_0 = \frac{\pi}{2}$, $m(t)$ appears on the Q-channel, and the I-channel is zero. Equation 5.29 shows that, for other values of ϕ_0, the resulting modulated signal is not distorted by ρ, but just multiplied by a constant gain factor. It can be concluded that, when no digital channel selection is performed ($\omega_0 = 0$), the modulation process is unaffected by amplitude deviation.

In the analysis of distortion in the demodulated signal, it can safely be assumed that out-of-band frequency components do not affect the signal fidelity. This is a fair assumption: Demodulators regard frequency components outside the desired signal's band as unwanted, and filter these out as carefully as practically possible to improve the demodulated signal-to-noise ratio. Consequently, only in-band distortion effects due to amplitude imbalance in the modulation process need to be considered here.

It should be noted, however, that out-of-band distortion is not necessarily less problematic than the in-band effects. When a modulated signal produces signals outside its allocated spectral range, it interferes with other transmissions. The extent to which this is permissible may depend on relevant frequency spectrum regulations, or the extent to which "crosstalk" and other interference-related noise effects can be tolerated in a system.

Define the bandwidth of the modulating signal as B. Inspection of Figure 5.12 shows that overlap (and therefore distortion) will occur when amplitude deviation is present, and

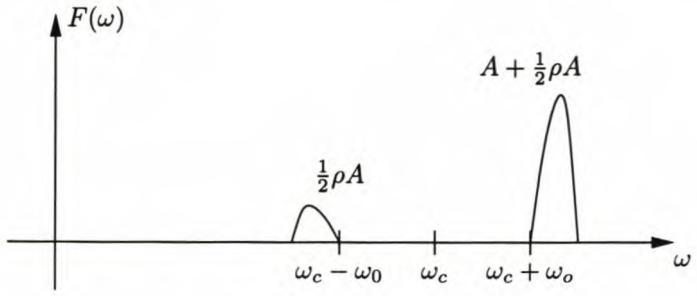

Figure 5.13: *Spurious sideband component caused by amplitude deviation in a single-sideband AM system, relative to a maximum amplitude A.*

$|\omega_0| < B$. The exact form of distortion depends on the modulating signal's spectrum, since it is signal overlapping (aliasing) that is taking place. A simulated example of overlapped distortion is shown on page 49.

Single-sideband AM

A quadrature modulator can be used to synthesise single-sideband AM signals by letting $a(t) = \tilde{m}(t) = m(t) + j\hat{m}(t)$. After quadrature mixing with amplitude deviation, Equation 5.8 (p. 42) produces

$$\begin{aligned} y(t) &= (1+\rho)\left[m(t)\cos\omega_0 t - \hat{m}(t)\sin\omega_0 t\right]\cos\omega_c t \\ &\quad - \left[m(t)\sin\omega_0 t + \hat{m}(t)\cos\omega_0 t\right]\sin\omega_c t\,. \end{aligned} \tag{5.30}$$

In this case, upper-sideband SSB has been assumed. Trigonometric expansion yields

$$y(t) = m(t)\cos(\omega_c+\omega_0)t - \hat{m}(t)\sin(\omega_c+\omega_0)t \tag{5.31}$$

$$+\tfrac{1}{2}\rho m(t)\cos(\omega_c+\omega_0)t - \tfrac{1}{2}\rho\hat{m}(t)\sin(\omega_c+\omega_0)t \tag{5.32}$$

$$+\tfrac{1}{2}\rho m(t)\cos(\omega_c-\omega_0)t + \tfrac{1}{2}\rho\hat{m}(t)\sin(\omega_c-\omega_0)t\,. \tag{5.33}$$

Term 5.31 represents the desired upper-sideband SSB signal—see, for example, [56, p. 149]. Term 5.32 is additive to the first term, and represents the amplitude increase (or decrease) produced by the amplitude error ρ.

The last term produces a spurious sideband signal due to the amplitude imbalance. It also has the form of a SSB signal, but is centred around $\omega_c - \omega_0$. The positive sign of $\hat{m}(t)$ indicates lower-sideband SSB, in contrast to the upper-sideband desired signal. Consequently, the error signal of Term 5.33 represents an error signal that is completely symmetrical around ω_c, but attenuated by ρ. This is illustrated in Figure 5.13. Once again, this result confirms that amplitude deviation produces a spurious sideband symmetric around the carrier frequency.

Similarly to the analysis that was done for double-sideband AM demodulation, Figure 5.13 (p. 56) indicates that an upper-sideband SSB signal will only overlap with its spurious sideband when ω_0 is negative and has a magnitude smaller than B. When this happens, both the desired and spurious sideband cross over ω_c, allowing them to overlap. Analogously,

a lower-sideband SSB signal will overlap with a spurious sideband caused by amplitude deviation when ω_0 is positive and smaller than B. As is the case for double-sideband AM, the distortion caused by this overlap depends only on the contents of the modulating signal—in contrast to FM, where the distortion was a more predictable "leakthrough" of the phasor rotation.

Figure 5.14 on page 58 simulates the effect of amplitude mismatch on a demodulated SSB signal. In the simulation, the error component was interpreted as if it lay within the demodulated signal bandwidth. The error appears as a spurious tone in the demodulated signal, that varies with the desired signal's amplitude. As was seen in all the previous simulations with an amplitude mismatch of $\rho = 10.8\%$, the spur is symmetrical to the desired signal, and lies exactly 25.8 dB below it, as predicted by Equation 5.10.

This concludes the analysis of the effect of amplitude imbalance on the transmitted and demodulated signals. The discussion now turns to DC offset error and local oscillator leakthrough in quadrature systems.

5.6 DC offset and oscillator leakthrough

In Equation 5.5 (p. 41) it was seen that DC offset and oscillator leakthrough cause a spurious component to appear at the transmitted oscillator frequency. In this section, the effects that these non-idealities have on the transmitted and received frequency spectra will be investigated.

In a physical quadrature transmitter or receiver, it is possible that the baseband I and Q channels have a DC offset relative to signal ground. This might be the result of imperfections in the digital-to-analogue conversion, or it might be generated purposely by the digital system (as will be seen later). When this happens, the I-Q channels' output can be written as follows:

$$\begin{aligned} I(t) &= \varepsilon_i + \mathcal{R}e\left\{a(t)\, e^{j\phi(t)}\right\} \\ Q(t) &= \varepsilon_q + Im\left\{a(t)\, e^{j\phi(t)}\right\}. \end{aligned} \tag{5.34}$$

The effect of this DC offset is a displacement of the circular phasor locus, as can be seen in Figure 5.15.

5.6.1 Frequency spectrum of the upmixed signal

When these displaced signals are upconverted by the quadrature mixer of Figure 5.1, the RF output can be calculated as

$$\begin{aligned} y(t) &= \left[\mathcal{R}e\left\{a(t)\, e^{j\phi(t)}\right\} + \varepsilon_i\right] \cdot \cos\omega_c t - \left[Im\left\{a(t)\, e^{j\phi(t)}\right\} + \varepsilon_q\right] \cdot \sin\omega_c t \\ &= \mathcal{R}e\left\{a(t)\, e^{j\phi(t)}\right\}\cos\omega_c t - Im\left\{a(t)\, e^{j\phi(t)}\right\}\sin\omega_c t + \varepsilon_i \cos\omega_c t - \varepsilon_q \sin\omega_c t \\ &= \mathcal{R}e\left\{a(t)\, e^{j[\phi(t)+\omega_c t]}\right\} + \alpha\cos(\omega_c t + \gamma), \end{aligned} \tag{5.35}$$

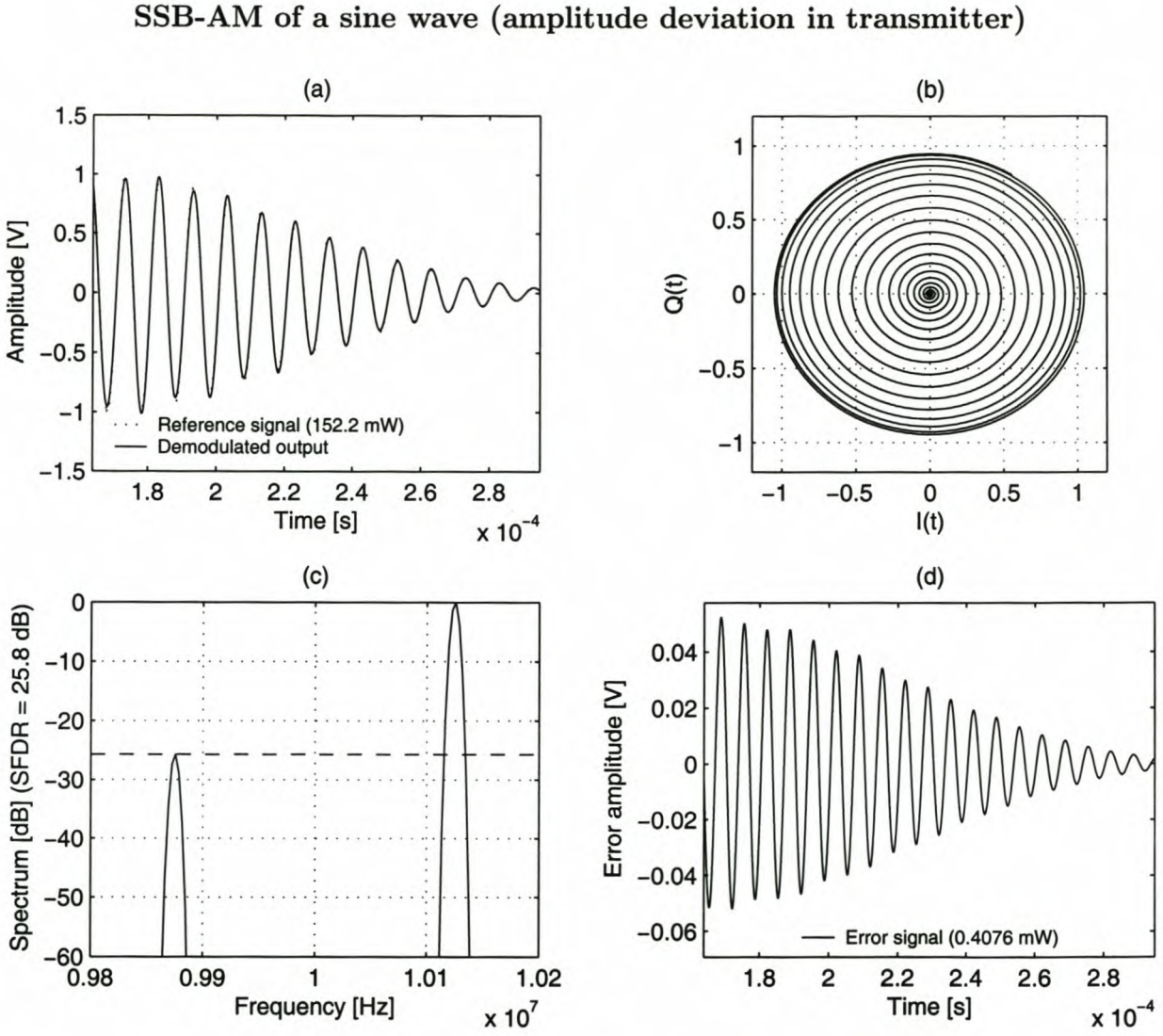

Figure 5.14: *Simulation of SSB amplitude modulation, with the transmitter's I-channel amplitude amplified by 10.8%. The carrier frequency offset is 25 kHz above the mixing frequency. (a) A decaying sine wave was used as modulating input signal. The output shows the greatest modulation errors near the signal peaks. (b) The inwardly-spiralling phasor is stretched horizontally due to the amplitude mismatch. (c) The amplitude mismatch causes a spurious sideband to appear. (d) The error signal shows both positive and negative excursions, and is proportional in magnitude both to the amount of amplitude mismatch and to the instantaneous amplitude of the modulating signal.*

Simulation reference: `ampdevssb`

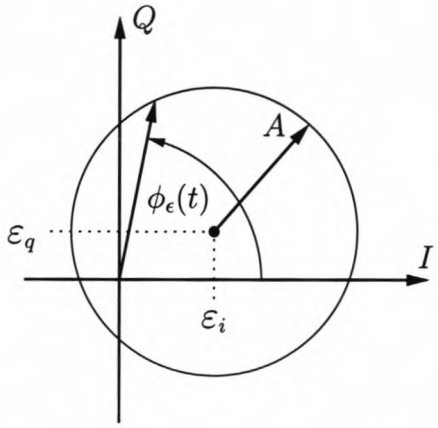

Figure 5.15: *The effect of DC offset and oscillator leakthrough on the I-Q phasor's locus, drawn for* $a(t) = A$.

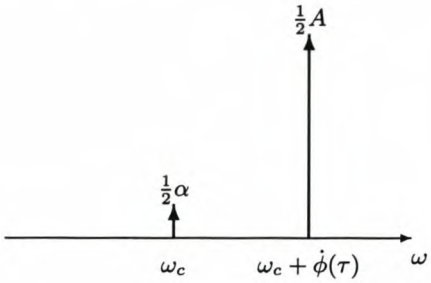

Figure 5.16: *LO leakthrough and DC offset both cause a frequency component to appear at the carrier frequency.*

with

$$\alpha = \sqrt{\varepsilon_i^2 + \varepsilon_q^2} \tag{5.36}$$

$$\gamma = \arctan \frac{\varepsilon_q}{\varepsilon_i}. \tag{5.37}$$

This leads to a very interesting result: When DC offset occurs on one or both of the I-Q channels, a spurious signal of constant amplitude and frequency is added to the RF output. This signal's frequency is exactly the carrier frequency, and its amplitude is equal to the displacement in the phasor diagram. Its phase, relative to the I-axis, is determined by the direction in which the locus is displaced from the origin.[6] Local oscillator leakthrough effectively takes place. Stated otherwise, local oscillator leakthrough and DC offset on the I-Q channels have exactly the same type of effect on the output signal.

[6]Note that Equations 5.35 and 5.37 assume no quadrature phase error in the quadrature mixing process. If quadrature phase error is present, it also affects the magnitude and phase of any carrier leakthrough component caused by DC offset. In such a case, $\alpha\cos(\omega_c t + \gamma)$ must be calculated by the full vector sum $\varepsilon_i \cos\omega_c t - \varepsilon_q \sin(\omega_c t - \lambda)$.

The frequency spectrum of a quadrature signal modulated with an I or Q offset follows directly from Equation 5.35. A single frequency component, with amplitude and phase as given by Equations 5.36 and 5.37, appears at the centre frequency. The SFDR is simply the ratio between the signal's maximum amplitude A, and this component's amplitude:

$$\mathrm{SFDR}_{\varepsilon} = 20 \log \left(\frac{A}{\alpha} \right) . \tag{5.38}$$

A simulation of a single transmitted tone with DC offset is shown in Figure 5.17. In this experiment, $\varepsilon_i = 0.15$ and $\varepsilon_q = 0.05$. This should produce a carrier component with amplitude $\alpha = 0.158$. According to Equation 5.38, this corresponds to an SFDR of 16.0 dB, which is exactly what is seen in the simulation. Although the spur is caused by DC offset, it is indistinguishable for oscillator leakthrough, as it lies precisely at the oscillator frequency.

5.6.2 Combined transmitter-receiver distortion

A downmixed receiver signal is likely to see a combination of DC offsets on the transmitter and receiver baseband signals, and oscillator leakthrough at both the transmit and receive mixer. In this section, it will be shown that, assuming coherent reception, all these non-idealities can be seen as a single DC offset on each baseband receiver channel. Even for non-coherent reception, the theory presented here makes it possible to model receiver distortion as if it originated in a coherent transmitter, allowing the reuse of transmitter distortion theory for the non-ideal receiver case.

When LO leakthrough (or I-Q DC offset) occurs in the transmission stage as well as in the reception stage, the received RF signal, prior to quadrature downmixing, is of the form

$$y(t) = \mathcal{R}e\left\{ a(t)\, e^{j[\phi(t)+\omega_c t]} \right\} + \alpha_{\mathrm{tx}} \cos(\omega_c t + \gamma_{\mathrm{tx}}) + \alpha_{\mathrm{rx}} \cos(\omega_c t + \gamma_{\mathrm{rx}}) , \tag{5.39}$$

where the oscillator leakthrough in the receiver has already been included. After downmixing, with the inclusion of I-Q DC offset in the receiver stage, the complex baseband signal can be written as

$$\begin{aligned} s(t) &= a(t)e^{j\phi(t)} + \alpha_{\mathrm{tx}} e^{j\gamma_{\mathrm{tx}}} + \alpha_{\mathrm{rx}} e^{j\gamma_{\mathrm{rx}}} \\ &= a(t)e^{j\phi(t)} + (\varepsilon_{i_{\mathrm{tx}}} + \varepsilon_{i_{\mathrm{rx}}}) + j(\varepsilon_{q_{\mathrm{tx}}} + \varepsilon_{q_{\mathrm{rx}}}) . \end{aligned} \tag{5.40}$$

From Equation 5.40, it can be seen that the total DC offset and LO leakthrough in the system manifests as a net DC offset in the receiver I and Q channels.

Once again, it will be shown in Section 6.6 that the coherent-carrier assumption ($\hat{\omega}_c = \omega_c$) is strictly necessary for this simplification to hold. As was the case for amplitude deviation, it is always possible to combine total quadrature distortion effects at either the transmitter or receiver. In the more general case where the mixer frequencies differ, transmitter and receiver distortion effects must be modelled (and compensated for) separately. Even then, the result presented here provides a way to reuse transmitter distortion analyses, even when the distortion takes place in the receiver.

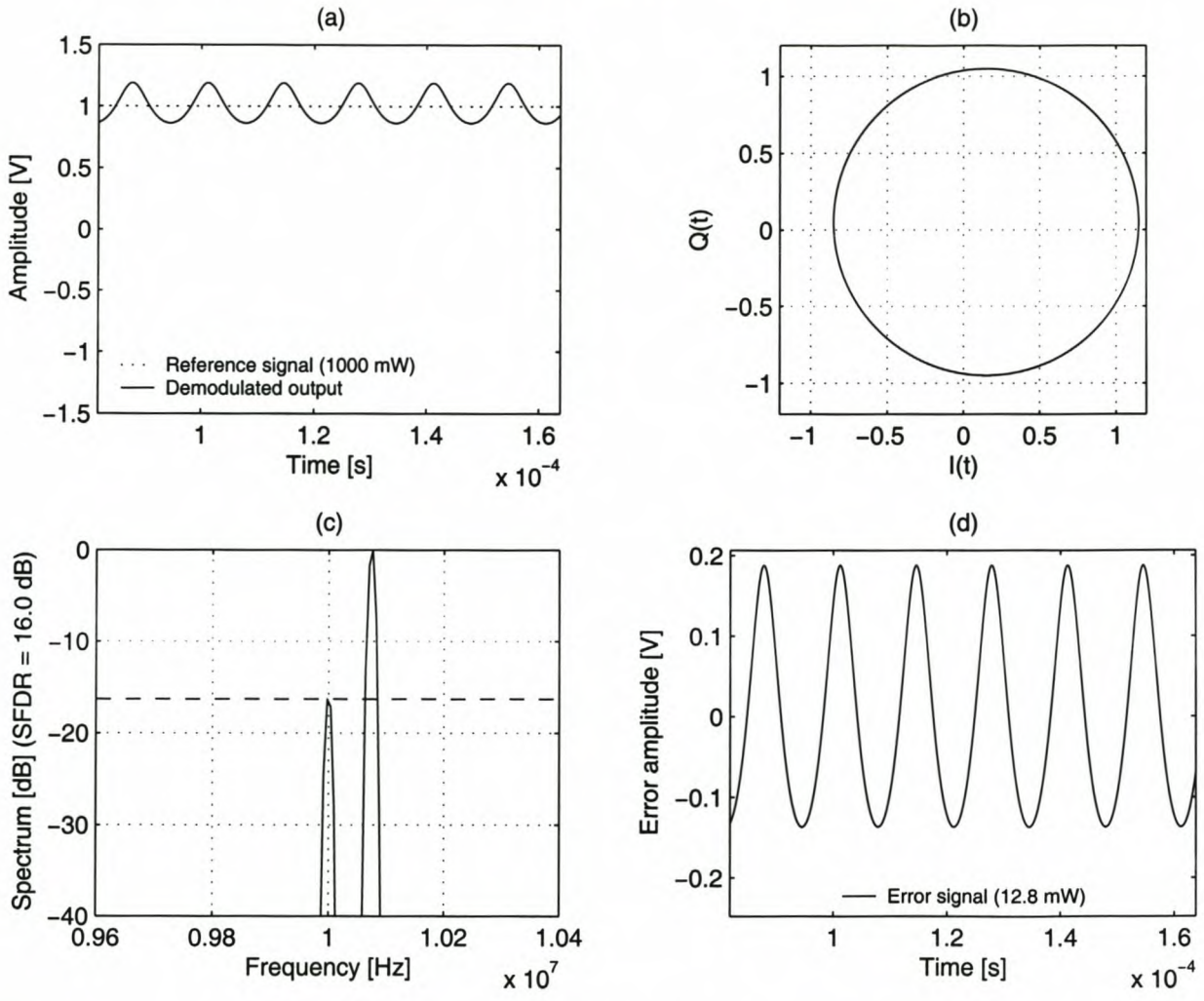

Figure 5.17: *Simulation of frequency modulation of an input DC signal, with DC offset on the transmitted baseband I and Q channels. 75 kHz frequency deviation was employed. (a) The demodulated signal shows an undesired 75-kHz oscillation, which is at its worst at the maximum excursions of the desired signal. (b) The received signal's phasor has shifted proportional to the DC offsets on the channels, but remains circular. (c) The DC offsets produce a spur at the carrier, indistinguishable from LO leakthrough. The spur lies 16 dB below the desired signal. (d) The error signal is not completely sinusoidal.*

Simulation reference: `ofserrdc`

5.6.3 Frequency spectrum of the downmixed signal

Equation 5.40 shows that LO leakthrough and DC offset cause a complex-valued DC offset to appear in the baseband receiver signal. This spurious component reduces the received SFDR of the system, and its effect on various modulation schemes will be investigated next.

5.6.4 Case studies

The general analysis presented above for baseband DC offset and RF oscillator leakthrough in quadrature mixers will now be applied to three practical analogue modulation schemes.

Frequency modulation

To investigate the effect of DC offset and oscillator leakthrough on the information in an FM signal, the distortion of the modulated signal's instantaneous frequency, as caused by the spurious carrier component, must be established. For this analysis, let the signal amplitude $a(t) = 1$. In Figure 5.15, the distorted phasor's phase angle is given by

$$\phi_\epsilon(t) = \arctan \frac{\sin\phi(t) + \varepsilon_q}{\cos\phi(t) + \varepsilon_i}. \tag{5.41}$$

As was done in Equation 5.22, the time derivative of Equation 5.41 can be taken to find the distorted phasor's frequency in terms of the desired frequency:

$$\frac{d\phi_\epsilon(t)}{dt} = \left(\frac{\varepsilon_i \cos\phi(t) + \varepsilon_q \sin\phi(t) + 1}{\varepsilon_i^2 + 2\varepsilon_i \cos\phi(t) + 2\varepsilon_q \sin\phi(t) + \varepsilon_q^2 + 1} \right) \cdot \frac{d\phi(t)}{dt}. \tag{5.42}$$

The factor in brackets in Equation 5.42 is best interpreted visually. Figure 5.18 shows a plot of Equation 5.42 for various values of the displacement factor α (in each case, the displacement angle was $\gamma = 0$ rad). For small offset errors, the error factor can be approximated by a sine wave. Larger displacements cause a decrease in demodulated amplitude near $\phi(t) = \gamma$ rad, and a sudden increase in frequency in the region near $\phi(t) = \gamma + \pi$ rad. As α approaches one, the demodulated amplitude is halved over a large region, with a sharp output spike at $\phi(t) = \gamma + \pi$ rad. For α greater than one (an unlikely scenario in a practical system), the error factor approaches an impulse function.

To determine distortion of the demodulated FM signal due to offset errors and LO leakthrough, Equation 5.42 must first be written in terms of the desired signal component and the error signal. To simplify the analysis, assume that ε_q is zero.[7] It then follows that

$$\frac{d\phi_\epsilon(t)}{dt} = \overbrace{\frac{d\phi(t)}{dt}}^{\text{desired demodulated signal}} - \underbrace{\left(\frac{\varepsilon_i + \cos\phi(t)}{\varepsilon_i + 2\cos\phi(t) + \varepsilon_i^{-1}} \right) \frac{d\phi(t)}{dt}}_{\text{error signal}}. \tag{5.43}$$

[7]This is equivalent to ignoring the phase of the error signal, and defining ε_i as the geometric mean of the I and Q offsets. It is a fair assumption, since the carrier phase can be assumed to be independent of the modulating signal information.

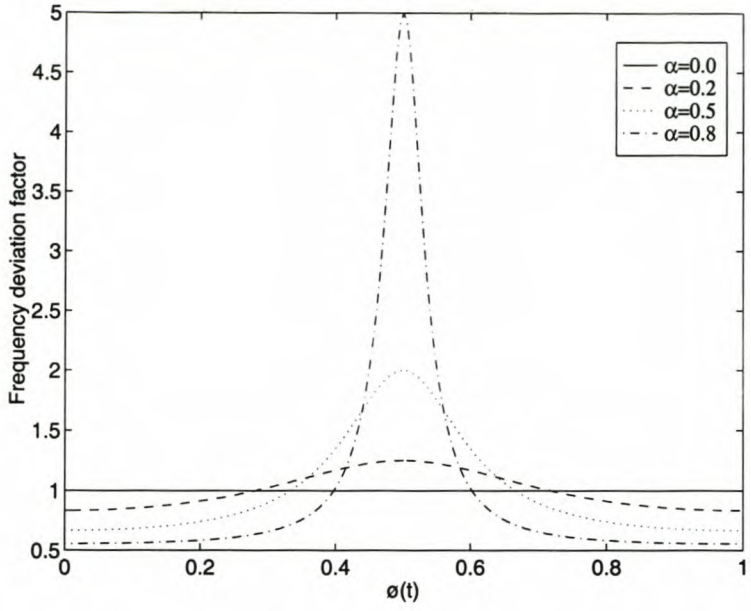

Figure 5.18: *The distortion wave $\dot{\phi}_\epsilon(t)/\dot{\phi}(t)$ for various values of the offset amplitude α (the x-axis was normalised by dividing by 2π)*

For small ε_i, the term ε_i^{-1} dominates the denominator in this equation. This leads to the approximation

$$\frac{d\phi_\epsilon(t)}{dt} \approx \frac{d\phi(t)}{dt} - \left[\varepsilon_i^2 + \varepsilon_i \cos\phi(t)\right] \frac{d\phi(t)}{dt}\,. \tag{5.44}$$

If the offset errors are small, the following happens to the demodulated output signal:

- The output signal is attenuated to $1 - \varepsilon_i^2$ of its full strength.
- A sinusoidal error signal is added to the output signal.
- The error signal has a frequency equal to the speed of phasor rotation—the phasor rotation "leaks" into the demodulated signal.
- The maximum amplitude of this sinusoidal error signal is equal to ε_i.
- The error signal is amplitude-modulated with the desired output signal. In other words, it is at its largest at the peaks and troughs of the modulating signal, $m(t)$, and zero when $m(t) = 0$.

Consequently, the error signal observed in the presence of offset error or quadrature leakthrough has the same basic form as that produced by amplitude deviation (Figure 5.7, p. 48). However, it produces an error signal at the rate of phasor oscillation, whereas the amplitude-deviation error signal oscillates at double the phasor frequency.

The simulation on page 61 has already shown part of the effect of LO leakthrough on the demodulated signal. In this simulation, the error signal does oscillate at the phasor

frequency of 75 kHz, and remains at constant amplitude. This result reinforces the idea that quadrature errors produce phasor "leakthrough" into the demodulated FM signal.

Figure 5.19 shows another simulation of the effects of DC offset and oscillator leakthrough on an FM signal. In this experiment, a sinusoidal signal is used as modulating input. It further illustrates the effect of Equation 5.42: Since the error factor is multiplied with the modulating signal, the difference signal in Figure 5.19 appears modulated in amplitude. When Figure 5.19 is compared to a similar experiment with amplitude deviation (Figure 5.5, p. 44), it is observed that the latter has a double-frequency error signal, as expected.

Double-sideband AM

Next, the effect of DC offset and LO leakthrough on double-sideband amplitude modulated signals will be considered. Such signals form a special case of the analysis presented thus far, with $a(t) = m(t)$, the real-valued modulating signal.

It was shown above that DC offset and LO leakthrough both inject a carrier frequency into the modulated RF signal. Whilst this has a fairly complex effect on the instantaneous frequency of the signal, as defined for FM, the possible effects on AM signals are as follows:

1. If no channel selection or digital carrier frequency adjustment is performed ($\omega_0 = 0$ in Equations B.8 and B.9 on page 171), the carrier component changes the AM signal's modulation index, without affecting the SFDR.

2. If $\omega_0 \neq 0$, but ω_c still lies within the signal band, a spurious frequency is induced that distorts the signal information. The resulting SFDR is

$$\mathrm{SFDR}_\varepsilon = 20 \log \left(\frac{\overline{a(t)}}{\alpha} \right) \tag{5.45}$$

   from Equation 5.38.

3. If $|\omega_0|$ is greater than the signal bandwidth, the spurious component does not interfere with the generated signal. However, it could interfere with adjacent channels. In this case, the SFDR is as given in Equation 5.45.

After imperfect transmission with LO leakthrough, DC offset, or both, the upmixed DSB-AM signal is of the form predicted by Equation 5.35:

$$y(t) = a(t) \cdot \cos\left[(\omega_c + \omega_0)t + \phi_0\right] + \alpha \cos(\omega_c t + \gamma)\,. \tag{5.46}$$

Quadrature downmixing is performed as per Equation 2.21 (p. 17):

$$s(t) = 2\left[y(t) \cdot e^{-j\omega_c t}\right]_{\mathrm{LPF}}\,, \tag{5.47}$$

Where coherent downmixing has again been assumed.[8] This produces the complex baseband signal

$$s(t) = a(t) \cdot e^{j[\omega_0 t + \phi_0]} + \alpha e^{j\gamma}\,. \tag{5.48}$$

[8] See Section 5.3 on page 39.

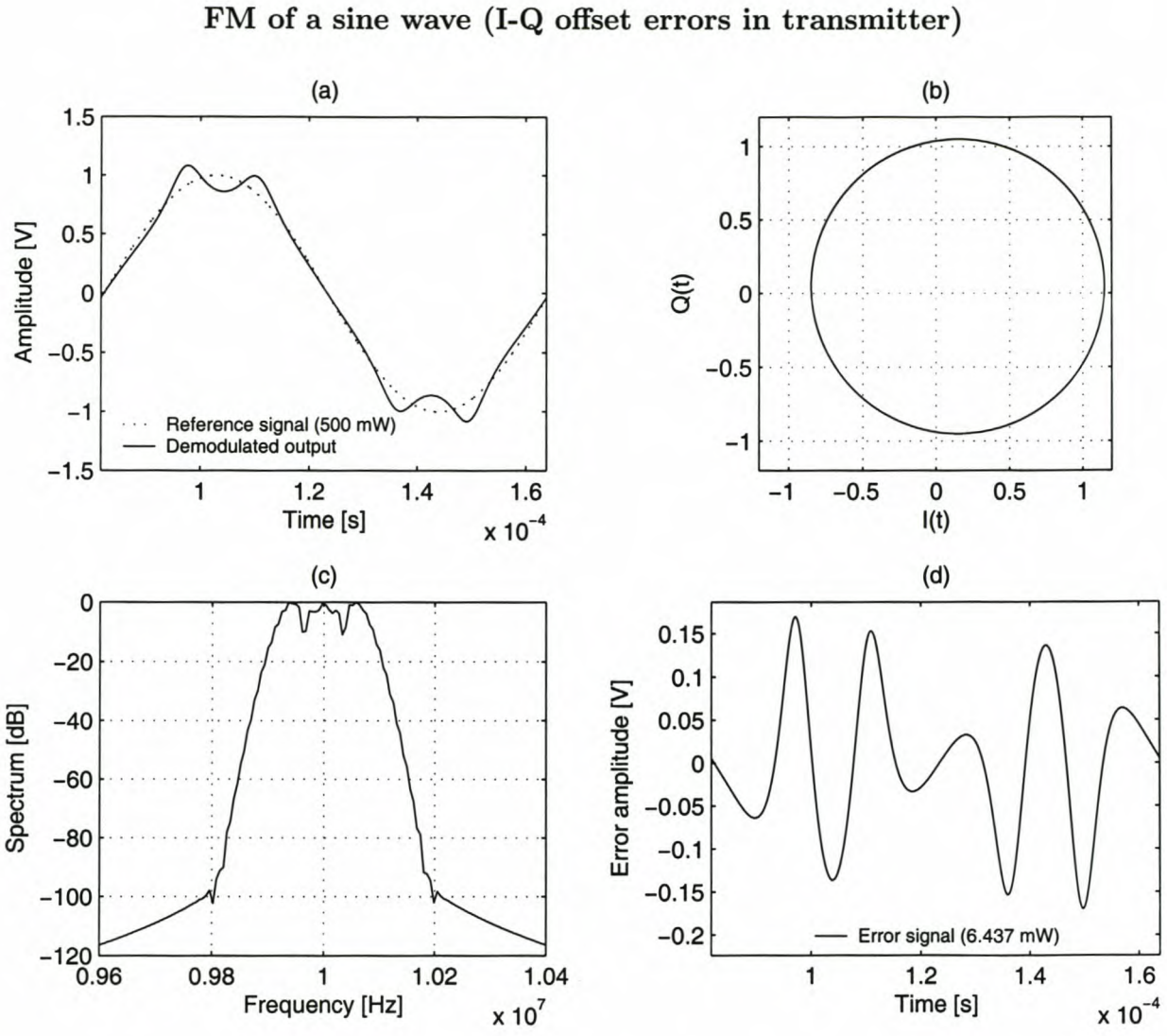

Figure 5.19: *Simulation of frequency modulation of an input sine wave, with DC offset on the transmitter's baseband I and Q channels (15% and 5%, respectively). 75 kHz frequency deviation was employed. (a) The demodulated signal shows an undesired 75-kHz oscillation, which is at its worst at the maximum excursions of the desired signal. (b) The received signal's phasor has shifted proportional to the DC offsets on the channels, but remains circular. (c) Because of the symmetry of the FM signal's spectrum, any spurious carrier component is obscured. (d) The error signal oscillates most rapidly and with highest amplitude near the desired signal's points of maximum excursion; at other points it is smaller, and oscillates slower (exactly equal to the speed of phasor rotation at that moment).*

Simulation reference: `ofserrfm`

The real and imaginary components of this complex-valued signal are

$$\begin{aligned} I(t) &= a(t)\cos(\omega_0 t + \phi_0) + \alpha\cos\gamma \\ &= a(t)\cos(\omega_0 t + \phi_0) + \varepsilon_i \qquad (5.49) \\ Q(t) &= a(t)\sin(\omega_0 t + \phi_0) + \alpha\sin\gamma \\ &= a(t)\sin(\omega_0 t + \phi_0) + \varepsilon_q\,. \qquad (5.50) \end{aligned}$$

It is shown in Section B.2.3 that a double-sideband AM signal can be demodulated by taking the magnitude of the complex-valued baseband signal.

$$m'(t) = \sqrt{I^2(t) + Q^2(t)}\,. \qquad (5.51)$$

When a carrier-leakthrough (or DC-offset) error is present, substitution of Equations 5.49 and 5.50 yields

$$m'^2(t) = a^2(t) + \alpha^2 + 2\alpha a(t)\cos(\omega_0 t + \phi_0 - \gamma)\,. \qquad (5.52)$$

This expression is best evaluated numerically, as in the simulation presented in Figure 5.20. The error signal is proportional in amplitude to α, and contains a strong 18.75-kHz component caused by the difference between the leakthrough carrier and the modulation carrier frequency offset. Also, the simulation again confirms the theorised relationship between DC offset and LO leakthrough. As per Equation 5.45, the vector magnitude of the offset is $\alpha = 0.1581$. The modulation carrier is $A = 0.5$, yielding

$$\mathrm{SFDR}_\epsilon = 20\log\left(\frac{0.5}{0.1581}\right) = 10.0\ \mathrm{dB}\,, \qquad (5.53)$$

which corresponds perfectly with the simulated SFDR.

A special case occurs when coherent demodulation of the AM signal is performed, with $\omega_0 = 0$ and $\phi_0 = \gamma$. Then Equation 5.52 becomes

$$m'^2(t) = [a(t) + \alpha]^2 \qquad (5.54)$$

so that

$$m'(t) = a(t) + \alpha\,. \qquad (5.55)$$

This means that for a coherent receiver without digital channel selection ($\omega_0 = 0$), LO leakthrough and DC offset simply produce DC offset in the received DSB-AM signal.

Single-sideband AM

A received single-sideband AM signal with transmitter LO leakthrough or DC offset is given by Equation 5.35 with $a(t) = \tilde{m}(t)$, which can be simplified to

$$\begin{aligned} f(t) &= m(t)\cdot\cos\left[(\omega_c + \omega_0)t + \phi_0\right] - \hat{m}(t)\cdot\sin\left[(\omega_c + \omega_0)t + \phi_0\right] \\ &\quad + \alpha\cos(\omega_c t + \gamma)\,. \qquad (5.56) \end{aligned}$$

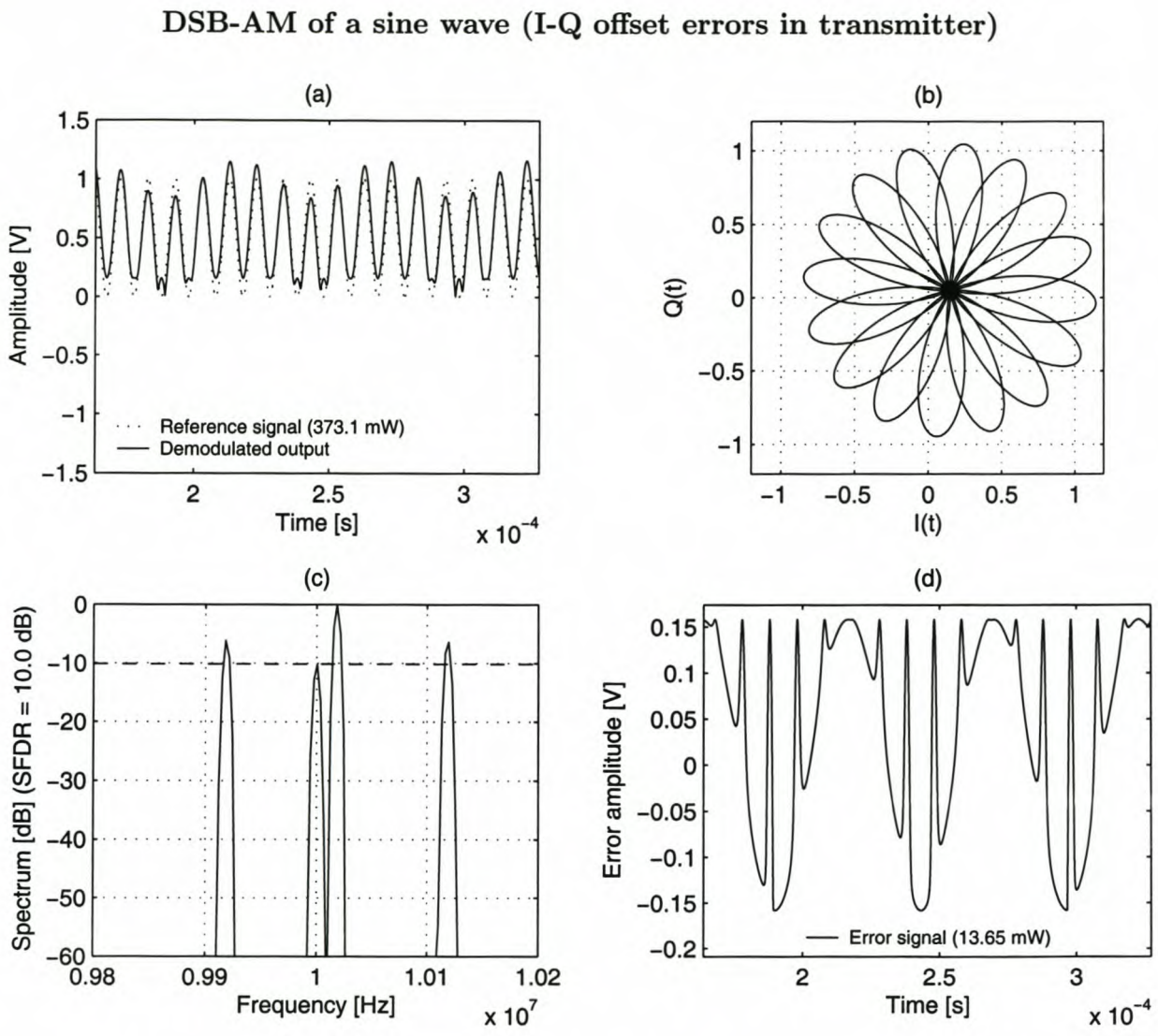

Figure 5.20: *Simulation of a DSB amplitude-modulated sine wave, with DC offset on the transmitter's baseband I and Q channels (15% and 5%, respectively). In this simulation, the carrier frequency was chosen to be 18.75 kHz above the mixing frequency of 10 MHz. (a) The demodulated signal shows considerable distortion, and the 18.75 kHz difference between the carrier frequency and the spurious component, translates into a 18.75-kHz "drift" in the demodulated signal. (b) The flower-shaped phasor of Figure B.3 has been shifted proportional to the DC offset. (c) After quadrature mixing, the DC offset in the baseband channels produces a strong spurious component at the mixing frequency. (d) The error signal shows a 18.75-kHz base component, with sharp spikes superimposed at the modulating signal frequency. The points of maximum excursion are equal to the magnitude of the complex-valued offset vector.*

Simulation reference: `ofserram`

This predicted spectrum may be verified by the simulation presented in Figure 5.21 (p. 69). A spurious component appears at the carrier frequency, with magnitude

$$\alpha = \sqrt{\varepsilon_i^2 + \varepsilon_q^2} = \sqrt{0.15^2 + 0.05^2} = 0.1581\,, \tag{5.57}$$

which, by Equation 5.45, corresponds to a carrier leakthrough component 16.0 dB below the fundamental. This is exactly what is observed in the simulation.

After quadrature downmixing (Equation 2.21) with a coherent carrier, the complex-valued baseband signal is

$$s(t) = m(t) \cdot e^{j[\omega_0 t + \phi_0]} - \hat{m}(t) \cdot e^{j\left[\omega_0 t + \phi_0 - \frac{\pi}{2}\right]} + \alpha e^{j\gamma}\,. \tag{5.58}$$

It is shown in Equation B.24 (p. 178) that an SSB signal can be demodulated by phase-locking onto its carrier, and performing complex coherent demodulation:

$$m'(t) = \mathcal{R}e\left\{s(t) \cdot e^{-j[\omega_0 t + \phi_0]}\right\}\,. \tag{5.59}$$

In this case, ideal phase locking has been assumed. Because the demodulation process described by Equation 5.59 is linear, the desired signal and LO leakthrough component can be considered separately. Ideal phase locking produces perfect reconstruction of the desired signal component. The error signal component then is

$$\begin{aligned} m_\epsilon(t) &= \mathcal{R}e\left\{\alpha e^{-j(\omega_0 t + \phi_0 - \gamma)}\right\} \\ &= \alpha \cos(\omega_0 t + \phi_0 - \gamma)\,. \end{aligned} \tag{5.60}$$

It can be concluded that LO leakthrough (or DC offset in the transmitter I and Q signals) produce an error tone in the demodulated signal equal to ω_0 (the difference between the receiver oscillator frequency and the SSB carrier offset). This is seen, for example, in the error signal from the simulation shown on page 69. In the special case where the receiver oscillator is exactly equal to the SSB carrier, a DC offset is produced in the demodulated signal.

5.7 Error in phase angle

The signal and spectral distortion of quadrature amplitude mismatch, DC offset and LO leakthrough have been investigated in some detail. The last type of quadrature non-ideality that must be investigated, is I-Q phase error.

The term *quadrature* implies that a system utilises two sinusoidal signals exactly $\pi/2$ radians out of phase. In a physical system, such a perfect phase relationship is virtually impossible to achieve. It is quite likely that a phase error could occur at either the I-Q input or output channels, or in the quadrature local oscillator signals. The phase accuracy of output I-Q channels is generally determined by the accuracy of the accumulator and the sine approximation, and is usually relatively accurate. It is more likely for a fairly large phase error to be present in the quadrature local oscillator signals. It is reasonable to suspect,

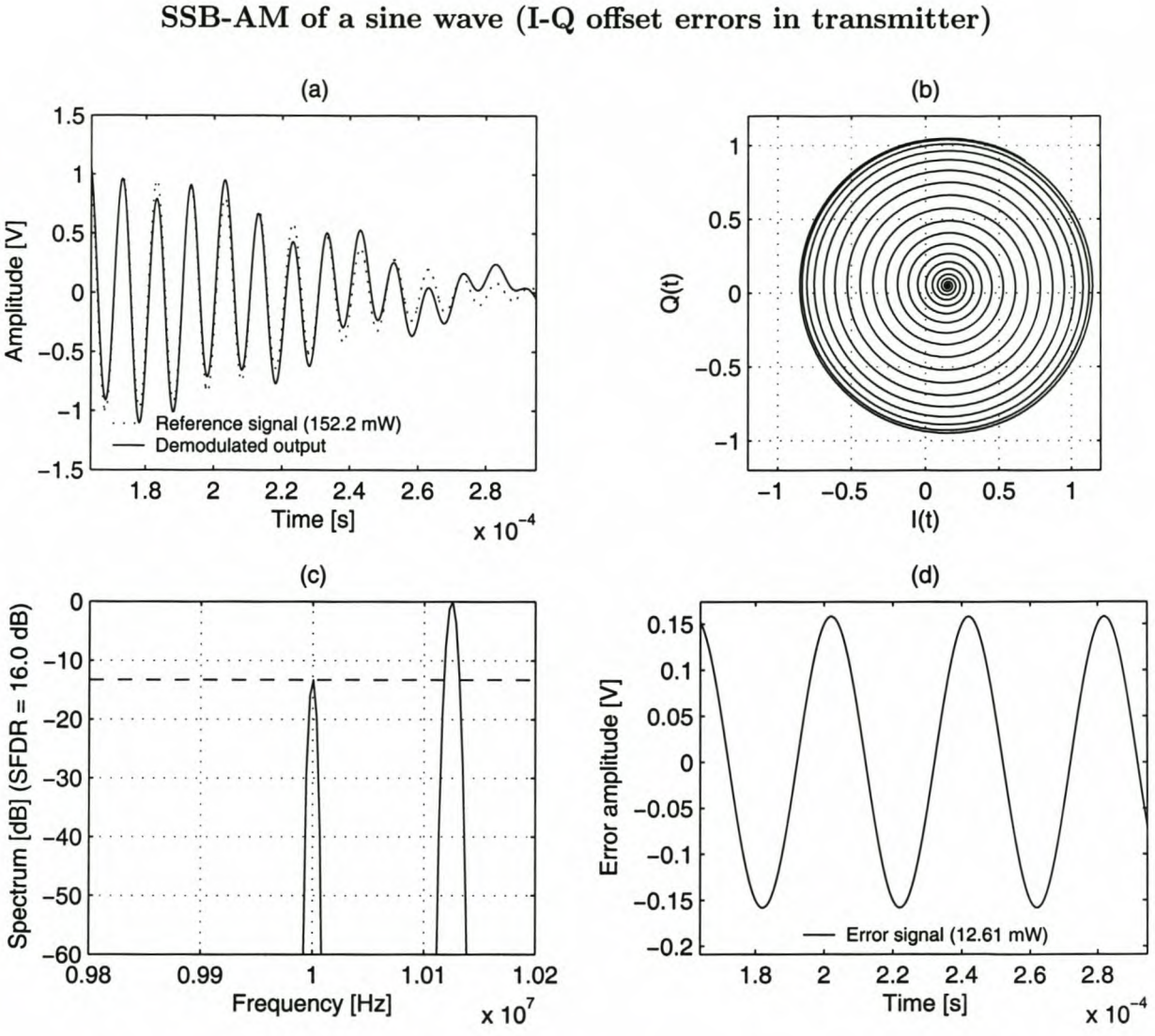

Figure 5.21: *Simulation of SSB amplitude modulation, with DC offset on the transmitter's baseband I and Q channels. The carrier frequency offset is 25 kHz above the mixing frequency. (a) The demodulated signal shows significant distortion. (b) The inwardly-spiralling phasor is shifted proportional to the DC offset. (c) The DC offset on the I-Q channels causes a spurious frequency component to appear at the mixing frequency. (d) Since the mixing frequency differs from the SSB carrier offset frequency by 25 kHz, the error signal manifests itself as a pure 25-kHz tone that is induced in the demodulated signal.*

Simulation reference: `ofserrssb`

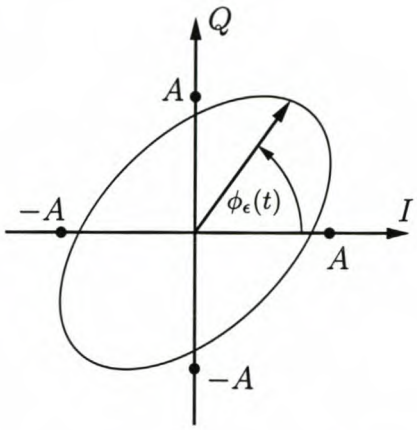

Figure 5.22: *The effect of phase error on the I-Q phasor's locus, drawn for* $a(t) = A$.

however, that a purposely generated phase error in the I-Q channels could in some way be used to compensate for an unwanted phase error in the mixing circuit.

Of the two types of quadrature phase error, baseband I-Q phase error may be defined as follows:

$$\begin{aligned} I(t) &= \mathcal{R}e\left\{a(t)\, e^{j\phi(t)}\right\} \\ Q(t) &= Im\left\{a(t)\, e^{j[\phi(t)-\kappa]}\right\} . \end{aligned} \tag{5.61}$$

Here the quadrature-phase signal of the baseband system lags the in-phase signal by κ radians. An equivalent definition (that will be used in the next section) is

$$\begin{aligned} I(t) &= \mathcal{R}e\left\{a(t)\, e^{j[\phi(t)+\kappa]}\right\} \\ Q(t) &= Im\left\{a(t)\, e^{j\phi(t)}\right\} . \end{aligned} \tag{5.62}$$

A similar phase error in the quadrature mixer may be defined as

$$\begin{aligned} M_I(t) &= \cos\omega_c t \\ M_Q(t) &= \sin(\omega_c t - \lambda) \end{aligned} \tag{5.63}$$

or, equivalently,

$$\begin{aligned} M_I(t) &= \cos(\omega_c t + \lambda) \\ M_Q(t) &= \sin\omega_c t . \end{aligned} \tag{5.64}$$

In some analyses, it will also prove convenient to divide the phase error equally between the I and Q signals. The relationship between phase error in the baseband signals and phase error in the local oscillator will be investigated next.

Figure 5.22 demonstrates the effect of phase error on the quadrature phasor's locus. As was the case for amplitude deviation, the locus turns into an ellipse, but for phase error, the ellipse's major axis is rotated anticlockwise through $\pi/4$ radians (for $\kappa, \lambda < 0$) or $-\pi/4$ radians (for $\kappa, \lambda > 0$). Stated differently, the major axis of the ellipse lies either on the line $Q(t) = I(t)$, or on the line $Q(t) = -I(t)$. The larger the phase error, the greater the ellipse's eccentricity; at $\kappa, \lambda = \pm\pi/2$ radians, the ellipse collapses to a straight line.

5.7.1 Baseband and oscillator phase error

Before the effects of the phase error on different signals are investigated, it is necessary to investigate the relationship between phase error in the baseband I-Q signals on the one hand, and the quadrature LO signals on the other. It will be shown that these two types of phase error cause identical effects in the RF and demodulated signals.

Firstly, assume that a quadrature phase error of κ radians occurs at the in-phase output of a quadrature transmitter, $I(t)$. Also, the quadrature mixer has a phase inaccuracy of λ radians at the quadrature output, $M_Q(t)$. Because the mixer is of the multiply-and-subtract type, the resultant RF signal is

$$y(t) = \mathcal{R}e\left\{a(t)\, e^{j[\phi(t)+\kappa]}\right\} \cos\omega_c t - Im\left\{a(t)\, e^{j\phi(t)}\right\} \sin(\omega_c t - \lambda)\,. \tag{5.65}$$

But

$$\sin(\omega_c t - \lambda) = \sin\omega_c t\, \cos\lambda - \cos\omega_c t\, \sin\lambda \tag{5.66}$$

and

$$\mathcal{R}e\left\{a(t)\, e^{j[\phi(t)+\kappa]}\right\} = \cos\kappa \cdot \mathcal{R}e\left\{a(t)\, e^{j\phi(t)}\right\} - \sin\kappa \cdot Im\left\{a(t)\, e^{j\phi(t)}\right\}\,. \tag{5.67}$$

Substitution and simplification produces

$$\begin{aligned} y(t) \;=\; & \cos\kappa \cdot \mathcal{R}e\left\{a(t)\, e^{j\phi(t)}\right\} \cos\omega_c t \;-\; \cos\lambda \cdot Im\left\{a(t)\, e^{j\phi(t)}\right\} \sin(\omega_c t) \\ & - (\sin\kappa - \sin\lambda) \cdot Im\left\{a(t)\, e^{j\phi(t)}\right\} \cos\omega_c t\,. \end{aligned} \tag{5.68}$$

This can be compared to the desired (error-free) RF output of

$$y_o(t) = \mathcal{R}e\left\{a(t)\, e^{j\phi(t)}\right\} \cos\omega_c t \;-\; Im\left\{a(t)\, e^{j\phi(t)}\right\} \sin(\omega_c t)\,. \tag{5.69}$$

It may be observed that phase error in the baseband I-Q signals, and phase error in the quadrature LO signals, cause similar effects and their effects are cumulative. In particular, by selecting $\kappa = \lambda$, it would seem to be possible to use phase error in the baseband signals to negate the effects of phase error in the quadrature mixer—a topic that will be pursued further in Chapter 6.

In the remainder of the section, phase error in the baseband signals and mixer will mostly be treated interchangably, since they cause identical effects in the RF signal. The quadrature demodulation case may be analysed by a similar argument.

5.7.2 Frequency spectrum of the upmixed signal

To analyse the frequency spectrum of the modulated signal, first write out the upmixed signal:

$$y(t) = \mathcal{R}e\left\{a(t)\, e^{j\phi(t)}\right\} \cos\omega_c t - Im\left\{a(t)\, e^{j[\phi(t)-\kappa]}\right\} \sin\omega_c t\,. \tag{5.70}$$

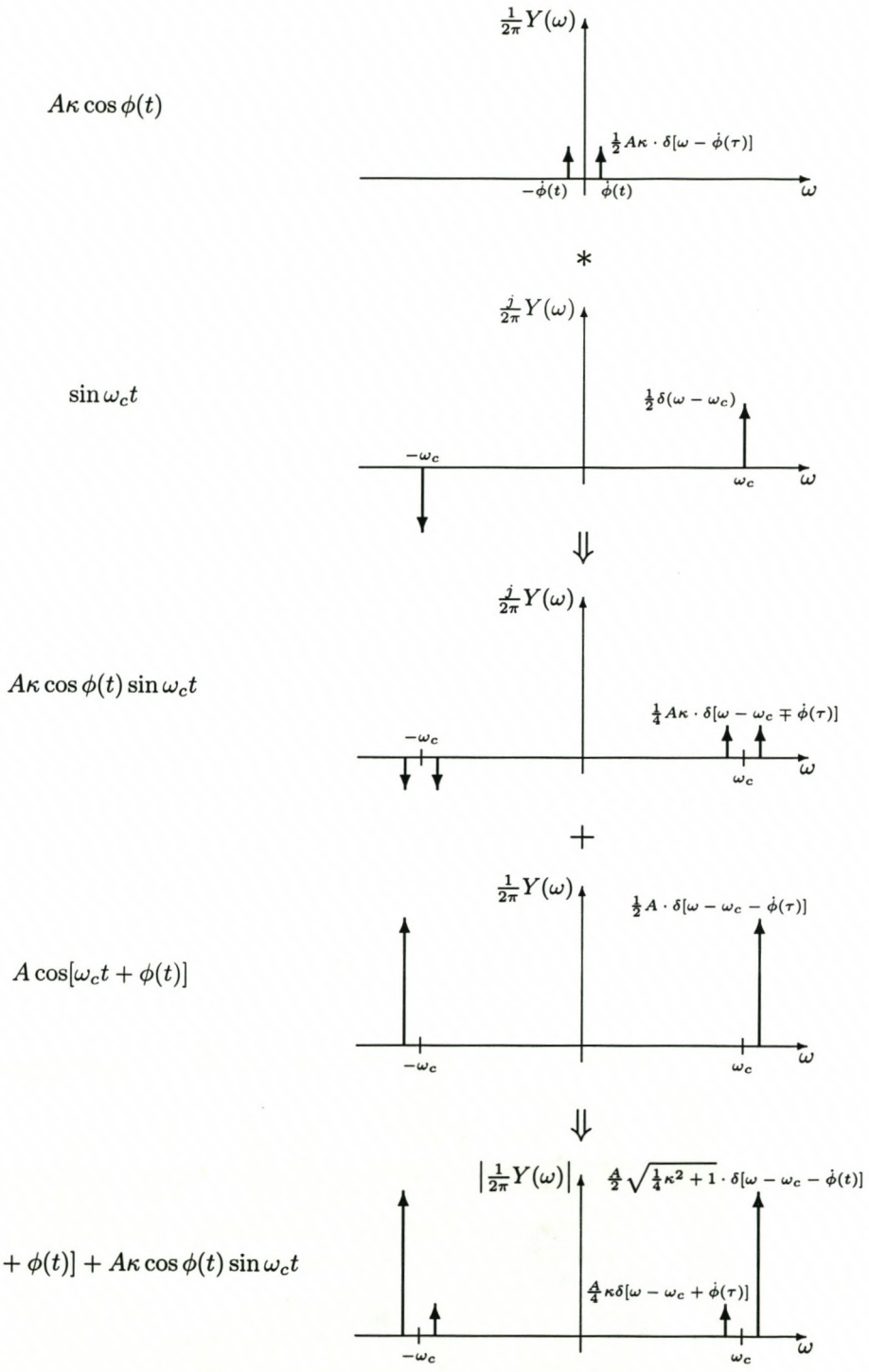

Figure 5.23: *Frequency diagram of I-Q mixing with small angular error.*

For small κ, $\sin\kappa \approx \kappa$ and $\cos\kappa \approx 1$ so that

$$y(t) \approx y_d(t) \; + \; \kappa \cdot \mathcal{R}e\left\{a(t)e^{j\phi(t)}\right\} \sin\omega_c t\,, \tag{5.71}$$

where $y_d(t)$ denotes the desired upmixed signal.

Figure 5.23 shows an analysis of this signal in the frequency domain (similar to the analysis done for amplitude deviation on page 46). In this figure, the (possibly complex-valued) amplitude $a(t)$ varies slowly enough to make the approximation $a(t) = A$ in the Fourier time window.

The spectral magnitude shown in the bottom graph is the magnitude of the phasor sum of the previous graphs. The desired signal peak is somewhat larger than would have been the case if κ were zero. A small sideband peak appears at a frequency symmetrical to the desired signal, with the carrier frequency as reflection point. This is a similar effect to what was found with amplitude deviation—this is to be expected, because the phasor locus has a similar (although rotated) shape.

The ratio between the desired signal peak and the spurious component, assuming a small phase error, is

$$\mathrm{SFDR}_\kappa = 20\log\left(\frac{\sqrt{\kappa^2+4}}{|\kappa|}\right). \tag{5.72}$$

κ must be measured in radians for this equation to hold.

Figure 5.24 (p. 74) illustrates the effect of quadrature phase error on single-tone synthesis. In this experiment, a phase error of 10° (0.1745 rad) occurred in the transmitter oscillator signals. As expected, a spur appears in the upmixed signal spectrum, symmetrical to the desired signal. According to Equation 5.72, the spur should lie 21.2 dB below the fundamental signal. This is what is observed in Figure 5.24, which supports the presented theory. Also, the baseband phasor takes on the shape of a tilted ellipse, as was hypothesised.

It was stated in Section 5.7.1 that baseband and oscillator phase error cause similar effects in the frequency spectrum. This is verified by the simulation shown in Figure 5.25 (p. 75). In this experiment, a 5° (87.27 mrad) phase error was generated in the I-Q baseband signals. According to the theory developed in this section, this should correspond to a spur with magnitude

$$S_{\kappa_1} = \frac{|\kappa_1|}{\sqrt{\kappa_1^2+4}} = 4.36\% \tag{5.73}$$

of the fundamental. The negative sideband caused by this phase error is indistinguishable from negative-frequency components in the desired signal, hence any additional spurious components caused by further non-idealities may be considered independent and cumulative to this spur. Therefore, the 5° phase error in the quadrature oscillators produce an additional spurious component at 4.36% of the fundamental signal amplitude. The total sideband spur must then be

$$\mathrm{SFDR}_\kappa = -20\log(8.72/100) = 21.2\ \mathrm{dB}\,. \tag{5.74}$$

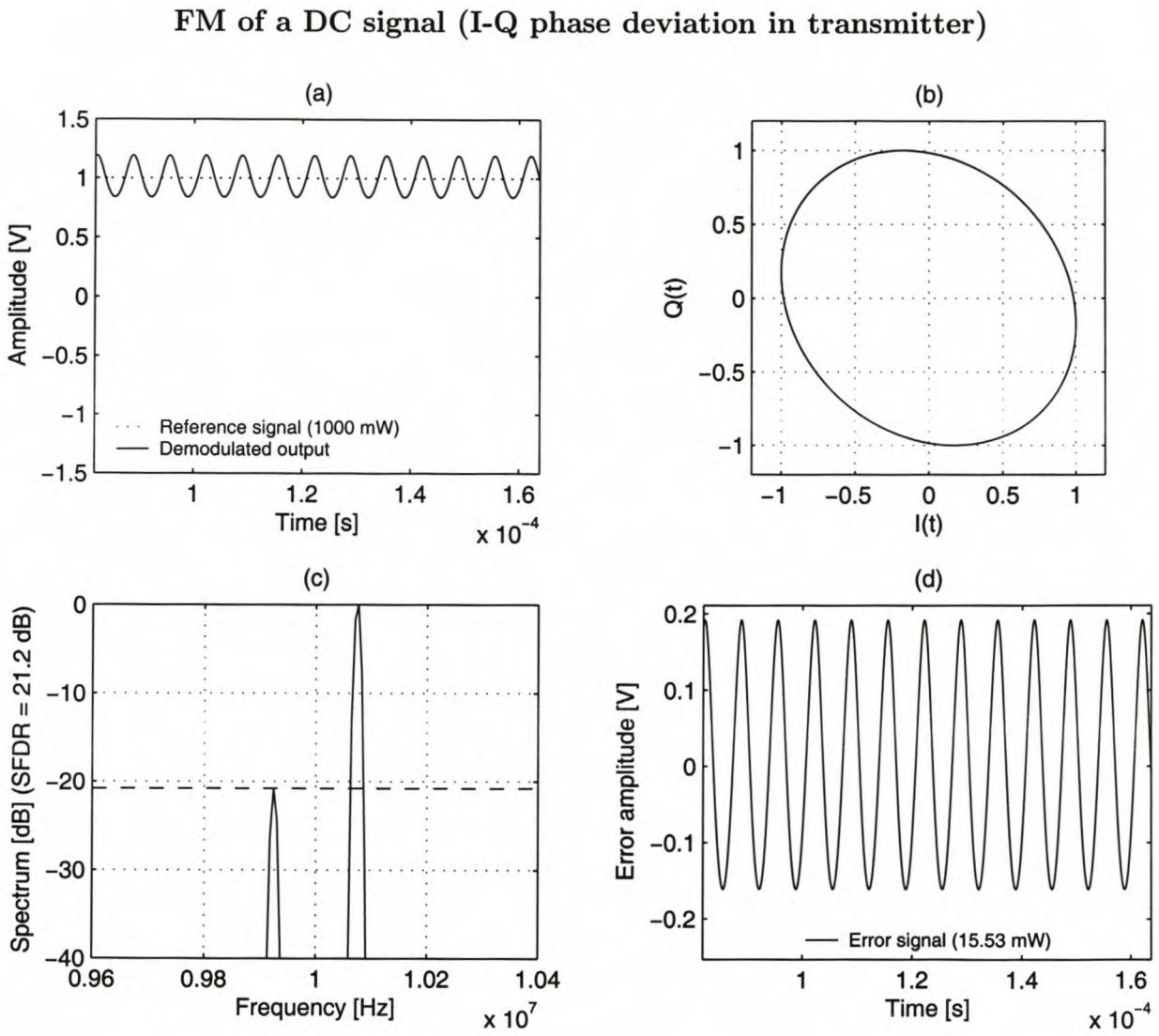

Figure 5.24: *Simulation of frequency modulation of an input DC signal, with the phase of $Q(t)$ lagging $I(t)$ by 10° in the quadrature upmixer. 75 kHz frequency deviation was employed. (a) The demodulated signal shows an undesired 150-kHz oscillation, which is at its worst at the maximum excursions of the desired signal. (b) Phase deviation produces an elliptical phasor locus in the received signal, rotated through 45°. (c) Like amplitude deviation, phase deviation produces a sideband component in the RF spectrum. In this case, the SFDR is 21 dB. (d) The 150-kHz sinusoidal error signal can be viewed as a "leakthrough" of the phasor rotation into the transmitted signal.*

Simulation reference: `phierrdc`

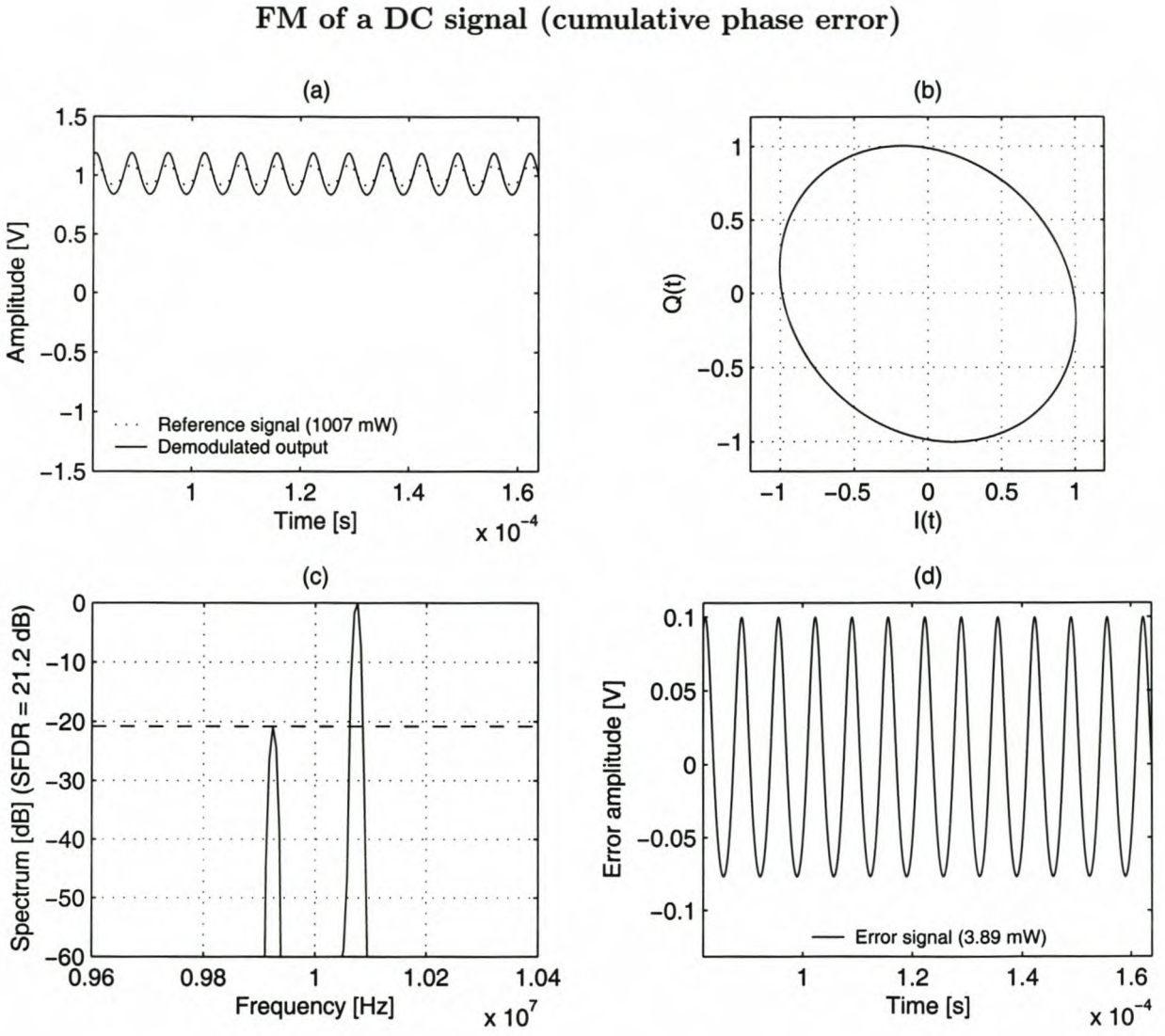

Figure 5.25: *Simulation of frequency modulation of an input DC signal with cumulative phase error. A* 5° *phase error existed in both the I-Q signals and the local oscillator signals of the transmitter. 75 kHz frequency deviation was employed. (a) The demodulated signal shows strong distortion.(b) The received signal's phasor is perfectly elliptical due to the transmitted phase error. (c) The RF spectrum shows a strong spurious sideband equivalent to that produced by a* 10° *phase error (see Figure 5.24, p. 74). (d) The error signal due to combined* 5°*-errors is identical to the error produced by a single* 10° *phase error (Figure 5.24). This strengthens the hypothesis that baseband and LO phase errors are produce equivalent, cumulative effects in the resultant signal.*

Simulation reference: `comptxphi`

This agrees with the spur observed in Figure 5.25(c). This result confirms that baseband and oscillator phase errors may be treated independently and equivalently, and that their cumulative contribution may be seen as a single phase error. In Chapter 6, it will be demonstrated that it is possible to use this idea to correct hardware phase inaccuracies, by causing a deliberate opposite phase error in the digitised signal.

5.7.3 Combined transmitter-receiver distortion

A quadrature baseband receiver signal may suffer from phase error effects originating in both the transmitter and the receiver. In this section, it will be demonstrated that these effects are cumulative for coherent demodulation. Also, it will be shown that quadrature phase error in the receiver can always be modelled as an equivalent phase error in a coherent transmitter, regardless of whether the true transceiver is coherent or not. This result allows the study of phase error effects to focus on transmitter non-idealities, because all results directly apply to the receiver as well.

For simplicity, it is assumed that all phase errors occur in the local oscillators of the quadrature mixers.[9] Also, the analysis is somewhat simpler if the phase error is split equally between the quadrature oscillators. The transmitter has quadrature local oscillators

$$\begin{aligned} M_I(t) &= \cos\left(\omega_c t + \tfrac{\lambda_{\text{tx}}}{2}\right) \\ M_Q(t) &= \sin\left(\omega_c t - \tfrac{\lambda_{\text{tx}}}{2}\right), \end{aligned} \tag{5.75}$$

and the receiver has

$$\begin{aligned} M_I(t) &= \cos\left(\omega_c t + \tfrac{\lambda_{\text{rx}}}{2}\right) \\ M_Q(t) &= \sin\left(\omega_c t - \tfrac{\lambda_{\text{rx}}}{2}\right). \end{aligned} \tag{5.76}$$

The transmitted baseband signal

$$s(t) = a(t)\, e^{j\phi(t)} = I_{\text{tx}}(t) + jQ_{\text{tx}}(t) \tag{5.77}$$

becomes, after quadrature upmixing with phase error λ_{tx},

$$y(t) = I_{\text{tx}}(t)\cos\left(\omega_c t + \tfrac{\lambda_{\text{tx}}}{2}\right) - Q_{\text{tx}}(t)\sin\left(\omega_c t - \tfrac{\lambda_{\text{tx}}}{2}\right). \tag{5.78}$$

After trigonometric manipulation, this RF signal can be written in the form

$$y(t) = \cos\left(\tfrac{\lambda_{\text{tx}}}{2}\right)\cdot y_d(t) + \sin\left(\tfrac{\lambda_{\text{tx}}}{2}\right)\cdot y_\epsilon(t), \tag{5.79}$$

where the first term contains the desired signal,

$$y_d(t) = I_{\text{tx}}(t)\cos\omega_c t - Q_{\text{tx}}(t)\sin\omega_c t, \tag{5.80}$$

[9] This does not affect the generality of the result—see page 71.

and the second term has an error component,

$$y_\epsilon(t) = Q_{\text{tx}}(t)\cos\omega_c t - I_{\text{tx}}(t)\sin\omega_c t\,. \tag{5.81}$$

The downmixed baseband channels at the receiver are given by

$$I_{\text{rx}}(t) = 2\left[y(t)\cos\left(\omega_c t + \tfrac{\lambda_{\text{rx}}}{2}\right)\right]_{\text{LPF}} \tag{5.82}$$

$$Q_{\text{rx}}(t) = -2\left[y(t)\sin\left(\omega_c t - \tfrac{\lambda_{\text{rx}}}{2}\right)\right]_{\text{LPF}}\,. \tag{5.83}$$

Substituting Equation 5.79 into Equations 5.82 and 5.83 yields the quadrature baseband receiver signals in terms of their transmitted counterparts:

$$I_{\text{rx}}(t) = \cos(\tfrac{\lambda_{\text{tx}}}{2} - \tfrac{\lambda_{\text{rx}}}{2})\cdot I_{\text{tx}}(t) + \sin(\tfrac{\lambda_{\text{tx}}}{2} + \tfrac{\lambda_{\text{rx}}}{2})\cdot Q_{\text{tx}}(t) \tag{5.84}$$

$$Q_{\text{rx}}(t) = \cos(\tfrac{\lambda_{\text{tx}}}{2} - \tfrac{\lambda_{\text{rx}}}{2})\cdot Q_{\text{tx}}(t) + \sin(\tfrac{\lambda_{\text{tx}}}{2} + \tfrac{\lambda_{\text{rx}}}{2})\cdot I_{\text{tx}}(t)\,. \tag{5.85}$$

Each baseband signal shows a desired component, plus undesired crosstalk from the other component. The result shows that combined transmitter-receiver phase error is indeed cumulative. Combined phase error may attenuate the desired signal, amplify the spurious signal, or both. For example, if $\lambda_{\text{tx}} = \lambda_{\text{rx}}$, the desired signal is not attenuated, but the crosstalk component is large. However, if $\lambda_{\text{tx}} = -\lambda_{\text{rx}}$, no error signal is present, but the desired signal is slightly attenuated. This last condition may be used to compensate for transmitter phase error by adding a deliberate phase error in a coherent-oscillator receiver, an idea that will be pursued further in Chapter 6.

The fact that receiver-transmitter phase error is cumulative means that their effects are identical in the demodulated signal. Hence, it is not necessary to investigate phase error in the receiver separately—all transmitter-related results apply. In a coherent transceiver, transmitter I-Q error, transmitter LO error, receiver LO error and receiver I-Q error may be modelled as a single parameter (e.g. as an equivalent transmitter LO error). Even in a non-coherent system, phase error in the receiver can be treated as if it were caused by an equivalent error in a fictional coherent transmitter, once again allowing the reuse of developed theory.

5.7.4 Frequency spectrum of the downmixed signal

The distorted baseband signals of Equations 5.84 and 5.85 show spurious crosstalk. The complex-valued baseband signal is

$$\begin{aligned} s'(t) &= I_{\text{rx}}(t) + jQ_{\text{rx}}(t) \\ &= \cos(\tfrac{\lambda_{\text{tx}}}{2} - \tfrac{\lambda_{\text{rx}}}{2})s(t) + j\sin(\tfrac{\lambda_{\text{tx}}}{2} + \tfrac{\lambda_{\text{rx}}}{2})s^*(t)\,. \end{aligned} \tag{5.86}$$

By substituting the desired signal $s(t) = a(t)\,e^{j\phi(t)}$,

$$s'(t) = \cos(\tfrac{\lambda_{\text{tx}}}{2} - \tfrac{\lambda_{\text{rx}}}{2})\cdot a(t)e^{j\phi(t)} + j\sin(\tfrac{\lambda_{\text{tx}}}{2} + \tfrac{\lambda_{\text{rx}}}{2})\cdot a^*(t)e^{-j\phi(t)}\,. \tag{5.87}$$

In terms of the frequency spectrum, this can be interpreted as follows: Quadrature phase error attenuates the desired signal slightly. Furthermore, a spurious sideband component

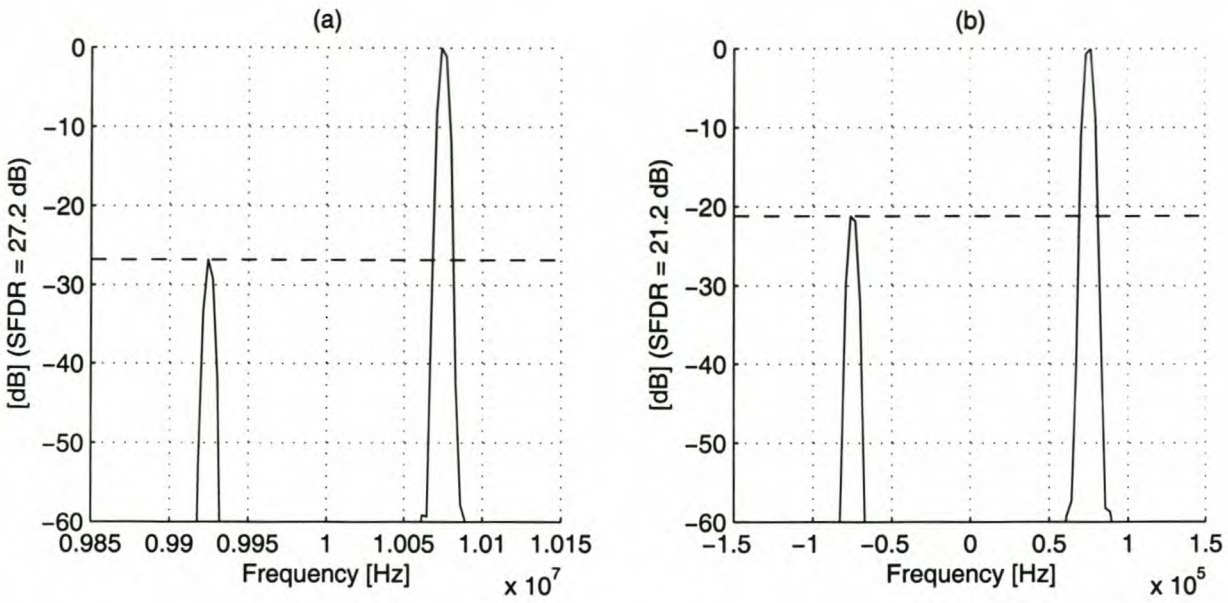

Figure 5.26: *Simulation of combined phase error in a quadrature transmitter and receiver. In this experiment,* $\lambda_{tx} = \lambda_{rx} = 5°$. *(a) Frequency spectrum of the upmixed signal. (b) Frequency spectrum of the downmixed signal, showing the effect of both transmitter and receiver phase error.*

appears, reflected around zero herz. Its envelope is the complex conjugate of the desired signal, shifted by $\pi/2$ radians (through the multiplication by j).

Many transmission schemes (such as FM and DSB-AM) employ real-valued $a(t)$; in such cases, the spurious signal would simply be a frequency- and phase-reflected sideband, shifted by 90 degrees. In this regard, phase error is very similar to amplitude mismatch, which also causes a negative sideband in the downmixed spectrum. The spurious sideband due to phase error, however, is orthogonal in phase to the one produced by amplitude mismatch. To calculate the total spur size, the vector sum of the two sidebands must be calculated.

Figure 5.26 shows the results of a simulation done to confirm that combined transmitter-receiver phase error is indeed cumulative. In this experiment, the transmitter had a phase error of $\lambda_{tx} = 5°$ (87.27 mrad). By Equation 5.72, this should cause a spur in the transmitted RF spectrum, 27.21 dB below the fundamental. This is precisely what is observed in the simulation. As expected, the spur forms an exact sideband to the desired signal.

According to the theory developed in this section, the receiver phase error of $\lambda_{rx} = 5°$ (87.27 mrad) should be cumulative to the transmitter phase error, producing a total received phase error of 10°. Equation 5.72 predicts an SFDR for 21.1 dB for this phase error, which also agrees with the simulation. This supports the theory that transmitter-receiver phase error is cumulative.

Note that the downmixed signal shows a negative-frequency reflection of the desired signal component, as expected.

5.7.5 Case studies

In this section, practical interpretation will be given for the results derived thus far, through the investigation of typical modulation schemes in the presence of phase error.

Frequency modulation

The effect of transmitter phase inaccuracy on a transmitted FM signal is considered first. Define the phase deviation as per Equation 5.61. For frequency modulation, the amplitude $a(t) = A$.

If the phasor locus in Figure 5.22 (p. 70) is compared with that of Figure 5.4 (p. 43), it can be seen that the former is a scaled rotation of the latter. Since the disturbance of the generated signal is affected by the shape of the phasor locus rather than by the scaled size, it can be deduced that amplitude and angular deviation cause similar disturbances to the demodulated signal. More specifically, for any given error in phase angle, an equivalent amplitude deviation can be found that will cause a demodulated disturbance of similar shape and amplitude, differing only in phase.

Firstly, write the erroneous phase angle in terms of the desired phase angle:

$$\phi_\epsilon(t) = \arctan \frac{\sin[\phi(t) - \kappa]}{\cos \phi(t)} . \tag{5.88}$$

FM information is contained in the rate of change of this angle, found by differentiating

$$\frac{d\phi_\epsilon(t)}{dt} = \left(\frac{\cos \kappa}{\cos^2 \phi(t) + \sin^2 [\phi(t) - \kappa]} \right) \frac{d\phi(t)}{dt} . \tag{5.89}$$

By noting that the rotation of the phasor ellipse from the amplitude deviation case does not change the size or shape of these oscillations (apart from a phase shift), it may be deduced that the demodulated error signal caused by phase deviation will be very similar to that caused by amplitude mismatch. The phasor is rotated by 45°, and causes two error signal oscillations per rotation (because it has two maximum and two minimum excursions from the origin). This double-frequency error signal oscillation was observed in the amplitude-deviation error signals.[10] The 45° phase shift of the phasor translates to a 90° phase shift in the frequency-doubled error signal.

This informal deduction would predict an error signal that is similar to that caused by amplitude mismatch, but shifted by 90° in phase. The simulation shown on page 80 confirms this theory. In this experiment, the 10° phase error in the transmitter causes the expected elliptic phasor locus for the received baseband signals. The demodulated signal shows distortion that is emphasised at the peaks of the modulating signal, as was found for amplitude deviation (compare Figure 5.5, p. 44). In fact, phase error and amplitude deviation produce very similar error signals, differing only by a 90° phase shift, as predicted.

As was the case for amplitude mismatch, the analysis of demodulation artefacts introduced by phase deviation is best done numerically, as in the simulation of Figure 5.27.

---

[10] See, for example, the simulations on pages 48 and 44.

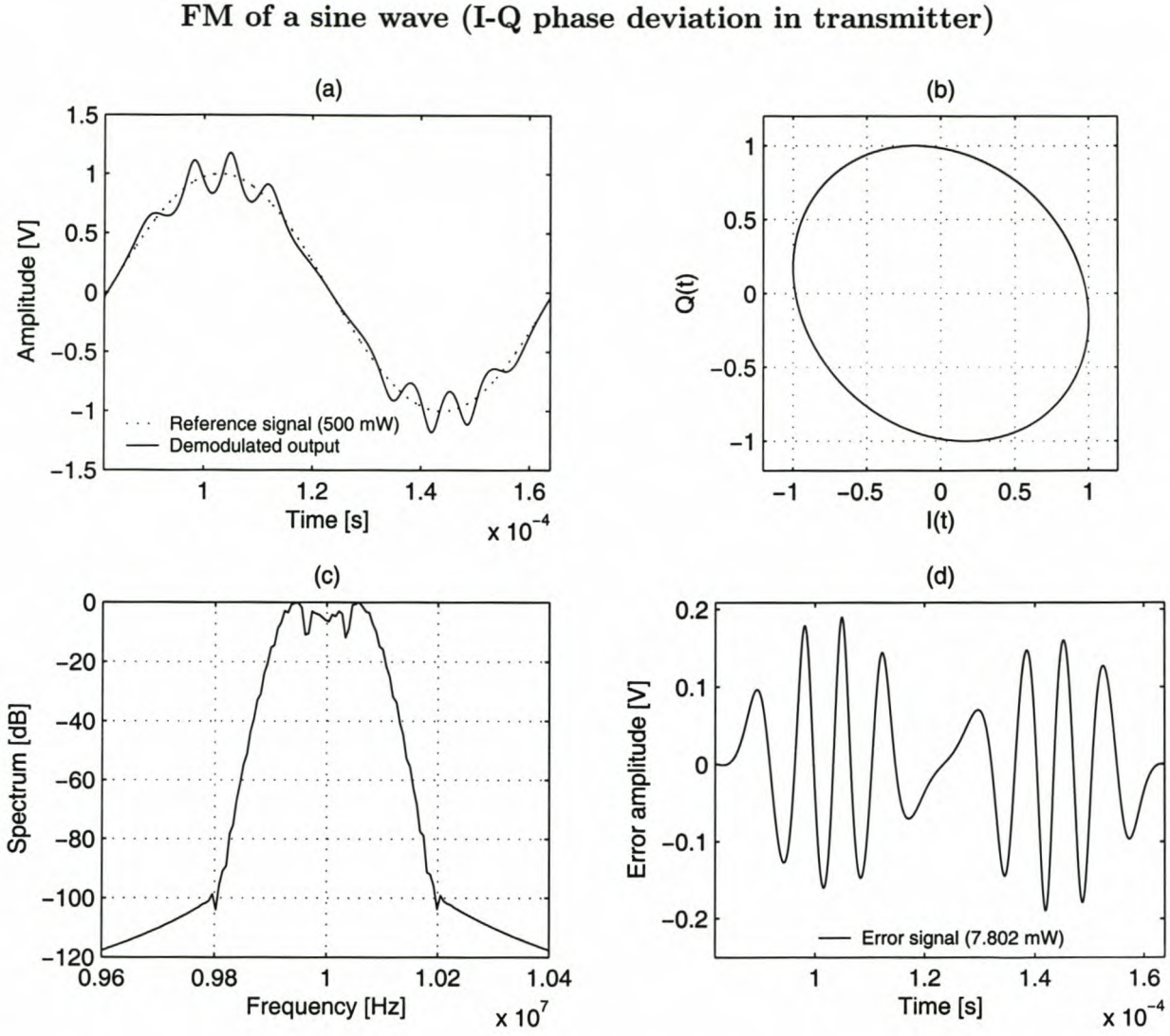

Figure 5.27: *Simulation of frequency modulation of an input sine wave, with the phase of $Q(t)$ lagging $I(t)$ by 10° in the quadrature upmixer. 75 kHz frequency deviation was employed. (a) The demodulated signal shows an undesired 150-kHz oscillation, which is at its worst at the maximum excursions of the desired signal. (b) Phase deviation produces an elliptical phasor locus in the received signal, rotated through 45°. (c) Because of the symmetry of the FM signal's spectrum, any spurious carrier component is obscured. (d) The error signal oscillates most rapidly and with highest amplitude near the desired signal's points of maximum excursion; at other points it is smaller, and oscillates slower (proportional to the speed of phasor rotation at that moment). It can be thought of as a "leakthrough" of the phasor rotation into the transmitted signal.*

Simulation reference: `phierrfm`

Double-sideband AM

The effect of quadrature phase error on the upmixed AM signal can, just as for FM, be derived from the general result presented in Equation 5.71 (where the assumption is made that $\kappa \ll 1$ rad). It is instructive to compare the development presented here to that performed for the amplitude-deviation case on page 54. For an AM signal, $\phi(t) = \omega_0 t + \phi_0$ to produce a centre frequency at $\omega_c + \omega_0$, and $a(t) = m(t)$ (the real-valued modulating signal). Then,

$$y(t) \approx \overbrace{m(t)\cos\left[(\omega_c + \omega_0)t + \phi_0\right]}^{\text{desired upmixed signal}} + \underbrace{m(t)\kappa\cos(\omega_0 t + \phi_0)\sin\omega_c t}_{\text{error signal}} . \tag{5.90}$$

Apart from a phase change, the result is identical to that obtained for amplitude deviation in Equation 5.27 (p. 54). It produces a similar spectrum to that of the single-tone case shown in Figure 5.23 (p. 72), except that the frequency impulses representing the FM signal's instantaneous frequency are now replaced by the double-sided spectrum of the modulating signal. As for the amplitude deviation case (p. 54), if $|\omega_0|$ is smaller than the modulating signal bandwidth, the spectra of the desired and error signals may overlap, causing signal distortion.

A simulation of an error signal that overlaps the desired AM signal is shown in Figure 5.28 (p. 82). In this experiment, the modulating signal is a sinusoid, and is DSB-modulated with a modulation index of 1 [43, p. 241]. A phase lag of 10° (0.1745 rad) in $Q(t)$ should produce spurs 21.2 dB below the desired signal component, according to Equation 5.72.

Examination of Figure 5.28(c) shows that this is exactly what happens: The three strong frequency components constitute the desired RF signal. Each desired component exhibits a sideband reflection around 10 MHz (the mixing frequency). Each spurious sideband is exactly 21.2 dB smaller than its desired counterpart, as is expected.

By comparing the demodulated error signal due to phase inaccuracy (Figure 5.28(d), p. 82), to the one caused by amplitude mismatch (Figure 5.8(d), p. 49), it can be seen that they are similar in shape. This can be attributed to the fact that the two forms of distortion both cause spurious sideband components in the downmixed complex-valued baseband signal, that differ only in phase.

A special case occurs when $\omega_0 = 0$ so that the LO frequency becomes the AM carrier frequency. For this case, Equation 5.90 reduces to

$$\begin{aligned} y(t) &\approx m(t)\cos(\omega_c t + \phi_0) + \kappa m(t)\cos\phi_0 \sin\omega_c t \\ &= m(t)\underline{/\phi_0} + m(t)\kappa\cos\phi_0\underline{/90°} . \end{aligned} \tag{5.91}$$

As was done for amplitude deviation in Section 5.5, the magnitude of the phasor sum can be calculated to determine the effect of phase mismatch on the modulated AM signal's amplitude:

$$|y(t)| \approx m(t)\sqrt{\kappa^2\cos^2\phi_0 + 2\kappa\cos\phi_0\sin\phi_0 + 1} . \tag{5.92}$$

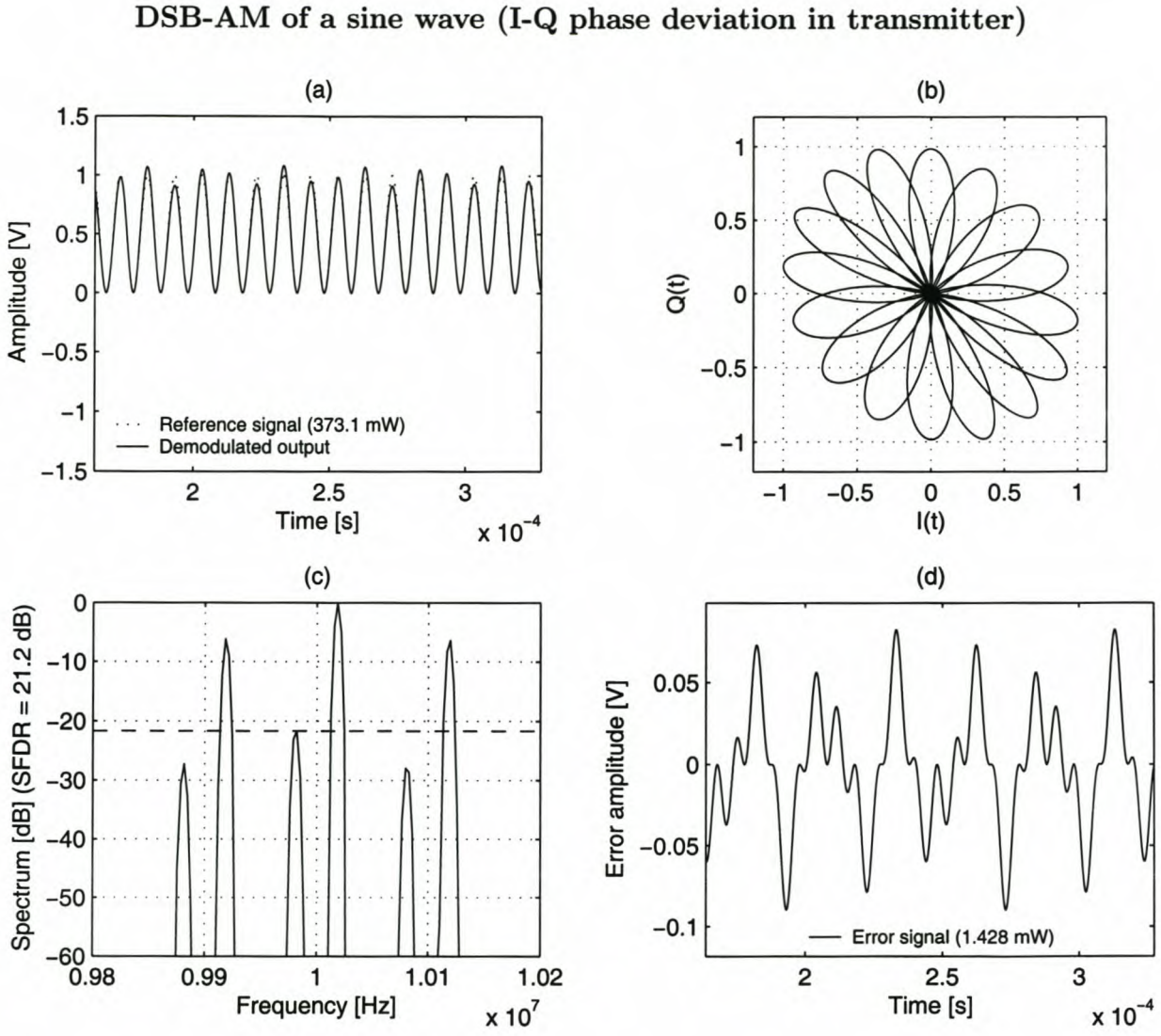

Figure 5.28: *Simulation of a DSB amplitude-modulated sine wave, with the phase of $Q(t)$ lagging $I(t)$ by 10° in the quadrature upmixer. In this simulation, the carrier frequency was chosen to be 18.75 kHz above the mixing frequency of 10 MHz. (a) The demodulated signal is unevenly distorted near its peaks. (b) The received AM signal's flower-like phasor is stretched diagonally, as is typical of the effect of phase error (see Figure 5.27, p. 80). (c) The frequency-domain distortion effect is similar to that seen in DSB-AM with amplitude deviation (Figure 5.8, p. 49): sidebands, symmetrical around the mixing frequency, appear to all the expected signal components. (d) The error signal due to phase error is similar to the one produced by amplitude deviation (Figure 5.8, p. 49), but differs in phase.*

Simulation reference: `phierram`

In the interpretation of the above equation, it should be kept in mind that the approximation is accurate for small κ. As for amplitude deviation, the modulated amplitude is multiplied by a constant gain. The gain is dependent on the phase deviation, κ, and the relative angle ϕ_0. Apart from this gain, the DSB-AM signal information is not affected.

Single-sideband AM

Section B.1.4 shows that upper-sideband SSB modulation at an offset frequency of ω_0 may be achieved by selecting $a(t) = \tilde{m}(t)$ and $\phi(t) = \omega_0 t$ in Equation 5.3 (p. 40). Then

$$I(t) = \mathcal{R}e\left\{\tilde{m}(t)\, e^{j\omega_0 t}\right\} = m(t)\cos\omega_0 t - \hat{m}(t)\sin\omega_0 t \tag{5.93}$$

$$Q(t) = Im\left\{\tilde{m}(t)\, e^{j\omega_0 t}\right\} = m(t)\sin\omega_0 t + \hat{m}(t)\sin\omega_0 t\,. \tag{5.94}$$

These baseband signals may be substituted into the equations for an upmixed signal with transmitter phase error (Equations 5.80 and 5.81). This produces a desired RF component

$$\begin{aligned} y'_d(t) &= \cos\tfrac{\lambda}{2}\left[m(t)\cos\omega_0 t - \hat{m}(t)\sin\omega_0 t\right]\cos\omega_c t \\ &\quad - \cos\tfrac{\lambda}{2}\left[m(t)\sin\omega_0 t + \hat{m}(t)\cos\omega_0 t\right]\sin\omega_c t\,. \end{aligned} \tag{5.95}$$

This represents an upper-sideband SSB signal (see Equation B.12, p. 173). Similarly, the error component in the RF signal is calculated to be

$$\begin{aligned} y'_\epsilon(t) &= \sin\tfrac{\lambda}{2}\left[\hat{m}(t)\cos\omega_0 t + m(t)\sin\omega_0 t\right]\cos\omega_c t \\ &\quad + \sin\tfrac{\lambda}{2}\left[\hat{m}(t)\sin\omega_0 t - m(t)\cos\omega_0 t\right]\cos\omega_c t\,. \end{aligned} \tag{5.96}$$

The error signal also has a single-sideband characteristic, but the positive sign between the two main terms indicates that it resides in the lower sideband. Furthermore, all terms inside square brackets have shifted by exactly ninety degrees in phase: $m(t)$ has been replaced by $\hat{m}(t)$, and $\hat{m}(t)$ by $-m(t)$. The error term is therefore a spurious sideband, reflected around the oscillator frequency and orthogonal in phase to the desired signal. This corresponds to the nature of the phase-deviation spur found for other modulation schemes.

It is useful to compare this result with the corresponding case for amplitude deviation (p. 56). Amplitude deviation also produces a spurious opposite sideband (see Figure 5.13), which is equal to the LSB-modulation of the original signal $m(t)$. In the phase-deviation case, the spurious sideband represents the LSB-modulation of $\hat{m}(t)$.

In Section 5.5.4 the effect of amplitude mismatch on a demodulated AM signal was considered. The similarities between amplitude mismatch and phase error observed so far would suggest that AM demodulation in the presence of phase error can also be analysed from previously developed theory.

The desired frequency component will be demodulated to the original modulated signal. The spurious component (if demodulated at all—it may lie completely out of the signal band) will produce an error signal superimposed on the desired signal. This error signal is similar to that caused by amplitude mismatch, except that it is shifted by 90°. The comments in Section 5.5.4 apply.

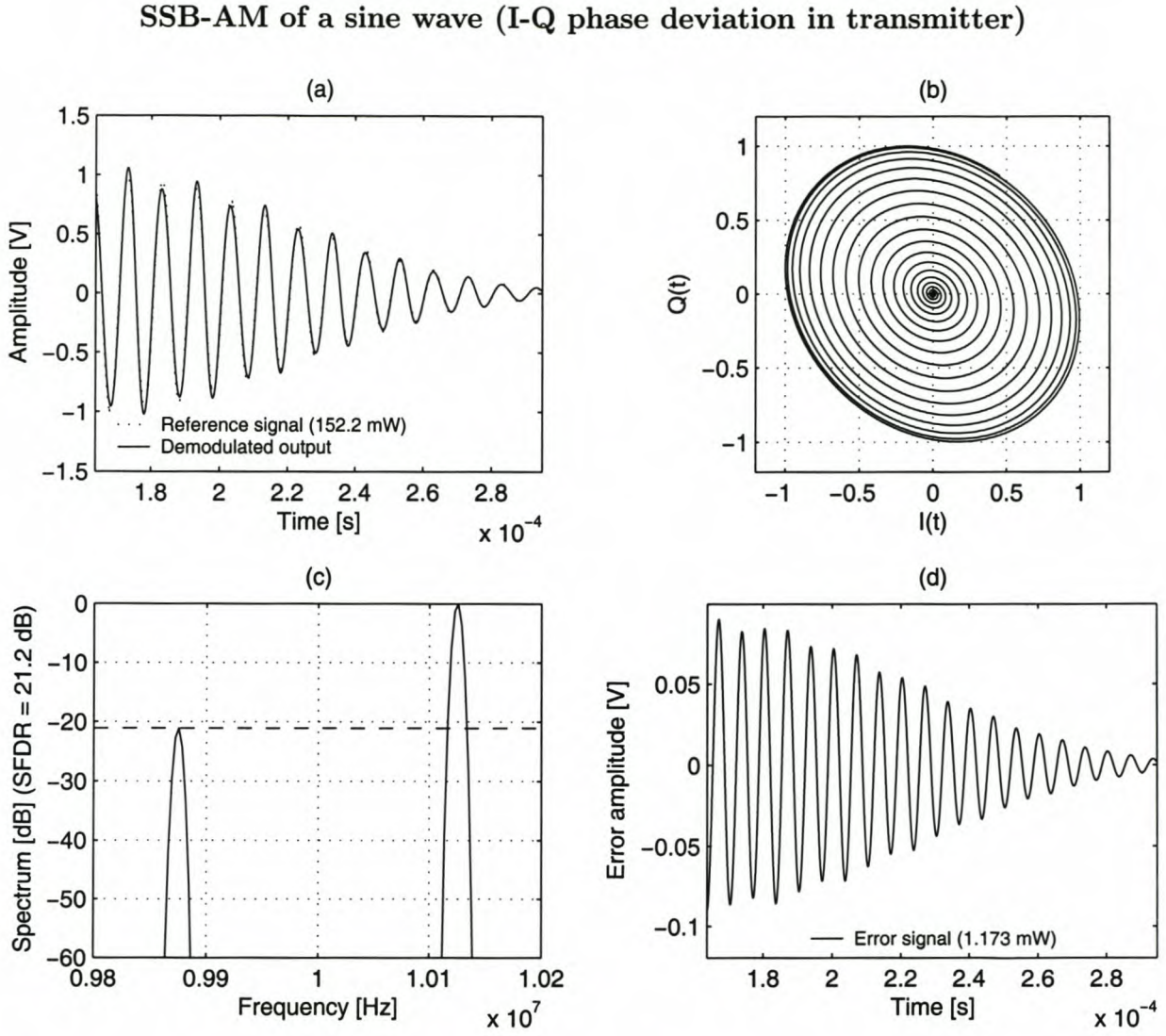

Figure 5.29: *Simulation of SSB amplitude modulation, with the phase of $Q(t)$ lagging $I(t)$ by 10° in the quadrature upmixer. The carrier frequency offset is 25 kHz above the mixing frequency. (a) Distortion is most evident at the peaks and troughs of the demodulated signal (b) The inwardly-spiralling phasor of the decaying-amplitude SSB signal is stretched diagonally, as is typical of a phasor's shape during I-Q phase error. (c) Phase error causes a spurious sideband to appear in the SSB-modulated signal's spectrum. The sideband is symmetrical around the mixing frequency, rather than around the SSB centre frequency, 25 kHz above the mixing frequency. (d) Apart from relative phase shift, the SSB error signal during phase error is similar to that found in an SSB signal during amplitude deviation (Figure 5.14, p. 58).*

Simulation reference: `phierrssb`

A simulation of SSB transmission with mixer phase error is shown in Figure 5.29 on page 84. The spurious sideband lies 21.2 dB below the desired signal, as predicted by Equation 5.72. The spur is symmetrical around the mixing frequency, rather than the SSB centre frequency. Since phase error, like amplitude error, causes a spurious sideband to appear (differing only in phase), the error signal in Figure 5.29(d) has the same frequency and relative amplitude as the error signal caused by amplitude mismatch (Figure 5.14(d), p. 58).

5.8 Combined quadrature errors

Thus far, only the individual effects of amplitude deviation, offset error, LO leakthrough and phase inaccuracies have been considered. In a practical system, all these effects are likely to be compounded. To analyse the compound effects, the general distortion model of Equation 5.5 (p. 41) must again be considered, and the following observations are made:

- The parameters α, γ, ε_i and ε_q, representing carrier leakthrough and DC offset, only appear in terms generating $\cos\omega_c t$ or $\sin\omega_c t$. Consequently, these parameters can only affect the spur at the carrier frequency.
- The parameter ρ, representing amplitude mismatch, only appears as coefficient of the double-sideband term $\mathcal{R}e\left\{a_i(t)e^{j\phi(t)}\right\}\cdot\cos\omega_c t$. It therefore affects the sideband component, but can have no effect on the carrier leakthrough component.
- The phase error in the baseband signal, κ, only affects the term $Im\left\{a_q(t)e^{j\phi(t)}\right\}\cdot\sin\omega_c t$. As this is also a double-sideband term, it follows that the baseband phase error only influences the sideband spur, and can have no effect on the carrier spur.
- The phase error in the quadrature mixer, λ, has an influence on both the $Im\left\{a_q(t)e^{j\phi(t)}\right\}\cdot\sin\omega ct$ term and on the $\varepsilon_q\sin\omega_c t$ term. It is therefore the only parameter that can affect the both the sideband and the carrier spur.

The calculation of the exact spur sizes caused by combined quadrature impairments can now be done, subject to the above considerations. As was done for the study of isolated quadrature inaccuracies, the analysis will focus on upmixing errors. Since all the quadrature inaccuracies in the downmixer may be modelled as equivalent upmixing inaccuracies, the downmixing case follows directly.

5.8.1 Carrier spur

From Eq. 5.5, Line 3, the total carrier spur can be calculated by the phasor sum

$$\alpha'\angle\gamma' = \alpha\angle\gamma + \varepsilon_i\angle 0 - \varepsilon_q\angle\left(\tfrac{\pi}{2}+\lambda\right). \tag{5.97}$$

It follows that when a phase error exists in a quadrature upmixer, the DC offset contribution to the carrier spur can no longer be calculated by the orthogonal summation of Equation 5.36

(p. 59). Instead, the quadrature phase error must be taken into account using the above vector sum.

The calculation produces an equivalent effective carrier leakthrough magnitude, α', and phase, γ', that may further be analysed in a similar way to the isolated carrier leakthrough case of Section 5.6. The carrier spur then lies

$$\mathrm{SFDR}_{\epsilon} = 20 \log \left(\frac{A}{\alpha'} \right) \text{ dB} \tag{5.98}$$

below the desired signal.

5.8.2 Sideband spur

The error signal due to amplitude inaccuracy has been shown on page 45 to be of the form

$$y_{\rho} = \rho \cdot \mathcal{R}e \left\{ a_i(t) e^{j\phi(t)} \right\} \cdot \cos \omega_c t \,. \tag{5.99}$$

Equation 5.5 shows this error term not to be dependent on phase error (i.e. the respective contributions to the total sideband error term may be calculated independently).

Phase error, on the other hand, causes an error term

$$y_{\kappa} \approx (\kappa - \lambda) \cdot \mathcal{R}e \left\{ a_i(t) e^{j\phi(t)} \right\} \cdot \sin \omega_c t \,, \tag{5.100}$$

for small phase errors, where $(\kappa - \lambda)$ is the total effective phase error caused by I-Q and local oscillator phase inaccuracy (Section 5.7.1).

Comparison of Equations 5.99 and 5.100 above shows that both error signals produce a double-sided (real-valued) spectrum, but with a 90-degree phase difference. From Equation 5.10 (p. 47), the relative spur magnitude due to amplitude deviation is

$$S_{\rho} = \frac{|\rho|}{2 + \rho} \,, \tag{5.101}$$

and Equation 5.72 gives the same for phase error:

$$S_{\kappa} = \frac{|\kappa - \lambda|}{\sqrt{(\kappa - \lambda)^2 + 4}} \,. \tag{5.102}$$

The sideband SFDR, in terms of the orthogonal vector sum of these two contributions, is then

$$\begin{aligned} \mathrm{SFDR}_{\mathrm{sb}} &= -20 \log \sqrt{S_{\rho}^2 + S_{\kappa}^2} \\ &= -10 \log \left(S_{\rho}^2 + S_{\kappa}^2 \right) = -10 \log \left[\frac{\rho^2}{(2+\rho)^2} + \frac{(\kappa - \lambda)^2}{(\kappa - \lambda)^2 + 4} \right] . \end{aligned} \tag{5.103}$$

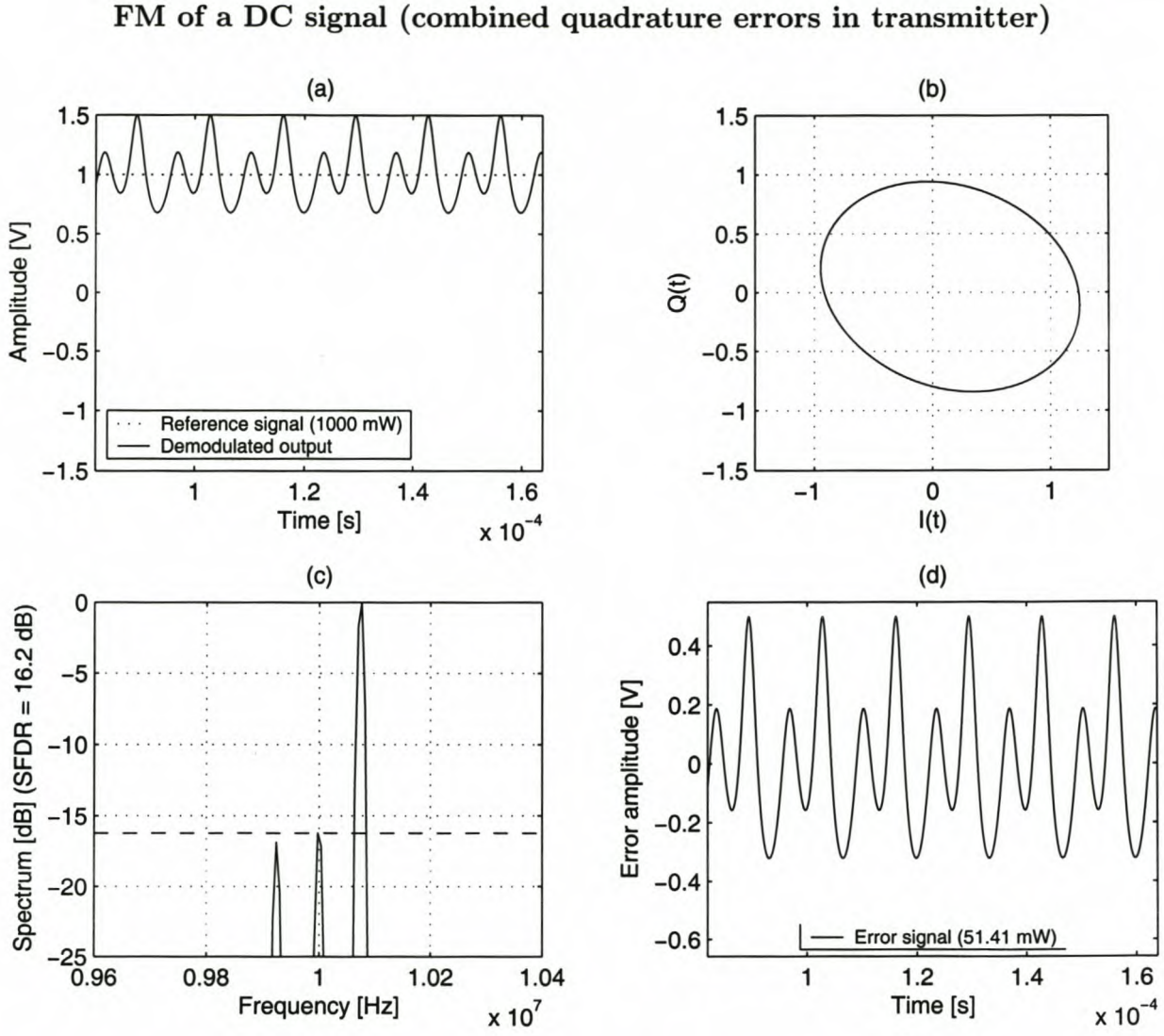

Figure 5.30: *Simulation of quadrature frequency modulation of an input DC signal, with combined quadrature distortion effects on the transmitter side. (a) The demodulated signal is distorted more strongly than for any of the individual non-idealities. (b) The received signal's phasor is elliptical, but none of the ellipse's axes lie on the I-axis or the ±45°-line any more. This confirms a combination of amplitude and phase distortion. (c) Two spurious components are visible. The carrier component is of the same strength as the one produced only by DC offset (Figure 5.17). The component at the sideband frequency is the vector sum of the spurs produced by amplitude deviation (Figure 5.7) and phase error (Figure 5.24) individually. (d) The error signal contains both the 75-kHz oscillation caused by DC offset, and the 150-kHz oscillation caused by amplitude deviation and phase error.*

Simulation reference: `combinedc`

DSB-AM of a sine wave (combined quadrature errors in transmitter)

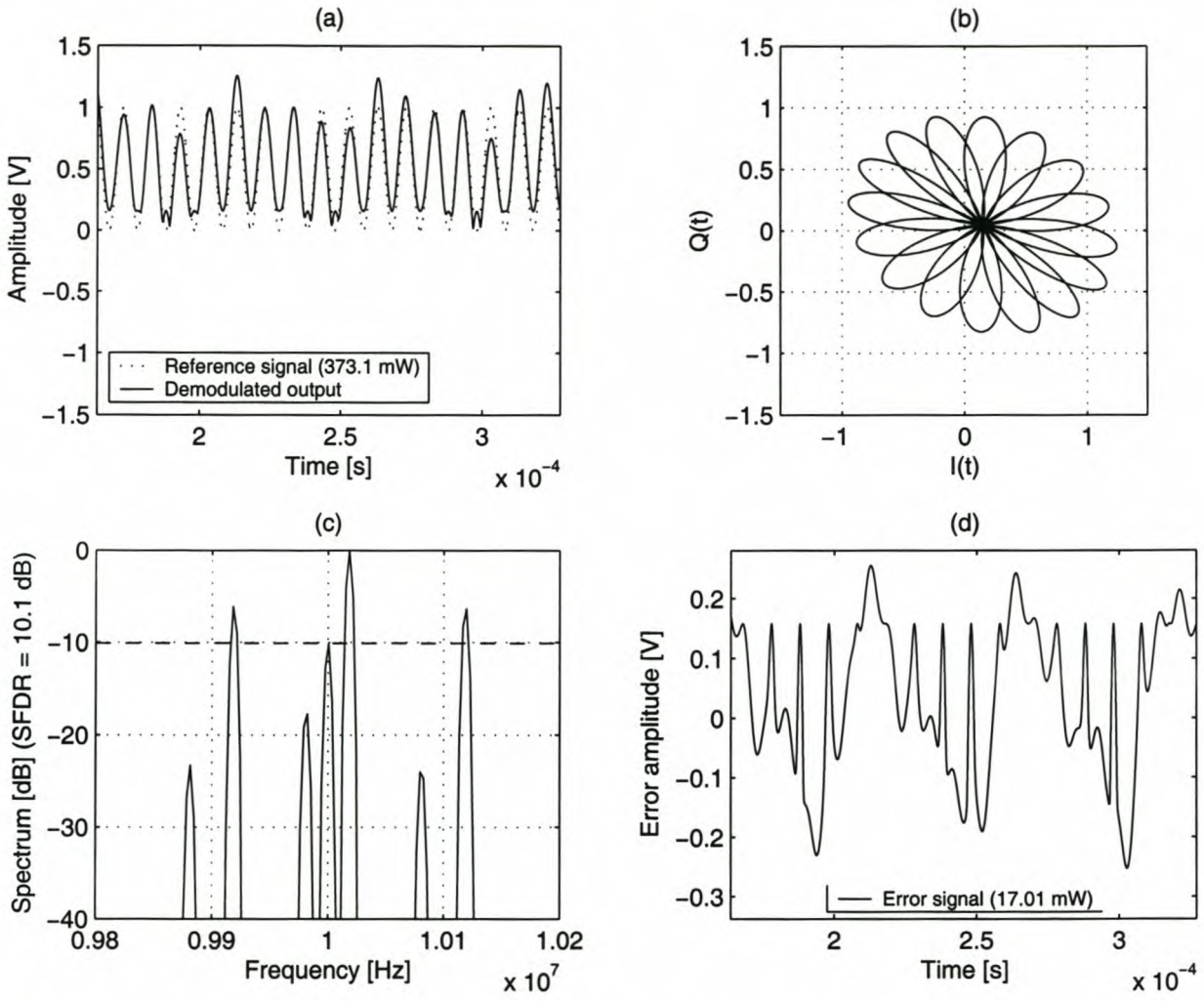

Figure 5.31: *Simulation of DSB amplitude modulation of an input sine wave, with combined quadrature distortion effects on the transmitter side. In this simulation, the carrier frequency was chosen to be 18.75 kHz above the mixing frequency of 10 MHz. (a) The demodulated signal is distorted more strongly than for any of the individual non-idealities. (b) The received signal's flower-shaped phasor is stretched, but not along either the I- or Q-axes, or the ±45°-line. This confirms a combination of amplitude and phase distortion. (c) Two sets of spurious components are visible. The component at the mixing frequency is of the same strenth as the one produced just by DC offset (Figure 5.20). The component at the sideband frequency is the vector sum of the spurs produced by amplitude deviation (Figure 5.8) and phase error (Figure 5.28) individually. (d) The error signal consists of an 18.75-kHz component (resulting from the strong peak at the mixing frequency, 18.75 kHz below the AM carrier), and a component at the signal frequency (indicating amplitude error in the demodulated signal).*

Simulation reference: `combineam`

5.8.3 Simulations

The simulations shown in Figure 5.30 (p. 87) and Figure 5.31 (p. 88) demonstrate the effects of combined quadrature inaccuracies. In the simulation of Figure 5.30, a single positive baseband tone is synthesised, and upmixed with the following quadrature errors:

- 23.75% amplitude mismatch ($\rho = 0.2375$).
- DC offset on the baseband I-Q output ($\varepsilon_i = 0.055$ and $\varepsilon_q = -0.0889$).
- Carrier leakthrough with $\alpha = 0.1581$ and $\gamma = 2.82$ rad.
- 10° phase error in the quadrature mixer ($\lambda = 0.1745$).
- No phase error in the baseband signals ($\kappa = 0$).

Substituting the relevant parameters into Equation 5.98 predicts a carrier leakthrough component of

$$\mathrm{SFDR}_{\epsilon} = 16.0 \text{ dB}. \tag{5.104}$$

This is confirmed by the simulation result in Figure 5.30. Directly substituting the values of κ and ρ into Equation 5.103 yields

$$\mathrm{SFDR}_{\mathrm{sb}} = 17.25 \text{ dB}, \tag{5.105}$$

which agrees with the sideband spur observed in the simulation.

A next simulation was done to confirm that, even in the presence of multiple quadrature impairments, a multitone signal still generates spurs only at the expected positions. This is demonstrated in Figure 5.31. The following parameters were used for this experiment:

- 23.75% amplitude mismatch ($\rho = 0.2375$).
- No DC offset on the baseband I-Q output.
- Carrier leakthrough with $\alpha = 0.1581$ and $\gamma = 2.82$ rad.
- 10° phase error in the quadrature mixer ($\lambda = 0.1745$).
- No phase error in the baseband signals ($\kappa = 0$).

The generated signal is an AM signal with a modulation index of unity, so that 50% of the signal power lies in the modulation carrier. Baseband channel selection is performed, so that, after upmixing, the AM carrier lies at 10 MHz + 25 kHz. The modulating input signal is a 100-kHz maximum-amplitude sinusoid.[11]

[11] See Appendix B.1.3 (p. 171) for an overview of quadrature AM, including baseband channel selection.

The spectrum in Figure 5.31(c) shows the modulation carrier at 10 MHz + 25 kHz, and the desired signal components 100 kHz to either side. 50% of the signal power lies in the carrier, and 25% in each sideband component, therefore the double sidebands lie 6.02 dB below the modulation carrier, as is observed in the simulated spectrum. Note that the modulation carrier is positioned 25 kHz above the local oscillator (mixer) frequency of 10 MHz, and that a spur lies at 10 MHz. Each of the three desired signal components also has its own sideband, reflected around the mixer frequency of 10 MHz. No other spurs appear.

Equation 5.98 predicts that the carrier spur should be 16.0 dB weaker than the desired signal. When compared to the modulation carrier at 10 MHz + 25 kHz, which already lies 6.02 dB below the total signal power, an SFDR of 10.0 dB can be predicted, and is also observed in the simulation.

Simarly, Equation 5.103 may be used to predict that all sidebands should lie 17.25 dB below their corresponding desired signal components (as in the previous experiment). This also corresponds to the simulated results.

5.9 Concluding remarks

This concludes the theoretical analysis of quadrature mixing non-idealities. It was shown that their effects in the time and frequency domain, for both the baseband and RF signals, are entirely deterministic. Furthermore, the resultant spurs are either single-frequency components (as is the case for DC offset or LO oscillator leakthrough), or frequency-reflected images of the desired signal (as is found for amplitude mismatch or quadrature phase error).

In particular, the magnitude of the spurious components are precisely predictable. In each case, there is a simple monotonic relationship between the magnitude of the quadrature error and the magnitude of the resultant spur (Equations 5.10, 5.38 and 5.72).

Digital compensation for deterministic hardware inaccuracies lies central to this dissertation. In the next chapter, it will be shown that all of the presented quadrature inaccuracies may be reversed by employing simple digital processing techniques with low computational overhead. The fundamental limitation in compensation accuracy will be shown to lie in the quantisation accuracy of the digital system, and the accuracy with which spurious artefacts can be measured.

Chapter 6

Digital Compensation

At the end of Chapter 3, a brief theory of compensation was presented, in order to motivate the study of hardware inaccuracies. It was stated that it is possible to compensate for hardware inaccuracies that are cascades of invertible transforms. The dissertation proceeded to analyse the distortion effects of SDR front-ends, in particular during quadrature mixing.

In this chapter it will be shown that these hardware models can be used to compensate for the hardware inaccuracies in the digital domain, as per Proposition A. Techniques to make the application of these principles practically feasible will then be presented.

6.1 Quadrature compensation

This section develops a compensation theory for quadrature mixer inaccuracies. Reversing individual impairments will be considered first, and it will then be shown how the principles may be applied to systems with a combination of quadrature inaccuracies.

The use of quadrature modulation using a physical mixer introduces many potential problems, and Chapter 5 analysed amplitude deviation, DC offset and phase angle error. In spite of these inaccuracies, quadrature modulation has the important advantage that it can employ software techniques to attempt to compensate for these hardware inaccuracies. This is possible because signal processing is performed at baseband frequencies which are more accessible to digital signal processing, by virtue of Proposition B. Digital compensation is a cheap, simple and efficient way of dealing with the quadrature inaccuracies.

6.1.1 Amplitude compensation

Quadrature mixing with amplitude mismatch is defined by Equation 5.6 on page 42:

$$\begin{aligned} I(t) &= (1+\rho)\,\mathcal{R}e\{a(t)e^{j\phi(t)}\} \\ Q(t) &= \mathit{Im}\{a(t)e^{j\phi(t)}\}\,. \end{aligned} \tag{6.1}$$

The SDR transmitter uses digital synthesis to create the I and Q signals, and can fully control the modulation process. Similarly, the SDR receiver can digitally process the received I and Q signals in an attempt to remove hardware distortion effects.

To compensate for amplitude deviation in an SDR transmitter, the synthesis software must scale the output of the I or Q output channel by multiplying the synthesised signal with a scaling factor before the result is passed to the DAC. For example:

$$I'(t) = \frac{I(t)}{1+\rho}, \quad Q'(t) = Q(t). \tag{6.2}$$

Similarly, an SDR receiver may compensate for amplitude mismatch by applying Equation 6.2 to the I and Q signals obtained from the ADC.

To measure amplitude mismatch in a transmitter or a receiver, a test RF signal of the form $\cos[(\omega_c + \omega_o)t]$ may be transmitted or received. The exact frequency offset, ω_o, is not important—as long as it allows the sideband to be easily measured. Equation 5.10 (p. 47) gives the relationship between ρ and the resultant sideband spur size. By making ρ the subject of the equation, it is possible to measure the level of amplitude distortion in a quadrature signal, by first measuring the relative sideband spur size, S_ρ:[1]

$$\rho = \frac{2S_\rho}{\pm 1 - S_\rho}, \tag{6.3}$$

where the sign is chosen to make ρ positive or negative as needed. If the phase relationship between the sideband spur and the desired signal can be measured (e.g. by an FFT calculation in a quadrature receiver), the sign of ρ can be chosen directly: From Equation 5.9 (p. 45), if the sideband is in phase with the desired signal, $\rho > 0$; if the sideband is 180° out of phase, $\rho < 0$.

Once ρ has been calculated from the spur measurement, Equation 6.2 can be applied to remove the spur.

In cases where the phase of the sideband cannot be measured (e.g. when using a spectrum analyser to measure transmitter distortion), the correct sign of ρ is quickly found by trial and error.

The extra multiplication required by the software compensation is a computational overhead that sometimes cannot be neglected. If the SDR hardware is capable of producing I and Q channels that are sufficiently matched in amplitude, it would be preferable to completely dispense of the software compensation. Section 5.5 provides an in-depth analysis of the effects of amplitude deviation that can be very valuable in determining the level of hardware accuracy required to achieve "sufficiently matched" amplitudes. To determine whether a certain degree of amplitude deviation can be tolerated, it is important to realise exactly what its effect will be on both the modulated and demodulated signals.

Figure 6.1 on page 93 shows a simulation in which a large amplitude mismatch in the transmitter was corrected in the coherent receiver. This is possible because, in coherent systems, it is possible to treat transmitter and receiver inaccuracies completely interchangably. Section 6.6 will show how non-coherent systems impose limitations on such inter-system compensation.

---

[1] $\mathrm{SFDR}_\rho \equiv -20 \log S_\rho$.

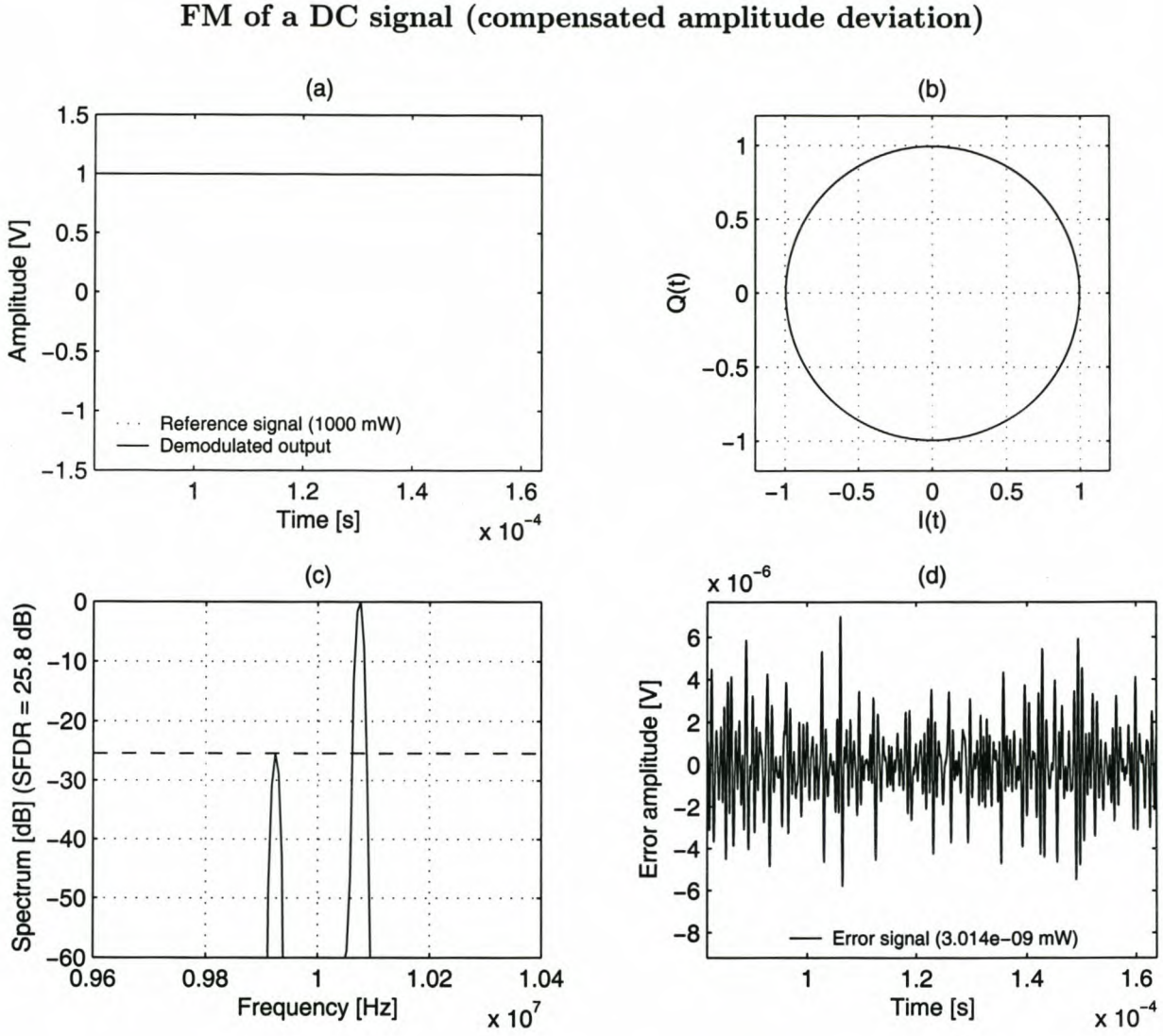

Figure 6.1: *Simulation of compensated frequency modulation of an input DC signal. A 10.8% error on the transmitter's I-channel amplitude was corrected in the receiver. 75 kHz frequency deviation was employed. (a) The modulating and demodulated signals are similar, suggesting that distortion caused by amplitude mismatch has successfully been cancelled. (b) The received signal's phasor is perfectly circular—no evidence of amplitude mismatch remains after compensation. (c) The RF spectrum shows a strong spurious sideband due to the amplitude error in the transmitter. (d) The error signal has the same level of post-filtering carrier residues seen in the completely undistorted simulation on page 169. It can be concluded that the distortion spur has been maximally suppressed.*

Simulation reference: `compamp`

6.1.2 Offset and oscillator compensation

Consider a transmitter with DC offset, as defined by Equation 5.34 on page 57:

$$\begin{aligned} I(t) &= \varepsilon_i + \mathcal{R}e\left\{a(t)\,e^{j\phi(t)}\right\} \\ Q(t) &= \varepsilon_q + Im\left\{a(t)\,e^{j\phi(t)}\right\}. \end{aligned} \tag{6.4}$$

It was shown in Section 5.6 that it is always possible to model a local oscillator leakage component in the RF signal as if it had been generated by an equivalent baseband DC offset in the above equation. It follows that it must be possible to compensate for the combined effects of baseband DC offset and RF carrier leakage by subtracting the cumulative effective DC offset in the digital domain:

$$I'(t) = I(t) - \varepsilon_i', \quad Q'(t) = Q(t) - \varepsilon_q'. \tag{6.5}$$

The above equation holds for both the transmission and the reception case, since they were shown to be symmetrical.

In a practical system, ε_i' and ε_q' must somehow be measured. In a receiver, this amounts to measuring the mean values of the received I and Q signals when a test tone is received. This technique will be further explored in Section 6.7. For a transmitter, the carrier spur must be measured, and converted into the equivalent DC offset values. From Equations 5.36 and 5.37 (p. 59):

$$\varepsilon_i' = \alpha\cos\gamma, \quad \varepsilon_q' = \alpha\sin\gamma. \tag{6.6}$$

Where α is the spur size, and γ is the phase difference between the spur and a generated test signal $\cos[(\omega_c+\omega_o)t]$. It is seldom practical to measure the phase of a transmitted signal; in such cases, α can be measured, but γ must be found by iteration. Such iterative calibration techniques will be studied later in this chapter.

Figure 6.2 shows a simulation that was performed to verify that a carrier spur can be removed. A +1 DC input signal was modulated without any amplitude, offset or phase errors. A sine wave with amplitude 0.12 and lagging the mixer's cosine signal with 19.8° was added to this modulated signal, producing the spur at the carrier frequency depicted by the dashed line in Figure 6.2. This corresponds to a (relatively poor) quadrature mixer with LO leakthrough of −18 dBc.

Next, the simulation was repeated, but this time an offset of −0.11 was added to the I signal, and an offset of −0.04 to the Q signal. This should induce an oscillator component with amplitude $\alpha = 0.117$ and phase $\gamma = -160°$, which is reasonably close to a 180°-shift of the LO leakthrough signal. The solid line in Figure 6.2 shows the simulation results: The LO spur is suppressed by the deliberate offset error.

The simulation on page 96 shows a transceiver system with an identical reference carrier, ω_c, in the transmitter and receiver. LO leakthrough in the transmitter was cancelled in the receiver by adding the corresponding DC offset to the received I-Q channels.

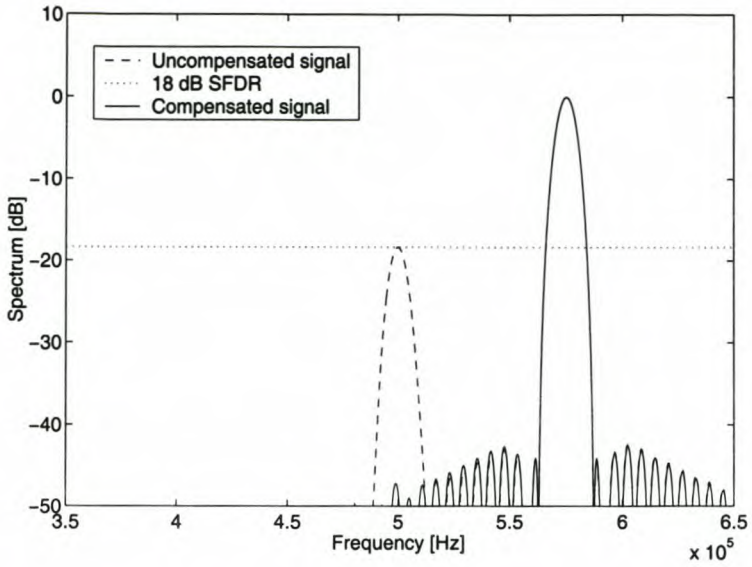

Figure 6.2: *Simulation to illustrate how deliberate I and Q offsets can be added to compensate for local oscillator leakthrough. The dashed line shows a modulated +1 DC input signal, to which a sine wave of -18 dBc was added, 19.8° lagging to the quadrature mixer's cosine signal. By adding I and Q offset errors, the spurious component at the carrier frequency was suppressed (solid line).*

In general, however, it cannot be assumed that transmitter leakthrough is easily compensated in the receiver, and *vice versa.* Transmitters and receivers seldom employ synchronous local oscillators, hence ω_c and $\hat{\omega}_c$ may differ. In such a system, it is still possible for the transmitter to compensate for transmitter leakthrough, and the receiver for the receiver effects, but cross-compensation becomes a more difficult problem which can no longer be solved by the simple addition of DC levels. It may be concluded that DC offset and LO leakthrough compensation is best performed at each stage where it occurs (transmission and reception). This idea is taken up again in Section 6.6.

6.1.3 Phase compensation

For a transmitter that has a phase error of κ radians in the baseband I-Q signals, and a phase error of λ radians in the quadrature mixing oscillator, Equation 5.68 (p. 71) predicts an RF signal of

$$\begin{aligned} y(t) \;=\; & \cos\kappa \cdot \mathcal{R}e\left\{a(t)\,e^{j\phi(t)}\right\}\cos\omega_c t \;-\; \cos\lambda \cdot Im\left\{a(t)\,e^{j\phi(t)}\right\}\sin(\omega_c t) \\ & -\,(\sin\kappa - \sin\lambda)\cdot Im\left\{a(t)\,e^{j\phi(t)}\right\}\cos\omega_c t\,. \end{aligned} \tag{6.7}$$

The third term represents the error signal (an undesired sideband in the upmixed signal). This term can be forced to zero by letting $\kappa = \lambda$. In a typical SDR transmitter, κ can easily be adjusted as part of the signal synthesis process; λ is usually a mixer characteristic that is out of the SDR designer's control.

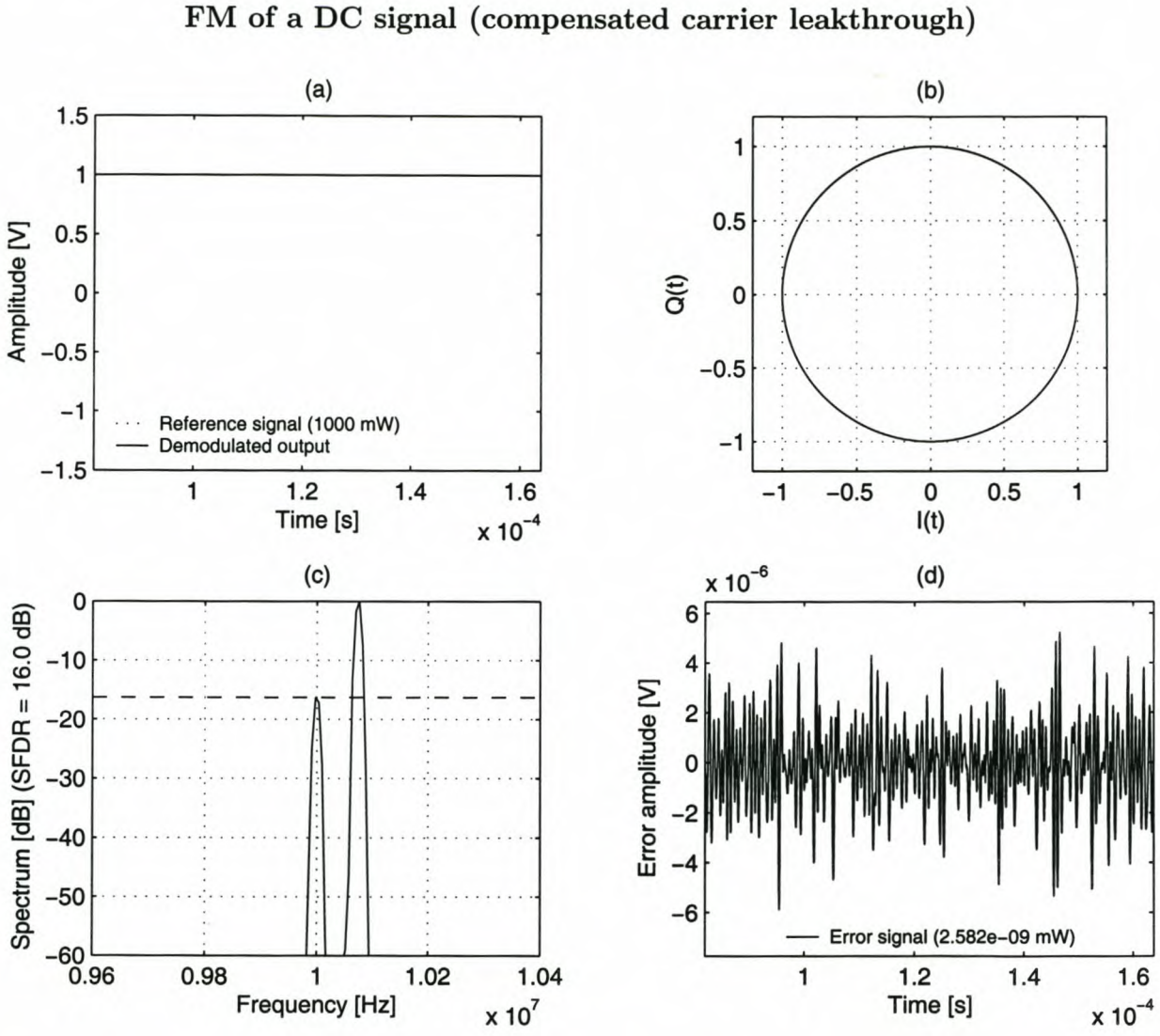

Figure 6.3: *Simulation of compensated frequency modulation of an input DC signal. Transmitter carrier leakthrough was corrected in the receiver. 75 kHz frequency deviation was employed. (a) The modulating and demodulated signals are similar, suggesting that distortion caused by carrier leakthrough has successfully been cancelled. (b) The received signal's phasor is perfectly centred—no evidence of carrier leakthrough or DC offset remains after compensation. (c) The RF spectrum shows a strong spur at the carrier. (d) The error signal has the same level of post-filtering carrier residues seen in the completely undistorted simulation on page 169. It can be concluded that the distortion spur has been maximally suppressed.*

Simulation reference: `compofs`

Section 5.7 demonstrated the symmetry between transmitter and receiver phase error. It follows that it is possible to perform similar phase compensation in a quadrature receiver by adjusting the phase relationship between the received I and Q signals.

This is illustrated in the simulation shown on page 98: A 10° phase error in the transmitter produces a strong sideband spur 21 dB below the desired signal. An error of equal magnitude in the coherent-carrier receiver serves to completely negate the transmitter phase error, so that the received signal's phasor is again perfectly circular. The error signal, which is the difference between the modulating and demodulated signals in Figure 6.4(a), contains only post-filtering residues similar to the distortion-free simulation shown on page 169.

Although this simulation illustrates the validity of the theory, its implementation is somewhat different from how phase compensation would be applied in a practical system. Practically, LO phase mismatch in a quadrature mixer would be measured, and an equal phase error would be induced in the synthesised I and Q signals. Such a phase adjustment could either be performed by all-pass filtering, or by transforming the phase error into an equivalent amplitude mismatch. Both these techniques will now be studied in more detail.

Hilbert filtering

Receiver phase compensation can be achieved by using a digital filter with a uniform phase response in the baseband. The simplest filter of this type is the Hilbert transformer. The ideal Hilbert transform induces a 90° phase shift over all frequencies. Practical FIR-filter Hilbert transformers are effective over a limited frequency band, and may induce some signal latency [32, pp. 657–662].

Assume a signal, $m(t)$, is passed through a Hilbert transformer to produce the signal $\hat{m}(t)$. From these two signals, any phase shift of the original signal can be obtained by calculating

$$m'(t) = \cos\theta \cdot m(t) + \sin\theta \cdot \hat{m}(t)\,. \tag{6.8}$$

This approach can be used to induce a phase shift of θ in one of the receiver I-Q signals to perform quadrature phase compensation.

The accuracy of the receiver compensation depends on how accurately the Hilbert transformer can be implemented in FIR filter form. In turn, the accuracy of the FIR filter ultimately depends on the numeric resolution of the digital system.

Phasor rotation and scaling

The study of quadrature phase error in Section 5.7 emphasised the similarity between the effects of quadrature amplitude mismatch, and the effects of quadrature phase inaccuracy. In particular, it was shown that, from a phasor-locus point of view, the two effects are identical except for a 45-degree rotation of the phasor. Hence, it should be possible to transform a phase error into amplitude mismatch by performing rotation in the complex plane, and then

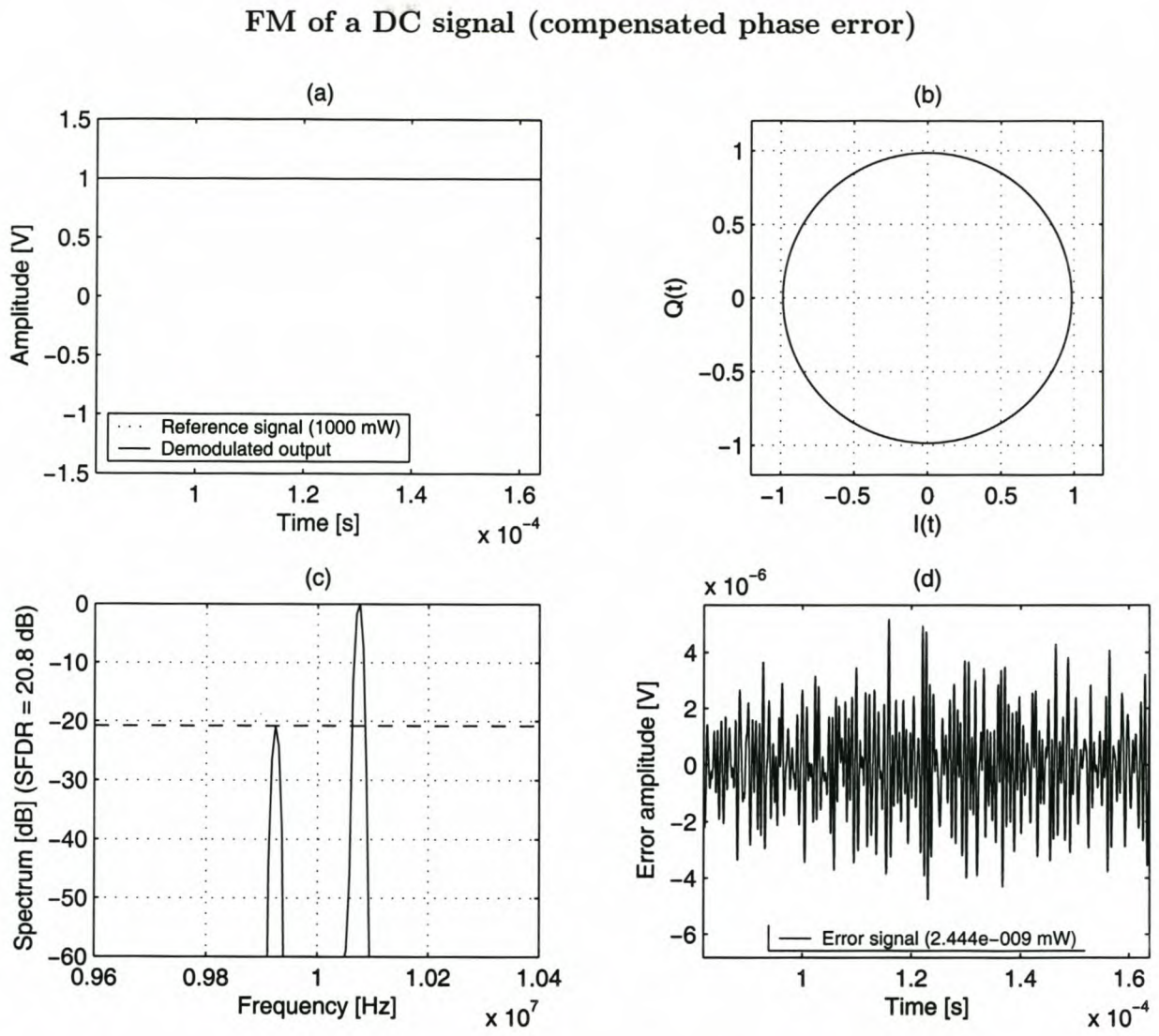

Figure 6.4: *Simulation of compensated frequency modulation of an input DC signal. A* 10° *phase error existed in the transmitter's local oscillator signals, but was cancelled by a compensation phase error in the receiver. 75 kHz frequency deviation was employed. (a) The modulating and demodulated signals are similar, suggesting that distortion caused by the phase error has successfully been cancelled. (b) The received signal's phasor is perfectly circular—no evidence of phase error remains after compensation. Note that the radius has dropped slightly below unity, indicating a slight loss of signal power due to the phase error. (c) The RF spectrum shows a strong spurious sideband due to the phase error in the transmitter. (d) The error signal has the same level of post-filtering carrier residues seen in the completely undistorted simulation on page 169. It can be concluded that the distortion spur has been maximally suppressed.*

Simulation reference: `compphi`

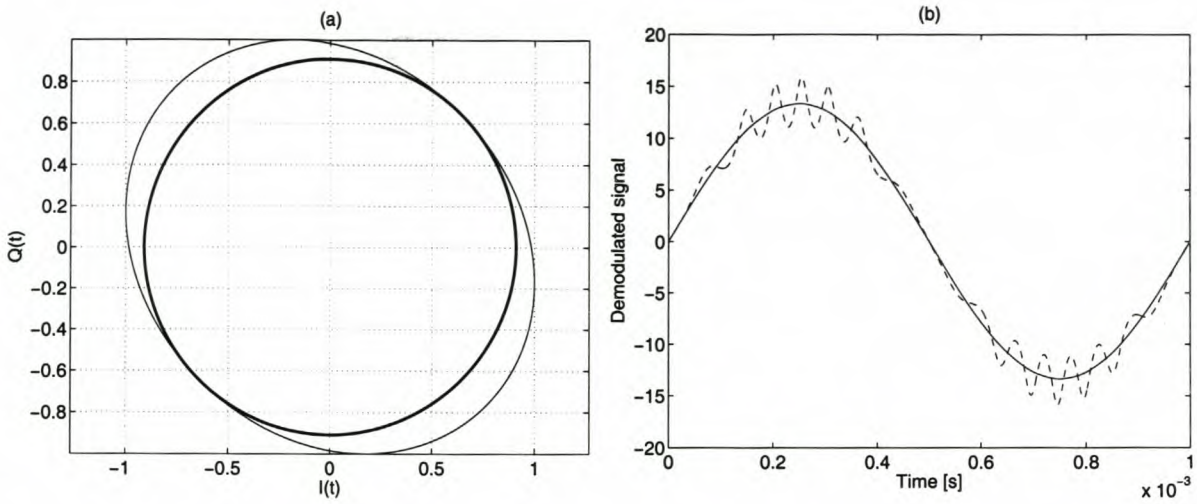

Figure 6.5: *Receiver phase error compensation by phasor rotation and scaling. (a) The original, elliptical phasor is rotated and scaled through two complex transformations. The resultant phasor is circular. (b) After compensation, the demodulated FM signal is received error-free. The dashed line shows the demodulated signal when no phase compensation is performed.*

scaling one of the axes (i.e. the I or the Q signal) as was done to compensate for amplitude mismatch. Complex rotation by 45° can be achieved by calculating

$$s'(t) = s(t) \cdot e^{j\frac{\pi}{4}}, \tag{6.9}$$

where $s(t) = I(t) + jQ(t)$ is the received complex-valued baseband signal.

The phase rotation of the phasor represents the phase difference between the amplitude mismatch error signal; it follows that the size of the elliptical eccentricity corresponds to the magnitude of the error signal. The rotation transforms the phase-inaccurate baseband signal into a signal with an equivalent amplitude inaccuracy, and it must now be established what the magnitude of this error signal will be for a given phase error.

If ρ and κ is chosen to produce error signals of equal magnitude, Equation 5.10 (p. 47) and Equation 5.72 (p. 73) may be equated:

$$\frac{|\rho|}{2+\rho} = \frac{|\kappa|}{\sqrt{\kappa^2+4}}. \tag{6.10}$$

Since both denominators are always positive, the absolute value signs may be dropped. Solving for ρ yields

$$\rho = \frac{2\kappa}{\sqrt{\kappa^2+4}-\kappa}. \tag{6.11}$$

This equivalent ρ can be used to scale the real part of the rotated baseband signal, $s'(t)$, as per Equation 6.2.

The simulation shown in Figure 6.5 demonstrates the use of phase compensation by rotation and scaling. An I-Q signal containing phase error is corrected by the following three lines of MATLAB code:

```
rho = 2*kappa / ( sqrt(kappa^2+4) - kappa );      % Equivalence
IQr = IQ*exp(j*pi/4);                             % Rotation
IQc = real(IQr)/(1+rho) + j*imag(IQr);            % Scaling
```

The compensated phasor is again circular, and the signal is demodulated without distortion. The advantage of this technique is that it may be performed on a sample-by-sample basis, as opposed to the long group delay associated with the FIR filtering of the Hilbert transformation technique. Phasor rotation and scaling will be employed in the SDR prototype of Chapter 7.

Measuring phase error

Measuring phase error is very similar to measuring amplitude mismatch, in that a test tone is transmitted or received, and the size of the sideband spur is measured. In this case, the sideband spur is 90° out of phase with the desired signal $\cos[(\omega_c+\omega_o)t]$. Equation 5.72 gives the relationship between the total phase error, κ, and the resultant sideband spur size. By making κ the subject of the equation, it is possible to measure the quadrature phase error by first measuring the sideband spur size, S_κ:[2]

$$\kappa = \frac{2S_\kappa}{\pm\sqrt{1-S_\kappa^2}}, \tag{6.12}$$

where the sign is chosen to make κ positive or negative as needed. As is the case when measuring amplitude mismatch, the phase relationship between the desired signal components and its sideband determines the sign of κ. From Equation 5.69: If the Fourier transform phase of the sideband is 90° below the phase of the desired signal, $\kappa > 0$; if the sideband phase is 90° above the phase of the desired signal, $\kappa < 0$.

Once κ has been calculated from the spur measurement, any of the above phase correction techniques may be applied to remove the spur. If the relative sideband phase cannot be measured, the correct sign of κ is easily found by trial and error.

Of course, measuring the value of κ (or ρ) becomes more problematic when a system contains both phase inaccuracy and amplitude mismatch. The following section will consider quadrature compensation in this general case.

6.1.4 Combined compensation

Section 5.8 investigated the interaction between the various quadrature impairments when they appear in combination. In particular, it was shown that the presence of phase mismatch

[2] $\text{SFDR}_\kappa \equiv -20\log S_\kappa$.

in the quadrature mixer may affect the relationship between the LO leakthrough spur and the baseband DC offsets. On the other hand, DC offset or LO leakthrough has no effect on the sideband spur. This suggests that LO leakthrough compensation should not be performed prior to sideband compensation, lest later phase adjustments re-introduce a LO spur. Once phase compensation has been performed, LO spur compensation can be done as per Section 6.1.2.

Direct measurement

It was shown on page 86 that the sideband spur is the orthogonal vector sum of the amplitude mismatch and phase error spur contributions:

$$S_{\text{sb}}\angle\theta = S_\rho + jS_\kappa\,, \tag{6.13}$$

giving the sideband spur magnitude and phase, relative to the desired signal component. If both the magnitude and phase of the sideband spur can be measured (as is usually the case in a quadrature receiver), the relative spur contributions must then be

$$S_\rho = S_{\text{sb}}\cos\theta\,, \quad S_\kappa = S_{\text{sb}}\sin\theta\,. \tag{6.14}$$

Once the individual spur contributions have been measured, amplitude compensation may be performed as per Section 6.1.1, and phase compensation as per Section 6.1.3. If the sideband spur phase is not measurable (e.g. in a transmitted RF signal), the amplitude and phase contributions cannot be separated directly. In such a case, an iterative compensation technique must be used, as will be developed below.

Combined quadrature compensation was tested in the simulation shown in Figure 6.6 (p. 102). In this simulation, various quadrature inaccuracies were introduced in the transmitter, and compensation was then performed for each individual inaccuracy in the coherent receiver, using the individual compensation techniques that were discussed in the previous sections. The resultant error signal (Figure 6.6(d), the difference between the modulating and demodulated signals) shows that the effects of the transmitted spurs have been completely removed.

Iterative techniques

In cases where the calibration setup does not make measurement of the spur phases possible (e.g. when using a spectrum analyser), the various compensation parameters can no longer be measured directly. For example, it might be known that the carrier spur has a magnitude of α, but the value of γ would be unknown. In such a case, the value of γ may be found by adjusting it on the range $[-\pi, \pi)$, compensating for the estimated values of ε_i and ε_q, and measuring the effect on the spur.

Figure 6.7 illustrates the search space for such an iterative adjustment. For this graph, it is assumed that a normalised error vector of $1e^{j\pi} = -1$ is present in a system. The magnitude of this vector, $A = 1$ is known, but its phase is unknown. The graph shows the

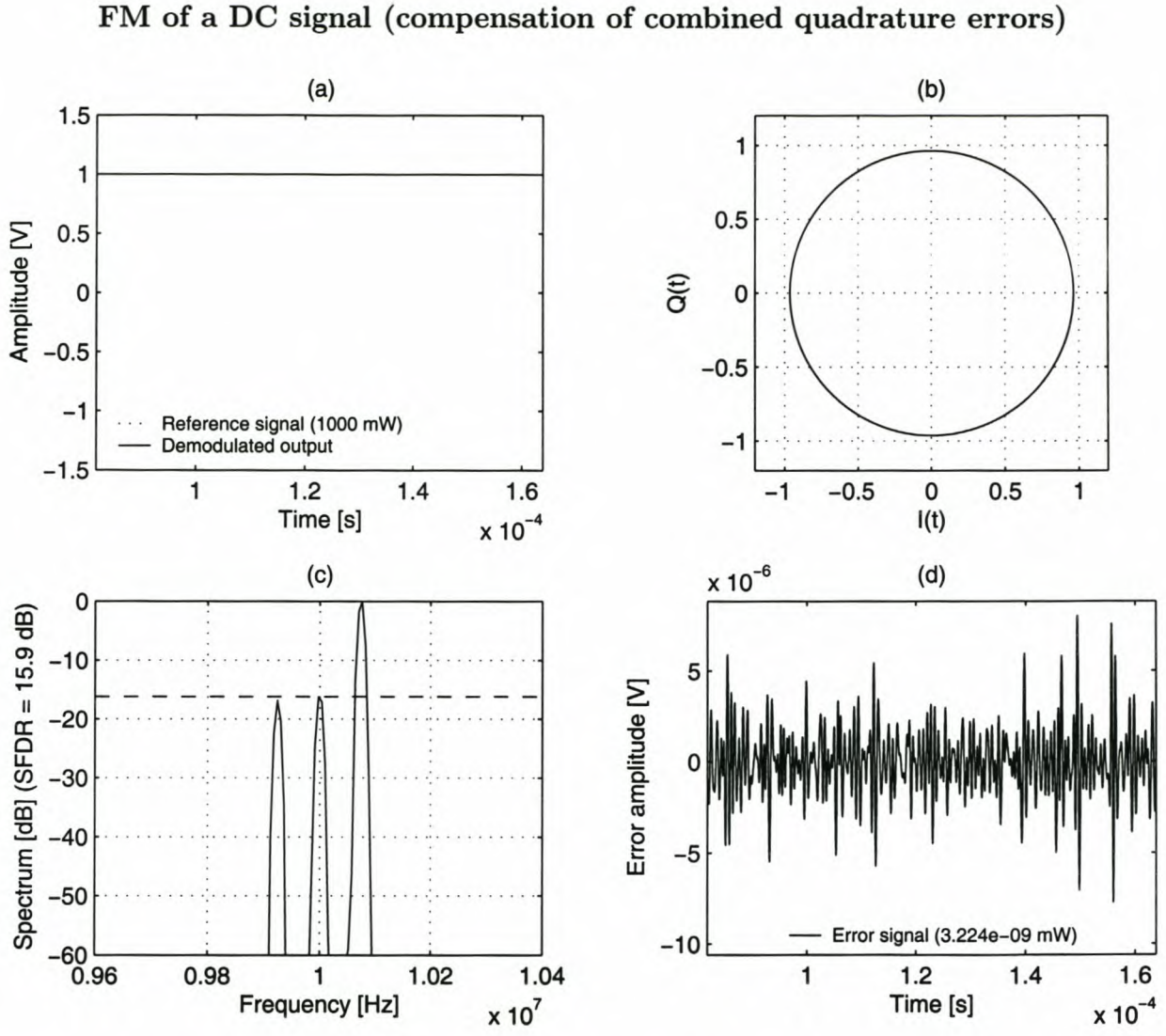

Figure 6.6: *Simulation of compensated frequency modulation of an input DC signal. Transmitter amplitude mismatch, carrier leakthrough and phase error were corrected in the receiver. 75 kHz frequency deviation was employed. (a) The modulating and demodulated signals are similar, suggesting that all the distortion effects caused by transmitter quadrature errors have been cancelled successfully. (b) The received signal's phasor is circular—no evidence of quadrature errors remains after compensation. (c) The RF spectrum shows a strong spurious sideband and carrier component due to the quadrature errors in the transmitter. (d) The error signal has the same level of post-filtering carrier residues seen in the completely undistorted simulation on page 169. It can be concluded that the distortion spurs have been maximally suppressed.*

Simulation reference: `compbine`

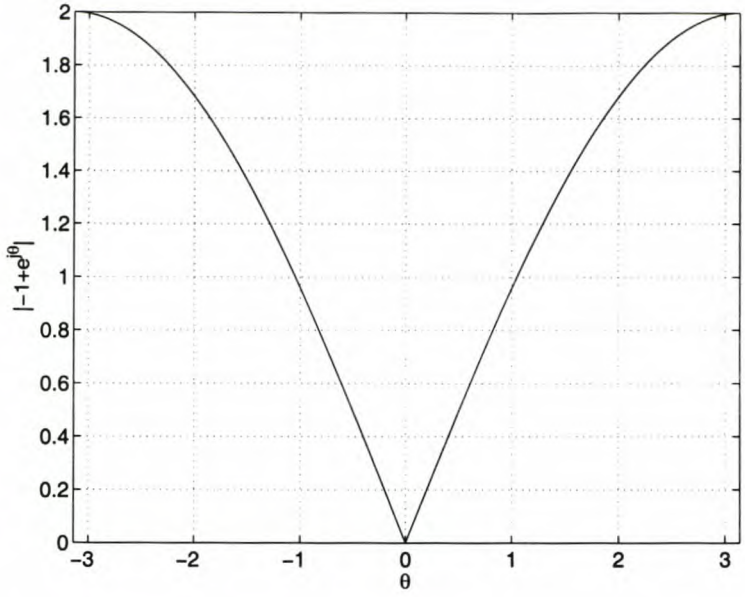

Figure 6.7: *Search space when estimating compensation phase. The search space is a graph of* $\left|-1+e^{j\theta}\right|$, *where* $\theta = 0$ *will fully compensate for the vector of* -1.

magnitude of the resultant sum vector when the compensation vector $e^{j\theta}$ is added to the error vector -1. Exact compensation is achieved when $\theta = 0$, for which the error magnitude drops to zero. In the worst case, when $\theta = \pi$, the compensation vector adds constructively to the error vector, and the total vector magnitude is doubled.

It can be shown by trigonometric manipulation that

$$\left|-1+e^{j\theta}\right| = 2\left|\sin\left(\frac{\theta}{2}\right)\right|, \tag{6.15}$$

so that, for a measured normalised vector sum magnitude, V,

$$\theta = \pm 2\sin^{-1}\left(\frac{V}{2}\right). \tag{6.16}$$

The smooth shape of the search space lends itself well to gradient-based algorithms to find an optimal value of θ within a few iterations. Figure 6.7 contains only a single local and global minimum, which guarantees that a gradient-based search will converge. One such algorithm, based on a steepest-descent search, is demonstrated by the MATLAB source code shown in Figure 6.8. An initial error magnitude measurement is taken (A), after which compensation is attempted with an initial phase of zero radians, and the error magnitude is measured again (a_1). The ratio $V = a_1/A$ is used in Equation 6.16 to find the required angle adjustment, $\pm\theta$. The sign ambiguity in $\pm\theta$ is resolved by first using $+\theta$ for compensation, and measuring whether an improvement in compensation results. If not, $-\theta$ is used.

Equation 6.16 represents a direct relationship between a measured error magnitude and compensation phase values. The algorithm described above will converge to the correct value of θ in a single iteration, assuming that all magnitude measurements are accurate (as in the

```
function [Vc, err] = descent(error, tolerance)
% DESCENT  Gradient search demonstration for vector compensation
%          Syntax: [Vc, err] = descent(error, tolerance)
%          This function demonstrates the use of a gradient-based algorithm to find
%          a compensation vector. The error vector is given by "error", and
%          "tolerance" specifies the maximum remaining error that may be present
%          after compensation. The function returns the total compensation vector,
%          "Vc", and the magnitude of the remaining error, "err".

done = 0;
Vc = 0;
i = 0;

while ~done
  A = abs(error+Vc);          % Measure the remaining error magnitude
  g1 = 0;                     % Initial compensation angle estimate
  v1 = -A*exp(j*g1);          % Corresponding compensation vector
  a1 = abs(error+Vc+v1);      % Measure error magnitude after further compensation
  i = i+1;                    % Count measurement
  relA = a1/A;                % Calculate relative error magnitude improvement
  g2 = 2*asin(relA/2);        % Estimate remaining angular error
  v2p = -A*exp(j*g2);         % Calculate new compensation vector estimate (positive angle)
  a2p = abs(error+Vc+v2p);    % Measure error magnitude after further compensation
  i = i+1;                    % Count measurement

  if (a2p < a1)               % Has error improved?
    Vc = Vc+v2p;              % Add compensation iteration to total compensation vector
    err = abs(a2p);           % Log remaining error size
  else                        % If not, we adjusted in the wrong direction
    v2n = -A*exp(-j*g2);      % Resolve angle ambiguity by measure negative angle
    a2n = abs(error+Vc+v2n);  % Measure error magnitude with negative angle compensation
    i = i+1;                  % Count measurement
    Vc = Vc+v2n;              % Add compensation iteration to total compensation vector
    err = abs(a2n);           % Log remaining error size
  end;

  done = (err < tolerance);   % Stop iterations when required tolerance has been reached
end;

disp(sprintf('%d measurements performed.', i));
```

Figure 6.8: *MATLAB source code demonstrating a gradient-based compensation algorithm. Only the error magnitude is used to calculate the compensation vector; the error phase is first guessed, and the change in total error magnitude allows a re-estimate of the phase error from Figure 6.7. The sign of the phase error is unknown, and is also found by trial. Because all "measurements" are ideal, only one iteration is performed when this program is run.*

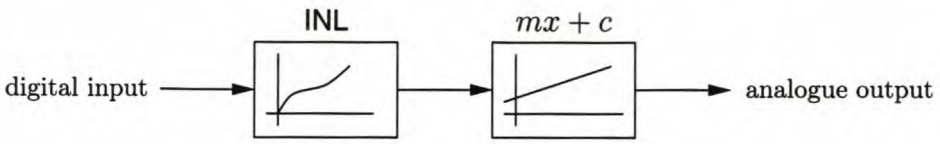

Figure 6.9: *Simplified model of a digital-to-analogue converter, containing integral nonlinearity and offset and gain error. An analogue-to-digital converter model would be identical to the diagram depicted here, with the direction of signal flow reversed.*

MATLAB simulation). In practice, more than one iteration may be needed to accommodate less accurate magnitude estimations.

The algorithm described here is equally suitable for sideband spur compensation (simultaneous amplitude and phase error) as for LO spur compensation (unknown LO leakthrough phase).

6.2 Linear compensation

Filters play a critical role in quadrature mixing, and non-idealities in the filter transfer functions could have a negative impact on quadrature compensation performance. In particular, if the I and Q low-pass filters do not have identical transfer functions, they may contribute to amplitude and phase mismatch in the quadrature signals. Such non-idealities are likely to be dependent on signal frequency, and it follows that any compensation function should also be frequency-dependent.

To compensate for a non-ideal filter transfer function, $H(s)$, an approximated inverse filter, $G(s) \approx H^{-1}(s)$ should be implemented in the digital domain. The approximation should be accurate within the significant frequency band of the signal. Any number of poles may be placed outside this frequency band. The nett effect of $G(s) \cdot H(s)$ should be an all-pass filter with a linear phase response within the frequency band of interest.

This process is called filter equalisation, and extensive literature is available on the subject. Su [44, p. 69] provides a useful frequency-domain approach, with particular reference to phase equalisation. Ziemer and Tranter [56] consider both frequency and time-domain approaches to designing equalisation filters. An overview of several techniques, specifically considering filter impulse responses, is given by Qureshi [33].

6.3 Harmonic compensation

Quadrature mixing is not the only contributor the spurious component in the signal spectrum: Signal converters, amplifiers and other non-ideal devices may induce signal distortion that manifests as undesired harmonics.

Consider, for example, the DAC model shown in Figure 6.9. It contains the main types of

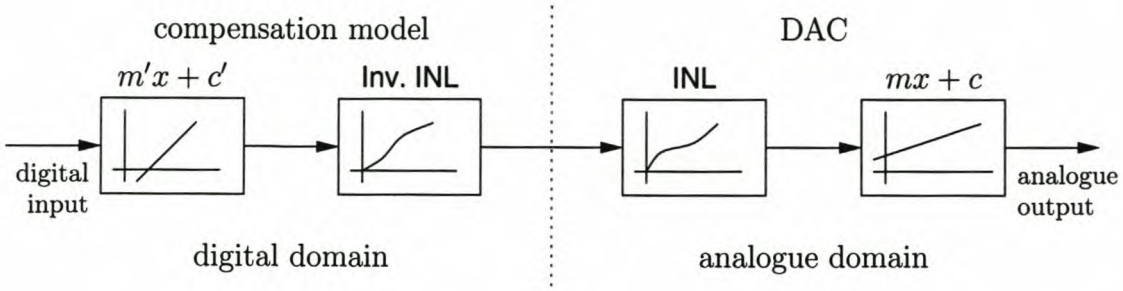

Figure 6.10: *Digital compensation for the DAC model shown in Figure 6.9. Compensation is performed in reverse order using the inverse INL mapping, and an inverted linear distortion.*

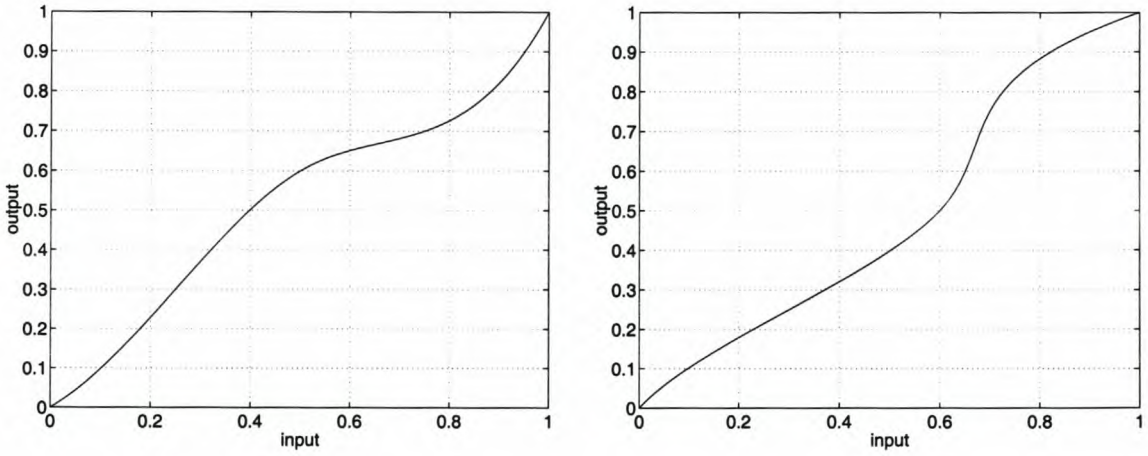

Figure 6.11: *(a) INL of the DAC used in the simulation. (b) Inverse INL.*

converter non-ideality discussed in Chapter 4: The input signal is first distorted in amplitude by an INL mapping, after which it is multiplied by a gain of m, and an offset of c is added—a linear transformation. By Proposition A, the blocks in Figure 6.9 must be invertible if compensation is to be performed.

The linear distortion is always invertible, because it is a one-to-one mapping. It is always possible to make x the subject of the equation to obtain an inverse mapping. Integral nonlinearity, on the other hand, may not be invertible. It can only be invertible when it is a one-to-one mapping, which is only true if the converter is monotonic. Monotonicity is therefore a necessary condition for converter compensation.

Figure 6.10 shows a block diagram of a compensated converter. The inverse transformations are applied in reverse order, as was discussed in Section 3.4. Effective compensation requires that a converter's gain, offset and INL errors are measured. The latter may be measured by spectral analysis [9].

The compensation technique of Figure 6.10 is now demonstrated by simulation. Consider

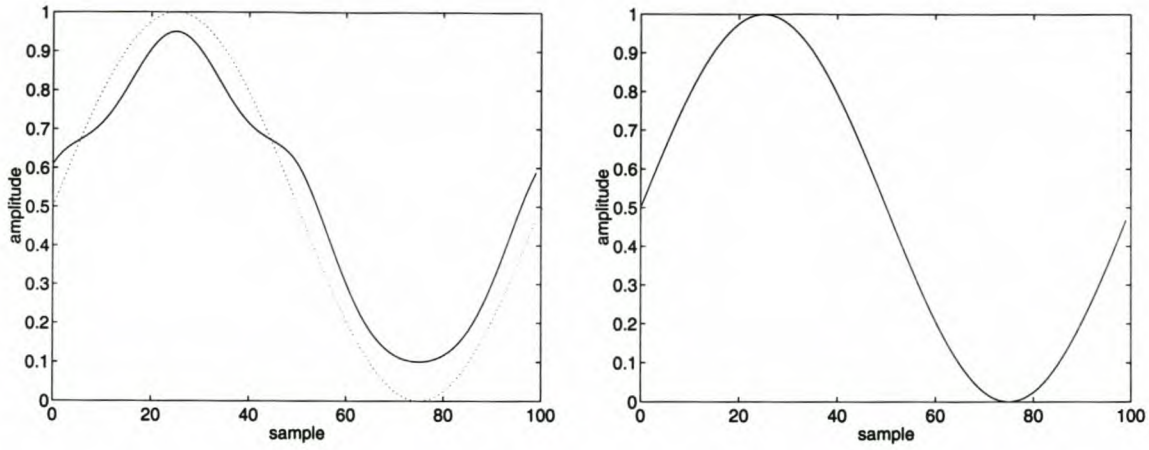

(a) (b)

Figure 6.12: *(a) Output signal of the DAC model prior to compensation. The dotted line shows the input signal. (b) Output signal of the DAC after the input signal has been passed through the compensation transforms.*

a DAC with INL as illustrated in Figure 6.11(a). The DAC also has a gain error of 0.85, and an offset error (after gain) of 0.1. The gain and offset errors can be modelled by the linear distortion

$$y = 0.85x + 0.1\,. \tag{6.17}$$

To perform converter compensation, the inverse distortion models must be calculated. If the INL is measured as in Figure 6.11(a), the inverse INL transform can be obtained by swapping the x and y axes. This inverse INL is shown in Figure 6.11(b). Similarly, the inverse linear distortion can be obtained by making x the subject of Equation 6.17:

$$x = 1.1765y - 0.1176\,. \tag{6.18}$$

Figure 6.12 shows the effect of converter inaccuracies and compensation. In Figure 6.12(a), a sine wave was provided as input to the uncompensated system, producing the severely distorted signal shown as the solid line. When the same signal was predistorted by passing it through the inverse linear distortion of Equation 6.18, and then through the inverse INL of Figure 6.11(b), the output was the signal in Figure 6.12(b). All distortion effects have disappeared, and the output signal is identical to the input signal again.

It can be concluded that the developed compensation techniques function correctly, and that they can be used to remove deterministic distortion effects in monotonic signal converters. The indirect DAC effect of sample-and-hold distortion (Section 4.1) can be negated in a similar way, by implementing an inverse digital filter prior to conversion.

The same compensation techniques may be applied to any devices that induce harmonics in the transmitted or received signals. Examples include amplifier and mixer compression.

6.4 Compensation accuracy

The compensation theory that was developed so far has made two significant assumptions: that distortion effects (such as spur sizes) can be measured with perfect accuracy, and that the compensation parameters (such as amplitude or phase correction) can be applied with perfect accuracy. Neither of these assumptions hold in a practical system, and the implication of finite-accuracy compensation will be studied in this section.

6.4.1 Measurement accuracy

In a practical system, it is possible that a spur with size S (either real or complex) is measured inaccurately, so that the measured value is

$$S' = S + s_\epsilon \,. \tag{6.19}$$

If compensation is performed using $-S'$, a residual spur with size $-s_\epsilon$ remains. This means that compensation can only be performed up to the accuracy with which the frequency-domain effects can be measured.

Tolerances on ρ, κ, ε_i and ε_q may be calculated by substituting a practical system's measurement tolerance, $-s_\epsilon$, into Equations 6.3, 6.6 and 6.12. In this way, residual distortion effects due to measurement inaccuracies may be calculated using the theory of Chapter 5.

6.4.2 Numeric accuracy

A fundamental limit on the accuracy of a software-defined radio is imposed by numeric quantisation, both during signal conversion and during signal processing. Consider an SDR system that uses N bits in its numeric representation.[3] Realisable quantisation levels lie

$$q = \frac{2}{2^N} \tag{6.20}$$

apart on a normalised signal that spans $[-1, +1)$. When attempting to represent an arbitrary signal value, the worst-case error would be

$$\frac{q}{2} = \frac{1}{2^N} \,, \tag{6.21}$$

which occurs when the correct signal value falls midway between two quantisation levels.

This worst-case error could occur when attempting to represent a DC value, or a signal of a particular amplitude. Due to quantisation, the amplitudes of two quadrature signals may

[3] If an SDR uses a different number of bits per sample during processing than during signal conversion, N corresponds to the smaller of the two. Also note that this text uses the convention that any signal converter, including oversampling devices (e.g. $\Delta\Sigma$ converters), can be modelled in terms of an equivalent Nyquist-rate converter, that has an effective N-bit quantisation accuracy within its corresponding Nyquist band [7]. It is therefore possible to focus on Nyquist-rate converters without loss of generality.

still differ by $\frac{q}{2}$, even after compensation. For $\rho = \frac{q}{2}$, Equation 5.10 predicts a remaining worst-case spur size

$$\mathrm{SFDR}_\rho = 20\log(2 \cdot 2^N) = (N+1) \cdot 6.02 \text{ dB} \tag{6.22}$$

below the fundamental signal.

Similarly, quantisation error would cause worst-case remaining DC offsets after compensation of $\varepsilon_i = \varepsilon_q = \frac{q}{2}$. That corresponds to

$$\alpha = \sqrt{\frac{q^2}{4} + \frac{q^2}{4}} = \sqrt{2} \cdot 2^{-N}. \tag{6.23}$$

Equation 5.38 predicts a worst-case spur size of

$$\mathrm{SFDR}_\epsilon = 20\log\left(\frac{2^N}{\sqrt{2}}\right) = N \cdot 6.02 - 3.01 \text{ dB} \tag{6.24}$$

below the fundamental signal.

Lastly, numeric accuracy also has an impact on how accurately phase differences can be represented within a digital system (see Appendix A.3.2, p. 164). For example, if a DDS-based SDR transmitter uses N bits as phase accumulator, a phase quantisation error of as large as

$$\kappa = \frac{q}{2} \cdot \pi \tag{6.25}$$

can be made. Equation 5.72 relates this to an SFDR of

$$\mathrm{SFDR}_\kappa = 10\log(\kappa^2 + 4) - 20\log\kappa. \tag{6.26}$$

For small κ, the first term can be simplified so that

$$\mathrm{SFDR}_\kappa = 6.02 - 20\log\left(\frac{\pi}{2^N}\right) = N \cdot 6.02 - 3.92. \tag{6.27}$$

Once again, it is seen that the system's quantisation accuracy has a direct effect on the worst-case remaining spur after compensation.

In general, residual spur sizes due to quantisation effects can be improved by 6.02 dB for each bit by which the numeric accuracy is increased.

6.4.3 Remarks

This section has demonstrated that compensation accuracy is limited by the precision with which spurs can be measured, and by the numeric accuracy of the digital system, including its converters (Proposition A). It is therefore possible to greatly increase the effective accuracy of mixer hardware by selecting an adequate numeric resolution for the SDR. In self-calibrating systems like those proposed in Section 6.7, the numeric accuracy also determines the measurement accuracy of the system.

6.5 Multistage compensation

In a practical system, quadrature compensation would most likely be combined with compensation for non-idealities in other parts of the transmission path. Such multistage compensation should preferably be performed according to the invertible-cascade model of Section 3.4 (p. 26) and of Proposition A.

For example, a typical transmitter would consist of DACs, followed by LPFs, followed by the quadrature mixer. Compensation must be performed in the opposite order, as was illustrated in Figure 3.2 (p. 27). Therefore the signal will be generated with compensated phase error in the phase accumulators, I-Q amplitude adjustment will be performed, and DC offsets added. Next, the inverse LPF will be applied to the generated signal. Lastly, the inverse DAC effects (such as inverse INL) will be added. If the hardware was modelled correctly, the compensated signal can be accurate to within the numeric or measurement accuracy of the system, as asserted by Proposition A (p. 4).

6.6 Non-coherent oscillators

In the development of much of the quadrature mixing theory thus far, it was assumed that the receiver local oscillator is coherent to the transmitter oscillator. Under this assumption, signal distortion caused by quadrature non-idealities was analysed, and compensation techniques were derived. In general, however, it cannot be assumed that the receiver is perfectly phase-coherent with the transmitter, since this would place demands on the front-end complexity that could be unacceptable in many systems.

This section investigates the non-coherent case, and its effect on the downmixed signals. It will be shown that non-coherent mixing produces more complex forms of signal distortion than the coherent case. However, it will also be shown that the compensation techniques derived in the chapter thus far still hold, under the limitation that transmitter inaccuracies can only be corrected at the transmitter, and *vice versa*.

6.6.1 Transmitter errors in an ideal receiver

A more general development for downmixed transmitter inaccuracies will now be done, with $\Delta\omega_c = \omega_c - \hat{\omega}_c \neq 0$. Receiver inaccuracies need not be analysed again, since they do not depend on the frequency or phase of the transmitter LO, neither therefore on $\Delta\omega_c$.

Amplitude deviation

It was shown in Equation 5.9 (p. 45) that an RF signal produced by a transmitter with quadrature amplitude deviation can be written in the form

$$y(t) = \overbrace{\mathcal{R}e\{a(t)e^{j\phi(t)}\}\cos\omega_c t - Im\{a(t)e^{j\phi(t)}\}\sin\omega_c t}^{\text{desired upmixed signal}} + \underbrace{\rho\cdot\mathcal{R}e\{a(t)e^{j\phi(t)}\}\cos\omega_c t}_{\text{error signal}} . \quad (6.28)$$

Quadrature downmixing by an estimated LO frequency is given by the equation

$$\begin{aligned} s(t) &= 2\left[y(t)\cdot e^{-j\hat{\omega}_c t}\right]_{\text{LPF}} \\ &= a(t)e^{j[\phi(t)+\Delta\omega_c t]} + \rho\cdot\mathcal{R}e\left\{a(t)e^{j\phi(t)}\right\}\cdot e^{j\Delta\omega_c t} . \end{aligned} \quad (6.29)$$

The first term represents the desired downmixed signal, translated in frequency by $\Delta\omega_c$. It was already motivated on page 19 why this frequency translation is acceptable in the digitised signal. The second term is the error term. Compare this to the coherent-demodulation case of Equation 5.19 (p. 51). The error term is now multiplied with the complex exponential $e^{j\Delta\omega_c t}$, which translates it in frequency, so that it no longer just produces a sideband of the desired signal. This spurious signal cannot be removed by simple amplitude adjustment in the receiver.

DC offset and LO leakthrough

A similar analysis can be done for DC offset and LO leakthrough at a transmitter, which is then downmixed with a non-coherent oscillator. In this case, Equation 5.35 predicts an RF signal of

$$y(t) = \mathcal{R}e\left\{a(t)e^{j[\phi(t)+\omega_c t]}\right\} + \alpha\cos(\omega_c t+\gamma) . \quad (6.30)$$

In the coherent-reception case, the transmitter inaccuracy translated to a simple DC offset in the received $I(t)$ and $Q(t)$ signals. For non-coherent reception, however,

$$\begin{aligned} s(t) &= 2\left[y(t)\cdot e^{-j\hat{\omega}_c t}\right]_{\text{LPF}} \\ &= a(t)\cdot e^{j[\phi(t)+\Delta\omega_c t]} + \alpha e^{j(\Delta\omega_c t+\gamma)} . \end{aligned} \quad (6.31)$$

The error term is no longer a constant signal offset, but a complex-valued oscillation at $\Delta\omega_c$. DC offset and LO leakthrough in the transmitter can no longer be corrected in the receiver by just adding an appropriate compensation offset.

Phase error

The analysis for quadrature phase error in the transmitter, with non-coherent reception, is very similar to the one for amplitude deviation given above. An upmixed signal with phase error can be written in the form of Equation 5.71:

$$y(t) \approx y_d(t) + \kappa\cdot\mathcal{R}e\left\{a(t)e^{j\phi(t)}\right\}\sin\omega_c t , \quad (6.32)$$

Non-coherent downmixing produces

$$\begin{aligned} s(t) &= 2\left[y(t)\cdot e^{-j\hat{\omega}_c t}\right]_{\text{LPF}} \\ &= a(t)e^{j[\phi(t)+\Delta\omega_c t]} + \kappa\cdot\mathcal{R}e\left\{a(t)e^{j\phi(t)}\right\}\cdot e^{j(\frac{\pi}{2}-\Delta\omega_c t)}. \end{aligned} \tag{6.33}$$

By the same argument as for amplitude deviation above, it can be concluded that noncoherent downmixing causes a spurious double-sideband signal to appear in the downmixed signal. In contrast to the coherent-downmixing case, this signal is not centred around 0 Hz, but shifted by $\Delta\omega_c$. Hence it cannot be cancelled by the compensation techniques developed thus far in this chapter.

6.6.2 Implication to compensation

The analyses above have shown that non-coherent downmixing in the presence of quadrature errors causes more complex artefacts in the received baseband signal. Although it would be possible to predict corresponding error signals for the various modulation schemes, little would be gained by such an exercise. Rather, the compensation techniques developed in Sections 5.5–5.7 should be revised for the non-coherent reception case.

It was shown in the earlier sections that, if coherent downmixing is performed, it is possible for a quadrature receiver to compensate for transmitter errors, and *vice versa*. This was exactly what was done in the simulations on pages 93 to 102. However, the analysis of the non-coherent case presented here shows that such simple forms of compensation can no longer be performed across the receiver-transmitter boundary.

In practice, this means that the transmitter can only compensate for quadrature errors originating at the transmitter, and the receiver for receiver errors. In a practical system, this may be a small cost to pay for the considerable simplification of allowing independent LO signals. It is still computationally simple to maximally suppress all quadrature-mixing spurs (originating at both the transmitter and the receiver) in the received signal, within the constraints of Proposition A.

Non-coherent mixing does not render compensation across the RX-TX boundary impossible, however, but it does make it considerably more involved. It would be possible to perform digital carrier estimation on the received signal, and use this information to estimate the transmitter sidebands. Such compensation techniques are not considered in the scope of this text, since (as will be shown in the next section) the issues of quadrature errors in non-coherent systems may be avoided if the receiver compensation is applied prior to calibrating the transmitter.

6.7 Calibration techniques

Before reception and transmission can take place, the software radio must be calibrated in order to compensate for hardware inaccuracies. Manual calibration can be a time-consuming

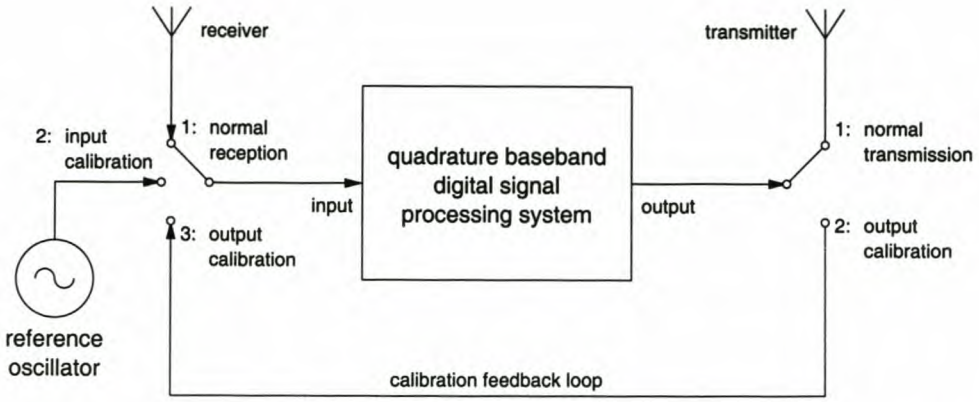

Figure 6.13: *Self-calibration system for quadrature-baseband software-defined radios.*

process that is particularly undesirable in devices that must be produced commercially. For this reason, a system was developed to help automate the compensation techniques presented in this chapter [51].

6.7.1 Single-reference calibration

Figure 6.13 shows a block diagram of this self-calibrating system: It is designed to perform calibration on a quadrature-baseband SDR transceiver, to compensate for non-idealities in the data conversion and quadrature mixing stages. The calibration method requires no external signal sources or measuring equipment. A single internal oscillator is used to calibrate the input stage, after which the corrected input can be used to calibrate the output stage.

During normal operation, the input and output stages of the SDR are switched to their respective amplifiers and antennas. When the system is to be calibrated, the input stage is first switched to position 2, from where it receives a signal generated by a reference oscillator. This signal may have a fairly arbitrary constant frequency within the allowed RF range of the receiver. The local oscillator is set to a frequency slightly below or above this reference frequency, and quadrature downmixing is performed.

Calibration is performed by analysis of the quantised complex baseband signal. The Fourier transform of the complex-valued signal is not symmetrical around zero. Assuming that the reference frequency is somewhat higher than the local oscillator frequency, the fundamental signal component will appear in the positive frequency spectrum. From here the signal harmonics can be analysed to determine the conversion non-linearities (see Section 6.3), and the signal sidebands and DC level can be analysed to determine the quadrature mixing inaccuracies (see Section 6.1).

Once the receiver stage has been calibrated, the receiver switch in Figure 6.13 switches to position 3, and the transmitter switches to position 2. The transmitter can now generate a test component, and the feedback to the calibrated receiver stage can be used to obtain

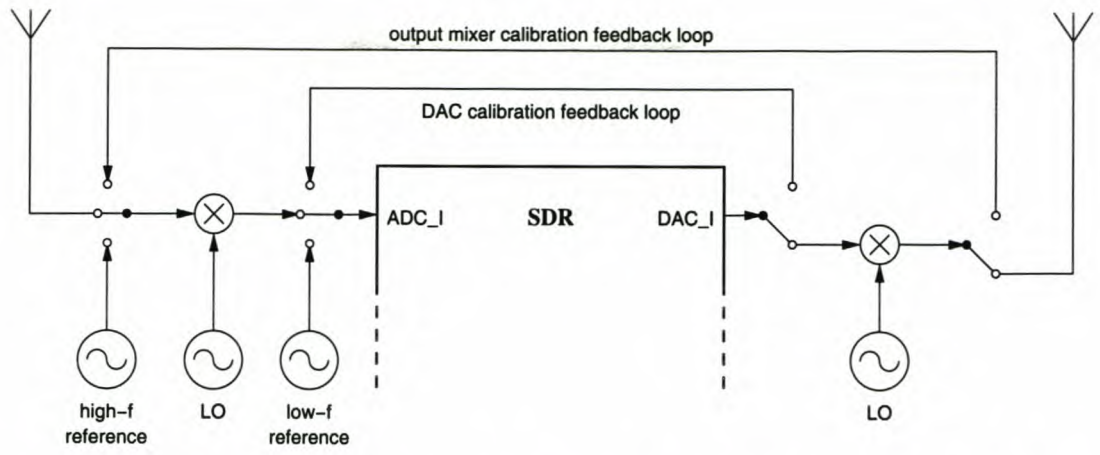

Figure 6.14: *A self-calibration system for SDR, with independent mixer and converter references. Only one of the input-output pairs is shown in the diagram, but the other pair is configured in an identical fashion.*

a reliable measurement of the transmitted signal spurs. After using this measurement to calculate the transmitter compensation parameters, the system switches back to normal operation (both switches in position 1).

6.7.2 Double-reference calibration

As an alternative to the single-reference calibration technique of the previous section, it may be possible to use two reference oscillators: a high-frequency oscillator (within the RF band) used to calibrate the quadrature mixer, and a low-frequency oscillator (frequency an order of magnitude lower than the ADC sampling rate) used to calibrate the digital converters. This approach isolates converter calibration from mixer calibration, and is illustrated in Figure 6.14. For this system, the calibration steps would be:

1. Connect both input ADCs to the low-frequency oscillator, and compensate for any harmonic distortion observed in the input signal.

2. Connect the output DACs to the input DACs, generate a test tone on the DACs, and compensate for any harmonic distortion observed in the output signal.

3. Switch the ADC inputs back to their respective quadrature downmixer outputs.

4. Switch the DAC outputs back to their respective quadrature upmixer inputs.

5. Connect the quadrature downmixer input to the high-frequency oscillator, and compensate for any quadrature errors observed in the complex baseband signal.

6. Connect the quadrature upmixer output to the quadrature downmixer input, and generate a test signal on the system output. Compensate for any quadrature errors observed in the output signal.

7. Switch the quadrature downmixer input back to the antenna for normal reception.

8. Switch the quadrature upmixer output back to the antenna for normal transmission.

Although this approach requires an additional reference oscillator, it has the advantage that it better characterises the hardware inaccuracies by completely separating error contributions of the converters from error contributions of the mixers.

6.8 Remarks

This chapter showed that it is possible to compensate for hardware non-idealities, in particular those associated with the quadrature mixer, and this result forms a central contribution of this dissertation. The fact that it is possible to counteract the non-idealities of a quadrature mixer makes its use in practical systems viable. Since quadrature mixing allows clear separation between signal translation and processing (Proposition B), which has significant advantages in terms of system complexity, the compensation of quadrature impairments is an important contribution.

In the next chapter, the developed theory is put into practice in the development and calibration of a simple SDR prototype.

Chapter 7

Practical results

The dissertation thus far has developed a theory of quadrature modulation and demodulation techniques, analysed their typical inaccuracies, and derived compensation techniques to ensure accurate signal transception. Numerous simulations were used to verify the theories presented throughout the text. The current chapter rounds off this research by describing the development of an experimental quadrature-based transceiver. The goals of the experiments described here are as follows:

1. To illustrate the development of a quadrature-based software-defined radio.
2. To demonstrate that quadrature mixing can be used to modulate and demodulate typical communications signals.
3. To compare observed artefacts with the theoretical predictions and simulations.
4. To verify the compensation theory, and to demonstrate that it is possible to suppress mixing artefacts to the point where they are no longer measurable (because they are obscured by noise) or adjustable (because the accuracy of the compensation factors have reached the numeric resolution of the SDR).
5. To confirm that it is possible to significantly improve the signal quality obtainable using low-cost mixers, by applying digital compensation.

7.1 General experimental setup

In this section the software, instrumentation and other hardware that make up the experimental setup, are described. In each experiment in Sections 7.2 and 7.3, the configuration of these components specific to that experiment will be documented.

7.1.1 Quadrature upmixer

The Rohde & Schwarz SMIQ-04B Vector Signal Generator supports quadrature upmixing of baseband I and Q signals to carrier frequencies of up to 4.4 GHz. The -3-dB modulation

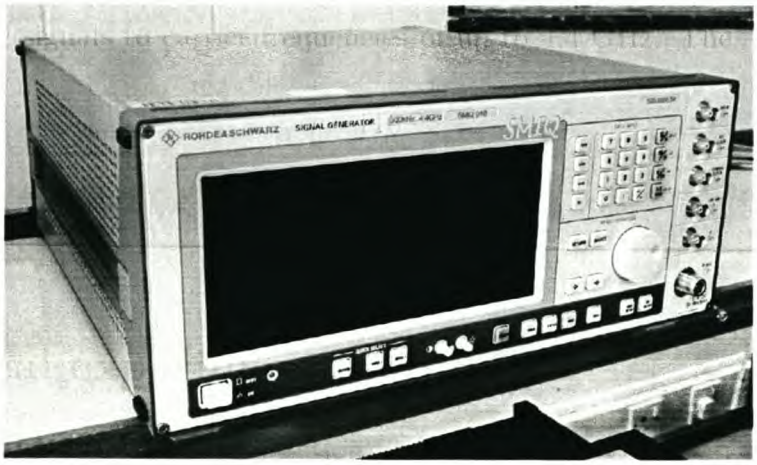

Figure 7.1: *The SMIQ-04B signal generator, with quadrature upmixing functionality.*

bandwidth is 30 MHz, and deliberate quadrature mixing errors (referred to as "quadrature impairments") can be set, making this instrument ideal for measuring and compensating for quadrature non-idealities.

Spectral purity during signal generation is specified to an SFDR of 70 dB for non-harmonic spurs, and 30 dB for harmonic spurs. The rated carrier-leakthrough SFDR is 45 dB, and the sideband spur size is not specified. Three "quadrature impairments" may be adjusted:

- Carrier leakage, as a percentage of the signal voltage (0% to 50%), at a resolution of 0.5%. The carrier leakage phase is not specified. The desired signal strength is lowered by an equal amount.

- Amplitude deviation, as a percentage of the full-scale voltage (−12% to +12%), at a resolution of 0.1%. The output power of the signal is maintained, so if the Q-signal's amplitude is increased, the I-signal's amplitude is decreased. This principle was also applied in all simulations, and is discussed in Appendix D. The ratio by which the I-channel amplitude must then adjust when the Q-channel amplitude changes, is given by Equation D.8 (p. 188).

- Quadrature phase offset, in degrees (−10° to +10°), at a resolution of 0.1°. The relationship between the phase error and the carrier leakage phase is not specified.

Although the adjustment resolution for each of these parameters is quoted in the product specifications [38], the tolerances on these parameter settings are not specified. It is therefore necessary to make the assumption that the accuracy of these quadrature impairments are approximately within the same order of magnitude as the specified adjustment resolutions.

From these specifications, and from the observed behaviour of the device, the SMIQ quadrature upmixing block diagram illustrated in Figure 7.2 may be deduced. The parameter ρ_g represents the percentage amplitude mismatch, κ_g is the quadrature phase error, α_g is the

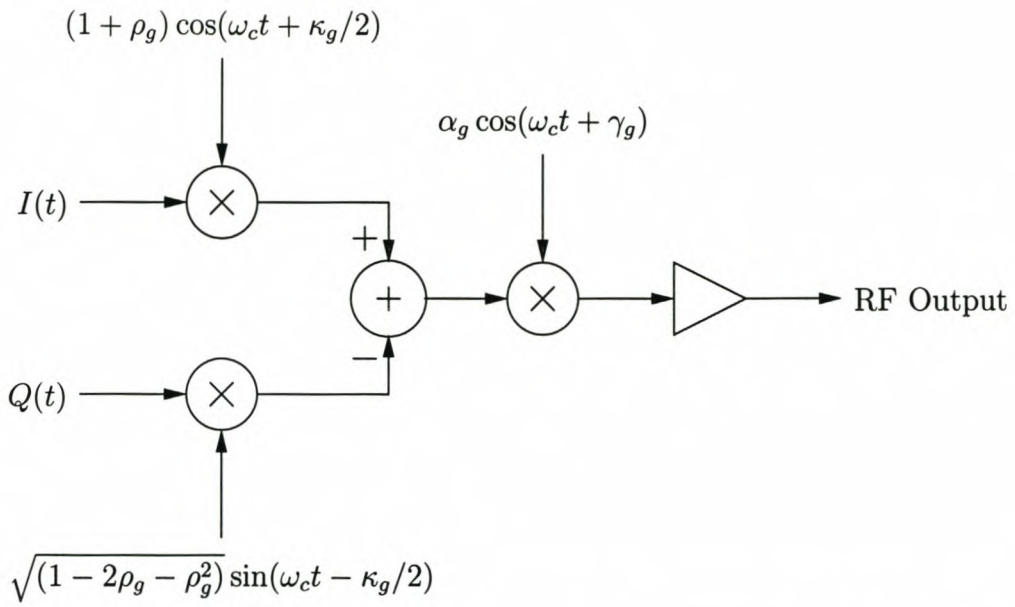

Figure 7.2: *Block diagram of the quadrature upmixing ("vector modulation") function of the Rohde & Schwarz SMIQ signal generator.*

Figure 7.3: *Screenshot of the adjustable I-Q impairment settings on the Rohde & Schwarz SMIQ signal generator [37].*

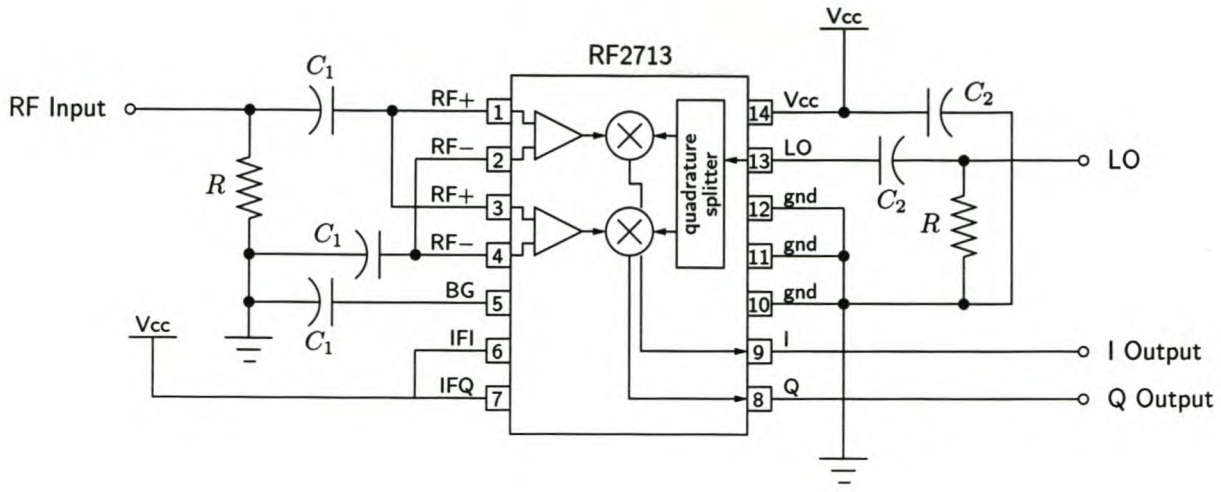

Figure 7.4: *Circuit diagram of the RF2713 quadrature mixer in a downmixing configuration [35]. In this diagram,* $R = 51$ kΩ, $C_1 = 10$ nF *and* $C_2 = 100$ nF.

Table 7.1: *Some specifications of the RF2713 quadrature mixer [35].*

Parameter	Typical	Worst-case
RF frequency range	0.1 to 250 MHz	
Baseband frequency range	DC to 50 MHz	
Noise figure	35 dB	
I-Q amplitude balance	0.1 dB (1.2%)	0.5 dB (5.9%)
Quadrature phase error	1°	
DC offset	< 10 mV	100 mV

carrier leakage percentage, and γ_g is the unknown carrier leakage phase. Figure 7.3 shows a block diagram of the SMIQ signal generator dialog by which the impairments may be adjusted.

7.1.2 Quadrature downmixer

Whilst a high-precision signal generator is used for the quadrature upmixing stage, the downmixing stage of the software-defined radio prototype employs a low-cost quadrature mixing IC: the RF2713 from RF Micro Devices [35]. The RF2713 is intended for general-purpose quadrature mixing, including zero-IF mixing (i.e. for quadrature-baseband modulation and demodulation of digital or analogue signals). The device may be connected in a modulating (upmixing) or demodulating (downmixing) configuration.

Figure 7.4 shows how the RF2713 can be configured as a quadrature downmixer [35]. This design was implemented on a printed circuit board. Table 7.1 lists a few relevant specifications of the mixer, including its typical quadrature inaccuracies.

7.1.3 Data acquisition card

In order to accurately synthesise and digitise analogue signals, a high-speed analogue-digital-analogue (ADA) device with a suitable software interface is required. The DAQ-2010 data acquisition card from Adlink is used for this purpose. It is capable of sampling four 14-bit input channels at 2 MS/s each, and two 12-bit output channels at 1 MS/s each [2]. This makes it well-suited for an SDR implementation with a bandwidth of up to approximately 1.4 MHz (reception) and 700 kHz (transmission).

Furthermore, all input and output channels have worst-case integral non-linearity errors (INL) of ± 1 LSB, which means that any spurious harmonics caused by deviation from the straight-line response must lie more than $12 \cdot 6.02 \approx 72$ dB (transmission) or $14 \cdot 6.02 \approx 84$ dB (reception) below the full-strength desired signal. This effectively eliminates the need for any further INL compensation, since any compensation distortion can be no more accurate than 1 LSB itself.

The DAQ-2010 interface that was developed for the SDR architecture is given in Appendix E. Dual-channel input and dual-channel output (for I-Q modulation) were supported in the software implementation.

7.1.4 Low-pass filters

Since the accuracy of quadrature modulation and demodulation depends on how well the I and Q channels are balanced, the channels' low-pass filters should be matched as closely as possible. For this purpose, two minimum-sensitivity Sallen-Key low-pass biquads are designed, and the difference between their frequency responses are measured in order to characterise the remaining imbalance. Active filtering is preferred in this application, since the output of the RF2713 quadrature mixer should be connected to a high-impedance load. Also, the Sallen-Key biquad contains no inductors; the poor tolerance on inductor values would make the design of well-matched low-pass filters more problematic.

The purpose of the low-pass filters is to remove sampling artefacts prior to upmixing, and to remove out-of-band noise and mixing images after downmixing. The bandwidth of the experimental system can be chosen so that its sampling artefacts may be adequately suppressed by a reasonably simple low-pass filter.

Filter design

The block diagram of the Sallen-Key biquad used for this design is shown in Figure 7.5. To ensure high input impedance, an operational amplifier in a voltage-follower configuration is used as input buffer. If it is assumed that the filter cut-off frequency will be at least an order of magnitude lower than the 100-kHz sampling rate of the data acquisition card, then the 4-MHz gain-bandwidth product of the LF351 operational amplifier makes it well suited as a filter component.

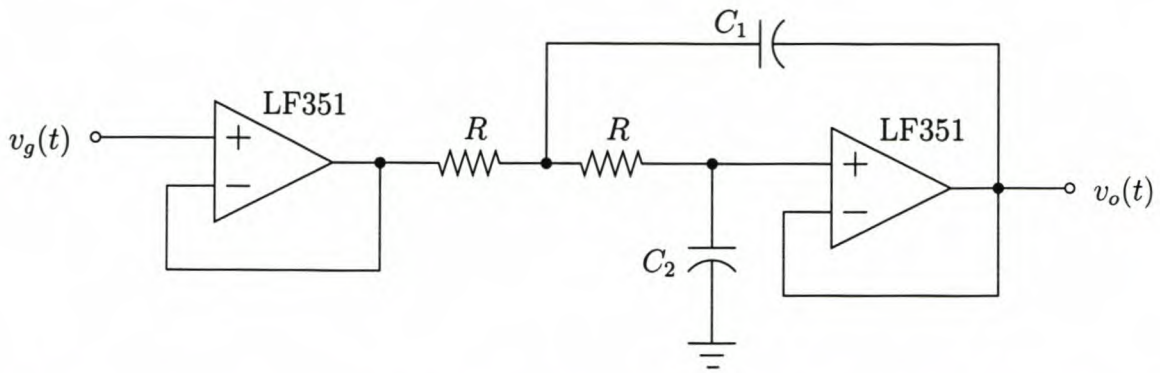

Figure 7.5: *Circuit diagram of a minimum-sensitivity, unity-gain Sallen-Key low-pass biquad.*

The design equations for a minimum-sensitivity Sallen-Key LPF is given by [44]:

$$R = k_z\ \Omega \tag{7.1}$$

$$C_1 = \frac{2Q}{k_z\omega_0}\ \mathrm{F} \tag{7.2}$$

$$C_2 = \frac{1}{2k_zQ\omega_0}\ \mathrm{F}\,, \tag{7.3}$$

where k_z represents an impedance scaling factor. A high quality factor (Q) produces a sharp cut-off between the passbands and stopbands (i.e. a relatively short transition region). However, it could produce a large gain peak near the corner frequency, and may require a large capacitance spread.

If the system is designed in such a way that the filter's transition region (including the resonant peak) falls within the "guard band" between the maximum signal frequency and the half Nyquist frequency, then the presence of a large gain peak is acceptable. After digital-to-analogue conversion, there is no signal content in the guard band, and the peak in the post-converter LPF's magnitude response will therefore not cause signal distortion. Similarly, any noise that is amplified by the filter prior to analogue-to-digital conversion may later be removed by digital filtering; the LPF here serves its primary purpose as anti-aliasing filter.

For these reasons, the filter is designed with as large a Q as produces a reasonable spread in capacitance values, in order to obtain a maximally flat passband and a short transition band.

To design the filter, two capacitance values with a reasonably large spread is chosen. By combining Equations 7.2 and 7.3, the quality factor may be calculated as

$$Q = \sqrt{\frac{C_1}{4C_2}}\,. \tag{7.4}$$

The next step is to calculate the impedance scaling factor, k_z, from these equations by including the desired cut-off frequency. The resistors' value, R, then follows directly.

Table 7.2: *Prototype filter design summary.*

Parameter	Value
Maximum signal frequency	1.5 kHz
Sampling frequency	100 kHz
LPF cut-off frequency	10 kHz
Filter attenuation of 98.5-kHz image	$40 \log \frac{98.5}{10} = 39.7$ dB
Sample-and-hold attenuation at 98.5 kHz	$20 \log[\text{sinc}(0.985)] = 36.4$ dB
Total worst-case image attenuation	76.1 dB

Cut-off frequency. The choice of filter cut-off frequency affects the maximum signal bandwidth, and the magnitude of alias spurs in the filtered spectra; acceptable specifications for the spur sizes should first be chosen. The SMIQ signal generator specifies 30-dBc harmonic spurs and 70-dBc non-harmonic spurs (Section 7.1.1)—a sensible specification for filter performance should therefore be that it suppresses in-band spurs and noise by at least 70 dB. By choosing a maximum signal frequency of 1.5 kHz, a filter cut-off frequency of 10 kHz and a sampling rate of 100 kHz, this constraint is met, as is summarised in Table 7.2.

The wide margin between the maximum signal frequency and the filter cut-off frequency also ensures that the signal is located within that slow-changing range of the passband that is least sensitive to component tolerances. This should ensure a better transfer function match between the I and Q filters.

Component choices. Choosing $C_1 = 470$ nF and $C_2 = 1$ nF allows the implementation of the filter using low-tolerance polycarbonate and polystyrene capacitors, respectively. The 1-nF capacitor is still more than an order of magnitude higher than parasitic capacitances that could be anticipated in the printed circuit board prototype [17]. These capacitor choices produce $Q = 10.84$. Substituting the capacitor values and the 10-kHz cut-off frequency into Equations 7.1 to 7.3 allows one to solve for the remaining component value, $R = 734\ \Omega$.

Simulated filter response

The predicted magnitude and phase responses of the filter is given in Figure 7.6. The filter has a flat, ripple-free passband with unity gain, that rises to a strong amplification peak at the cut-off frequency (caused by the choice of quality factor). The response then drops at 40 dB per decade in the stopband. The phase response varies little in the passband and stopband, but changes rapidly near the cut-off frequency—also as a result of the size of Q [44]. The flat, almost linear filter response in the passband ensures that component tolerances will have minimum impact on how well the I and Q filters match.

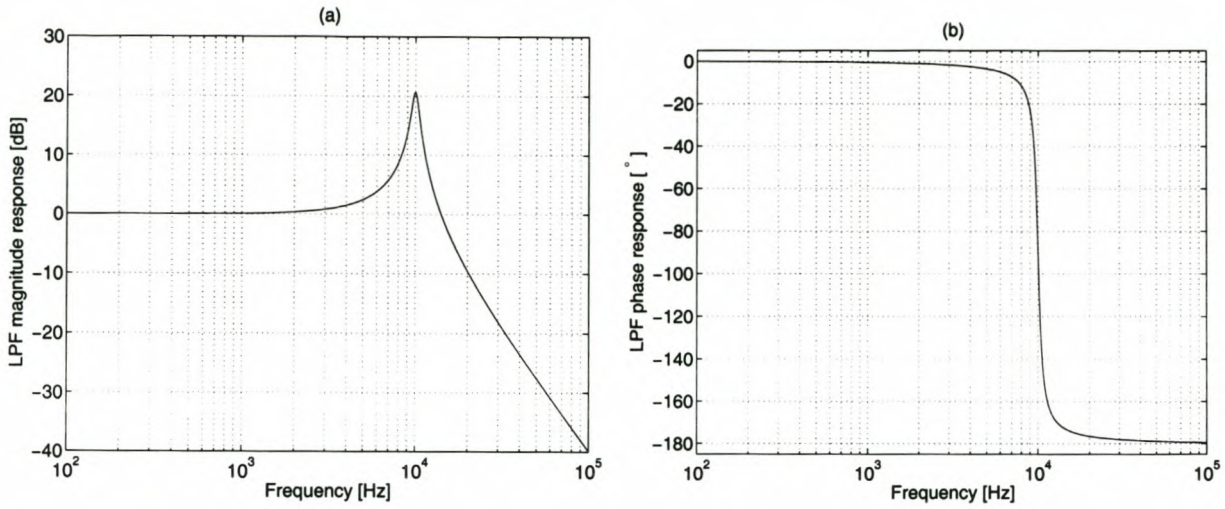

Figure 7.6: *Predicted Sallen-Key low-pass biquad frequency response. (a) Magnitude response. (b) Phase response.*

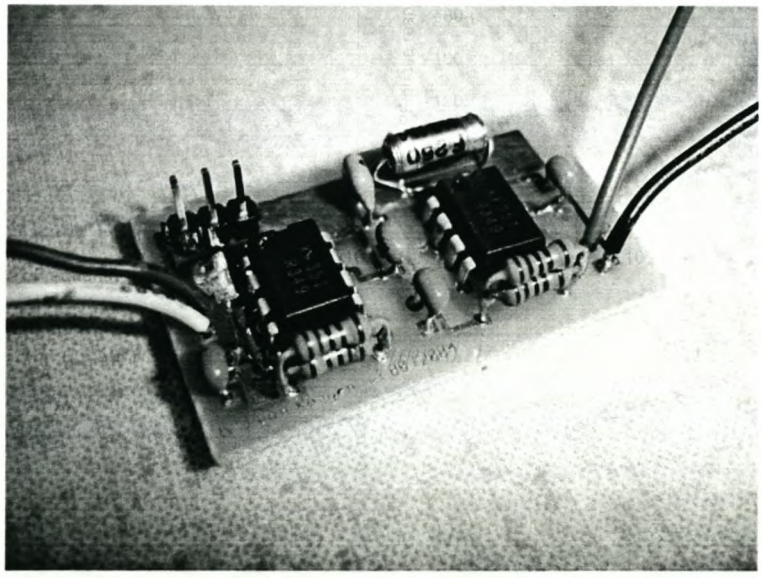

Figure 7.7: *A constructed Sallen-Key low-pass filter.*

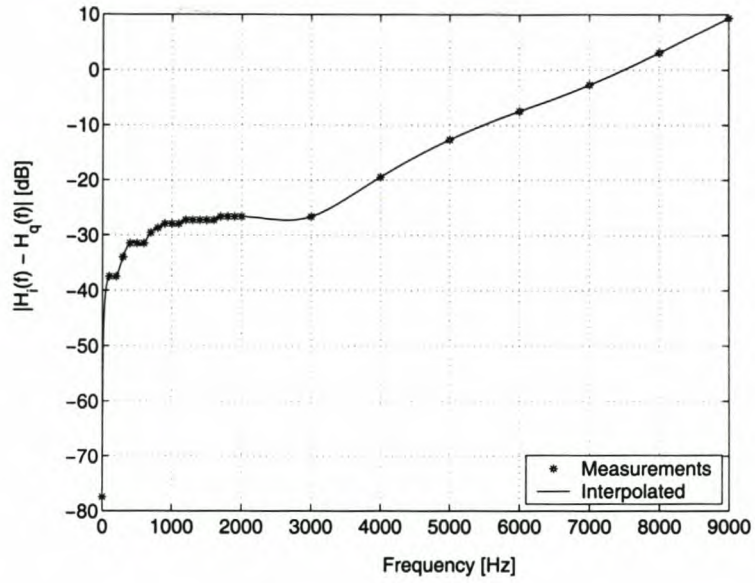

Figure 7.8: *Graph of the filters' common-mode rejection over baseband frequencies. The magnitude of the error phasor is approximately constant between* −28 *and* −26.5 dB *from 1 kHz to 3 kHz. At higher frequencies the filters approach their sensitive region near the cut-off frequency, and the mismatch becomes progressively worse.*

Filter construction

The block diagram of Figure 7.5 was implemented using the chosen component values. A fully constructed filter on a printed circuit board is shown in Figure 7.7.

Measurement of filter accuracy

To test whether the filters are well matched, a common-mode test was performed, in which a sinusoid of variable frequency was connected to the inputs of both filters. The difference between the two filter outputs was then measured. Note that both amplitude mismatch and phase mismatch at the test frequency would cause an error sinusoid to appear in the difference signal. The magnitude of this error phasor was then measured.

The results of the filter measurements are shown in Figure 7.8. Very little mismatch occurs at DC (the amplitude of the error signal is about 77.5 dB below the input signal), and the mismatch in the 1–3 kHz range is approximately constant around −27 dB. Above 3 kHz, the filters' transfer functions enter a range of rapid change in both magnitude and phase, indicative of the Sallen-Key biquad's low damping ratio. In this range the filters exhibit high sensitivity to component tolerances, and are poorly matched.

If the reliable passband of the filters is chosen to lie below 3 kHz, the worst-case error of −26.5 dB (140-mV error signal for a 3-V signal, or 4.467%) occurs exactly at 3 kHz. If only the magnitude of this error signal is considered, Equation 5.10 (p. 47) predicts a sideband

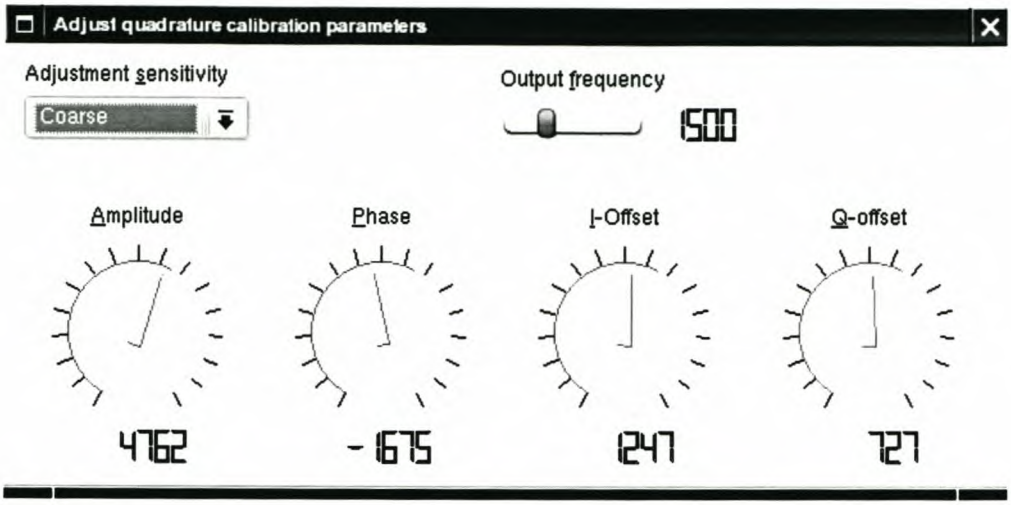

Figure 7.9: *Screenshot of the SDR calibration application that was written to compensate for quadrature mixing errors.*

spur size in the upmixed signal, due to filter mismatch in the baseband, of

$$\mathrm{SFDR}_{\mathrm{sb}} = -20\log\left(\frac{0.0467}{2-0.0467}\right) = 32.8 \text{ dB} \tag{7.5}$$

Filter mismatch produces a dependence on frequency in the quadrature errors. Even if the system is perfectly compensated by using a specific test frequency, the relative filter responses may differ at another frequency, and cause slightly different quadrature errors. Equation 7.5 places an upper bound on the magnitude of such post-compensation spurs.

7.1.5 Software

The software for the SDR transceivers used in the practical measurements was written within the Software Defined Radio Architecture developed in the Digital Signal Processing and Telecommunications Group of the University of Stellenbosch. The SDR Research Project started as an extension of the Ph.D. research of this dissertation. It consists of a software architecture that allows the rapid development of new SDR configurations by using a library of SDR components. The library consists of modulators, demodulators, filters, coders, decoders, hardware interfaces, etc. For more information on the SDR Architecture and Component Library, see Appendix E.

One of the SDR applications that was developed specifically for these experiments, is the quadrature calibration tool shown in Figure 7.9. It allows the various quadrature DDS parameters to be adjusted, while the effects that the adjustments have on the RF signal may be monitored on a spectrum analyser.

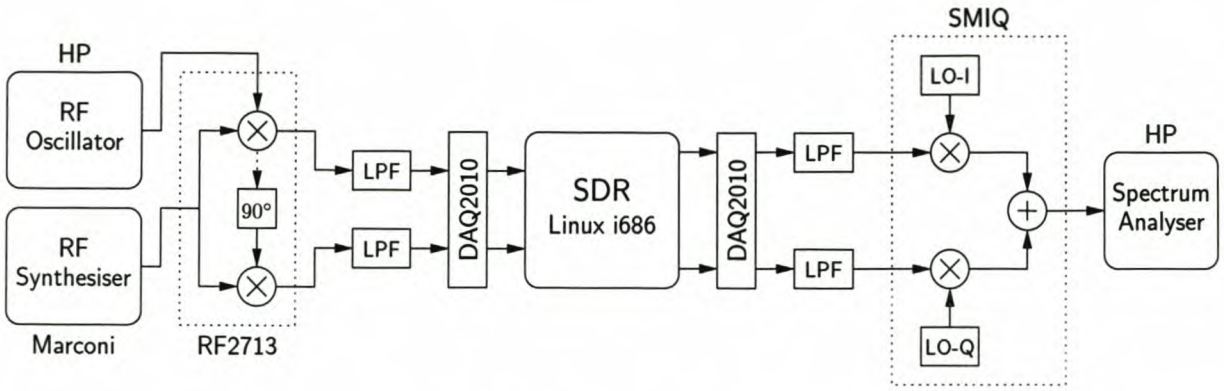

Figure 7.10: *Block diagram of the experimental setup.*

7.1.6 Measurement setup

The general measurement setup used in all the following experiments, is illustrated in Figure 7.10. In addition to the hardware and software components that were already discussed, the measurement setup makes use of a Hewlett-Packard 8590L spectrum analyser and a Marconi 2019 communications signal synthesiser (capable of generating FM and AM signals).

7.2 Transmission tests

The first set of experiments will test the transmission quality of a software-defined radio that uses quadrature upmixing. The system will be tested prior to any compensation, to measure the inherent quadrature inaccuracies of the system (Section 7.2.1). An initial calibration will then be performed to suppress the observed quadrature spurs to the RF signal's noise floor (Section 7.2.2). This calibrated system will then form the basis for further tests, in which deliberate errors are introduced to the quadrature mixing process (using the programmable impairments capability of the SMIQ quadrature upmixer, Section 7.2.3). Quadrature compensation is then applied to these known errors (Section 7.2.4), after which the transmitter is tested with multi-tone and dynamic signals (Sections 7.2.6 to 7.2.8).

7.2.1 Pre-compensation tests

Firstly, the transmission will be tested with no deliberate distortion. This test gives an indication of the absolute accuracy of the experimental system.

Experimental setup

A baseband tone of +1.5 kHz is generated without any predistortion, and sampled at 100 kHz. The quadrature baseband signals are filtered using second-order Sallen-Key low-pass filters with a cut-off frequency of 10 kHz. The resulting I and Q signals are then upmixed by

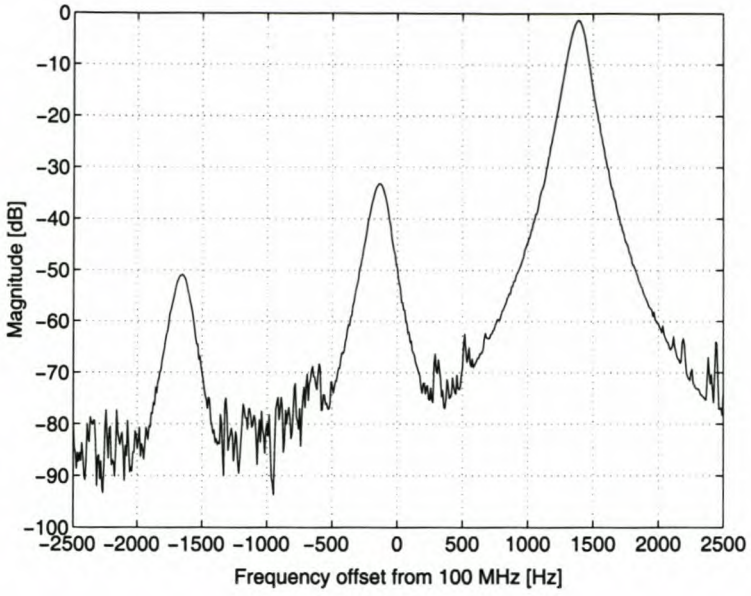

Figure 7.11: *Spectrum of the upmixed signal prior to any compensation. The rightmost spur is the desired signal. A carrier leakthrough component may be observed at* -31.9 dBc, *and a sideband component (due to amplitude mismatch and phase inaccuracy) at* -49.5 dBc.[2]

100 MHz using the SMIQ signal generator's "vector modulation" capability, with "quadrature impairments" set to zero. The resultant RF spectrum is then measured.

Expected results

Since a positive baseband frequency is used, quadrature upmixing should produce a desired component at 100 MHz + 1.5 kHz. Since no compensation is performed, it is to be expected that the system could include all types of quadrature inaccuracies. According to the theory developed in Chapter 5, these inaccuracies should produce a sideband component at 100 MHz − 1.5 kHz (due to amplitude mismatch and phase inaccuracy), and a carrier leakthrough component at 100 MHz.

Measurements

The measured RF signal spectrum is shown in Figure 7.11. Although the desired signal at 100 MHz + 1.5 kHz produces the strongest peak, the carrier and sideband spurs are also clearly visible. The SMIQ data sheet specifies a typical carrier leakthrough component of -45 dBc; the stronger observed spur of -31.9 dB suggests that the DACs and filters may contribute some DC offset. Although the SMIQ data sheet does not specify how large the sideband spur may be during quadrature mixing, the observed spur of -49.5 dBc does indicate that some amplitude mismatch and phase inaccuracy occur in the converters, filters and mixer.

Table 7.3: *Quadrature compensation parameters for the initial transmission calibration.*

Amplitude	I Offset	Q Offset	Phase
$\rho = 2.239 \cdot 10^{-3}$	$\varepsilon_i = -22.92 \cdot 10^{-3}$	$\varepsilon_q = -19.26 \cdot 10^{-3}$	$\kappa = 3.462 \cdot 10^{-3}$

Conclusion

The uncompensated system shows spurs at the expected frequencies. These spurs are the net effect of inaccuracies in all the subsystems of the analogue front-end. Regardless of how these inaccuracies are distributed between the subsystems, Proposition A, on which the compensation principles of Chapter 6 was built, only requires knowledge of their net effect. If this proposition is correct, it should be possible to compensate for these spurs in the experiments that follow.

7.2.2 Initial calibration

In the next experiment, the software radio's amplitude mismatch, DC offset and quadrature phase inaccuracy are adjusted, according to the compensation algorithm proposed in Section 6.1.4, until the sideband and carrier spurs are optimally suppressed. This calibration point will then form a basis for further tests, in which deliberate quadrature errors will be introduced.

Experimental setup

The basic experimental setup is identical to that of the previous experiment (Section 7.2.1). The compensation algorithm is executed using the manual calibrator shown in Figure 7.9 (p. 125), while observing the spur changes on the spectrum analyser.

Expected results

The compensation algorithm of Section 6.1.4 is simple enough to execute manually, and it should be possible to compensate for the quadrature spurs up to the point where the spurs are obscured by the noise floor of the synthesised signal. When the spur heights can no longer be measured, further compensation becomes impossible, and the synthesised signal is sufficiently compensated.

Measurements

Figure 7.12 shows the results of the initial calibration. The exact parameters required to compensate the system are listed in Table 7.3.

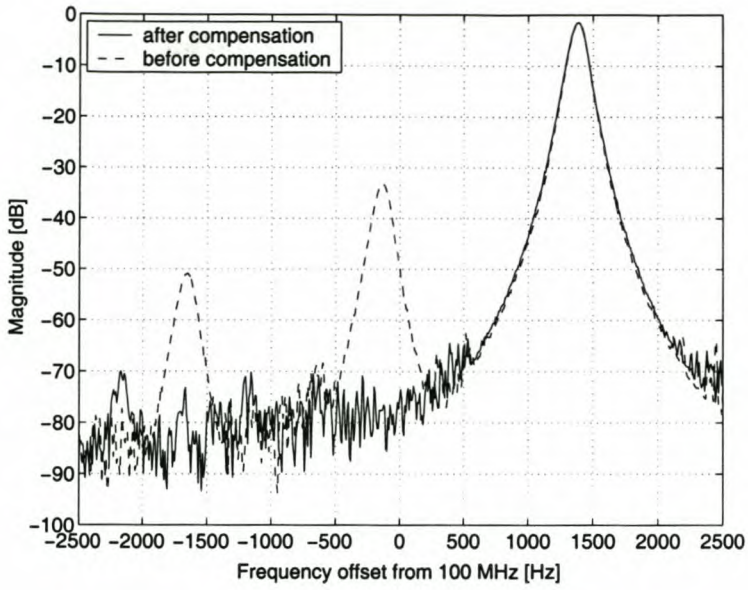

Figure 7.12: *RF spectrum after of the transmitted signal after initial calibration.*

Conclusion

Although the accuracy of quadrature compensation will only be accurately tested in Section 7.2.4, this experiment already shows the effectiveness of the quadrature compensation techniques. The carrier and sideband spurs have been suppressed so that they are completely indistinguishable from the transmission noise floor. The transmission system is now free from the effects of quadrature upmixing errors, and can be used in further experiments as a basis for the introduction of, and compensation for, various deliberate quadrature errors.

7.2.3 Deliberate quadrature errors

The calibrated system can now be used as basis for the next set of experiments, in which individual and compound quadrature errors are deliberately introduced in the upmixing stage. The resultant spurs in the RF spectrum can then be measured to verify that the theory of quadrature inaccuracies, as presented in Chapter 5, is accurate.

Experimental setup

The calibrated system of Section 7.2.2 is re-used for this experiment. The SMIQ signal generator, which is used as quadrature upmixing stage, supports the generation of deliberate quadrature errors (see Section 7.1.1, p. 116). Using this functionality, the following tests are to be performed:

1. 1% amplitude mismatch; no other quadrature impairments.

2. 5% amplitude mismatch; no other quadrature impairments.

Table 7.4: *Predicted and measured quadrature upmixing spurs*

Nr	Leakage		Amplitude		Phase		Predicted [dB]		Measured [dB]	
	SMIQ	α	SMIQ	ρ	SMIQ	κ	Spur	Err	Spur	Err
1	–	–	1%	0.02031	–	–	−40.0	±3.56	−40.2	+0.2
2	–	–	5%	0.10830	–	–	−25.8	±1.58	−26.0	+0.2
3	–	–	–	–	1°	0.01745	−41.2	±0.84	−41.4	+0.2
4	–	–	–	–	5°	0.08727	−27.2	±0.17	−27.2	+0.0
5	1%	0.0101	–	–	–	–	−39.9	±0.83	−39.7	−0.2
6	5%	0.0526	–	–	–	–	−25.6	±0.18	−25.0	−0.6
7	1%	0.0101	1%	0.02031	1°	0.01745	−37.5	–	−37.5	+0.0
8	1%	0.0101	1%	0.02031	1°	0.01745	−39.9	–	−36.3	−3.6

3. 1° quadrature phase error; no other quadrature impairments.

4. 5° quadrature phase error; no other quadrature impairments.

5. 1% carrier leakthrough; no other quadrature impairments.

6. 5% carrier leakthrough; no other quadrature impairments.

7. Combined quadrature impairments of 1% amplitude mismatch, 1° quadrature phase error and 1% carrier leakthrough. In this experiment, only the sideband spur size is measured.

8. Combined quadrature impairments as in Test 7, except that the carrier spur is now measured.

For each test, the resultant spur sizes will be measured and compared with the theoretical predictions. Hereby, the theory regarding the effects of quadrature inaccuracies (Chapter 5) can be experimentally verified.

Expected results

The expected spurs due to the individual quadrature errors may be calculated using the theory presented in Chapter 5. The predicted results for the various experiments are summarised in Table 7.4. The various columns represent the following:

- **Nr.:** The experiment number, as described above.
- **Leakage:** The carrier leakthrough component, as specified on the SMIQ "Impairments" dialog[3] (α_g), and in terms of the equivalent leakthrough amplitude (α) as

[3]Figure 7.3, p. 118

described in Section 5.6. The SMIQ signal generator expresses this leakthrough amplitude as a percentage of the total output amplitude [37], therefore the signal amplitude decreases by an equal amount. This is different from the way α was defined on page 59, so that

$$\alpha = \frac{\alpha_g}{1 - \alpha_g} \tag{7.6}$$

The predicted spur size then follows from Equation 5.38 (p. 60), with $A = 1$.

- **Amplitude:** The amplitude mismatch, as specified on the SMIQ "Impairments" dialog (ρ_g), and in terms of the equivalent parameter ρ defined in Section sec:QComp:Amp. By comparing the way the SMIQ Signal Generator implements amplitude mismatch (see Figure 7.2, p. 118) with the definition of ρ on page 42, their relationship may written as

$$\rho = \frac{1 + \rho_g}{\sqrt{1 - 2\rho_g - \rho_g^2}} - 1 \tag{7.7}$$

This value of ρ allows the spur size to be predicted using Equation 5.10 (p. 47).

- **Phase:** The phase values on the SMIQ "Impairments" dialog (κ_g) must first be converted to radians,

$$\kappa = \frac{\pi}{180}\kappa_g \tag{7.8}$$

before it can be substituted in Equation 5.72 (p. 73) to calculate the predicted spur size.

In order to confirm the theory of quadrature spurs developed in Chapter 5, the measurements in experiments 1 to 6 should agree closely with the predicted values. If it is assumed that the tolerances on the SMIQ signal generator's quadrature impairment parameters are approximately equal to their adjustment resolutions (see p. 117), error estimates may be made by calculating the difference between the spur sizes caused by the nominal error and its worst-case deviation. These error estimates are also listed in the "Predicted" column of Table 7.4.

The pre-calibrated system of Section 7.2.2 forms a good starting point for introducing quadrature errors and predicting their effects, but it should be noted that there is one measurement where the precompensation in the SDR could affect the current experiment: Introducing deliberate phase error in the mixer will affect the precompensation of the carrier leakthrough spur. Recall that Section 6.1.4 recommends that phase and amplitude compensation be done prior to carrier leakthrough compensation, because the phase accuracy of the system affects the way in which the compensation DC offsets combine to form the compensation carrier. Consequently, when an SMIQ phase impairment is set, the carrier

leakthrough compensation of Section 7.2.2 is invalidated, and the uncompensated carrier spur of Figure 7.11 (p. 127) may start to re-appear. Since the SMIQ data sheets do not specify the phase of its deliberate carrier leakage impairment, it is impossible to predict the exact size of this spur.

Fortunately, this will not affect the compensation experiments in Section 7.2.4, provided that phase compensation is performed prior to carrier leakthrough compensation, as per the principles of Chapter 6.

As expected, the introduction of phase error counteracts the carrier spur compensation that was performed in Section 7.2.2's initial calibration. The spur size lies 53.4 dB below the desired signal, which is considerably smaller than the original carrier spur of −31.9 dBc. This reinforces the notion that this is just a partial reappearance of the original carrier spur, because the original compensation was compromised.

Measurements

Figure 7.13 shows the measured RF spectra for the smaller errors, and the observed spurs are summarised in Table 7.4, together with the spur measurements for the larger quadrature errors. The measured spurs agree very well with the predictions, and the prediction errors are generally below the assumed tolerances of the SMIQ signal generator's impairment settings. The single exception is for the 5% leakage error experiment, which seems to exhibit a somewhat larger inaccuracy than predicted just by the tolerance assumption. Nevertheless, the 0.6 dB (7.2%) prediction error still represents fair accuracy, in particular when considering that the SMIQ leakage tolerance is not specified in the datasheet [37, 38].

Conclusion

The theory of how quadrature inaccuracies affect a transmitted signal's RF spectrum, developed in Chapter 5, has now been verified both by simulation and by practical measurement. When specific quadrature inaccuracies are introduced, the measured spurs lie at exactly the expected frequencies, and their sizes are very close to the predicted values—to within a range that can reasonably be attributed to the instrumentation inaccuracies.

7.2.4 Quadrature compensation

In the last experiment, a combination of quadrature errors were introduced to a precalibrated system, producing sideband and carrier spurs of predictable magnitudes. In the current experiment, it will be shown that it is possible to fully compensate for a combination of such quadrature errors: 1% amplitude mismatch, 1% carrier leakthrough and 1° phase error. According to the theory developed in Chapter 6, the compensation errors should be inverses of the mixing errors.

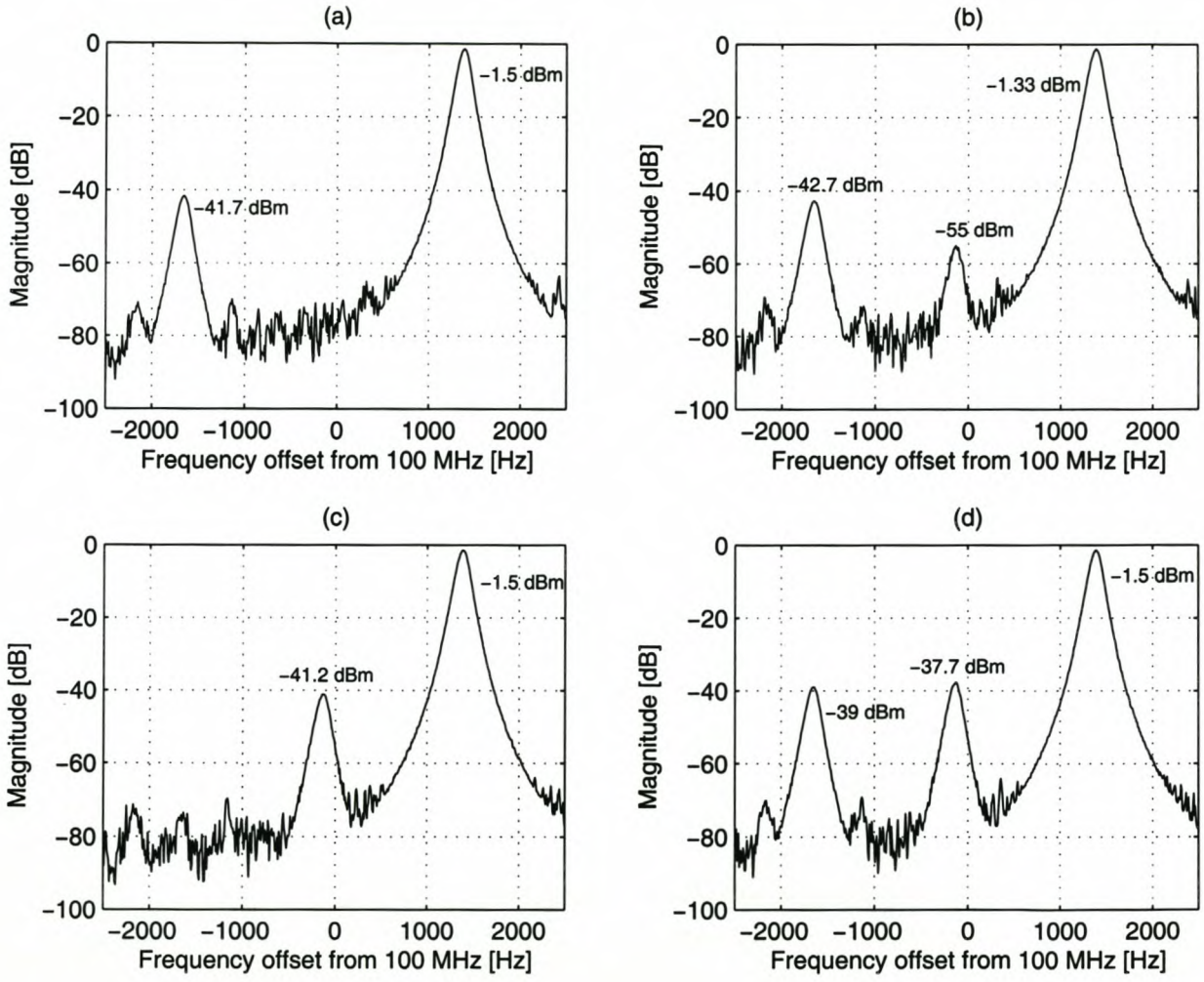

Figure 7.13: *The effect of deliberate quadrature errors on the frequency spectrum of a transmitted signal. (a) 1% amplitude mismatch; (b) 1° phase error; (c) 1% local oscillator leakthrough; (d) combined quadrature errors.*

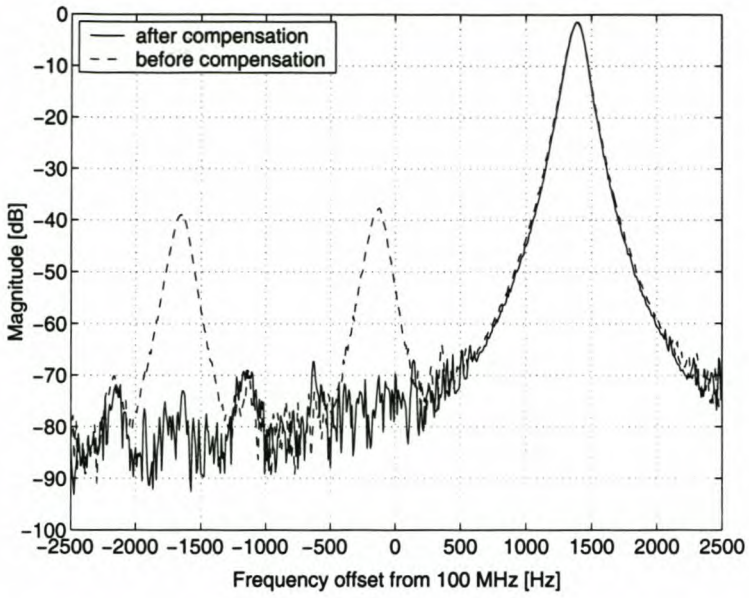

Figure 7.14: *RF spectrum of the transmitted signal, after compensating for the quadrature errors illustrated in Figure 7.13(d).*

Experimental setup

The experimental setup from the previous experiment (Section 7.2.3) is re-used for this experiment. As in the experiment of Section 7.2.2, compensation is performed using the manual calibrator shown in Figure 7.9 (p. 125).

Starting from the deliberately-impaired setup of the previous experiment, manual calibration is again performed using the algorithm of Section 6.1.4. After the spurs have been suppressed to the level of the noise floor, the compensator's amplitude, offset and phase adjustments are compared to the quadrature impairment settings on the SMIQ Signal Generator.

Expected results

To verify the theory presented in Chapter 6, the compensation parameters should be inverses of the signal generator impairments, to within the adjustment tolerance of the SMIQ Signal Generator (0.1% amplitude, 0.5% carrier leakthrough and 0.1° phase tolerance).

Measurements

After performing the calibration routine of Section 6.1.4, the quadrature spurs are again suppressed to the point where they become indistinguishable from the system noise floor (Figure 7.14). In itself, this result demonstrates that quadrature compensation is indeed effective. Furthermore, it will be useful to verify that the size of the compensation errors in the SDR are in fact inverses of the quadrature mixing errors in the signal generator.

Table 7.5: *Comparison of compensation parameters to known quadrature inaccuracies.*

Parameter	Initial	Compensated	Adjustment	SMIQ	Error	Tolerance
Amplitude	0.2239%	−0.8034%	-1.027%	1%	0.027%	0.1%
Offset / Carrier	2.994%/−140°	1.498%/−117.5°	1.566%/38°	1%	0.566%	0.5%
Phase	0.1984°	1.2198°	1.0214°	1°	0.0214°	0.1°

Table 7.5 compares the parameters that produced minimum spur sizes during calibration, with the known mixer errors. The "Initial" column of the table lists the initial calibration parameters (from Section 7.2.2), and the "Compensated" column shows the values of the same parameters, after compensating for the combined quadrature errors introduced in the mixer. The difference is listed in the "Adjustment" column, which indicates the parameter changes that were needed to return to the optimal compensation point. The size of these adjustments should be the inverses of the mixer errors (which are listed in the "SMIQ" column).

The compensation parameters correspond very well to the nominal values of the quadrature impairments introduced by the SMIQ mixer. The listed error values lie below the assumed tolerance of the signal generator settings, except for the carrier adjustment, which is slightly higher. This again suggests that the actual carrier leakage inserted by the signal generator might differ slightly from the nominal value on the "Impairments" dialog. Note that even under normal "impairment-free" operation, the SMIQ specifies carrier suppression of only −45 dBc (Section 7.1.1), which corresponds to 0.56% of the full signal strength.

Conclusion

Not only is it possible to suppress multiple quadrature errors to the level of the transmitted signal's noise floor, but these required adjustment sizes correspond very well to the theoretical predictions. This confirms that the theory developed in Chapter 6 is reliable. This experiment demonstrates that quadrature compensation (Proposition A) allows a quadrature mixer to perform far better than its specified rating—as is illustrated by the carrier spur that has been suppressed well below its rated level of −45 dBc.

7.2.5 Filter effects

Since no filter equalisation is performed in this prototype, and the filters exhibit non-zero common-mode rejection (Figure 7.8, p. 124), it is to be expected that the calibration accuracy (in particular the sideband compensation accuracy, which is affected by the filters' relative magnitude and phase responses) will deteriorate somewhat for output frequency components remote from the calibration point.

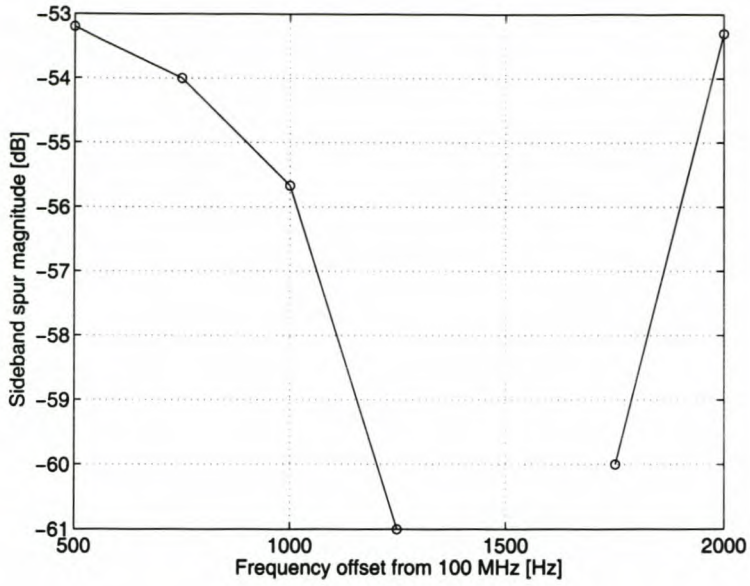

Figure 7.15: *Sideband spur measurements away from the calibration frequency.*

Experimental setup

The compensated quadrature transmitter of Section 7.2.4 is used, but the transmitted tone is varied from +500 Hz to +2000 Hz (relative to the carrier).[4] The relative size of the sideband spur is then measured.

Expected results

Exactly at the calibration frequency of 1500 Hz, the system from Section 7.2.4 is fully compensated, and no sideband should be visible. As the output frequency is adjusted away from 1500 Hz in either direction, the sideband spur is expected to reappear and grow due to the slight mismatch in filter transfer functions. The spur should never be larger than the worst-case predicted by the common-mode rejection ratio test of Section 7.1.4 (p. 124), namely 32.8 dB below the desired signal component.

Measurements

Sideband spur measurements are shown in Figure 7.15. No spur is measured at +1500 Hz, but away from the calibration frequency, a sideband spur reappears, and grows as the distance from +1500 Hz increases. A worst-case spur of −53.2 dB is measured.

No carrier leakthrough component was observed in any of the measurements.

---

[4]Measuring at a smaller offset than about +500 Hz is not practical, since the spectrum analyser has a minimum frequency resolution bandwidth of 300 Hz. For small frequency offsets, the desired signal lobe obscures the sideband.

Conclusions

Filter mismatch has a demonstrable effect on the accuracy of quadrature compensation. The extent to which filter matching is achieved, diminishes the worst-case sideband spur. Analogue filter matching may be complemented by digital filter equalisation, to further improve the magnitude and phase accuracy of the I and Q channels, in order to ensure reliability of compensation over a wide range of output frequencies [56, p. 507], [33, 43].

7.2.6 Multi-tone transmission

In all the previous tests, a single RF tone was transmitted, and its sidebands and carrier leak-through were investigated and removed by compensation. For the theory presented in this dissertation to apply to information-bearing signals, it must be shown that the compensation techniques also apply to multitone signals. In this experiment, a multitone SSB-AM signal is subjected to quadrature inaccuracies in the upmixing, and its spectrum is investigated prior to and after quadrature compensation.

Experimental setup

The baseband signal

$$f(t) = \tfrac{8}{9}e^{j\pi 750t} + \tfrac{1}{9}e^{j\pi 1500t} \tag{7.9}$$

is first generated by the uncompensated system with deliberate error used in the experiment of Section 7.2.3, and then by the compensated system of Section 7.2.4. Exactly the same quadrature impairments are set, and the quadrature compensation parameters of the previous experiment are re-used, without any additional adjustments.

Expected results

Chapter 5 predicts that each desired frequency in the multitone signal should produce its own sideband frequency in the uncompensated signal. Each sideband spur should be proportional to its corresponding desired frequency, with spur sizes as predicted by Equations 5.10 (p. 47) and 5.72 (p. 47). Besides sideband spurs and the carrier spur, no other spurs are predicted.

After compensation, all spurs should be suppressed. While it is possible that the slight differences in the filter transfer functions could re-introduce quadrature errors at frequencies away from the calibration point, the filter mismatch measurements of Section 7.1.4 place an upper bound on the expected spur residues.

Measurements

The experiment's results are shown in Figure 7.16(a). The quadrature errors produce side band spurs, and a sideband tone is observed for each desired SSB tone. After compensation is switched on, all these sidebands collapse flush with the noise floor. In the wider spectrum

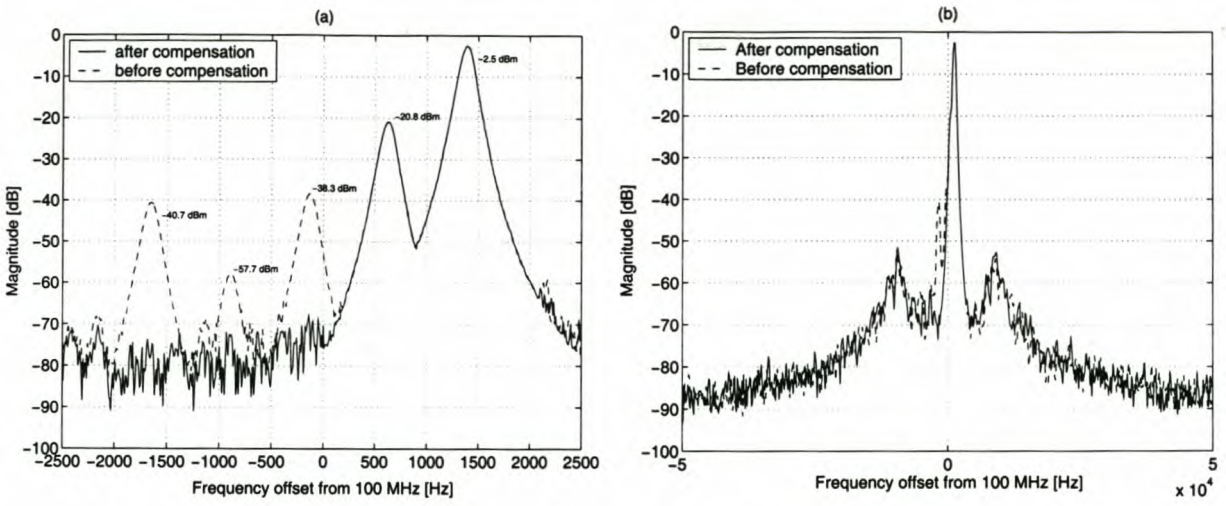

Figure 7.16: *Spectrum of a multitone SSB-AM signal before and after quadrature compensation. (a) Spectrum around the carrier. The uncompensated signal shows a carrier spur, and sideband spurs corresponding to both the desired tones. These spurs are suppressed to the noise floor after compensation. (b) A wideband view of the signal. No out-of-band spurs appear either before or after compensation. The bulges in the noise spectrum near* ± 10 kHz *follow the baseband LPFs' magnitude responses.*

of Figure 7.16(b), it can be seen that, even for the multitone case, no spurs occur outside the allocated signal bandwidth.

Conclusion

The compensation techniques generalise to multi-frequency signals, as expected. This experiment demonstrates that, even without additional filter equalisation, the quadrature transmission system can produce an SSB signal that is virtually indistinguishable from one produced by heterodyne upmixing: All the spurs that characterise the quadrature mixing process have successfully been suppressed, using exactly the same parameters as for the single-tone case.

7.2.7 FM transmission

To demonstrate the synthesis of an information-bearing signal, the next experiment investigates the spectrum of a frequency-modulating signal. For this purpose, a sine wave is used as modulating signal, so that the Bessel-shaped spectrum of the resulting signal may be verified [56, 43].

Experimental setup

The compensated system of Section 7.2.4 is re-used in this experiment. In this case, the software-defined radio generates an FM signal with 200 Hz frequency deviation. This system

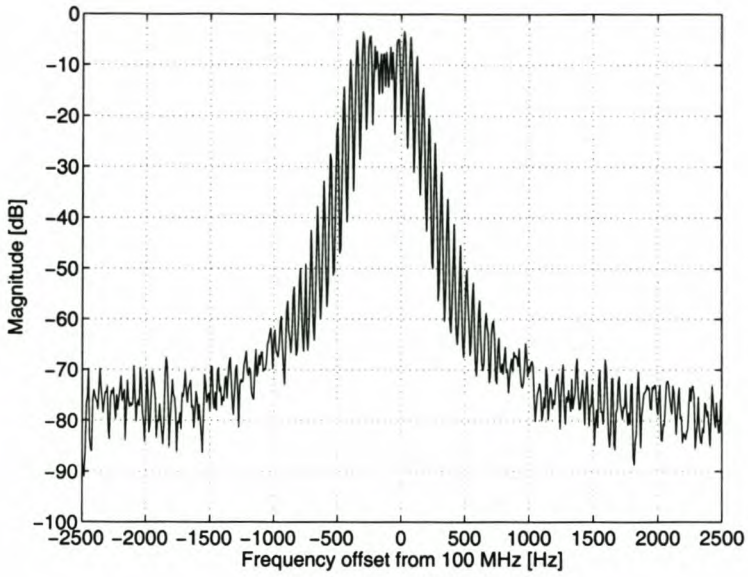

Figure 7.17: *Spectrum of a transmitted frequency-modulated signal. 200-Hz frequency deviation was employed, and a 50-Hz sine wave was used as modulating signal.*

is used to frequency-modulate a a 100-MHz carrier with an input sinusoid of 50 Hz. The resultant RF spectrum is then measured.

Expected results

When a sinusoid is frequency-modulated, the resultant spectrum consists of discrete frequency components, spaced ω_m apart, where ω_m is the frequency of the modulating sinusoid [56, 43]. The significant bandwidth of the modulated signal may be approximated by Carson's rule as [56, 43]

$$B \approx 2(\omega_d + \omega_m)\,, \tag{7.10}$$

where ω_d is the frequency deviation (200 Hz in this case). The measured FM spectrum should therefore have a -3-dB bandwidth of approximately 500 Hz.

Measurements

The observed signal spectrum after frequency modulation is shown in Figure 7.17. The discrete Bessel components, spaced at exactly 50 Hz, are clearly visible in the spectrum. Components -4 and $+4$ lie 1.7 dB below the signal maximum, 500 Hz apart. Components -4 and $+4$ lie 5.5 dB below the signal maximum, 600 Hz apart. This corresponds well with the -3-dB signal bandwidth approximation by Carson's rule.

No anomalous components can be observed in the signal spectrum.

In a related FM experiment, the 10-kHz Sallen-Key low-pass filters were replaced by 100-kHz RC filters. A recorded music signal was used as modulating input, and used to frequency-modulate a quadrature-baseband carrier. The signal was then upmixed to 110 Mhz, and

transmitted at 0 dBm, with 75 kHz frequency deviation. The music could clearly be received using a conventional radio receiver. Although such a music test does not provide a strong quantatitive measurement of the system's performance, it does confirm that a quadrature modulator can be used effectively in the synthesis of useful modulated signals.

Conclusion

This experiment demonstrates that the compensated quadrature system performs as expected when used to synthesise a dynamic signal. In the observed spectrum, no anomalous spurs or out-of-band components can be measured. A modulated signal can also be reliably demodulated with a test receiver.

7.2.8 Noise transmission

The study of quadrature transmission indicated that the transmitted signal bandwidth is exactly equal to the bandwidth of the complex baseband signal. Furthermore, it is possible to limit any out-of-band transmissions by employing low-pass filters on the quadrature baseband signals (as opposed to the significantly more difficult problem of controlling the bandwidth of an RF signal, especially when the desired signal bandwidth is narrow compared to the transmission frequency).

In this experiment, it will be verified that the RF signal bandwidth can be controlled by the use of low-pass filters on the baseband outputs prior to mixing. This is done by generating a white-noise signal in the baseband, and demonstrating that the bandwidth of the resulting RF signal can be controlled by using low-pass filters in the baseband.

Experimental setup

A software-defined radio is used to generate uniformly distributed phase samples in the range

$$\Theta = [0, 2\pi)\,, \tag{7.11}$$

which is then used to generate the complex-valued white noise signal

$$f(t) = e^{j\Theta}\,. \tag{7.12}$$

The signal is sampled at 100 kS/s on both channels, which results in a total double-sided baseband bandwidth of 100 kHz. The noise signal is then upmixed using the SMIQ signal generator as quadrature mixer. No deliberate quadrature impairments are introduced, and no compensation is performed.

In the first part of the experiment, the noise signal is not filtered prior to its connection to the mixer. Next, the Sallen-Key low-pass biquads of Section 7.1.4 are connected to the baseband output signals. In both cases, the spectral magnitude of the resultant RF signal is measured.

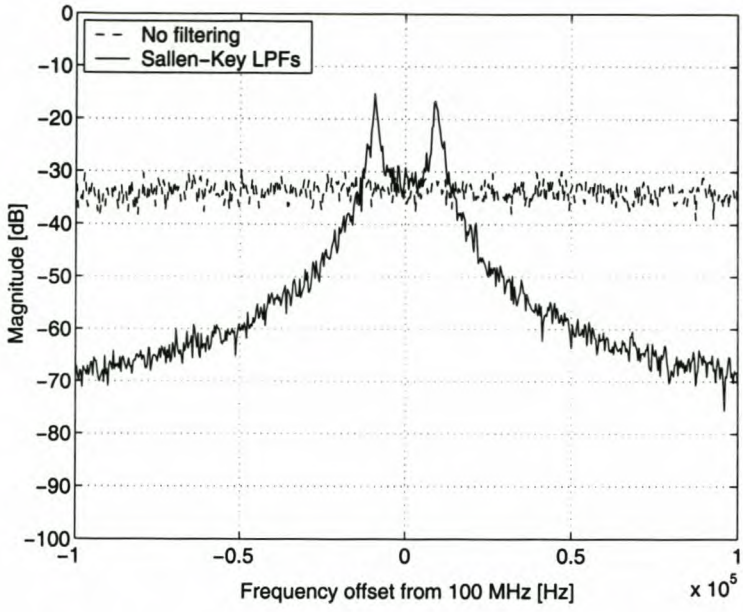

Figure 7.18: *The effect of baseband filtering on a transmitted noise spectrum. With no baseband filters, the transmitted white noise signal has a uniformly flat spectrum within its sampling bandwidth. However, when the signal is first low-pass filtered in the baseband, the resultant RF spectrum follows the filters' magnitude response. This demonstrates that the RF bandwidth can be controlled from the baseband.*

Expected results

The experiment without low-pass filtering should produce a signal with relatively broad bandwidth and a uniform power density within that band. On the other hand, when filters are used in the baseband, the resulting RF power density should no longer be flat, but will follow the magnitude response of the filters.

Measurements

The spectra observed for the tests with and without filters are shown in Figure 7.18. The spectrum corresponding to the unfiltered baseband signals has the expected white-noise characteristic. As soon as the filter is added, the RF spectrum takes on the filter characteristic—it is as if the origin of the filter's magnitude response (Figure 7.6) has moved to the carrier frequency. Out-of-band components (in this case, outside 100 MHz $\pm$ 10 kHz) are suppressed by the baseband filters, while the desired frequency band is unaffected.

Conclusion

This experiment illustrates baseband control over the RF spectrum. No bandpass filtering is required at the transmission frequency, nor at any other intermediate frequency—the low-pass filters control the contents of the transmitted signal. In this way, it becomes possible

to accurately obtain a very narrow-spectrum signal (in this case, $Q = \frac{100\text{ MHz}}{20\text{ kHz}} = 5000$) using only two second-order low-pass filters.

7.3 Reception tests

In the next set of experiments, the quadrature compensation techniques will be verified on a software radio receiver prototype. For these experiments, a COTS quadrature downmixer is used, with initially unknown quadrature impairments. The quadrature inaccuracies are characterised, and compensation parameters are calculated. The fidelity of the compensation is then tested for various transmitted signals.

7.3.1 Pre-compensation tests

In the first experiment, the quadrature inaccuracies of the downmixing circuit is measured, and compared to the typical values specified in the RF2713 datasheet. Other artefacts in the received spectrum are also investigated.

Experimental setup

Firstly, 110 MHz was identified as a potential carrier frequency in a reasonably quiet part of the RF spectrum. The SMIQ signal generator is used to provide a reference oscillator of 220 Mhz to the RF2713 quadrature mixer, which in turn produces the 110-MHz quadrature references (see Figure 7.10, p. 126). The input RF signal is provided by the Marconi 2019 signal generator; for this experiment, it is a stable −29-dBm sinusoid of frequency 110 MHz + 1.5 kHz. The RF2713 produces two quadrature-baseband output signals, which are passed through the Sallen-Key low-pass biquads of Section 7.1.4 and then digitised using the Adlink DAQ-2010 data acquisition card.

The received signals are recorded using the `rx_logger` SDR program (see Appendix E). The baseband signal spectrum can then be visualised in Matlab.

Expected results

The specified quadrature inaccuracies for the RF2713 quadrature mixer are listed in Table 7.1 on page 119. From the typical inaccuracy ratings, the sideband spur may be calculated to have a size of

$$\begin{aligned} \text{SFDR}_{\text{sb}} &= -20\log\sqrt{S_\rho^2 + S_\kappa^2} \\ &= -10\log\left[(5.964\cdot 10^{-3})^2 + (8.726\cdot 10^{-3})^2\right] \\ &= 39.5\text{ dB} \end{aligned} \tag{7.13}$$

Since this is lower than the pre-compensation filter mismatch (see Figure 7.1.4, p. 124), the filter's sideband contribution can be expected to dominate.

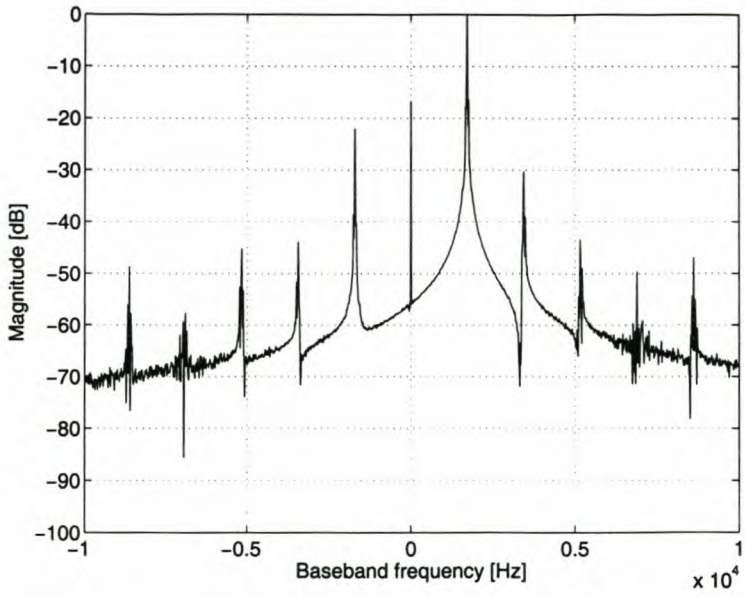

Figure 7.19: *Baseband spectrum of a received* +1.5-kHz *frequency, prior to quadrature compensation. The sideband spur is* 22 dB *below the desired signal, and the second harmonic lies at* −30 dBc. *Several higher-order harmonics are present.*

The carrier spur is less predictable: The I and Q signals have a DC bias of about $V_{cc}/2$, so a very large initial DC spur can be predicted. The estimated bias of 2.5 V will be removed prior to more accurate DC compensation. However, the RF2713 data sheet additionally specifies a typical DC mismatch ($|I_{\mathrm{dc}} - Q_{\mathrm{dc}}|$) of up to 100 mV [35]; for a 25-mV output signal (as in this experiment), this means that, even after removing the nominal DC bias, the carrier spur may still be 12 dB *higher* than the desired component.

Furthermore, the internal Gilbert cell transistor configuration of the mixer cannot be expected to have a completely linear response: It is very likely that some harmonics will be introduced in the downmixed signals. The RF2713 data sheet does not specify typical distortion levels—in practice it was found to be strongly dependent on the input signal strength.

Just as the desired signal is expected to produce a sideband component in the presence of quadrature inaccuracies, so the harmonics of the desired signal will also produce sideband components. Consequently, the baseband signal spectrum can be expected to contain a picket-fence of spurs, separated by the fundamental frequency.

Measurements

The baseband signal spectrum is shown in Figure 7.19. The spectrum illustrates why quadrature mixers are generally considered to be inferior to heterodyne mixing solutions: The spectrum is rife with spurs, and the SFDR is only 17 dB. The sideband spur is considerably larger than predicted by the "typical" inaccuracy, indicating that further amplitude

and phase errors are being introduced by the filter mismatch. Spurs are observed at all the harmonic frequencies, and at their sideband frequencies.

Conclusion

The quadrature downmixing process shows significant impairment. However, all spurs occur at expected frequencies, and it should be possible to compensate for the spurs due to quadrature inaccuracies. Harmonic distortion is not specific to quadrature mixing, but it should also be possible to improve the signal's harmonic accuracy by using the appropriate inverse digital transform.

7.3.2 Quadrature compensation

Next, the quadrature compensation parameters must be determined. This is done by performing the phasor-rotation algorithm described in Section 6.1.3. The compensation parameters are then tested on several input signals, to assess the reliability of the compensation techniques.

Experimental setup

All input signals are obtained using the same hardware as described in the previous experiment. The experiment consists of the following steps:

1. Input: a -29-dBm signal of $+1.5$ kHz.
2. Obtain quadrature compensation parameters using the phasor-rotation algorithm with seven iterations (`qparams.h`, Appendix E).
3. Obtain harmonic compensation curve by using analysing the received signal distortion (`hparams.h`, Appendix E).
4. Discard the training sequence, and apply the compensation parameters to a new input signal (`qcomp.m` and `hcomp.h`, Appendix E).
5. Investigate the compensated signal's phasor and spectrum.
6. Using the same compensation parameters, measure the spectra of -29-dBm input signals with frequencies $+2.0$ kHz and -1.5 kHz, to establish whether the compensation parameters are applicable at frequencies removed from the calibration point.

Expected results

At the calibration frequency, it should be possible to optimally compensate for quadrature errors, so that they are no longer distinguishable in the signal spectrum. It should also be possible to reduce the harmonic spurs produced in the mixing process.

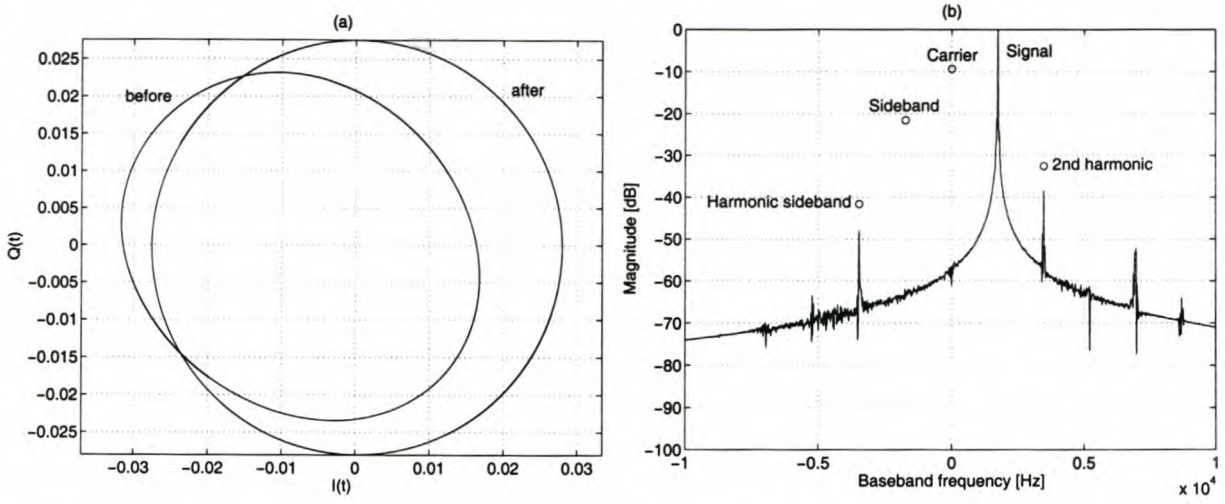

Figure 7.20: *The effect of baseband quadrature compensation on a received signal's phasor and spectrum. (a) Prior to compensation, the received phasor is a rotated, translated ellipse, indicative of all types of quadrature impairment in the receiver. After compensation is performed, the phasor becomes a circle centred at the origin. (b) The signal spectrum of the received signal after compensation. The pre-compensation spur heights are indicated with circles and labels. Quadrature compensation has optimally suppressed the formerly dominant carrier and sideband spurs.*

The compensation accuracy is expected to deteriorate slightly at frequencies removed from the calibration point, due to slight mismatches in the filter responses.

Measurements

The results of the quadrature compensation process is shown in Figure 7.20. The phasor in Figure 7.20(a) is no longer an off-centre ellipse, but has been transformed into a circle centred at the origin—the phasor which is typical of two equal-amplitude sinusoids in the correct quadrature relation. Figure 7.20(b) shows the compensated signal's spectrum, with the initial spur sizes indicated as circles. No visible residue of the carrier (0 Hz) or sideband (-1.4 kHz) spurs remain. The harmonic distortion spurs, typical of any mixer (not just quadrature mixers), now dominate, although the harmonic inversion has also served to reduce their size.

Figure 7.21 shows the received spectrum for input signals at frequencies away from the calibration frequency of $+1.5$ kHz. As expected, the slight differences in filter responses cause small quadrature spurs to reappear. However, these spurs are still far below the initial quadrature spurs of the uncompensated system (Figure 7.19). The harmonic spur sizes are unaffected by the specific input frequency, and continue to dominate the spectrum.

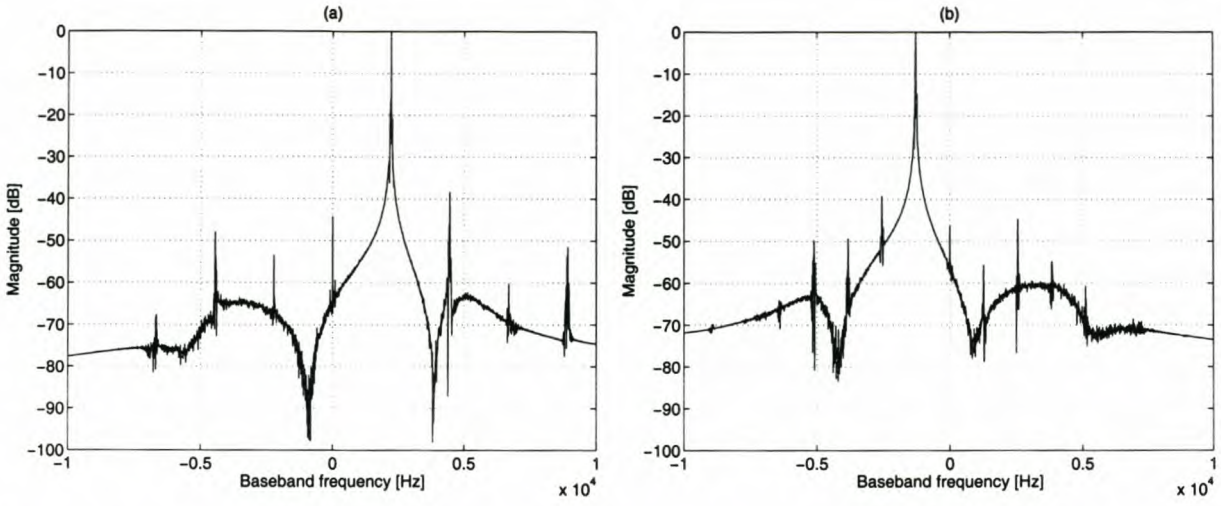

Figure 7.21: *Spectra of received frequencies away from the calibration point. (a) +2 kHz. (b) −1.5 kHz.*

Conclusion

The reception-side quadrature compensation techniques of Chapter 6 have been demonstrated to reliably suppress the quadrature mixing spurs. Compensation is best at the frequency where the quadrature inaccuracies are measured—filter mismatch at other frequencies could diminish the compensation accuracy. It should be noted, however, that it was opted (for this prototype) to implement two reasonably well-matched filters, and not perform filter equalisation in the digital domain. The compensation accuracy may be further improved by measuring the magnitude and phase of the sideband spur at various input frequencies, and then use that to synthesise digital equalisation filters to reduce the filter mismatch.

The compensation techniques allow the quadrature mixer to operate far beyond its accuracy ratings: The analysis in Section 7.3.1 indicated that the sideband spur, for example, can at best be expected to lie 39.5 dB below the desired component; in practice, the mixing setup was found to perform much worse prior to compensation (Figure 7.19 showed an a carrier spur of −22 dBc). Also, it was shown in Section 7.3.1 that a carrier spur of +12 dBc may be expected even if the nominal DC bias is subtracted. The experiments shown in Figure 7.21, however, show that the mixer now operates at −53 dB (sideband) and −45 dB (carrier) even away from the calibration frequency. Software compensation makes it possible to reverse fundamental hardware inaccuracies (Proposition A).

7.3.3 FM reception

In the final reception test, a frequency-modulated signal is generated using a reference FM exciter. This FM signal is then downmixed from the VHF band using the RF2713 quadrature

mixer, and then filtered and digitised. Software compensation and demodulation is then performed, and the received signal's time-domain and frequency-domain representations are analysed, in order to establish whether quadrature downmixing can reliably demodulate a dynamic, multi-frequency waveform such as an FM signal.

Experimental setup

The Marconi 2019 is used to generate an FM signal at 110 Mhz, with 1-kHz frequency deviation and a signal strength of -29 dBm. A 1-kHz modulating signal bandwidth is allocated, and for this test a 300-kHz sinusoid is generated as modulating signal.

The downmixing, digitisation and compensation setup of the previous experiment (Section 7.3.2) is re-used here. The compensated signal is demodulated by numerically differentiating the complex-valued baseband signal's instantaneous phase (`fmdemod.m`, Appendix E). The demodulated signal is then downsampled to a 20-kHz sampling rate, which is better suited to representing the demodulated signal. Lastly, out-of-band noise is removed by passing the signal through an 8th-order Butterworth low-pass filter with a 1-kHz cut-off frequency.

Expected results

A 300-Hz sinusoid should be observed after demodulation. If the quadrature compensation and demodulation techniques are reliable and practical, the signal should exhibit very little demodulated distortion, since the modulated SFDR has been shown in the previous experiment to be around 40-dB, which should induce very little observable distortion after quadrature demodulation.

Measurements

As can be seen in Figure 7.22, the 300-kHz modulating sinusoid is demodulated correctly. The spectrum is shown on the right-hand side: The desired demodulated signal's spurs dominate. The mismatch between the RF signal's true centre frequency, and the local oscillator of the mixer, causes a frequency offset in the baseband modulated signal, which in turn produces a DC offset in the demodulated FM signal. In a system where such a DC offset would have been undesirable, it can be removed by digitally shifting the downmixed signal to the correct frequency offset (for example, by using a digital frequency translation stage).

From the demodulated signal, and the knowledge that the desired signal is a pure sinusoid, the received signal-to-noise ratio may be calculated to be approximately 24 dB.

Conclusion

In this last experiment, it was shown that after quadrature demodulation and compensation, a modulated signal which continuously varies in instantaneous frequency can be received and

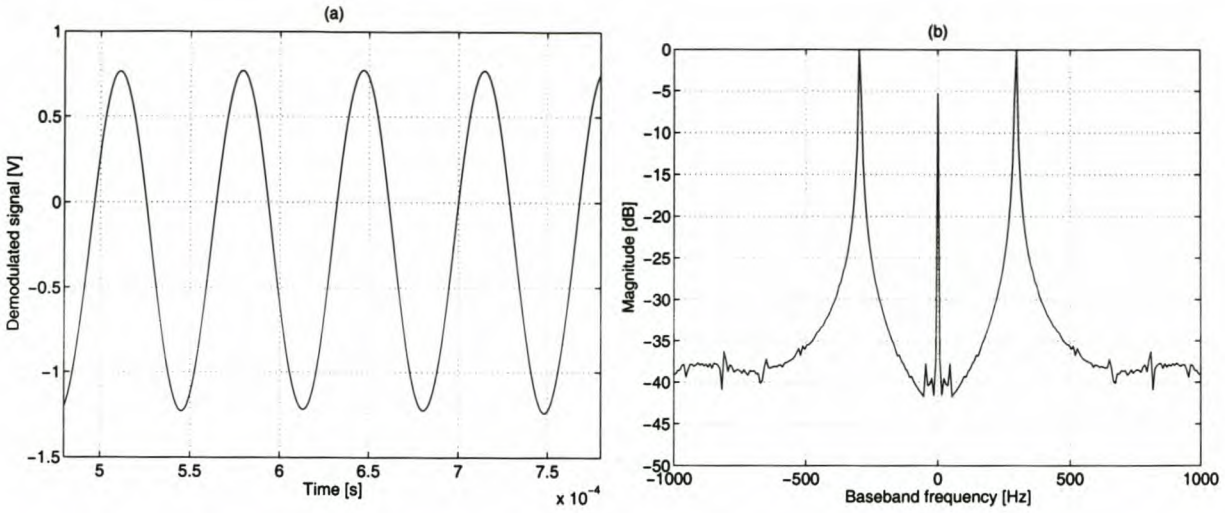

Figure 7.22: *Results of the FM demodulation test. (a) Time-domain representation of the demodulated 300-kHz sinusoid. (b) Spectrum of the demodulated signal.*

demodulated reliably. This is a significant test, because it requires correct compensation over a range of frequencies. However, the compensation procedure is just as simple as for the single-tone case: The complex-valued downmixed signal is rotated and scaled on the complex plane.

7.4 Remarks

The practical experiments performed in this chapter firstly serve to verify the theory developed in Chapter 5, regarding the nature of quadrature mixing errors. Furthermore, it demonstrates that the techniques used to compensate for these errors, as developed in Chapter 6, are indeed practical to implement, and deliver a considerable improvement in both the transmitted RF and received baseband signal spectra.

The experimental prototype uses single-stage quadrature mixing, and confirms that it is possible to obtain a clean separation between signal translation and signal processing. Although RF signals of 100 and 110 MHz was used, digital signal conversion was done at only 1 MHz, and the signal information was processed at this lower rate.

The transmitted signal bandwidth was shown to be completely controllable by the low-pass filters in the baseband: By using two 10-kHz LPFs, it was possible to obtain a signal bandwidth of 20 kHz at 100 MHz ($Q = 5000$), and out-of-band components were tightly controlled by the filter roll-off. The choice of centre frequency was fairly arbitrary: Using the same filters and mixer, a 20-kHz wide signal could have been produced at 250 MHz ($Q = 12500$); another filter could have placed the signal at 1.4 GHz ($Q = 7 \cdot 10^4$) or higher. This level of reliability in the production of extremely narrowband signals would have been prohibitively difficult to achieve using heterodyne mixing with bandpass filters.

In summary, the theoretical claims of this dissertation are supported by the practical measurements. While the prototype may certainly be further improved (for example, by better filter matching or filter equalisation), the prediction and compensation of quadrature spurs will still proceed in a similar fashion.

Chapter 8

Conclusions

The preceding chapters presented the theoretical development and practical verification of baseband compensation principles for defects in quadrature signal conversion and processing. In this last part of the dissertation, the specific results will again be related to the central goals of the research. The relevance of these results to the broader research community will be estimated, and avenues for related future research will be identified.

8.1 Research results and contributions

8.1.1 Compensation as design principle

Chapter 1 introduced two propositions central to the research presented here. Consider again the first proposition:

> **Proposition A:**
> A digital processing system can always compensate for deterministic distortion effects in its analogue front-end (limited only by the accuracy of its numeric representation, and by the accuracy with which the distortion effects can be measured) under the condition that all these analogue inaccuracies are cascades of invertible transforms, and that their net effect is fully known.

Chapters 4 and 5 were devoted to identifying these "analogue inaccuracies" typically found in SDR systems, and to analyse their effects on signal accuracy. The primary contribution, however, was to show that these effects can all be modelled as invertible transforms susceptible to compensation. This allowed the derivation of signal processing principles in Chapter 6 that allow compensation for effects such as converter INL, amplifier non-linearities, and quadrature amplitude, offset and phase errors. To this end, automatic calibration techniques were developed (Section 6.7). The theoretical compensation theories were tested by simulation throughout the text, and finally verified by practical measurement (Chapter 7).

Proposition A requires not only that individual distortion effects be known and modelled, but that their net effect also be characterised. The dissertation demonstrated that the most significant accuracies found in the typical front-end of an SDR (in particular those employing

quadrature mixing) are individually invertible, and can be compensated for individually. Furthermore, it was shown that, when individually invertible distortion effects occur in cascade, it is possible to compensate for their net effect by applying the respective inverse transforms in reverse order. It can be concluded that, if individual distortion effects are invertible and known, and the order in which they occur are known, the net distortion effect is also known and invertible.

The numerical accuracy of the digital processing places bounds on the accuracy of any compensation performed. Furthermore, since the compensation transform is the inverse of a model of some hardware inaccuracy, the quality of compensation also depends on how accurately the distortion effects are measured and modelled. The distortion models developed in Chapters 4 and 5 were simple enough to allow compensation with low computational cost, yet provided a significant improvement in the performance of a sample system (Chapter 7). Further refinement of compensation models will be addressed in Section 8.2 below.

Although the text focused on a specific (though significant) selection of distortion effects, Proposition A lays down a principle that has much wider application than these particular non-idealities: Hardware limitations should not dictate the complexity of the entire signal processor or SDR—complexity is an information-theoretical consideration, as stated by Proposition B. Rather, hardware non-idealities should be modelled, and cancelled in the digital domain.

This principle diverges from the SDR truism that system flexibility is improved by moving "digitisation closer to the antenna" [26, 27, 4]. Rather, this research demonstrated that it is more desirable to extend the "range of influence" of the digital signal processing over as large a part of the signal path as possible. The use of a hardware front-end need not compromise the flexibility and accuracy of an SDR, nor should compensating for it increase the digital processing complexity. Instead, designing by this principle may turn otherwise disregarded components into viable options to reduce digital processing complexity. For example, the use of quadrature instead of heterodyne mixing allows digitisation and processing at baseband rates, rather than a frequency dictated by the chosen IF.

8.1.2 Quadrature mixing as front-end of choice

In addition to the central proposition above, a supporting proposition was stated on page 5:

> **Proposition B:**
> Signal processing and frequency translation are distinct components of any transceiver system. Signal processing concerns the embedding and extraction of *information* into and from a signal. *Signal processing complexity is a function of information rate.* Frequency translation involves the placement of a signal at a prescribed or convenient position in the frequency spectrum. It does not affect the information content in any way, and is thus only a function of the translation distance.

Proposition B stands in support of the central proposition, because it is based on the observation that the use of a hardware front-end (instead of signal conversion directly at the antenna) may allow the use of lower sampling rates and fewer computational resources. The proposition is an attempt to formalise this observation, and to lay a theoretical basis for the separation of frequency translation (mixing) and signal processing (conversion, modulation and demodulation).

This dissertation presented the quadrature mixer, in both modulating and demodulating configuration, as the frequency translation device that best embodies this principle. As was shown in Chapter 2, the quadrature mixer allows the signal bandwidth to be divided between the in-phase and quadrature channels. Signal processing can be performed at this baseband rate by using, for example, the quadrature modulation and demodulation techniques described in Appendix B. Since the I and Q channels each contain frequency information no higher than half the total bandwidth of the signal (because the signal band can be spread equally over both positive and negative frequencies), signal conversion can be performed at a rate equal to the bandwidth, by Nyquist's criterion [30].

Chapter 4 showed that converter performance deteriorates at higher sampling rates, possibly lowering the effective quantisation accuracy of a system. Also, a trade-off exists between high precision and high speed in DACs and ADCs, so obtaining a desired SQNR at a high sampling rate may be costly or even impossible. Quadrature frequency translation places the lowest possible constraint on converter rate, and therefore allows a more cost-effective front-end solution, with a greater selection of high-accuracy devices. High-accuracy signal conversion is important in an SDR-like system, because, by Proposition A, the signal quantisation represents a fundamental limit on obtainable signal accuracy.

Furthermore, since a digitally compensated quadrature mixer avoids the aliasing that plagues heterodyne mixing, frequency translation can be implemented in a single stage. Filtering is theoretically limited to low-pass filtering in the baseband (although some form of bandpass filtering may be required at a receiving antenna to limit the input signal power). The entire frequency translation stage is simpler and more cost-effective than the multiple mix-and-filter approach typical to heterodyne front-ends [45].

Besides the cost-effectiveness of such a simplified hardware front-end, it has a second advantage that a simpler hardware configuration leads to less complex compensation requirements. In this regard, Proposition B stand in further support of Proposition A.

Lastly, an important principle stated by Proposition B is that a modulated signal's centre frequency should not be related to the signal content. In particular, the choice of centre frequency should not affect the choice of signal bandwidth, which is in the first place an information-theoretical (and therefore content-related) consideration. Section 2.4 illustrated this principle by showing that compensated quadrature techniques can be used to produce extremely narrowband systems at arbitrarily high centre frequencies. In this regard, the quadrature-mixing approach allows finer channel selectivity than its heterodyne counterparts, because channel selection filtering in receivers is only done after translation to

the baseband.

8.1.3 Future applicability of the propositions

It may be argued that the principles advocated by the above propositions will gradually become obsolete as signal conversion technology improves. To quote a typical source: [4]

> As technology progresses, an SDR can move to an almost total SR, where digitization is at (or very near to) the antenna and all of the processing required for the radio is performed by software residing in high-speed digital signal processing elements.

Such a statement makes the implicit assumption that radio communication will always occur at a fixed range of broadcast frequencies that will eventually be overtaken by signal conversion and processing rates. Although this may be true for specific technologies (e.g. GSM cellular communication that has a fixed frequency allocation), it cannot be held true in general. With currently conceivable future technologies, there will always be parts of the radio spectrum beyond the reach of the state of the art in signal conversion and processing. Consequently, software radio can never be a general communications solution if it relies on digitisation at the antenna.

In contrast, this dissertation proposes a configuration that is limited by signal bandwidth rather than centre frequency. This approach combines the frequency reach of an analogue front-end with the flexibility of digital signal processing. It remains applicable to communication frequencies beyond the reach of current or future signal converters and processors.

8.1.4 Practical results and contributions

The propositions above represent the main theoretical contribution of this dissertation. In addition, several more practical contributions were made in support of these theses, confirming their usefulness as design principles.

Compensation techniques

Proposition A theorised that it is possible to compensate for hardware inaccuracies insofar as such inaccuracies can be measured, and insofar as the numeric resolution of the system allows the inaccuracies to be corrected. The development of novel compensation techniques formed a central part of the research described in this dissertation. Chapter 6 developed computationally efficient techniques to compensate for the most significant quadrature mixer and signal conversion inaccuracies. Simulation and practical testing confirmed the derivations, and the simulation software and prototype system contribute to the experimental tools available for SDR research.

Self-calibration system

The effectiveness of the compensation techniques depends on the accuracy and ease with which hardware inaccuracies can be modelled. In Section 6.7 a novel technique for automating SDR calibration was described. The self-calibration scheme allowed compensation for converter and quadrature mixer inaccuracies, using only switching techniques and one or two stable reference oscillators. Although the switching and the parameter extraction was performed manually in Chapter 7, the techniques are simple enough to easily be automated.

The simple self-calibration technique demonstrates that the compensation principles advocated by Propositions A and B are not merely theoretical niceties, but practical enough to be implemented in even a very basic prototype.

The quadrature demodulation techniques of Appendix B demonstrate this simplicity. Although the techniques were developed as part of this research, they are simple enough to make novelty unlikely. However, within the context of quadrature compensation they gain new relevance as signal processing techniques.

8.1.5 Theoretical contributions

In support of the main propositions of the dissertation, in-depth theoretical studies of significant forms of front-end distortion were presented. The first of these, on the topic of DAC and ADC non-linearities, consisted of a study of related research. The second study, however, concerning the effects of quadrature non-idealities on signal modulation and demodulation (specifically in the context of quadrature mixing as SDR front-end frequency translation mechanism), represents an original research contribution. Chapter 6 studied the artefacts caused by quadrature non-idealities on the modulated signal spectrum and the demodulated received signal. Deviation from a circular phasor locus was used as analytic tool in the study of these effects, and it was shown that such phasor loci can be used to quickly identify the types of distortion present in a received I-Q signal.

The characterisation of distortion effects, as presented by Chapter 6, formed the basis for the development of the compensation techniques. The distorted signals provided references for the evaluation of the effectiveness of compensation.

8.2 Current research and further work

Moving SDR signal processing to the baseband facilitates the use of relatively low-speed platforms (such as desktop PCs) in the study of radio telecommunications. Such "virtual radios" can be used to combine the ease of development, use and reconfigurement that characterise PCs, with seamlessly integrated radio applications. The PC already allows an enormous level of integration between wire-based networking, multimedia, sound (and more general signal) processing, peripheral hardware and the user interface. This environment would make the computer an attractive choice for integrated SDR applications.

The practical results of Chapter 7 show the ease with which complex baseband radio applications can be developed on a PC, and how radio signals can be processed by using general-purpose data acquisition hardware and simple external quadrature mixers. The Software-Defined Radio Research Project of the University of Stellenbosch was founded with the development of such virtual radios in mind [47]. The research of the SDR Group is strongly focused on firstly developing the theories of this dissertation into specific applications, and secondly on further extending the theory of quadrature baseband processing.

Current research projects include the development of an SDR software architecture for the rapid development of software radios, the implementation of automated calibration systems, the study of front-end emulation techniques for modelling hardware inaccuracies, the development of radio transceiver applications using quadrature front-ends, the design of low-cost front-end circuits, the development of more robust quadrature demodulation techniques, and the application of this theory on non-radio applications such as modems.

Some immediate opportunities arise for the further development of the principles, theory and studies set out in this dissertation:

- Many other hardware non-idealities remain to be modelled, in order to find possible compensation techniques. In particular, preliminary investigation has shown intermodulation distortion to possibly be invertible [54]. Such hardware models could be used to improve not just quadrature mixing front-ends, but also more general mixer solutions.

- By Proposition B, signal processing rates (and, by implication, signal conversion rates) should be a function of a signal's information content. However, spread-spectrum modulation techniques such as CDMA spread a relatively small amount of information over a wide bandwidth, and the simple front-end used in this document would not be able to sample at the much lower information rate. This apparent contradiction of Proposition B arises from the fact that a pseudorandom signal (such as the spreading signal used in CDMA) is fully deterministic, and therefore cannot contain any information [31]. However, if the simple front-end of Chapter 3 were used to receive a CDMA signal, the pseudorandom sequence would effectively be unknown prior to digitisation—and a sampling rate proportional to the signal bandwidth would be required.

  Further research is required on techniques that would allow despreading to become part of the frequency translation stage, so that signal conversion can occur at the information rate.

8.3 Summary

The research presented in this dissertation presented a case for applying hardware compensation techniques in software, in order to allow a greater choice of front-end technologies in software-defined radio systems. In particular, quadrature mixing was proposed as

a technique that could benefit greatly from such compensation techniques. The dissertation further proposes that, when adequately compensated, quadrature mixing becomes the frequency translation technique of choice: It allows a system to clearly separate frequency translation and signal processing—a distinction motivated by information theory that places signal processing requirements at a theoretical minimum.

Although these compensation techniques were thoroughly developed, and tested both in simulation and by practical prototype, the techniques in themselves do not form the central thesis of this dissertation. What is more fundamental is the principles that underlie these compensation techniques.

The first principle is that a well-designed signal processing system should combat hardware inaccuracies by inverting them in the digital domain. This principle influences hardware design: It becomes less important to design a highly accurate front-end, and more important to design for invertibility. In practice it was found that typical SDR front-end components can be represented by simple models, and compensation can be performed efficiently. When invertibility is a weaker constraint than hardware accuracy, it becomes possible to make use of lower-cost hardware.

The second principle is that digital processing complexity should be dictated by the information complexity of the signal being processed. Since half of a DAC or ADC lies in the digital domain, it also participates in digital signal processing. Consequently, signal conversion should be a function of signal information. Frequency translation is not an information-related problem, and should, by this principle, not form part of the digital signal processing. It should rather be performed in a hardware front-end—in this regard, it was shown that quadrature mixing allows a very effective baseband representation of the signal, in the sense that a minimum sampling rate can be used.

With this in mind, one may reconsider the comment quoted on page 3, namely that designers would be "likely to reject" quadrature mixing front-ends, because their hardware inaccuracy is a "significant problem". By addressing such inaccuracies using simple, efficient forms of compensation, this powerful signal translation technique can indeed come to its right.

Bibliography

[1] ADLER, E. A. *et al.*, "Frequency Translation of a Baseband Signal." *RF Design*, April 1993, Vol. 16, No. 4, pp. 41–44.

[2] ADLINK. *NuDAQ DAQ-2010 4-Ch, Simultaneous, High Performance Multi-function Data Acquisition Card — User's Guide*, 2003.

[3] BEACH, M. *et al.*, *Radio Frequency Translation for Software Defined Radio*, Ch. 2. In Tuttlebee [45], 2002.

[4] BLUST, S., *Software Based Radio*, Ch. 1. In Tuttlebee [45], 2002.

[5] BRANNON, B. *et al.*, *Data Conversion in Software Defined Radios*, Ch. 4. In Tuttlebee [45], 2002.

[6] BURACCHINI, E., "The Software Radio Concept." *IEEE Communications Magazine*, September 2000, pp. 138–143.

[7] CANDY, J. C. and TEMES, G. C., *Oversampling Delta-Sigma Data Converters*. IEEE Press, 1992.

[8] COHEN, L., *Time-Frequency Analysis*. Englewood Cliffs: Prentice-Hall, 1995.

[9] CROOK, D. and CUSHING, R., "Sources of Spurious Components in a DDS/DAC System." *RF Design*, April 1998, pp. 28–42.

[10] CUSHING, R., "Single-Sideband Upconversion of Quadrature DDS Signals to the 800-to-2500-MHz Band." *Analog Dialogue*, May 2000, Vol. 34, No. 3.

[11] DOMÍNGUEZ, J. B. and RIERA SALIS, J. M., "PM and FM Generation with DDS: Effects of Sampling the Modulating Signal." *Electronics Letters*, March 1995, Vol. 31, No. 7, pp. 516–517.

[12] ERLICH, S., "Digital FM Modulator." May 1992. United States Patent No. 5,111,163.

[13] FINNEY, R. L. and THOMAS, G. B., *Calculus*. Second edition. Reading, Massachusetts: Addison-Wesley, 1994.

[14] FRY, R. J., *Harris DIGIT FM Exciter—Facts and Features*. Harris Corporation, August 1995.

[15] HENDRIKS, P., "Tips for Using High-Speed DACs in Communications Design." *Electronic Design*, January 1998.

[16] HENTSCHEL, T. *et al.*, "The Digital Front-End of Software Radio Terminals." *IEEE Personal Communications*, 1999.

[17] HOROWITZ, P. and HILL, W., *The Art of Electronics*. Second edition. Cambridge: Cambridge University Press, 1996.

[18] JENQ, Y. C., "Digital Spectra of Nonuniformly Sampled Signals—Digital Look-Up Tunable Sinusoidal Oscillators." *IEEE Transactions on Instrumentation and Measurement*, September 1988, Vol. 37, No. 3, pp. 358–362.

[19] KESTER, W. (Ed.), *High Speed DACs and DDS Systems*, Ch. 6. In Kester [20], 1996.

[20] KESTER, W. (Ed.), *High Speed Design Techniques*. Analog Devices, 1996.

[21] KROUPA, V. F. (Ed.), *Direct Digital Frequency Synthesizers*. New York: IEEE Press, 1998.

[22] KUNG, S. Y. *et al.*, "A Highly Concurrent Algorithm and Pipelined Architecture for Solving Toeplitz Systems." *IEEE Transactions of Acoustics, Speech and Signal Processing*, January 1983, Vol. ASSP-31, pp. 66–76.

[23] MANASSEWITSCH, V., *Frequency Synthesizers—Theory and Design*. Second edition. New York: Wiley, 1980.

[24] MATHWORKS, I., *MATLAB Version 5 Language Reference Manual*. Natick, Massachusetts: Mathworks, 1996.

[25] MEHRGARDT, S., "Noise Spectra of Digital Sine-Generators Using the Table-Lookup Method." *IEEE Transactions on Acoustics, Speech and Signal Processing*, August 1983, Vol. 31, No. 4, pp. 1037–1039.

[26] MITOLA, J., "The Software Radio Architecture." *IEEE Communications Magazine*, May 1995, pp. 26–41.

[27] MITOLA, J., "Software Radio Architecture: A Mathematical Perspective." *IEEE Journal on Selected Areas in Communications*, April 1999, Vol. 17, No. 4, pp. 514–539.

[28] NIEZNAŃSKI, J., "An Alternative Approach to the ROM-less Direct Digital Synthesis." *IEEE Journal of Solid-State Circuits*, January 1998, Vol. 33, No. 1, pp. 169–171.

[29] NOSAKA, H. and NAKAGAWA, T., "A Phase Interpolation Direct Digital Synthesizer with a Symmetrically Structured Delay Generator." *IEICE Transactions on Electronics*, July 1999, Vol. E82-C, No. 7, pp. 1067–1072.

[30] NYQUIST, H., "Certain Topics in Telegraph Transmission Theory." *Transactions of the AIEE*, February 1928, Vol. 47, pp. 617–644.

[31] PEEBLES, P. Z., *Probability, Random Variables, and Random Signal Principles*. Fourth edition. McGraw-Hill, 2000.

[32] PROAKIS, J. G. and MANOLAKIS, D. G., *Digital Signal Processing: Principles, Algorithms, and Applications*. Third edition. New Jersey: Prentice-Hall, 1996.

[33] QURESHI, S., "Adaptive Equalization." *IEEE Communications Magazine*, March 1982, Vol. 20, No. 2, pp. 9–16.

[34] RAZAVI, B., "Design Considerations for Direct-Conversion Receivers." *IEEE Transactions on Circuits and Systems—II: Analog and Digital Signal Processing*, June 1997, Vol. 44, No. 6.

[35] RF MICRO DEVICES, Greensboro. *RF2713 Quadrature Modulator/Demodulator*, 2003.

[36] ROBERTSON, D., "DACs for DDS." *EDN*, October 1997. (Letter).

[37] ROHDE & SCHWARZ. *Operating Manual: SMIQ Vector Signal Generator*, 2002.

[38] ROHDE & SCHWARZ. *Specifications for Vector Signal Generator R&S SMIQ*, 2002.

[39] SCHWEBER, B., "Give DACs Due Diligence for Superior DDS Performance." *EDN*, July 1997.

[40] SHANNON, C. E., "A Mathematical Theory of Communications." *Bell System Technical Journal*, July 1948, Vol. 27, pp. 379–423, 623–656.

[41] SMITH, D., "Signals, Samples and Stuff: A DSP Tutorial (Part 1)." *QEX*, March 1998, pp. 3–16.

[42] STEGMANN, J., "Simulations of quadrature demodulation techniques." Preliminary findings for Masters Thesis, University of Stellenbosch, June 2003.

[43] STREMLER, F. G., *Introduction to Communication Systems*. Third edition. Reading: Addison-Wesley, 1990.

[44] SU, K. L., *Analog Filters*. London: Chapman & Hall, 1996.

[45] TUTTLEBEE, W. (Ed.), *Software Defined Radio*. West Sussex: Wiley, 2002.

[46] TWITCHELL, E. R., "A Digital Approach to an FM Exciter." *IEEE Transactions on Broadcasting*, June 1992, Vol. 38, No. 2, pp. 106–109.

[47] UNIVERSITY OF STELLENBOSCH, "SDR Research Group Homepage." http://www.dsp.sun.ac.za/sdr, September 2003.

[48] VAN ROOYEN, G.-J., "Design and Implementation of an FM Exciter using Direct Digital Synthesis." Undergraduate thesis: University of Stellenbosch, 1998.

[49] VAN ROOYEN, G.-J. and LOURENS, J. G., "A Quadrature Baseband Approach to Direct Digital FM Synthesis." *IEEE Transactions on Broadcasting*, September 2000, Vol. 46, No. 3, pp. 227–230.

[50] VAN ROOYEN, G.-J. and LOURENS, J. G., "Advances in Direct Digital Frequency Synthesis." *Elektron*, July 2001, pp. 39–42.

[51] VAN ROOYEN, G.-J. and LOURENS, J. G., "Baseband Digital Signal Processing System with Digital Spur Compensation." October 2002. South African Patent Application 2002/7909.

[52] VAN ROOYEN, G.-J. and LOURENS, J. G., "Baseband Digital Synthesis and Analysis for High-Frequency Software Radio Applications." *Proceedings of IEEE Africon*, October 2002, Vol. 1, pp. 371–376.

[53] VANKKA, J., "Methods of Mapping from Phase to Sine Amplitude in Direct Digital Synthesis." *IEEE Transactions on Ultrasonics, Ferroelectrics, and Frequency Control*, March 1997, Vol. 44, No. 2, pp. 526–534.

[54] WITKOWSKY, J., "A Hardware Emulator Testbed for Software-Defined Radio." Master's thesis, Peninsula Technikon, 2003.

[55] WITKOWSKY, J. and VAN ROOYEN, G.-J., "A Hardware Emulator Testbed for Software Defined Radio." *Proceedings of IEEE Africon*, October 2002, Vol. 1, pp. 383–388.

[56] ZIEMER, R. E. and TRANTER, W. H., *Principles of Communications: Sytems, Modulation and Noise*. Fourth edition. New York: John Wiley & Sons, 1995.

Appendix A

Direct-digital synthesis

The primary aim of this dissertation is to present a detailed analysis of quadrature-baseband modulation and demodulation techniques, and their use for arbitrary-accuracy signal processing. In order to understand quadrature modulation in particular, its prerequisite technology is summarised here: the standard technique of performing single-signal direct-digital synthesis (DDS), by which arbitrary waveforms can be generated from a fixed reference frequency.

A.1 Single-signal DDS

The idea behind direct-digital synthesis is to digitally "sculpt" a desired analogue signal. To do this, a digital-to-analogue converter (DAC) operating at a fixed sampling frequency is employed. Different output frequencies are obtained by sampling a sine wave at various intervals. For example, to obtain a higher output frequency, the sine wave is sampled at larger phase increments. Likewise, to generate a lower output frequency, smaller phase increments are used when sampling the sine wave. In short, the rate of phase change (effectively the phase derivative) determines the resultant output frequency.

A schematic representation of a DDS system is shown in Figure A.1. The heart of

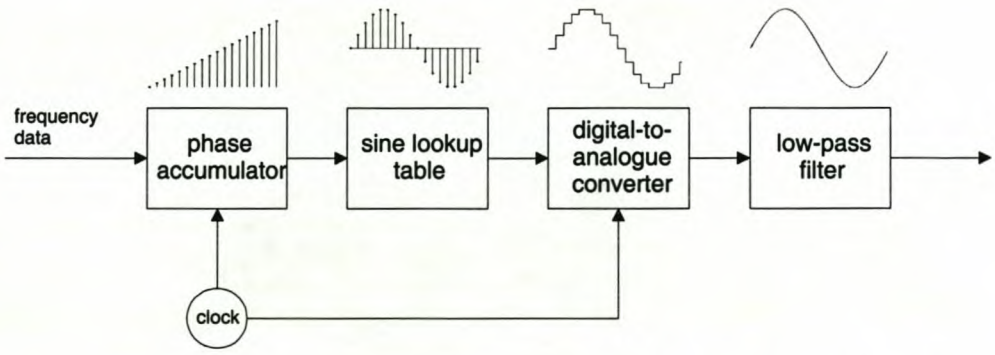

Figure A.1: *Schematic overview of a single-signal direct-digital synthesiser.*

the system is the phase accumulator—an R-bit number that represents the current phase ($0 \leq \phi < 2\pi$ rad) of the output sine wave. During each clock cycle the phase accumulator is incremented with $\Delta\phi$; the size of this increment is directly proportional to the output frequency. Phase wrap from 2π to 0 rad is accomplished by simply ignoring the phase accumulator overflow. The phase accumulator is used as an index to a phase lookup table, which produces a sampled sine wave. Finally, digital-to-analogue conversion and low-pass filtering are applied to produce the output sine wave.

Although a lookup table is used in this diagram (and in most practical DDS systems), it is not the only technique that can be used to map phase values to wave amplitudes. Various alternatives have been developed, such as sine compression [53], Taylor series approximation [13], ROM-less DDS [29, 28], and digital oscillators [32, p. 352], [22].

If $\Delta\phi$ were constant, the phase would increase in a linear fashion and the output frequency would be constant. Manassewitsch [23] shows that an output frequency of f_o can be produced if the phase increment is

$$\Delta\phi = 2\pi \left(\frac{f_o}{f_s}\right) \text{ rad}, \tag{A.1}$$

with f_s being the sampling frequency (also called the reference clock frequency). A digital phase accumulator with R bits represents 2π rad. This means that the previous equation can also be expressed as

$$\Delta\phi = 2^R \left(\frac{f_o}{f_s}\right). \tag{A.2}$$

By dynamically adapting the phase increment, it is possible to implement a wide range of modulation schemes. Phase modulation, for example, can easily be achieved by using an input signal as offset to the phase accumulator during sine lookup:

$$\phi(nT) = \Delta\phi \cdot nT + k_\phi m(nT), \tag{A.3}$$

where $k_\phi m(nT)$ is the (scaled) modulating input signal and $\phi(nT)$ is the phase to use during the sine lookup (both at discrete time nT). The carrier frequency is determined by the phase increment, $\Delta\phi$. Frequency modulation is quite similar, and will be considered in the next section. Amplitude modulation can be achieved by generating a constant frequency (by setting $k_\phi = 0$ in Equation A.3) and multiplying this carrier with the modulating signal on a sample-by-sample basis.

A.2 A typical application: frequency modulation

Direct-digital synthesis can be used for the generation of any arbitrary band-limited wave, provided that the sampling rate is above the Nyquist frequency. In this dissertation the focus will mostly fall on sinusoidal signal synthesis, because most existing modulation schemes use sinusoidal basis functions. In general, however, DDS can synthesise any periodic waveform

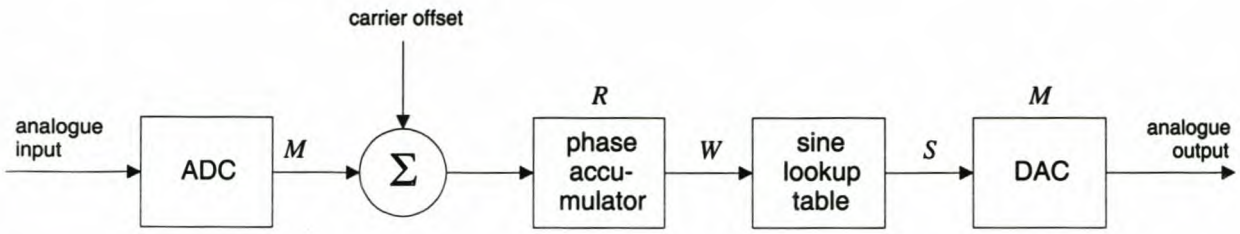

Figure A.2: *Block diagram of a DDS system showing each component's number of bits.*

(when using a lookup table) and any aperiodic waveform (when using algorithm-based sample calculation).

A DDS system capable of generating a sine wave of arbitrary amplitude, phase offset and frequency can easily be employed to generate a variety of analogue and digital modulation schemes. In this section, a typical application of DDS is analysed, namely frequency modulation (FM).

In analogue FM, the phase angle at any instant t is given by

$$\phi(t) = \omega_c t + k_f \int_0^t m(\tau)\, d\tau + \phi_0\,, \tag{A.4}$$

where ω_c is the carrier frequency, k_f is the deviation constant, $m(t)$ is the modulating signal, and ϕ_0 represents the phase angle at time $t = 0$. To perform modulation in discrete time, as is required in a DDS system, Equation A.4 must be rewritten as

$$\phi(nT) = nTF_c + k_f T \sum_{k=1}^{n} m(kT) + \phi_0\,. \tag{A.5}$$

In this equation, T is the sampling interval and n is the sample number. F_c is a constant that determines the carrier frequency of the discrete-time output signal. Each sample produced by this equation can be used as the phase index to a sine lookup table, to obtain a sampled FM signal. If all significant frequency components are below the half-Nyquist frequency, an analogue FM signal can be generated by low-pass filtering the sampled FM signal. If ideal components were used, the resultant analogue signal would be identical to the one produced by the ideal analogue FM modulator of Equation A.4 (within the signal bandwidth).

The DDS FM exciter can generate an FM signal directly at the desired broadcast frequency, or an intermediate frequency can be employed. When the signal is generated directly at the broadcast frequency, only minimal filtering is required. The use of an intermediate frequency requires one or several stages of filtering and mixing [14].

A.3 Design considerations

In a direct-digital synthesiser, the designer must choose the number of bits in the phase accumulator, the number of entries in the sine lookup table, and the bit accuracy of the sine

information and the DAC. These parameters directly affect the spurious noise levels in the modulated frequency spectrum. The effect that various design parameters have on a DDS FM exciter will be investigated next.

A.3.1 Number of ADC bits

A DDS FM exciter performs frequency modulation by using a sampled and quantised representation of the input signal. In an FM signal, each possible *amplitude level* of the input signal is represented as a unique *frequency* in the output signal. For each possible output frequency, the phase increment, $\Delta\phi$, must have a unique value—in other words, $\Delta\phi$ must be able to take on as many values as there are quantisation levels on the input signal.

For example, if the modulating input signal is sampled with M-bit resolution, it has 2^M quantisation levels. Since each amplitude level must translate to a unique frequency, determined by the size of the phase increment per clock cycle, $\Delta\phi$ must also take on 2^M different values. As the frequency deviation is in the range $-\omega_d$ to $+\omega_d$, the frequency resolution of the DDS system is

$$\Delta\omega = \frac{2\omega_d}{2^M} \text{ rad}. \tag{A.6}$$

For example, in a commercial radio broadcasting application the deviation frequency is $\omega_d = 75$ kHz. For 16-bit input quantisation, the corresponding DDS frequency resolution is about 2.29 Hz.

The fact that the modulating input signal is sampled (therefore discretised both in amplitude and in time) accounts for many of the spurious components in the DDS output. This arises from the fact that a sampled signal has an infinite number of reflected (alias) components that also affect the synthesis. For a detailed analysis of the effects of sampling the modulating signal, see Domínguez and Salis [11].

A.3.2 Number of accumulator bits

Although the *phase increment* has only 2^M possible values, an M-bit value is too small to represent the actual *phase* in the phase accumulator. This is because the phase increment must be offset by a value that produces the centre frequency. Suppose that the 16-bit input signal must be frequency modulated ($\omega_d = 75$ kHz) at a centre frequency of 5 MHz. If the phase resolution is 2.29 Hz, the accumulator must have enough bits to represent

$$\phi_{\max} = \frac{2(5 \cdot 10^6 + 75 \cdot 10^3)}{2.29} = 4.43 \cdot 10^6, \tag{A.7}$$

where the factor two is necessary to satisfy the Nyquist sampling criterion. Consequently, the accumulator must have at least 23 bits to satisfy the required frequency resolution. The higher the centre frequency, the more bits are required (roughly one extra bit for each octave

that the centre frequency rises). In general, the required number of bits is[1]

$$R = \left\lceil \log_2 \left(\frac{2(\omega_c + \omega_d)}{\Delta\omega} \right) \right\rceil . \tag{A.8}$$

This effect is one of the most serious shortcomings of single-signal DDS. A high centre frequency places demands on the bit and memory requirements of the DDS system. A low output centre frequency can only be converted to a higher frequency through (often several stages of) mixing and filtering.

To summarise, the size of the phase accumulator is dictated by the required centre frequency and the acceptable quantisation of the input signal. It has no effect on the noise floor of the modulated RF signal.

A.3.3 Number of lookup table entries

It is not strictly necessary for each value of the phase accumulator to address a unique value in the sine lookup table. Instead, the phase accumulator can be kept at the resolution dictated by Equation A.8, (R bits) as the internal representation of the phase, while only the W most significant bits are used as index to the sine lookup table. The extreme case is the 1-bit lookup table: The MSB of an R-bit accumulator selects the output level, and a square wave is generated. Only two output values are possible, but the square wave frequency and phase are generated with R-bit accuracy.

This technique has the advantage that it can significantly save on memory requirements for the lookup table. However, it leads to spurious noise: The quantisation of phase bits in the DDS process causes phase noise in the modulated signal. This phase noise appears as spurs in the RF spectrum (in the extreme case, the large harmonics of a square wave). Jenq [18] shows that the spurs in the modulated signal's spectrum will generally lie between $6.02W - 3.92$ dBc and $6.02W - 5.17$ dBc. This can deteriorate a modulated signal's spurious free dynamic range, or SFDR (introduced in Section 3.2).

Phase truncation can be very useful when good output frequency resolution is required, but a comparatively high RF noise floor can be tolerated. For example, if a commercial FM signal is generated at a high output frequency (such as 108 MHz), at least 26 accumulator bits are required for 16-bit sound quality. A sine lookup table with a 26-bit phase index would contain 67.1 million entries.

A.3.4 Number of sine data and DAC bits

The choice of word length for the sine data words and the digital-to-analogue converter (DAC) is simply dependent on the allowable quantisation noise in the modulated signal. For example, if the noise must be kept lower than 90 dB below the carrier, 15-bit (or preferrably

[1] $\lceil x \rceil$ is the ceiling function, which rounds its argument to the nearest integer towards plus infinity.

16-bit) resolution is required. This follows from the rule of thumb that each output bit produces a 6-dB improvement in quantisation noise. A more detailed analysis is given by Jenq [18].

Appendix B

Quadrature modulation and demodulation techniques

Chapter 2 has given a very generic interpretation of quadrature modulation and demodulation. This appendix describes some practical techniques to achieve the modulation of analogue and digital signals in quadrature-based signals.

B.1 Quadrature modulation techniques

As was described in Chapter 2, Equation 2.8 (or its generalised expressions, Equations 2.13 and 2.14) can be implemented in the block diagram of Figure 2.3 (p. 13). The sine and cosine of $\theta(t)$ can be generated by using the single-signal DDS technique of Appendix A.[1] These components are then multiplied by the carrier frequency's corresponding sine and cosine waves, and the difference is used as RF output.

The quadrature modulation techniques are developed here to show that it is possible to reproduce the most important analogue modulation schemes using quadrature-baseband DDS. Propositions A and B are not limited to these modulation schemes, but the techniques described here do illustrate the field of the propositions' application. The quadrature signal theory forms an important part of the analysis of quadrature non-idealities in Chapter 5, and the modulation schemes are used extensively in simulations and in the practical system of Chapter 7.

B.1.1 Quadrature frequency modulation

The synthesis of an analogue FM signal at a carrier frequency ω_c is considered first. An FM signal (as is used in commercial radio broadcasting, for example) consists of a single sinusoid of which the instantaneous frequency modulates in time, proportional to the amplitude of

[1] Or, in the case of multitonal synthesis, $\theta_i(t)$ for each of the component tones can be used to look up the sine and cosine of the respective angle from the table. The calculated amplitudes are than added together, as per Equations 2.13 and 2.14, prior to analogue conversion and mixing.

a modulating input signal. In terms of Section 2.2.2, this description categorises it as a single-tone RF signal with time-variant frequency but constant amplitude and phase offset. From this, Equation 2.8 can be written as

$$y(t) = \cos[\phi(t) \cdot t] \cos \omega_c t - \sin[\phi(t) \cdot t] \sin \omega_c t\,, \tag{B.1}$$

where $\phi(t)$ represents the time-varying phase argument of Equation A.5 (p. 163), so that $\theta(t) = \phi(t) \cdot t$. To generate the two modulated baseband signals, $I(t) = \cos\theta(t)$ and $Q(t) = \sin\theta(t)$, Equation A.5 must be applied for baseband FM. In this equation, F_c is the carrier frequency; for baseband FM, $F_c = 0$. The discrete modulating signal is $m(kT)$, and can be positive or negative. Therefore, the two modulated baseband signals can be generated in the following way:

$$I(nT) = \cos\left[k_f \sum_{k=1}^{n} m(kT)\right] \tag{B.2}$$

$$Q(nT) = \sin\left[k_f \sum_{k=1}^{n} m(kT)\right]. \tag{B.3}$$

The deviation factor k_f is calculated from the desired maximum frequency deviation so that

$$\Delta\phi_{\max} = k_f \cdot [m(kT)]_{\max}\,. \tag{B.4}$$

This maximum phase increment can be calculated by substituting the maximum frequency deviation and the sample frequency in Equation A.1 (p. 162), and then solving for k_f in Equation B.4 above.

Digital-to-analogue conversion and low-pass filtering is performed to obtain $I(t)$ and $Q(t)$ from their discrete-time counterparts.

FM of an input DC signal is simulated in Figure B.1 on page 169. FM of an input sine wave is simulated in Figure B.2 on page 170.

B.1.2 Quadrature phase modulation

Assume that the carrier at frequency $\omega_c + \omega_o$ is to be modulated in phase, where ω_c is the local oscillator (LO) frequency, and ω_o is the frequency offset between the LO frequency and the desired carrier frequency. Note that ω_o can be negative, and can be zero in cases where the LO frequency represents the exact carrier frequency (this is not assumed to be the case here, for purposes of generality). Then the phase argument of the synthesised I-Q signals is

$$\theta(nT) = \omega_o nT + k_\phi m(nT)\,. \tag{B.5}$$

Using the same DDS lookup table technique as for frequency modulation, Equations B.2 and B.3 can be modified for phase modulation to

$$I(nT) = \cos[\omega_o nT + k_\phi m(nT)] \tag{B.6}$$

$$Q(nT) = \pm\cos\left[\omega_o nT + k_\phi m(nT) - \frac{\pi}{2}\right]. \tag{B.7}$$

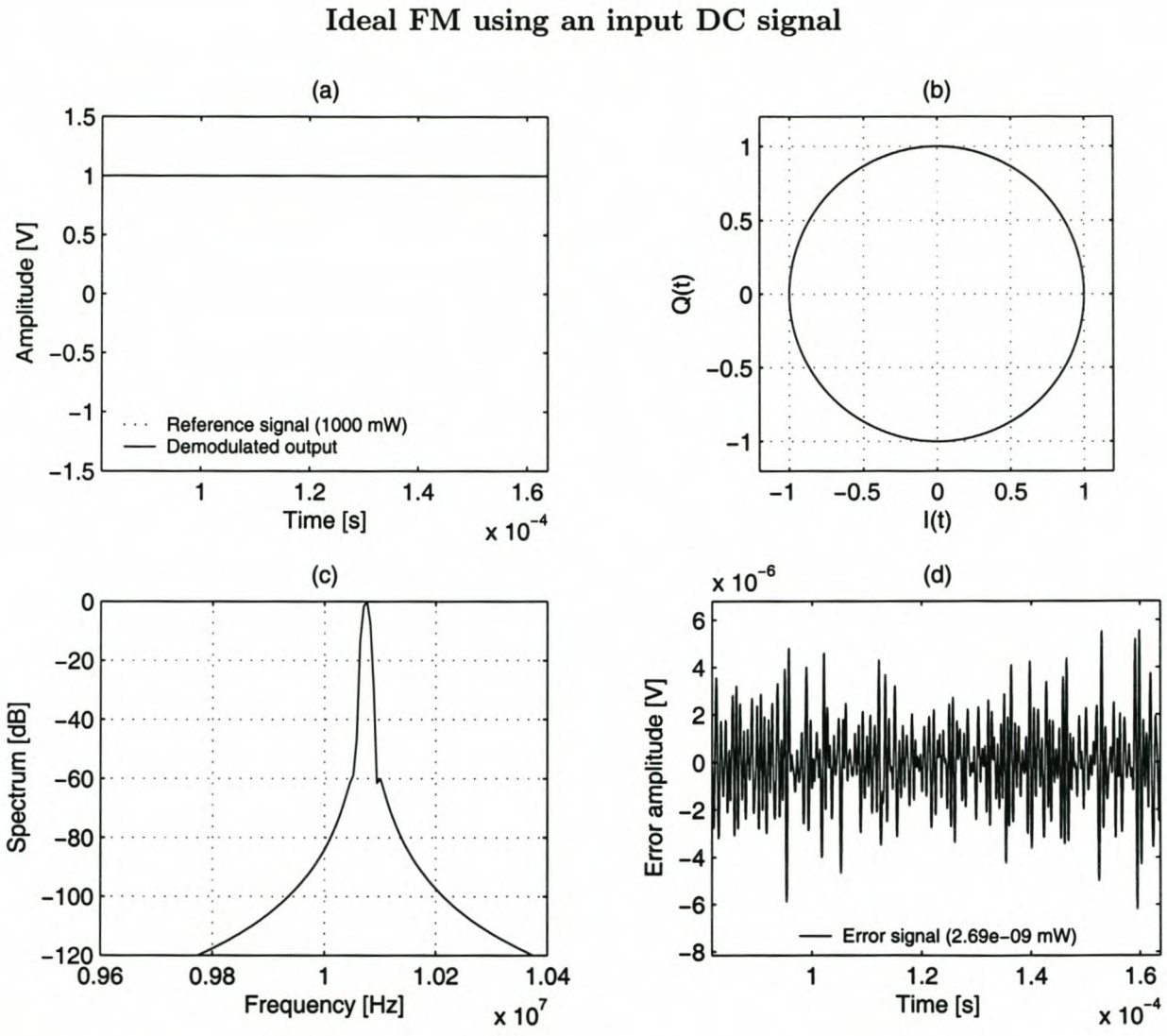

Figure B.1: *Simulation of ideal frequency modulation of an input DC signal. (a) The modulating and demodulated signals are visually identical. (b) The phasors of both the transmitted and received signals are perfectly circular, indicating zero quadrature impairment. (c) The frequency spectrum of the modulated signal shows a single component at maximum frequency deviation (75 kHz above 10 MHz). (d) The error signal mostly contains post-filtering carrier residues.*

Simulation reference: `cleandc`

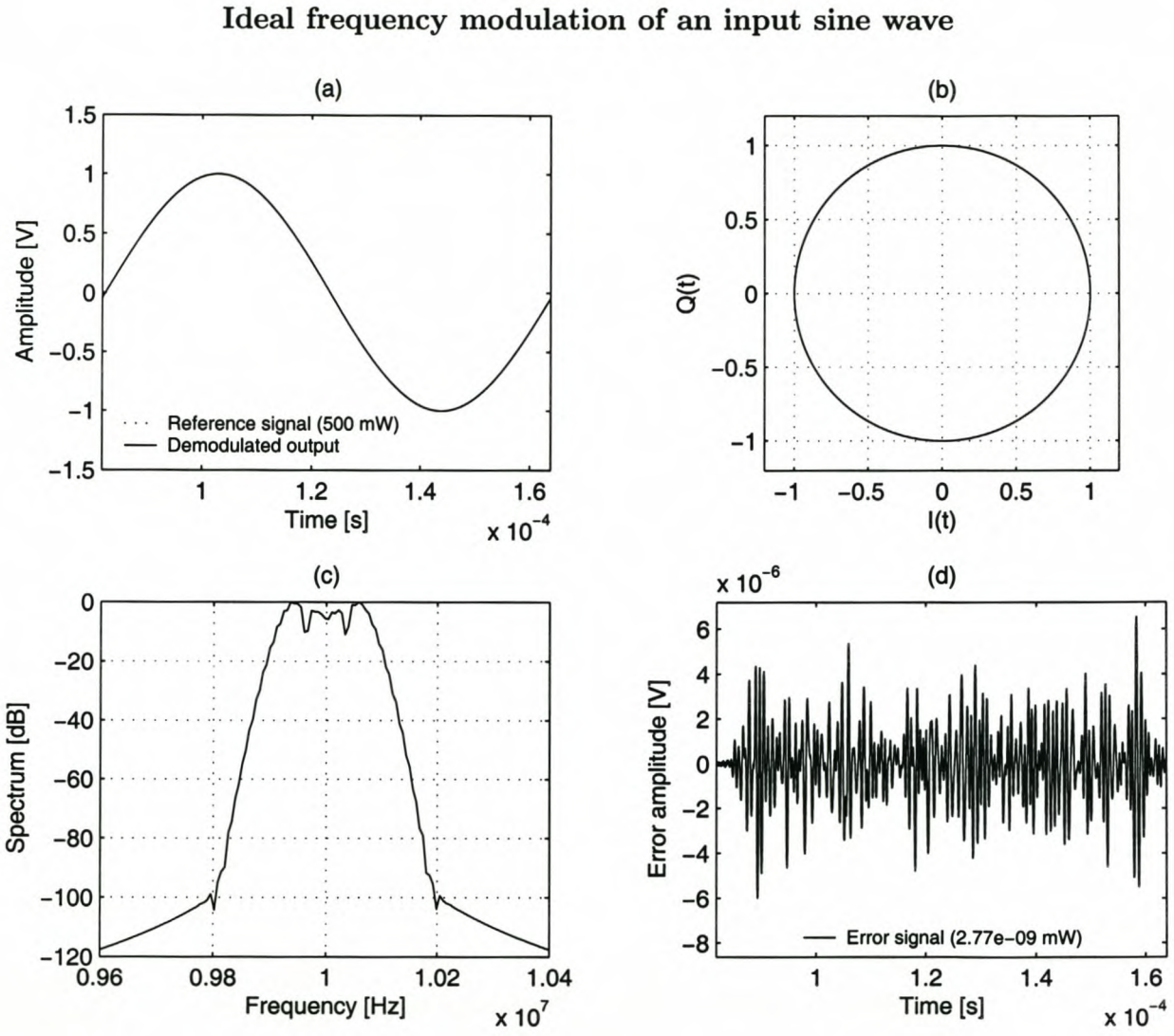

Figure B.2: *Simulation of ideal frequency modulation of an input sine wave. (a) The modulating and demodulated signals are visually identical. (b) The phasors of both the transmitted and received signals are perfectly circular, indicating zero quadrature impairment. (c) The frequency spectrum of the modulated signal shows the range of frequency modulation. (d) The error signal mostly contains post-filtering carrier residues.*

Simulation reference: `cleanfm`

The sign of $Q(nT)$ is chosen to be the same as the sign of ω_o, producing the lead-lag phase relationship between $I(nT)$ and $Q(nT)$ that distinguishes between positive and negative frequencies in the baseband signal. The signals are synthesised by the lookup-table DDS technique of Chapter A. The quadrature phase-modulated $I(nT)$ and $Q(nT)$ are then converted and filtered to produce $I(t)$ and $Q(t)$, and then mixed as illustrated in Figure 2.3.

The phase deviation constant k_ϕ is easily calculated by dividing the desired maximum phase deviation by $[m(nT)]_{\max}$.

B.1.3 Quadrature amplitude modulation (DSB)

Double-sideband amplitude modulation is achieved by synthesising two carrier signals in quadrature relationship at a carrier frequency $\omega_c + \omega_o$, where ω_c once again represents the local oscillator frequency, and ω_o the offset of the centre frequency. Following a similar analysis as in the previous paragraphs,

$$I(nT) = m(nT)\cos(\omega_o nT) \tag{B.8}$$

$$Q(nT) = \pm m(nT)\cos\left(\omega_o nT - \frac{\pi}{2}\right), \tag{B.9}$$

where the modulating input signal $m(nT)$ is assumed to have the correct scaling and offset to produce the desired modulation index, and the sign of $Q(nT)$ is equal to the sign of ω_o. The signal is then also synthesised using DDS and subsequently converted to continuous analogue signals, and mixed according to Figure 2.3.

If $\omega_o = 0$, no quadrature mixing is required, and $I(nT) = m(nT)$ whilst $Q(nT) = 0$. For non-zero ω_o, it may be more efficient to use a digital oscillator than a lookup table, since the feedback coefficients need only be calculated for possible carrier frequencies.

Figure B.3 shows a simulation of an DSB-AM signal.

B.1.4 Quadrature amplitude modulation (SSB)

Single-sideband amplitude modulation (SSB) can be accommodated without any alteration of the system hardware of Figure 2.3. Equation 2.9 is easily adapted to the equation for SSB [56, p. 148] by letting

$$I(nT) = m(nT) \quad \text{and} \quad Q(nT) = \pm\hat{m}(nT), \tag{B.10}$$

where $\hat{m}(nT)$ represents the Hilbert transform of $m(nT)$, and the sign of $Q(nT)$ determines whether upper-sideband SSB (positive sign) or lower-sideband SSB (negative sign) is produced. For Equation B.10 these sidebands will be symmetrical around the mixer's local oscillator frequency, ω_c. To implement such a system digitally, a digital Hilbert transform filter [32] must be implemented, but no sinusoidal synthesis or lookup is required.

In systems where software-based channel selection is to be performed, the SSB centre frequency can be adjusted to $\omega_c + \omega_0$ (where ω_0 is a positive or negative frequency offset). To achieve this, time-domain multiplication by a complex exponential (resulting in frequency

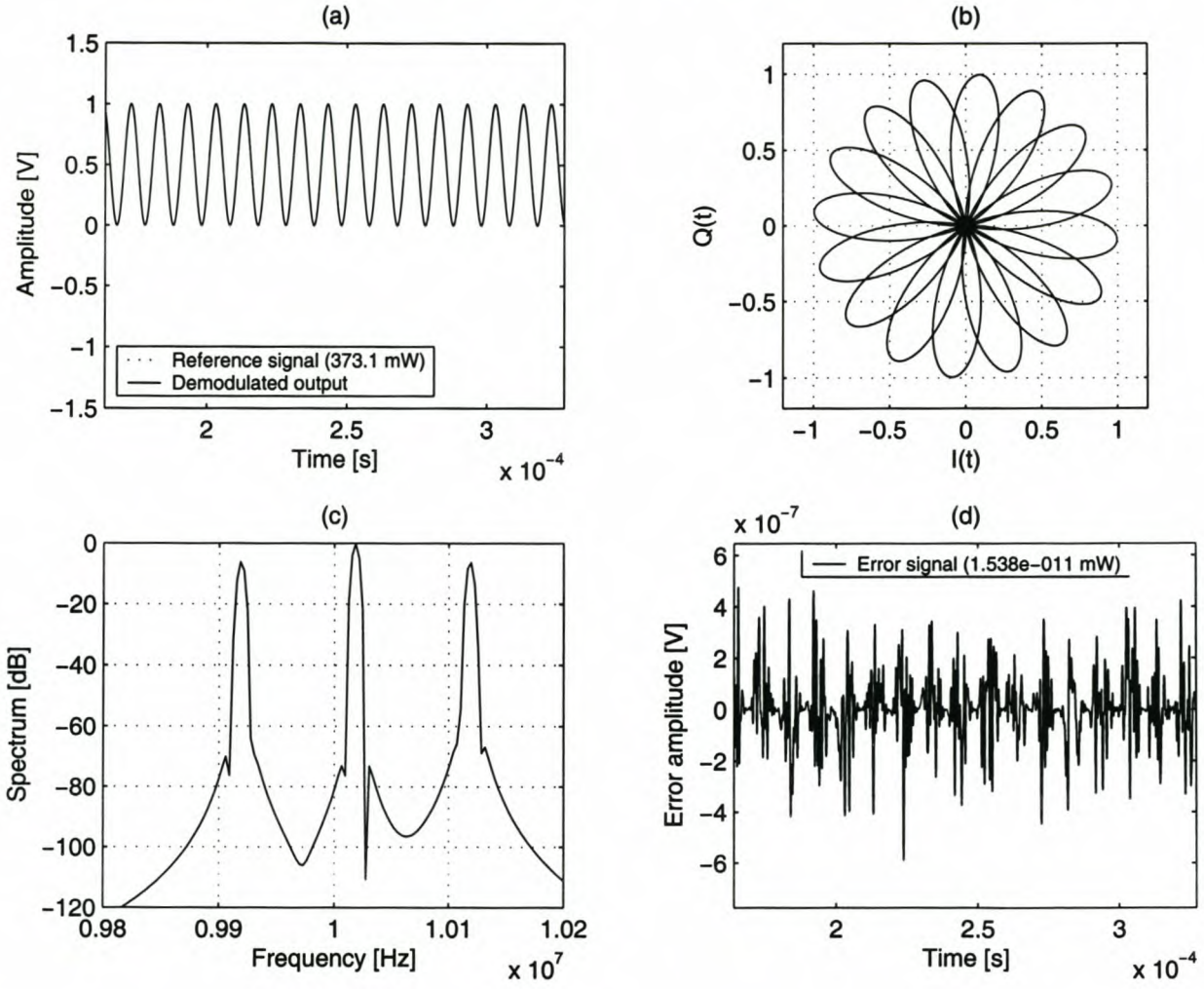

Figure B.3: *Simulation of ideal DSB amplitude modulation of an input sine wave, with a carrier frequency above the mixing frequency. In this simulation, the carrier frequency was chosen to be 18.75 kHz above the mixing frequency of 10 MHz. (a) The modulating and demodulated signals are visually identical. (b) Because the phasor is modulating in amplitude whilst it is rotating at a constant frequency, it produces this attractive flower-like graph. (c) The large-carrier AM signal produces a strong frequency component at 10.025 Mhz. The double-sideband modulation is clearly visible, as are the small sidebands produced by the windowing of the modulating signal. (d) The error signal mostly contains post-filtering carrier residues.*

Simulation reference: `cleanamofs`

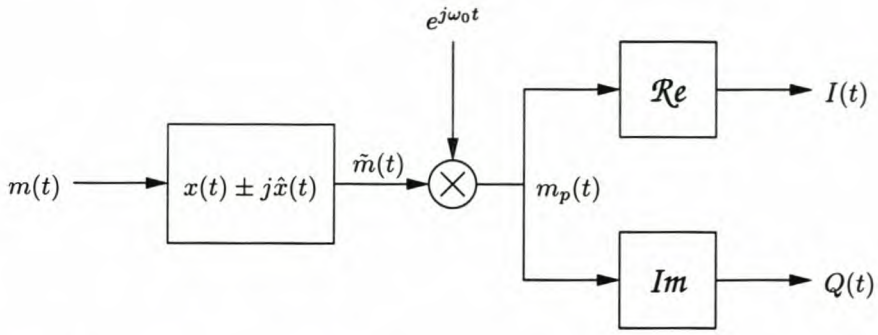

Figure B.4: *Block diagram of an SSB modulator with channel selection. The sign of the analytic transform determines whether an USB (negative) or LSB (positive) signal is produced. Note that ω_0 may also carry its own sign.*

translation—see Section 2.2) must be performed while the signals are still in the digital domain, as is illustrated by Figure B.4. The modulating signal is first converted to its single-sided representation by the analytic transform [56, p. 98]

$$\tilde{m}(nT) = m(nT) \pm j\hat{m}(nT)\,. \tag{B.11}$$

The conjugation sign in Equation B.11 is negative for upper-sideband SSB, and positive for lower-sideband SSB. Instead of directly performing quadrature mixing on the real and imaginary components of the analytic signal (as is done in the conventional implementation of SSB), the complex-valued analytic signal can be translated in frequency by multiplying it with a complex exponential. This represents the first stage of upmixing, and is performed in the digital domain—typically to achieve channel selection. The real and imaginary components of this signal can be further translated to the actual band centre frequency by using the quadrature mixing techniques of Section 2.2 in the analogue front-end.

For the practical realisation of Figure B.4, a Hilbert transform filter must be implemented. Digital mixing with the complex exponential is achieved by noting that the translated signal is

$$\begin{aligned} m_p(nT) &= [m(nT)\cos\omega_0 nT - \hat{m}(nT)\sin\omega_0 nT] \\ &\quad + j\,[m(nT)\sin\omega_0 nT + \hat{m}(nT)\cos\omega_0 nT]\,, \end{aligned} \tag{B.12}$$

where the complex exponential was decomposed into its trigonometric form by Euler's identity. The sine and cosine of $\omega_0 nT$ can be created by lookup-table DDS. However, if $\omega_0 nT$ is limited to a small set of frequencies (as is typically the case for channel selection), or if a slight delay is permissible while new loop coefficients are calculated when ω_0 changes, a coupled-form oscillator might be better suited to the task [32, p. 354].

B.1.5 Extension to digital modulation schemes

The modulation techniques described thus far assume an analogue input signal. By modulating frequency, phase and amplitude, they represent a general starting point for developing

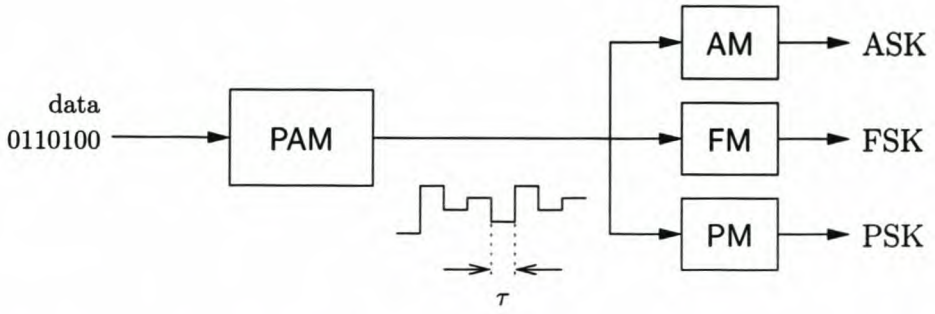

Figure B.5: *Digital modulation can be implemented in terms of analogue modulation schemes. The binary data is grouped into data words, and each word is treated as a symbol that maps to a corresponding amplitude level. The resulting pulse-amplitude modulated (PAM) signal has as many amplitude quantisation levels as there are digital symbols, and is used as input to an analogue modulator.*

other modulation schemes. This section briefly illustrates how to extend the developed theory to digital modulation schemes.

Parameter-based digital modulation schemes such as amplitude-shift keying (ASK), frequency-shift keying (FSK) and phase-shift keying (PSK) transmit information by using a set of N symbols (i.e. discrete amplitudes, frequencies or phases) that can be transmitted at a rate of $1/\tau$, where τ is the symbol length. A convenient intermediate waveform that encapsulates the commonality between these digital modulation schemes, is pulse amplitude modulation (PAM),[2] which is illustrated in Figure B.5. A useful technique in digital software-defined radios, is to translate an information stream into a PAM representation (each data word or symbol produces a quantisation level), and to use this wave as input to one of the quadrature analogue modulators described in Sections B.1.1 to B.1.3.

Because a PAM signal takes on only predetermined (quantised) amplitude levels, and maintains them for a period τ, which is often long compared to the carrier period, the modulation techniques may in certain cases be simplified as described further in this section.

To maintain its general applicability, this dissertation will mostly present modulation from the analogue point of view, since digital modulation schemes can often be seen as special cases of their analogue counterparts.

---

[2]The use of the term "PAM" here is somewhat unconventional. It is intended to convey the observation that any digital signal can be represented as a PAM-like signal that can take on only discrete amplitude values. Each amplitude represents a digital symbol. Using this discrete-valued, non-return-to-zero PAM as the modulating input to an AM, FM or PM system, results in ASK, FSK or BPSK respectively. Therefore this specialised PAM signal is a useful intermediate representation of digital data, and is helpful to build digital modulation schemes from their analogue counterparts.

Frequency-shift keying

For FSK, the number of symbols, N, is usually relatively low, and the requirements on DDS frequency resolution may be relaxed accordingly. It may be impractical to use a digital oscillator instead of lookup-table DDS, since phase continuity is usually a requirement during symbol transitions. Unless an integral relationship exists between the sampling rate, symbol rate and symbol frequency positions, it would be necessary to re-calculate the oscillator coefficients at each symbol transition.[3]

Phase-shift keying

PSK (including all its derivatives, such as QPSK and QAM) require very accurate phase synthesis, and digital oscillation may be unpractical for such purposes. The lookup table can be greatly optimised by choosing $\omega_o = 0$ in Equation B.5, with the disadvantage that channel selection must be done by adjusting the local oscillator frequency of the quadrature mixer. In this case, only the symbol phase shifts, ϕ_i, and the associated symbol amplitudes need to be stored or calculated. In fact, this means that the DDS technique just simplifies to the traditional I-Q method of generating QPSK or QAM. The quadrature compensation techniques that will be developed in Chapter 6 still hold and can be used to impove the bit error rate of such a system.

In software-defined radio systems, software channel selection and adjustable symbol constellations are often priorities. If so, a full lookup table that minimises phase and amplitude quantisation noise (Section A.3) may be required.

Amplitude-shift keying

Given an amplitude-modulating PAM signal representing digital symbols, generating an amplitude-shift keyed signal is almost trivial. A digitally generated complex subcarrier is multiplied by the PAM amplitude values and synthesised as I and Q signals. Since only a limited number of subcarriers need to be generated (of which $\omega_0 = 0$ may be one), ASK is well suited to the use of a digital oscillator.

B.2 Quadrature demodulation techniques

It can now be demonstrated how the quadrature downconversion technique of Equation 2.21, and its practical realisation depicted in Figure 2.5, can be used to perform baseband demod-

[3]Digital sinusoidal oscillators require recalculation of the loop parameters to produce a continuous-phase change in frequency. Knowledge of the current phase position is required at the frequency transition, and the sine of the phase at the new frequency must be determined. A frequency-modulating oscillator would therefore also require a lookup table (or a similar technique), and a simpler solution would be to use only a lookup table to generate the sinusoid, eliminating the need for a feedback loop.

ulation of received modulated signals. These demodulation techniques make use of the derivation on page 19 that a received signal of the form

$$f(t) = a(t) \cdot \cos \phi(t) \tag{B.13}$$

becomes

$$s(t) = a(t) \cdot e^{j[\phi(t) - \omega_c t]} \tag{B.14}$$

after quadrature frequency translation. These demodulation techniques are used in the simulations and practical system of Chapters 5, 6 and 7 to verify the developed theory.

B.2.1 Quadrature phase demodulation

Although the baseband signal of Equation B.14 shows frequency translation, the signal's original phase argument, $\phi(t)$, stays intact and may be demodulated.

Coherent reception

First, consider the case where the carrier frequency is estimated precisely. In such a scenario, the received signal may be

$$f(t) = A \cdot [\omega_c t + \phi(t)] \,, \tag{B.15}$$

representing a constant-amplitude signal at carrier frequency ω_c, with the modulated phase information in $\phi(t)$. After quadrature downmixing by Equation B.14 with a coherent carrier signal, the complex-valued baseband signal to be processed digitally is

$$s(t) = Ae^{j\phi(t)} \,. \tag{B.16}$$

Usually the downmixed signal is digitised as two quadrature baseband signals, $I(t) = \mathcal{R}e\{s(t)\}$, and $Q(t) = \mathit{Im}\{s(t)\}$. Then the desired phase argument is

$$\phi(t) = \arctan\left[\frac{Q(t)}{I(t)}\right] \,. \tag{B.17}$$

Non-coherent reception

In general, it cannot be assumed that the local oscillator of the quadrature mixer is exactly phase coherent with the modulated signal carrier—indeed, such an assumption would imply that the receiver is not a fully software-defined radio. In such a case, the downmixed signal becomes

$$s(t) = Ae^{j[\phi(t) + (\omega_c - \hat{\omega}_c)t]} \,. \tag{B.18}$$

Taking the arctangent produces a linear phase drift due to the frequency error $\omega_c - \hat{\omega}_c$. However, high-pass filtering can be used to remove this phase drift, as illustrated in Figure B.6.

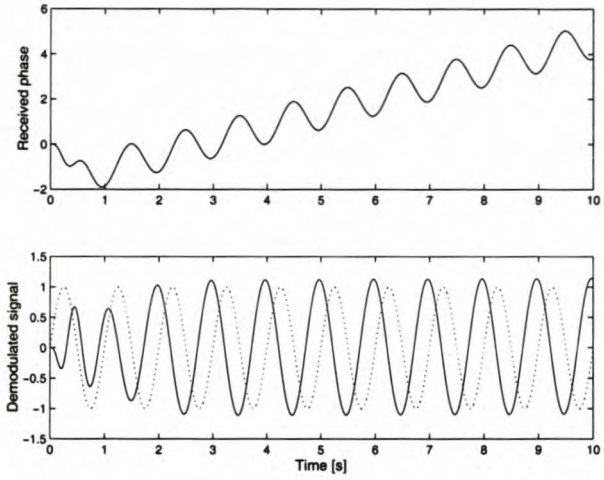

Figure B.6: *Phase drift caused by imperfect carrier estimation during quadrature phase demodulation can be cancelled by filtering out the drifting DC component. The top diagram shows the phase of a received quadrature signal; the average rate of increase represents the frequency difference between the signal carrier and the receiver carrier estimate. The lower diagram shows the same signal after high-pass filtering to remove the DC drift component. Apart from group delay caused by the filtering, the demodulated signal is identical to the modulating signal (shown as a dotted line).*

B.2.2 Quadrature frequency demodulation

Frequency demodulation may be achieved by differentiating the complex phase of Equation B.18. This produces the instantaneous frequency

$$\omega_i(t) = \dot{\phi}(t) + (\omega_c - \hat{\omega}_c)\,. \tag{B.19}$$

The frequency error term represents a DC offset that is easily removed by high-pass filtering.

A simple digital differentiator may be realised by calculating the difference between successive samples. During frequency demodulation, it is particularly important to again perform low-pass filtering after demodulation (with a cut-off frequency just above the highest signal frequency), in order to minimise the quadratically-rising noise power density spectrum caused by this differentiation process [56]. Preemphasis and deemphasis may also be used as part of the modulation scheme to whiten the demodulated noise spectrum [43].

B.2.3 Quadrature amplitude demodulation: AM

After quadrature downmixing, a received DSB-AM signal has the form

$$s(t) = a(t)e^{j(\omega_c - \hat{\omega}_c + \omega_0)t + j\phi_0}\,. \tag{B.20}$$

The real and imaginary components of this complex-valued signal are $I(t)$ and $Q(t)$ respectively. For amplitude demodulation, the magnitude of this complex signal is of interest, and

thus

$$m(t) = \sqrt{I^2(t) + Q^2(t)} \tag{B.21}$$

regardless of the exact frequency and phase of the downmixed signal. In particular, Equation B.21 holds when $\omega_0 = 0$ and $\omega_c = \hat{\omega}_c$ (coherent demodulation).

B.2.4 Quadrature amplitude demodulation: SSB

A received single-sideband AM signal (as generated in Section B.1.4 on page 171) with an unknown carrier frequency offset ω_0 from the local oscillator frequency, and an unknown phase offset of ϕ_0, can be written in the form [56, p. 151]

$$f(t) = m(t) \cdot \cos\left[(\omega_c + \omega_0)t + \phi_0\right] - \hat{m}(t) \cdot \sin\left[(\omega_c + \omega_0)t + \phi_0\right] . \tag{B.22}$$

In this case, upper-sideband SSB has been assumed. The derivation for lower-sideband SSB is identical, with the exception of a sign change between the two terms of $f(t)$ above. After quadrature downmixing by $-\omega_c$, the complex-valued baseband signal is of the form

$$s(t) = m(t) \cdot e^{j(\omega_0 t + \phi_0)} - \hat{m}(t) \cdot e^{j(\omega_0 t + \phi_0 - \frac{\pi}{2})} , \tag{B.23}$$

where the identity $\sin(A) = \cos(A - \frac{\pi}{2})$ was used to write the translated version of the second term of Equation B.22. It will now be demonstrated that the modulating signal $m(t)$ can be retrieved through the operation

$$m'(t) = \mathcal{R}e\left\{ s(t) \cdot e^{-j(\hat{\omega}_0 t - \hat{\phi}_0)} \right\} , \tag{B.24}$$

where $\hat{\omega}_0 t$ and $\hat{\phi}_0$ are estimates of the exact signal parameters of Equation B.22. By substituting Equation B.23 in Equation B.24,

$$m'(t) = \mathcal{R}e\left\{ m(t) \cdot e^{j[(\omega_0 - \hat{\omega}_0)t + (\phi_0 - \hat{\phi}_0)]} - \hat{m}(t) \cdot e^{j[(\omega_0 - \hat{\omega}_0)t + (\phi_0 - \hat{\phi}_0) - \frac{\pi}{2}]} \right\} . \tag{B.25}$$

For convenience, let

$$\Delta\omega_0 \equiv \omega_0 - \hat{\omega}_0 \qquad \text{and} \qquad \Delta\phi_0 \equiv \phi_0 - \hat{\phi}_0 . \tag{B.26}$$

Then,

$$\begin{aligned} m'(t) &= m(t) \cdot \cos(\Delta\omega_0 t + \Delta\phi_0) - \hat{m}(t) \cdot \cos(\Delta\omega_0 t + \Delta\phi_0 - \tfrac{\pi}{2}) \\ &= m(t) \cdot \cos(\Delta\omega_0 t + \Delta\phi_0) - \hat{m}(t) \cdot \sin(\Delta\omega_0 t + \Delta\phi_0) . \end{aligned} \tag{B.27}$$

Depending on the values of $\Delta\omega_0$ and $\Delta\phi_0$, three demodulation cases can be identified:

1. In the ideal case, $\Delta\omega_0 = 0$ and $\Delta\phi_0 = 0$. Then Equation B.27 reduces to

$$m'(t) = m(t) \tag{B.28}$$

and the modulating signal is perfectly reconstructed.

2. If the offset frequency is correctly estimated, but a phase error remains, $\Delta\omega_0 = 0$ but $\Delta\phi_0 \neq 0$. When this happens,

$$m'(t) = m(t)\cos(\Delta\phi_0) - \hat{m}(t)\sin(\Delta\phi_0)\,. \tag{B.29}$$

The Hilbert-transformed modulating signal leaks through into the demodulated signal. This crosstalk term can produce serious signal distortion if $\Delta\phi_0$ is not small. This is similar to the distortion caused by poor demodulation carrier estimation in non-quadrature systems [56, p. 151].

3. If the offset frequency is incorrectly estimated ($\Delta\omega_0 \neq 0$), Equation B.27 shows that both $m(t)$ and $m'(t)$ will be present in the recovered signal, and that the output will oscillate between them at a rate of $\Delta\omega_0$. This represents an unacceptable level of distortion.

From the observations above, it can be concluded that some form of frequency and phase estimation is required in the demodulator to recover ω_0 and ϕ_0 from the received signal. A complex digital phase-locked loop can be applied for this purpose [42].

B.2.5 Extension to digital modulation schemes

The analogue quadrature demodulation techniques described thus far are equally well suited to digital demodulation. All the above techniques generate a demodulated waveform that can be interpreted as a PAM signal. A typical digital demodulator then proceeds to perform symbol synchronisation, noise integration and threshold detection to identify the received symbols. Once the symbol stream is extracted, the symbols can be decoded into their binary representations, word synchronisation can be performed, and the data can be processed.

Extensive processing of the demodulated PAM waveform is possible in software, making flexible and robust demodulators possible. Such signal processing is beyond the scope of this text, however.

B.2.6 Practical implementation

The quadrature demodulation techniques described in this section have been implemented and tested as part of the Software-Defined Radio Project of the Digital Signal Processing and Telecommunications Group of the University of Stellenbosch [47]. This research confirmed that quadrature demodulation is a simple, flexible technique that can be used to robustly demodulate a wide variety of demodulation schemes [42]. Furthermore, advanced digital processing tools such as adaptive filtering may be employed to use *a priori* knowledge of a modulating signal's statistical properties to further improve the fidelity of the demodulation process.

These quadrature demodulation techniques were also implemented as part of the SDR Architecture developed by the SDR Group [47]. Appendix E contains references to the

source code, and the practical measurements of Chapter 7 show how quadrature modulation can be used very effectively in practice.

Appendix C

Simulations

To aid the analysis of quadrature mixing inaccuracies in software-defined radio systems, an SDR simulation system was developed in MATLAB. Figure C.1 on page 182 gives a graphical overview of the various simulation modules, and how they interact. This chapter will summarise the operation of the simulation modules. For in-depth documentation on the use of the software, the reader is referred to the help provided with the source code. See Appendix E for details on how to obtain the simulation source.

C.1 Overview of the simulation modules

The simulation modules attempt to mimic the behaviour of analogue signals by representing them as vectors of signal samples. At the very least, signals must be sampled at twice the maximum frequency component of the signal. If signal visualisation (especially in the frequency domain) is important—and in a simulation it most often is—the sampling frequency is best chosen much higher.

When a transceiver is simulated, there is a large difference in the frequency content of signals at various stages of transmission. However, to avoid the added complexity (and subsequent additional measurement uncertainty) of sampling rate conversion, a uniform sampling rate is used throughout a given simulation. Most of the simulation modules described below take the sampling rate (in Herz) as one of their parameters. Other modules, such as the one performing amplitude demodulation, can perform its task without knowledge of the exact sampling rate. This is possible because the same input and output sampling rate is assumed.

All full-page simulation results contained in the text were produced using the `simulate.m` program, with the "simulation reference" listed at the bottom of the page used as argument. For example, to replicate the simulation shown on page 169, the command `simulate cleandc` may be executed under MATLAB.

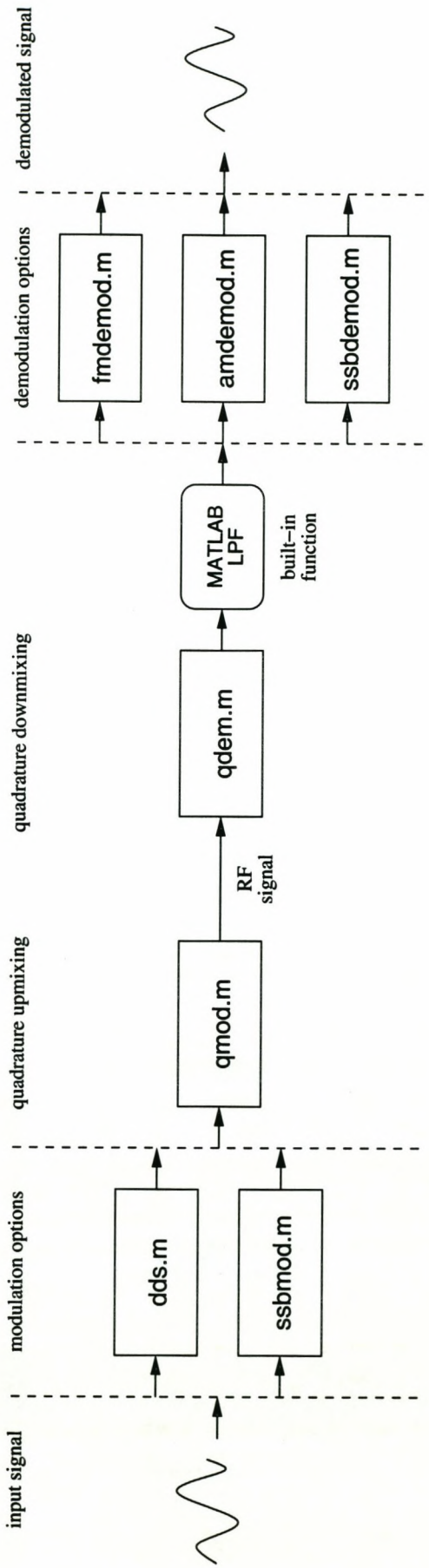

Figure C.1: *Overview of the MATLAB simulation modules.*

C.1.1 Baseband modulation

dds.m performs quadrature-baseband direct-digital synthesis. It takes an amplitude-modulating and frequency-modulating signal as input, and produces a complex-valued output baseband signal, $I(t) + jQ(t)$. It can add a deliberate phase error between the I and Q signals. The DDS technique used is identical to the one discussed in Chapter 2.

ssbmod.m performs single-sideband amplitude modulation at a specified offset frequency in the baseband. It produces a complex-valued output signal of the same form as the one produced by dds.m.

C.1.2 Quadrature mixing

qmod.m performs quadrature upmixing on a complex-valued baseband input signal, and produces an RF output signal at the specified mixing frequency. It can add deliberate amplitude, offset and phase errors, and can introduce LO leakthrough in the output signal.

qdem.m is qmod.m's downmixing counterpart. It takes a real-valued RF signal as input, and multiplies it with the sine and the cosine of a specified mixing frequency, to produce a complex-valued output signal. It supports the same quadrature inaccuracies as qmod.m. Note that qdem.m performs no output filtering, and therefore contains a double-frequency image component.

C.1.3 Baseband demodulation

fmdemod.m is a very simple quadrature FM demodulator that calculates the time derivative of the input signal's instantaneous phase. The instantaneous phase is approximated by subtracting successive samples. The entire demodulation process is contained in the code lines

```
phi = angle(IQ);
dPhi = wrap([phi 0] - [0 phi]);
Fi = dPhi(1:length(IQ))*Fs/(2*pi*dF);
```

where `IQ` is the complex-valued input signal vector, `Fs` is the sampling frequency and `dF` is the FM frequency deviation. `Fi` is the output.

amdemod.m is an even simpler quadrature DSB-AM demodulator. It simply calculates the magnitude of the complex-valued input signal:

```
Ai = abs(IQ);
```

ssbdemod.m is a single-sideband demodulator based on the theory of Section B.2.4. In addition to the complex-valued baseband signal, it requires the sampling frequency,

the offset frequency (ω_0 in Equation B.24) and the starting phase (typically zero). Its algorithm is a direct implementation of Equation B.24:

```
m = real(IQ.*exp(-j*2*pi*Fo*t-Phi0));
```

Here, `IQ` is the complex-valued input signal, `Fo` is the offset frequency in Herz, `t` is the signal's time axis and `Phi0` is the starting phase.

C.2 Simulation premises

- The simulations were run under MATLAB Version 5, but should be compatible with any later MATLAB version.
- MATLAB uses IEEE-754 double-precision floating point numbers. For the simulations, this implies a precision (mantissa) of 53 bits and an exponent of 11 bits.
- The modulating input signal was assumed to always be in the range -1 to $+1$ V.
- A simulation sampling frequency of 100 MHz was used throughout.
- A quadrature mixing frequency of 10 MHz was used throughout.
- For simulations where the signal carrier was offset from the mixing frequency, an offset frequency of 25 kHz was used.
- For FM modulation, 75 kHz/V frequency deviation was used.
- Simulation runs consisted of 16 384 samples for FM, and 32 768 samples for AM and SSB.
- A Blackman window function was used to precondition the RF signal prior to calculating its spectrum.
- An 8th-order Butterworth low-pass filter, with a cut-off frequency of 1.5 MHz was experimentally found to produce the best results in distortion-free simulations when placed after the output of the qdem.m function. The non-ideality of the filter results in a small error signal even in the "ideal" simulation runs, because a small RF component remains in the signal output.
- The error signal displayed in the simulations represents the difference between the demodulated received signal and a reference signal. The reference signal was obtained by performing the same demodulation on the transmitted I-Q signal, without quadrature impairments. The error signal therefore only exposes errors produced by the quadrature upmixing and downmixing process.

- Amplitude deviation (qmod.m) is applied in such a way that the total signal power of the baseband signal stays constant. If one axis is scaled by a factor k_ρ, the other axis must be scaled by $\sqrt{2 - k_\rho^2}$ (see Equation D.8 on page 188).

C.3 Observations

The simulation results are discussed throughout the main text of the document, in the sections to which they apply. A few comments are, however, appropriate here—specifically with regard to the "ideal" simulation runs without quadrature distortion.

Since Matlab uses double-precision floating point numbers for its calculation, it has an effective 52 bits of numeric accuracy. Consequently, quantisation error is not likely to place a fundamental bound on the simulation accuracy. Rather, the effects of non-ideal filtering will play a larger role in establishing the maximum achievable simulation accuracy.

A point in case is the simulation shown in Figure B.1 on page 169. In this simulation, a DC signal is frequency modulated and demodulated again, without any quadrature distortion. The resultant signal error in Figure B.1(d) should give an indication of the simulation accuracy.

The error signal has an average power of about $2.4 \cdot 10^{-12}$ W, which lies approximately 116 dB below the original signal power. This error signal consists of remnants of the RF signal that are not fully removed by the 8th-order Butterworth low-pass filter.

During the quadrature-distortion simulations, the resultant signal error completely dominates this accuracy error. During the quadrature compensation simulations, maximum compensation is achieved when the error signal is again suppressed to below 116 dB and below.

Appendix D

Further derivations and proofs

D.1 Finding ratios by continued fraction expansion

A rational representation of a real number x can be found by writing it as a continued fraction of the form

$$x \approx \frac{n}{d} = d_1 + \frac{1}{\left(d_2 + \frac{1}{\left(d_3 + \cdots + \frac{1}{d_k}\right)}\right)}. \tag{D.1}$$

The values d_i are found by repeatedly taking the integer part of the fraction, and by then taking the reciprocal of the remaining fractional part. If x has a rational representation, the continued fraction will eventually terminate. If x is not a rational number, the fraction continues indefinitely, but can be truncated after k terms to approximate x by a rational representation. For example, truncating the continued fraction representation of π after two terms, yields the familiar rational approximation of 22/7.

The Matlab User's Guide [24] states:

> The accuracy of the approximation increases exponentially with the number of terms and is worst when $x = \sqrt{2}$. For $x = \sqrt{2}$, the error with k terms is about $2.68 \cdot (0.173)^k$, so each additional term increases the accuracy by less than one decimal digit.

D.2 Power transmitted by an elliptical phasor locus

This section shows a simple derivation for the total power transmitted after quadrature modulation, in the general case where the phasor locus is elliptical and centered at the origin. The derivation is done for the specific case where the ellipse's axes coincide with the I-Q axes (amplitude deviation, see Section 5.5). Since an offset in the phasor's phase angle represents a shift in phase in the output signal, and therefore does not influence the transmitted power, the proof will also hold for the general case where the ellipse's axes may

be rotated. This may, for example, occur when the quadrature mixing process suffers from poor phase separation (Section 5.7).

Let the I-Q channels of the quadrature modulator of Figure 2.3 on page 13 be

$$\begin{aligned} I(t) &= A_i \cos\phi(t) \\ Q(t) &= A_q \sin\phi(t)\,. \end{aligned} \tag{D.2}$$

These two equations conform to the standard parametrisation of an ellipse [13, p. 654]. The phasor locus is similar to that of Figure 5.4 on page 43. Without loss of generality, it can be assumed that the total amplitude of the output signal is determined by the amplitude of the I-Q channels, so that quadrature mixing is performed by using the following unity-amplitude sinusoids:

$$\begin{aligned} M_i(t) &= \cos\omega_c t \\ M_q(t) &= \sin\omega_c t\,. \end{aligned} \tag{D.3}$$

The ellipse traced by Equation D.2 has a radius of A_i along the one axis, and a radius of A_q along the other axis. Let the greater of these be the major radius, and the other the minor radius. Next, let us calculate the power of the transmitted signal. According to Parceval's theorem, the total transmitted power of a signal is equal to the power contained in the signal's Fourier components. The transmitted signal is

$$y(t) = A_i \cos\phi(t)\cos\omega_c t - A_q \sin\phi(t)\sin\omega_c t\,. \tag{D.4}$$

The Fourier transform of this signal, at time $t = \tau$ in the joint time-frequency domain, produces

$$\begin{aligned} \mathcal{F}\{y(t)\}|_{t=\tau} &= \frac{A_i}{2}\left\{\delta[\omega - \dot\phi(\tau)] + \delta[-\omega + \dot\phi(\tau)]\right\} * \frac{1}{2}\left\{\delta[\omega-\omega_c] + \delta[-\omega+\omega_c]\right\} - \\ &\quad \frac{A_q}{2j}\left\{\delta[\omega - \dot\phi(\tau)] - \delta[-\omega + \dot\phi(\tau)]\right\} * \frac{1}{2j}\left\{\delta[\omega-\omega_c] - \delta[-\omega+\omega_c]\right\} \\ &= \frac{A_i + A_q}{4}\left\{\delta[\omega + \omega_c + \dot\phi(\tau)] + \delta[\omega - \omega_c - \dot\phi(\tau)]\right\} + \\ &\quad \frac{A_i - A_q}{4}\left\{\delta[\omega + \omega_c - \dot\phi(\tau)] + \delta[\omega - \omega_c + \dot\phi(\tau)]\right\}\,. \end{aligned} \tag{D.5}$$

A plot of Equation D.5 is given in Figure D.1, showing the frequency positions and amplitudes of the impulses at time $t = \tau$. It can easily be seen that, if $A_i = A = A_q$, the outer impulses have an amplitude of $A/2$, and the inner impulses disappear completely. This corresponds to having a circular phasor locus, and is the ideal condition for frequency synthesis.

Using Equation D.5 and Parceval's theorem, the signal power can be calculated as

$$\begin{aligned} P &= 2\left[\left(\frac{A_i}{4} - \frac{A_q}{4}\right)^2 + \left(\frac{A_i}{4} + \frac{A_q}{4}\right)^2\right] \\ &= \frac{1}{4}\left(A_i^2 + A_q^2\right)\,. \end{aligned} \tag{D.6}$$

From this result, the following conclusion can be drawn:

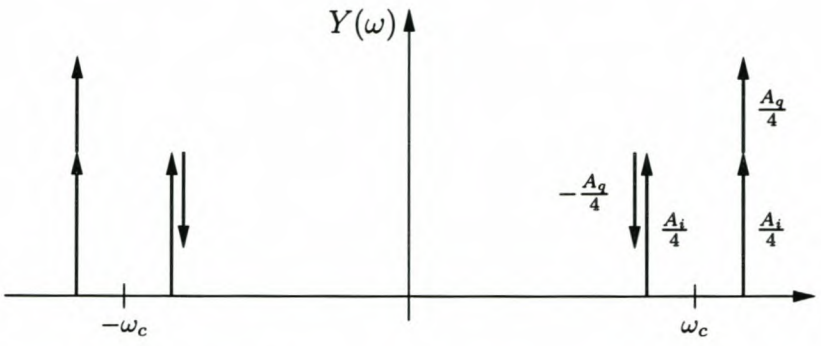

Figure D.1: *Frequency domain plot of a quadrature signal that has an elliptical phasor locus.*

> Consider a quadrature signal that describes an elliptical phasor locus centered at the origin. When this signal is upmixed with a unity-amplitude quadrature carrier frequency, the power of the resultant signal is equal to a quarter of the sum of the squares of the elliptical phasor locus's major and minor axes [i.e. $P = (A_i^2 + A_q^2)/4$]. In the special case of a circular locus, the power is equal to half the square of the radius [i.e. $P = A^2/2$].

During simulation, it is often useful to keep the total power in the complex baseband signal constant when one of A_i or A_q change. If unity amplitude is taken as the norm, the constant output power must be

$$\begin{aligned} P &= \frac{1}{4}\left(A_i^2 + A_q^2\right) \\ &= \frac{1+1}{4} = \frac{1}{2}. \end{aligned} \tag{D.7}$$

When the amplitude of one of the baseband signals changes, and the total power must remain constant, the expression above can be solved for the dependent parameter:

$$\begin{aligned} \frac{1}{4}\left(A_i^2 + A_q^2\right) &= \frac{1}{2} \\ A_i^2 + A_q^2 &= 2 \\ A_q &= \sqrt{2 - A_i^2}. \end{aligned} \tag{D.8}$$

Appendix E

Source code

Distribution copies of this dissertation should have a CD inside the back cover. The CD contains full source code for the simulation modules and the practical SDR prototype, plus additional documentation related to the research. If the CD is missing or unreadable, please do not hesitate to contact the author at g-j@ieee.org.

Source code can also be downloaded from the following website:

http://www.dsp.sun.ac.za/~gvrooyen/phdsrc.zip

In the event that the source code cannot be retrieved from the above address, please contact the author at g-j@ieee.org to have a copy of the source sent by email.